The Physiological and Proteomic Response of Two Strains of the Diatom *Thalassiosira oceanica* to Copper and/or Iron Limitation

by

Anna Angelika Hippmann

Dipl. Biol., Johannes Gutenberg University of Mainz, Germany, 2005

A THESIS SUBMITTED IN PARTIAL FULFILLMENT OF

THE REQUIREMENTS FOR THE DEGREE OF

DOCTOR OF PHILOSOPHY

in

THE FACULTY OF GRADUATE AND POSTDOCTORAL STUDIES

(Oceanography)

THE UNIVERSITY OF BRITISH COLUMBIA

(Vancouver)

December 2017

Abstract

Diatoms are responsible for over 20% of the Earth's photosynthetic productivity, thus impact global fisheries, biogeochemical cycles and climate. However, marine primary productivity is limited by the micronutrient iron (Fe) in ~40% of the ocean. Diatoms inhabiting these regions have evolved unique physiological strategies to survive under these extremely low Fe conditions. Several physiological adaptations to Fe-limitation in diatoms require an increased dependency on copper (Cu), suggesting an interaction between Fe and Cu nutrition and the potential for Fe-Cu co-limitation in these regions. Though some published work has illustrated transcriptomic and proteomic adaptations of some diatoms to low Fe, there is limited knowledge on diatoms' acclimation strategies to low Cu or Fe-Cu co-limitation.

My thesis research focused on elucidating concomitant physiological and proteomic responses of two strains of the open ocean diatom *Thalassiosira oceanica* (CCMP1003 and CCMP1005) acclimated to Fe, Cu, and Fe-Cu limiting conditions. I measured over 20 physiological parameters, including carbon assimilation rate, oxygen production, respiration rate, an array of photosynthetic parameters [such as electron transport rate of photosystem II (ETR_{PSII}), non-photochemical quenching (NPQ), and antenna absorption cross section of photosystem II, σ_{PSII}], and photosynthetic rates as a function of light intensity. Moreover, I investigated the differential expression of proteins in *T. oceanica* in response to these three metal limitations, using stable isotope dimethyl labelling proteomics.

I first describe the physiological and proteomic responses to Cu limitation in *T. oceanica*, focusing on the changes to and the interplay among proteins and pathways involved in the light reactions of photosynthesis, the carbon and nitrogen metabolisms, and the prevention of

oxidative stress. I then compare unique changes to the photosynthetic apparatus induced by each metal limitation (Fe, Cu and Fe-Cu) *vs.* changes induced by general cellular stress. Furthermore, given that my research investigated two strains of *T. oceanica*, I uncovered stunning intraspecific differences in their proteomic and physiological responses to trace metal limitation. My research unveiled a comprehensive restructuring of the photosynthetic apparatus, and a sophisticated interaction among metabolic pathways in *T. oceanica* (CCMP1003) in response to low metal availability (especially Cu), demonstrating exceptional adaptations to low trace metal availabilities.

Lay Summary

Diatoms are one of the most important groups of algae in our oceans. Indeed, a quarter of the oxygen we breathe is produced by diatoms. These microorganisms support global fisheries and modulate nutrient cycles and climate. However, their growth is limited by iron (Fe) availability in over one-third of the global ocean. Diatoms have adapted to survive in these Fe-limited regions using a higher number of copper (Cu) containing proteins and thus diatoms may potentially experience co-limitation by Fe and Cu *in situ*. On-going anthropogenic changes to our oceans, such as ocean acidification and higher temperature, are expected to affect Fe and Cu bioavailabilities. Thus, to predict future changes in marine primary productivity, we need to understand how diatoms may adapt to low trace metal conditions. My research provides insights on different physiological and proteomic strategies employed by two open ocean diatoms in response to three different metal limitation scenarios.

Preface

Chapter 2 is the Methods chapter for Chapters 3-5. This chapter is a modified version (i.e. more detailed, and including the Fe and Fe-Cu co-limiting conditions) of the method section published in:

Hippmann, A.A., Schuback, N., Moon, K.-M., McCrow, J.P., Allen, A.E., Foster, L.J., Green, B.R., and Maldonado, M.T. (2017). Contrasting effects of copper limitation on the photosynthetic apparatus in two strains of the open ocean diatom *Thalassiosira oceanica*. PLoS ONE *12*, e0181753.

The experiments were designed by AAH with help from MTM, BRG, LJF, and AAE. AAH wrote most of the chapter. The section on FRRf parameters was originally drafted by NS, the section on differential proteomics was originally drafted by KMM, and the section on the EST library generation was drafted by AAH and AEA.

Chapter 3 has been published as:

Hippmann, A.A., Schuback, N., Moon, K.-M., McCrow, J.P., Allen, A.E., Foster, L.J., Green, B.R., and Maldonado, M.T. (2017). Contrasting effects of copper limitation on the photosynthetic apparatus in two strains of the open ocean diatom *Thalassiosira oceanica*. PLoS ONE *12*, e0181753.

The experiments were designed by AAH with help from MTM, BRG, LJF, and AAE. AAH was responsible for the culturing and harvesting of the diatoms, the determination and extraction of cellular proteins and their separation into soluble and insoluble fractions. AAH also determined all physiological parameters, except the FRRf measurements, which were conducted by NS.

MKM was responsible for stable isotope dimethylation and LC-MS/MS, as well as running the MASCOT® software. Cells for the EST library were grown by AAH, while the DNA extraction, sequencing, and EST library assembly were conducted by JPM and AEA. AAH interpreted the data and wrote the manuscript, with help from MTM, BRG, and LJF.

Chapters 4 and 5 are in preparation for submission to peer-reviewed scientific journals. The co-authors are: Hippmann, A.A., Schuback, N., Moon, K.-M., McCrow, J.P., Allen, A.E., Foster, L.J., Green, B.R., and Maldonado, M.T.

The experiments were designed by AAH with help from MTM, BRG, LJF, and AAE. AAH was responsible for the culturing and harvesting of the diatoms, the determination and extraction of cellular proteins and their separation into soluble and insoluble fractions. AAH also determined all physiological parameters, except the FRRf measurements, which were conducted by NS. MKM was responsible for stable isotope dimethylation and LC-MS/MS, as well as running the MASCOT® software. Cells for the EST library were grown by AAH, while the DNA extraction, sequencing, and EST library assembly were conducted by JPM and AEA. AAH interpreted the data and wrote the chapters, with help from MTM, BRG, and LJF.

Table of Contents

List of Tables

List of Figures

List of Symbols

$1/n_{PSII}$	mol of chl*a* associated with each RCII (mol chl*a* mol $RCII^{-1}$)
α	initial slope of the PvsE curve, quantifies the linear light-dependent increase of the rate of photosynthesis under sub-saturating light conditions (mol e-/RCII)/(µmol quanta / m2 * s)
e^-	electron
F’	steady-state chl*a* fluorescence yield in the light-regulated state
F_m	maximum chl*a* fluorescence yield in the dark-regulated state
F_m'	maximum fluorescence in actinic light
F_o	minimum chl*a* fluorescence yield in the dark-regulated state
F_o'	minimum chl*a* fluorescence yield in the light-regulated state
F_q'	(= F_m' - F′), ‘quenched’ variable chl*a* fluorescence yield in the light-regulated state
F_v	(= F_m - F_o), variable chl*a* fluorescence yield in the dark-regulated state
F_v/F_m	maximum quantum yield of PSII photochemistry
F_v'	(= F_m' - F_o'), variable chl*a* fluorescence yield in the light-regulated state
σ_{PSII}	functional PSII absorption cross section ($Å^2$ $RCII^{-1}$)
$\Phi_{e:C}$	electron requirement for carbon fixation (mol e^- mol C^{-1}), note that the more recent symbol for this parameter is KC

List of Abbreviations

1,3BPG	1,3-bisphosphateglycerate
2K3D-PG	2-keto-3-deoxyphosphogluconate
2PG	2-phosphoglycerate
3PG	3-phosphoglycerate
6PG	6-phosphogluconate
AA	amino acid
AAT	aspartate aminotransferase
ACAS	acetyl-CoA synthase
ACC	acetyl-CoA carboxylase
ACO	aconitase hydratase
ADP	adenosine diphosphate
Agm	agmatinase
Allox	alloxanthin
AMT	ammonium transporter
APX	ascorbate peroxidase
Arg	arginase
argD	n-acetylornithine aminotransferase
AsL	argininosuccinate lyase
AsuS	argininosuccinate synthase
ATCase	aspartate carbamoyltransferase
ATP	adenosine triphosphate
C	carbon
cbbX	rubisco expression protein
CCMP	culture collection of marine phytoplankton
CET	cyclic electron transport
Chl	chlorophyll
Chl*a*	chlorophyll *a*

Chl*b*	chlorophyll *b*
ChlF	chlorophyll *a* fluorescence
CO_2	carbon dioxide
CS	citrate synthase
Cu	copper
Cys	cysteine
CYS	cysteine synthase
Dd	diadinoxanthin
DHAP	dihydroxyacetone phosphate
DHAR	dehydroascorbate reductase
DLDH	dihydrolipoamide dehydrogenase
DLHC	disconnected light-harvesting complexes
Dt	diatoxanthin
EDA	2-keto-3-deoxyphosphogluconatealdolase
EDD	6-phosphogluconate dehydratase
E_K	light-saturation parameter (from PvsE curves)
ENO	enolase
ETC	electron transport chain
ETR	electron transport rate
ETR_{RCII}	electron transport rate (RCII-specific rate of charge separation)
F2BP	fructose-1,6-bisphosphatase
FA	fatty acid
FBA I	fructose-bisphosphate aldolase class-I
FBA II	fructose-bisphosphate aldolase class-II
Fe	iron
Fe-NiR	Nitrite reductase (ferredoxin-dependent)
FH	fumarate hydratase
FNR	ferredoxin:$NAD(P)^+$ reductase
FRRF	Fast repetition rate fluorometer /fast repetition rate fluorometry

Fru-1,6-bis-P	fructose-1,6-bisphosphate
Fru-6P	fructose 6-phosphate
Fx	fucoxanthin
GAP	glyceraldehyde 3-phosphate
GAPDH	glyceraldehyde 3-phosphate dehydrogenase
GCL	glutamate cysteine ligase
GDCP	glycine decarboxylase p-protein
GDCT	glycine decarboxylase t-protein
GDH	glutamate dehydrogenase
GF/F	glass fibre filter
glu	glutamate
Glu 6-P	glucose 6-phosphate
GOGAT	glutamate synthase
GPI	glucose 6-phosphate isomerase
GR	glutathione reductase
GRX	glutaredoxin
GSI	glutamine synthetase I
GSII	glutamine synthetase II
GSIII	glutamine synthetase III
GSS	glutathione synthetase
GTR	glutathione transporter
HNLC	high-nutrient low chlorophyll
HPLC	high pressure liquid chromatography / high performance liquid chromatography
IDH	isocitrate dehydrogenase
LC-MS/MS	liquid chromatography - tandem mass spectrometry
LDH	L-lactate dehydrogenase
LED	light emitting diode
LET	linear electron transfer chain
LHCs	light-harvesting complexes

MDH	malate dehydrogenase
ME	malic enzyme
NAD(P)H-NiR	nitrite reductase (NAD(P)H-dependent)
NAD(P)H	nicotinamide adenine dinucleotide (phosphate), reduced
NiRT	formate/nitrite transporter
NPQ	non-photochemical quenching (Stern-Volmer quenching)
NPQ_{NSV}	non-photochemical quenching (normalized Stern-Volmer quenching)
NR	nitrate reductase
NRT	nitrate/nitrite transporter
O_2	oxygen
OAA	oxaloacetate
OCD	ornithine cyclodeaminase
OdC	ornithine decarboxylase
OGD	2-oxoglutarate dehydrogenase
OTC	ornithine carbamoyltransferase
P_{680}	chlorophyll molecule in RCII
PAR	photosynthetically available radiation
PC	pyruvate carboxylase
pc	plastocyanin
PCR	polymerase chain reaction
PDH-E1	pyruvate dehydrogenase-E1 component
PDH-E2	pyruvate dehydrogenase E2 component (dihydrolipoamide acetyltransferase)
PEPC	phosphoenolpyruvate carboxylase
PEPCK	phosphoenolpyruvate carboxykinase
PEPS	phosphoenolpyruvate synthase
PFK	phosphofructokinase
PGAM	phosphoglycerate mutase
pgCPSII	carbamoyl-phosphate synthase II
PGK	phosphoglycerate kinase

PGM	phosphoglucomutase
PK	pyruvate kinase
P_{max}	maximum photosynthetic rate
PPDK	pyruvate, phosphate dikinase
PQ	plastoquinone
PSI	photosystem I
PSII	photosystem II
PTOX	plastid terminal oxidase
P*vs*E	productivity /photosynthesis *vs.* light curve
QA	primary stable electron acceptor after charge separation in RCII
QB	secondary stable electron acceptor after charge separation in RCII
*q*PCR	real-time quantitative PCR
rbcL	ribulose-bisphosphate carboxylase large chain
rbcS	ribulose-bisphosphate carboxylase small chain
RCI	reaction center I
RCII	reaction center II
ROS	reactive oxygen species
RPE	ribulose-5-phosphate epimerase
RPI	ribose-5-Phosphate-isomerase
RT-PCR	reverse-transcript PCR
RuBisCO	ribulose-bisphosphate carboxylase
RuBisP	ribulose-bisphosphate
SD	standard deviation
SSLC	steady-state light curve
ST	single turnover
SUCLA	succinate CoA synthetase
TPI	triose-phosphate isomerase
TPT	putative location of triose-phosphate-transporter
TXN	thioredoxin

unCPS (CPSase III)	carbamoyl-phosphate synthase
Ure	urease
URT	Na/urea-polyamine transporter
γ-glu-cys	γ-glutamylcysteine

Acknowledgements

I want to express my sincere gratitude for the guidance and mentorship provided throughout my PhD by my supervisor Maite Maldonado. Your door was always open, and the time discussing trace metal physiology, concentrations and interactions was always stimulating. Especially your eye for detail without losing sight of the big picture implications was and is inspiring. It has been a long journey, but your support was unwavering. Maite, when I thought I wouldn't even start my PhD because I was pregnant, your exuberant reaction was "Anna, this is great!!! Both motherhood and a scientific career are wonderful!!!! If you want to do it, you can do it." And you were right! However, just as the saying goes "It takes a village to raise a child", the same is true for a PhD.

Beverley Green, who has become my unofficial co-supervisor, especially in everything related to LHCs and metabolic pathways. Thank you for many hours of insightful discussions and digging deeper into the photosynthetic apparatus, diatom phylogeny, and sequence homologies. Our trip to Seattle will not be forgotten! Both you and Maite are true role models, scientifically and personally.

Thank you to my whole advisory committee: Maite Maldonado, Beverley Green, Leonard Foster and Michael Murphy: The fruitful discussions, your different perspectives and insights were challenging and motivating. I could not have imagined a more supportive committee. You never caged me in, but instead listened to my ideas and gave valuable feedback and guidance.

I would also like to thank our collaborators in San Diego. I learned so much in the week I spent at JCVI. Andy Allen, John McCrow, James McCarthy, Jeff McQuaid, and Talina Konotchick: the time we spent discussing iron physiology in diatoms −ISIPs in particular− and how to best map the transcriptome to the genome, opened yet another window for me.

Thank you to Jenny Moon of the Foster Lab and Angele Arrieta of the Murphy Lab for patiently guiding me through and answering all my questions related to differential proteomics and PCR, respectively.

Our group, the Tornadoes! Your friendship, camaraderie, understanding, support and advice throughout the years will be treasured: Alyssia Herr, Ania Posacka, Carolyn Duckham, Chen Zeng, Dave Capelle, Dave Semeniuk, David Cassis, Eva Jordison, Florian Baier,

Genevieve Savard, Iselle Flores Ruiz, Jade Schiller, Jian Guo, Kang Wang, Kristina Brown, Lauren Mocchia, Lindsey Fenwick, Mirkko Flecken, Nina Schuback, Robert Izett, Tereza Jarnikova, Will Burt, Xinjuan, Yuanji Sun.

In particular, Dave Semeniuk – for challenging scientific, educational, political and artistic views, not for the mere challenge but to really try to get to the bottom of it (btw, still so sorry about the desk!!!); Nina – my photosynthesis-FRRF-yoga-bike guru, your calm and funny dry humor in really any situation is awe-inspiring; Ania – for moral, R, and chocolate support in the lab and beyond; Robert – for meeting-menthos and your re-freshening unruffledness; Pia – thanks for care packages and postcards and just being you and there; Randolf – for funny PhD wisdom exactly when needed on the other end of the email and insights from the chemistry perspective; Carlos – for never questioning supplying yet another laptop, printer, screen, and other office supplies as soon as I needed them.

This thesis would not have been possible without coffee, dark chocolate, and the ceaseless love and unwavering support of my family. My parents, Mama und Papa (Nana und Bopa), even an ocean apart, really, just a phone call away −or even just a 10-hour flight when really needed− you supported me and us throughout these years; similarly, Tim's parents Dieter and Martina (Oma und Opa); Ben, Max, und Johanna, my fearless warriors, you were often so patient and even made breakfast, when mom was so tired in the mornings; Tim, no words can express my gratitude, love, and amazement at how you have supported our family throughout these years. Finally: "I'll be finished by Christmas!" I love you. 2248

To my family

“Think left and think right and think low and think high.
Oh, the things you can think up if only you try!”
(Dr. Seuss)

“just use bleach” (Carlos Chiu)
“NO!” (Angelina)

Chapter 1: Introduction

Here I provide a brief unifying context to the experimental work presented in Chapters 3-5, discussing the significance of diatoms in global nutrient cycles and their dependency on the two trace metals of interest in this thesis; iron (Fe) and copper (Cu). I describe the phylogenetic ancestry of diatoms and the resulting chimaeric genomic makeup that enables them to develop unique strategies to adapt to multiple environmental conditions. I also introduce my model diatom species, *Thalassiosira oceanica* (Figure 1.1). This chapter concludes with a summary of the overall research objectives and structure of this work.

1.1 Global ocean, phytoplankton, and climate

The global ocean covers over 70% of our planet. Besides containing many diverse ecosystems that support humans economically and ecologically, it has an intricate relationship with our atmosphere and ultimately our climate. This relationship is due to differential gas solubility constants and resulting gas exchange between the liquid phase of the ocean and the gaseous phase of the atmosphere. The concentrations of gases, such as carbon dioxide (CO_2) or oxygen (O_2), in the ocean-atmosphere boundary layer, are, thus, dependent on physical and biological processes in the surface ocean, such as mixing, photosynthesis and respiration.

Marine phytoplankton are unicellular, microscopic algae that are able to use the energy of the sun to reduce CO_2 to organic carbon. The fate of this organic carbon varies. It can be 1) used as a storage, structural, or other metabolic component in the cell, thus temporally removing CO_2 from the atmosphere, 2) reoxidized by respiration within the mitochondria to supply cellular energy, thereby releasing CO_2 back to the environment, 3) remineralized by heterotrophic bacteria once the cell has died (which also releases CO_2), 4) ingested by zooplankton after the

cell has been grazed, or 5) exported to the deep ocean as dead cells sink, most likely, inside zooplankton fecal pellets. The latter is called the biological carbon pump as it effectively removes CO_2 from the atmosphere sequestering it into the deep ocean as organic carbon (de la Rocha, 2007).

Marine phytoplankton account for approximately 40% of the global primary productivity and are responsible for the export of 16 gigaton (10^{12} kg) of fixed CO_2 to the deep ocean (Nelson et al. 1995; Field et al. 1998). Variations in the magnitude of this organic C export affect the CO_2 content of the upper ocean which in turn regulates atmospheric CO_2 levels (Archer 2003). To fully understand the global carbon cycle, it is thus essential to establish the factors controlling oceanic phytoplankton productivity.

1.2 Diatoms

Diatoms are eukaryotic, single-celled microalgae found in almost every aqueous environment, both freshwater and marine. Diatoms have a very complex highly ornamented, silicified cell wall called the frustule. Despite evolving relatively recently, diatoms are among the most successful phytoplankton groups (Falkowski et al. 2004) and are ubiquitous in the well-lit surface layer (i.e. euphotic zone) of the ocean. They are estimated to account for ~ 40% of the ocean's net primary production and for ~ 50% of the carbon sequestration into the deep ocean (Falkowski et al. 2004). In other words, the oxygen in every 4th breath that we take has been produced by diatoms. Furthermore, given their productivity, diatoms largely support global fisheries and influence biogeochemical cycles of both macronutrients (e.g. carbon, nitrogen, phosphorous, and silica) and micronutrients (e.g. Fe, Mn, and Cu).

1.3 Photosynthesis

Photosynthesis is arguably the most important metabolic pathway on our planet. In it, the energy of the sun is absorbed to create the cellular reducing equivalent NAD(P)H and energy equivalent ATP, while releasing oxygen (O_2). NAD(P)H and ATP can then be used to fix CO_2 into organic compounds. This organic carbon can fuel phytoplankton growth, as well as organisms in higher trophic levels. A schematic overview of the photosynthetic electron transport chain is illustrated in Figure 1.2. Light is absorbed by special pigmented light-harvesting complexes (LHCs). Some of the absorbed energy is channelled towards photosystem II (PSII) in which a special pigment pair (Chl*a*) is excited in such a way that induces charge separation. The electron is then transferred via several proteins (plastoquinone, cytb_6f complex, plastocyanin/cytc_6) to the second photosystem (PSI). Photosystem I (PSI) also has its own LHC antennae complex and special pigment pair (Chl*a*), where charge separation also occurs and the electron is transported via a ferredoxin (Fdx) and ferredoxin:$NADP^+$-reductase (FNR) to $NADP^+$ thus generating the cellular reducing equivalent NAD(P)H. During several of these steps, protons (H^+) are pumped into the lumen generating a pH gradient that in turn is used for ATP synthesis, the cellular energy currency. The two photosynthetic reactants, ATP and NAD(P)H, can then be used in the Calvin-Benson-Bassham cycle to fix CO_2 into carbohydrates. Thus, in photosynthesis, light energy is transformed into chemical energy (carbohydrates) that is accessible to all life forms. This process is called primary productivity.

1.4 Phytoplankton productivity

Phytoplankton primary productivity varies among oceanic regions. As observed in terrestrial systems (Longhurst 1995), there are highly productive regions (i.e. eutrophic) such as coastal and

open ocean upwelling regions, where more than 1 mg C m^{-3} are fixed annually. In contrast, low productivity regions (i.e.oligotrophic) convert less than 0.1 mg C m^{-3} every year (Field et al. 1998). However, even though carbon fixation per m^3 is over an order of magnitude larger in eutrophic than oligotrophic waters, the vast regions of oligotrophic waters in the ocean account for over 23% of the total ocean net primary productivity (NPP) compared to 19% for the eutrophic waters (mesotrophic waters accounting for 56 % and macrophytes for 1%).

Phytoplankton productivity depends on physical, chemical, and biological parameters e.g. light, temperature, mixing, nutrients and predator assemblages. These parameters have a direct influence on planktonic organisms, populations, and community structure. In addition to carbon, macronutrients such as nitrate and phosphate are needed by phytoplankton in a conserved molar stoichiometry, 106 mol C:16 mol N:1 mol P, the so-called Redfield ratio (Redfield 1934, 1958). Trace elements, such as iron (Fe), zinc (Zn), manganese (Mn), cobalt (Co), or copper (Cu) occur in extremely low concentrations in the open ocean (~10^{-9} M), but are essential for phytoplankton growth. These trace elements are required in minuscule amounts (0.5-100 µmol mol C^{-1}) and are so-called essential micronutrients. Ho et al. (2003) measured the elemental composition of representative phytoplankton phyla and derived an extended Redfield ratio including trace elements (subscript indicates mol; note that macronutrient values are multiplied by 1,000): $(C_{124}\,N_{16}\,P_1\,S_{1.3}\,K_{1.7}\,Mg_{0.56}\,Ca_{0.5})_{1,000}$ - $Sr_{5.0}\,Fe_{7.5}\,Zn_{0.80}\,Cu_{0.38}\,Co_{0.19}\,Cd_{0.21}\,Mo_{0.03}$ (Ho et al. 2003). If the concentration of any one of these micronutrients is too low, growth and hence primary productivity will be limited.

Even though nitrate was thought to be the main limiting resource for marine primary productivity, in at least 30% of the ocean, nitrate concentrations are not depleted, suggesting that another nutrient limits phytoplankton. The regions with excess nitrate are the subarctic and

equatorial Pacific, as well as the Southern Ocean. Since the 1990s, extensive research, including several mesoscale iron fertilization experiments (Boyd et al. 2007), has indicated that 30-40% of the global ocean is indeed Fe limited (Moore et al. 2004). Furthermore, more recent work has suggested the possibility of Fe-Cu co-limitation in some of these areas (Coale 1991; Peers and Price 2006).

1.5 Iron in the ocean

In the modern, oxygenated ocean, Fe is stable as its oxidized species, ferric ion (Fe^{3+}), which tends to form insoluble Fe hydroxides, such as $Fe(OH)_2^-$ (Millero 1998). Iron concentrations in the ocean vary by two orders of magnitude, with higher concentrations at the coast relative to those in the open ocean. The mean dissolved Fe concentration in open ocean waters (> 50 km away from the coast) is 0.07 nM (Johnson et al. 1997). In surface waters, approximately 99.9% of the dissolved Fe is bound to strong organic ligands, resulting in 0.07 pM dissolved inorganic Fe (Rue and Bruland 1995; Wu and Luther III 1995).

1.6 Iron - cellular demand

There are two compelling reasons supporting the important role of Fe in essential cellular redox systems. First, Fe was readily available in the reducing Archaean ocean when pathways such as respiration and later photosynthesis evolved (Catling and Claire 2005). Second, the standard electrochemical potential E^0 (0.77 V) between Fe (II) and Fe (III) gives Fe a wide applicability to catalyze metabolic redox reactions (Hunter and Boyd 2007). Furthermore, depending on the protein matrix to which the Fe is bound, the redox potential can be modulated from +550 mV to -700 mV (Capozzi et al. 1998). Therefore, Fe is the best redox catalyst in nature.

The two main classes of Fe-containing electron transfer proteins are the heme-containing cytochromes (cyt) and iron-sulphur (Fe-S) proteins. In heme proteins, the Fe is bound to one of nine porphyrin systems and can be used to channel electrons, bind oxygen, or both, depending on the localization of the heme (or multiple hemes) within the protein. Most prominent heme-containing protein classes include cytochromes (cyt), oxygenases, peroxidases, and catalases. Iron-sulphur (Fe-S) proteins contain one or more Fe ions that are coordinated by thiol ligands from cysteine residues provided by the protein, and bridged by sulphide ions. Besides some representatives that are involved in enzymatic activity (e.g. mitochondrial aconitases (Jordan et al. 1999); nitrite reductase (Adhikari and Rahman 2017); sulphite reductase (Hermann et al. 2015)), the vast majority of Fe-S proteins are ferredoxins and rubredoxins that participate solely in electron transfer reactions. Important Fe-S containing proteins include Rieske-Proteins (involved in mitochondrial cytbc_1 and plastidial cytb_6f complex, (Schmidt and Shaw 2001)), ferredoxins (in electron transfer e.g. in photosynthesis, (Hanke and Mulo 2013)), and nitrogenases (globally important as the only nitrogen-fixing proteins (Smith 1999; Hoffman et al. 2011)).

Several essential metabolic pathways have a high Fe demand; for example, the respiratory electron transport chain in the mitochondrion (~28 Fe atoms), the photosynthetic electron transport chain in the chloroplast (~22 Fe atoms) (Raven et al. 1999), and nitrate assimilation (~7 Fe atoms). Furthermore, Fe is needed in several proteins involved in the detoxification of reactive oxygen species (ROS), such as ascorbate peroxidases and Fe-containing representatives of superoxide dismutase (Alscher et al. 1997).

Cellular Fe:C quotas can differ among species and depend on the nutritional status of the cells. For example, under Fe replete conditions, Fe:C quotas in diatoms can range from 26-102

μmol Fe:mol C, while under Fe-limiting conditions these decrease to 0.65 - 18 μmol Fe:mol C (Maldonado and Price 1996).

1.7 Copper in the ocean

In the modern ocean, Cu is stable as cupric ion (Cu^{2+}) and forms inorganic complexes, such as $CuCO_3$, $CuOH^+$, and $CuOH_2$ (van den Berg 1984). Photochemical processes in surface waters may also produce significant amounts of transient Cu^+ (Moffett and Zika 1983). Interestingly, as with Fe, the speciation of dissolved Cu is dominated by organic complexation with strong and weak ligands that bind > 97% of dissolved Cu in the ocean (van den Berg 1984; Coale and Bruland 1988). Moffet and Brand (1996) have provided strong evidence that these ligands are biogenic. However, in contrast to Fe-binding ligands that are thought to be released by bacteria in order to acquire Fe more efficiently (Trick 1989), Cu-binding ligands are released in response to high Cu levels to lower the free cupric ion concentration, and thus its toxicity (Moffett and Brand 1996; Moffett et al. 1997).

Concentration gradients of Cu in marine surface waters are not as distinct as those for Fe. In the open ocean, Cu concentrations range from 0.5 nM to 1.4 nM in the Pacific (Bruland 1980; Boyle et al. 1981) and 0.6 to 1 nM in the Atlantic (Rutgers et al. 1997). In coastal waters, due to anthropogenic sources, Cu concentrations may range from 4-6 nM in non-polluted areas (Boyle et al. 1981; Moffett et al. 1997) to ~100 nM in moderately polluted estuaries, such as San Francisco Bay (Buck et al. 2006).

1.8 Copper – cellular demand

Why is there a need for Cu when Fe is the best redox catalyst for metabolic pathways? As mentioned above, Fe was readily available in the Archaean ocean (> 2.5 Gyr ago) when photosynthesis and respiration evolved. These two features, suitable physicochemical characteristics and bioavailability, were crucial in determining the metal of choice incorporated into a protein. Approximately 2.32 Gyr ago, atmospheric oxygen levels rose considerably (Bekker et al. 2004), changing the solubilities of a variety of metals. As summarized by Kaim and Rall (1996), the oxidizing atmosphere had two distinct advantages for the incorporation of Cu into proteins: while the formerly soluble Fe(II) was now oxidized to insoluble Fe(III) hydroxides, the former Cu (I), trapped in insoluble sulfides, was now oxidized to soluble Cu (II).

Depending on the protein matrix, Cu^{+}/Cu^{2+} enzymes may have redox potentials ranging from 180 - 790 mV. In addition to redox reactions, Cu proteins are key in numerous enzymatic reactions involving dioxygen, such as transport, oxidases, oxygenases, and detoxification (Fetherolf et al. 2017). However, even though Cu is essential for eukaryotes and prokaryotes, it is also potentially toxic due to its high reactivity with oxygen and tendency to generate reactive oxygen species (ROS, Knauert and Knauer 2008). Therefore, Cu homeostasis is essential for any living cell. Strikingly, Rae et al. (1999) have deduced that the free Cu ion concentration in yeast is maintained below 1 Cu atom per cell (Rae et al. 1999). Indeed, within the cell, Cu is transported and delivered to various destinations by specialized Cu-binding chaperones and metallothioneins (Blaby-Haas et al. 2014).

The majority of Cu proteins are involved in either electron transfer reactions or binding and activation of small molecules such as oxygen or nitrous oxide (as reviewed by Kaim and Rall 1996). The group of Cu proteins almost exclusively responsible for electron transfer

reactions are blue Cu proteins, with plastocyanin as the most prominent representative (De Rienzo et al. 2000). Plastocyanin can be found in photosynthetic bacteria, green algae and plant chloroplasts. It ferries electrons in the photosynthetic electron transport chain from cytb_6f to the reaction centre of photosystem I (P700) thus being an analogue to cytc_6, which is used by more ancient photosynthetically active phytoplankton (reviewed by Navarro et al. 1997). Depending on Cu availability, some algae (e.g. the green alga *Chlamydomonas reinhardtii* and others) have the option to switch between the Cu-containing plastocyanin and the Fe-containing cytc_6 (Sandmann and Böger 1980; Merchant and Bogorad 1986).

The second group of abundant Cu proteins involved in dioxygen reactions, includes blue Cu oxidases, cyt*c* oxidases and superoxide dismutases. Multicopper oxidases are widespread in bacteria, fungi, plants and animals and catalyze sequential substrate oxidation by transferring 4 electrons to O_2, resulting in 2 H_2O (Messerschmidt 1998). Copper- (and Fe-) containing cyt*c* oxidases are of global importance as they catalyze the final reduction of dioxygen to water in the respiratory chain.

In the well-studied freshwater green algae *Chlamydomonas reinhardii*, the most abundant Cu proteins are cyt*c* oxidase, plastocyanin, and a multicopper oxidase, which is involved in Fe acquisition (La Fontaine et al. 2002; Merchant et al. 2006). Interestingly, until recently, plastocyanin was thought to be only used by plants and eukaryotic marine phytoplankton in the green lineage. Surprisingly, 10 years ago, the oceanic diatom, *Thalassiosira oceanica*, was shown to use plastocyanin instead of cytc_6 in its photosynthetic apparatus (Peers and Price 2006).

Comparable to Fe:C quotas, Cu:C quotas vary as well, depending on species and nutritional status. In coastal isolates, Cu:C quotas range from 0.4 to 2.67 μmol Cu:mol C under Cu replete conditions and from 0.32 to 1.96 μmol Cu:mol C under Cu limiting conditions. In

general, in oceanic isolates, Cu:C quotas are higher than those in coastal phytoplankton, ranging from 1.84 to 6.32 μmol Cu : mol C under Cu replete conditions and from 0.32 to 2.58 μmol Cu : mol C under Cu-limiting conditions (Annett et al. 2008).

1.9 Algal trace-metal physiology – iron, copper and their interaction

Trace metal requirements of oceanic and coastal phytoplankton vary, reflecting the trace metal conditions in their respective habitats (Brand et al. 1983; Sunda and Huntsman 1995). Most prominently, oceanic species have to adapt to 100 times lower Fe concentrations compared to coastal species. As mentioned above (section 1.5; Iron in the ocean), Fe concentrations in vast ocean regions were deemed too low to support the growth of even the smallest photosynthetic cell (Raven 1988; Sunda et al. 1991). However, oceanic phytoplankton have evolved unique mechanisms to lower their trace metal demands while optimizing trace metal transport in environments with limiting trace metals such as Fe, Mn, and Zn (Brand et al. 1983). For example, to reduce its Fe requirement, the model open ocean diatom *T. oceanica* has altered the stoichiometry of its photosynthetic apparatus by reducing the concentration of the Fe-rich photosystem I (12 atoms Fe) by 5-fold and that of the cytb_6f complex (5 atoms Fe) by 7-fold relative to the model coastal species *T. weisfloggii* (Strzepek and Harrison 2004). Furthermore, *T. oceanica* has been shown to use the Cu-containing plastocyanin instead of the Fe-containing cyt$c_{6,}$ lowering the cellular Fe requirement by 10% (Peers and Price 2006). This protein substitution is particularly interesting as plastocyanin was only known to exist in Chl*b* containing photosynthetic organisms (e.g. green algae and plants) and cyanobacteria. In photosynthesis, two additional atoms of Fe can be saved by substituting ferredoxin with flavodoxin, even though the latter has a lower specific reaction rate (Raven et al. 1999).

However, the full mosaic of phytoplankton adaptations to various trace metal deficiencies is not well understood. Historically, investigations on Cu and phytoplankton interactions have focused on Cu as a toxic metal (Rueter et al. 1979; Brand et al. 1986; Croot et al. 2000; Davis et al. 2006). More recently, several studies acknowledged the importance of Cu as a micronutrient for phytoplankton physiology, and the intricate relationship between Fe and Cu nutrition in oceanic phytoplankton (Wells et al. 2005; Peers and Price 2006; Annett et al. 2008). Relative to their coastal counterparts, oceanic phytoplankton require more Cu for growth (Peers et al. 2005), and have a higher cellular Cu content (Annett et al. 2008). Even though Peers and Price (2006) argue that the higher Cu requirement of *T. oceanica* can be solely accounted for by their use of plastocyanin, other studies suggest higher Cu demands due to the involvement of additional Cu-containing proteins in other metabolic pathways. Maldonado et al. (2006) for example showed an up to 60 fold up-regulation of a putative multi Cu-containing oxidase (MCO), which is believed to be involved in the high-affinity Fe uptake system of marine diatoms.

1.10 *T. oceanica* - a model species for open ocean diatoms adapted to low Fe

For several decades, *Thalassiosira pseudonana* (also known as *Cyclotella nana*) strains have been isolated and successfully grown for various morphological and physiological experiments (Guillard and Ryther 1962). The coastal strain 3-H (CCMP 1335) was isolated in coastal waters off the coast of Long Island and was the first diatom whose whole genome was sequenced (Armbrust et al. 2004). The oceanic strain 13-1, which was regarded as a typical oceanic diatom, was isolated in the oligotrophic Sargasso Sea and was only identified as the distinct species *T. oceanica* in 1983 (Hasle 1983). Since then, other strains have been isolated from the Sargasso Sea and identified as *T. oceanica*, including strains CCMP 1003 and CCMP 1005, isolated in

1977 and 1958, respectively. These two latter strains are the *T. oceanica* strains investigated in the present study (Figure 1.1).

For decades, both strains have been used as model open ocean diatoms and important traits in their trace metal physiology have been revealed compared to their coastal counterparts. Most importantly, these oceanic strains have succeeded in adapting to their low Fe environment by both lowering their Fe requirements and increasing the efficiency of Fe acquisition mechanisms. Interestingly, both strategies required a higher physiological Cu dependency (Peers et al. 2005; Peers and Price 2006; Maldonado et al. 2006).

T. oceanica has a 25% lower cellular Fe demand (2 µmol Fe:mol C) than *T. pseudonana* to achieve maximal growth rates (Sunda et al. 1991). Under Fe limitation, both species engage an inducible, Cu-dependent, high-affinity uptake system which allows them to access Fe bound to strong organic ligands (Maldonado et al. 2006). However, under the same conditions, *T. oceanica* shows faster Fe uptake rates and higher Cu dependency compared to its coastal counterpart. Copper dependency is so severe that Cu limitation might, in fact, induce Fe limitation in this species (Maldonado et al. 2006). Incidentally, and in contrast to its lower cellular Fe content, *T. oceanica* has a 50% higher Cu demand than *T. pseudonana* (2.93 *vs.* 1.9 µmol Cu: mol C, respectively, (Annett et al. 2008). In accordance with its more efficient Fe uptake system, *T. oceanica* has 2-fold faster Cu uptake rates than *T. pseudonana* at identical Cu concentration. In addition, the K_m of the proposed high-affinity Cu uptake system in *T. oceanica* is three times lower than its coastal counterpart (48.3 nM *vs.* 188.4 nM) (Guo et al. 2010).

The alteration of PSII: PSI ratio (Strzepek and Harrison 2004), and the use of Cu-containing plastocyanin instead of Fe-containing cytc_6 in the photosynthetic electron transport chain (Peers and Price 2006) explain the lower Fe requirement and higher Cu-demand in oceanic

species. It has been suggested that this high Cu-dependency of Fe-limited phytoplankton may lead to Fe-Cu co-limitation in the field (Coale 1991; Peers and Price 2006). It is thus surprising that no study has examined the proteomic effects of Cu limitation or Fe-Cu co-limitation in these diatoms.

1.11 Diatoms – their phylogenetic ancestry as key to their success

Humans are part of one phylum −chordate−, which includes dinosaurs, birds, and fish. In contrast, aquatic phytoplankton are part of at least 12 eukaryotic and 2 prokaryotic phyla, highlighting the huge diversity of these microbes. After some debate, strong evidence suggested that eukaryotic phytoplankton were derived from a single endosymbiotic event in which an ancient cyanobacterium was engulfed by a eukaryote and eventually became a totally dependent endosymbiont, the chloroplast (Rodríguez-Ezpeleta et al. 2005; Reyes-Prieto et al. 2007) (see Figure 1.3).

Three distinct lineages evolved from this primary endosymbiosis event: glaucophytes, red algae, and green algae. From the latter, land plants evolved. However, species from both red and green algae went through secondary endosymbiosis events in which they were engulfed by a heterotrophic eukaryote (Keeling 2004; Archibald 2005). The red algal endosymbiont gave rise to a diverse group of organisms referred to as chromalveolates, although they may have originated via several separate secondary endosymbiosis events (Burki et al. 2016). They include dinoflagellates, haptophytes, heterokontophytes (including bacillariophyta = diatoms), cryptophytes and others. In the evolution of the organisms derived from secondary endosymbiosis, what is left from the original red and green algae are the chloroplast and the outer membranes resulting generally in 4 chloroplast membranes. The inner two membranes

belong to the original cyanobacterium (plastid envelope, inner and outer membrane), the third is the outer membrane of the primary host (i.e. red algae), and the fourth membrane represents the phagosomal membrane of the secondary host (i.e. heterotrophic eukaryote) (McFadden 1999; Archibald and Keeling 2002). This fourth, outermost plastid membrane is part of the host's endoplasmatic reticulum. Genes from both the nucleus and chloroplast have been transferred to the host nucleus, leaving only a small number of genes in the chloroplast genome itself (McFadden 1999).

Importantly, the proposed sequential secondary endosymbiosis of both a green and red alga (Moustafa et al. 2009), combined with bacterial horizontal gene transfer, resulted in an unprecedented chimaeric genome in diatoms. There are genes derived from their green algal, red algal and original heterotrophic ancestor as well as bacterial genes. This has been exemplified in the diverse ancestry of genes involved in the heme biosynthesis pathway (Oborník and Green 2005) and the five isoenzymes of fructose-bisphosphate aldolases (Allen et al. 2012).

Other surprising traits were revealed when the first two diatom genomes were sequenced (*T. pseudonana* (Armbrust et al. 2004); *Phaeodactylum tricornutum* (Bowler et al. 2008)), including 1) a high amount of transposable elements that appear to self-prime reverse transcription in a novel manner, 2) proteins responsible for a complete urea cycle (previously only found in heterotrophic eukaryotes), 3) proteins possibly involved in C4-like carbon concentrating mechanisms (common in certain land plants), and 4) an unusual polyunsaturated fatty acid metabolism resulting in the storage compound chrysolaminarin. However, still half of the genes of *T. pseudonana* are of unknown function, mainly because there are no homologous proteins in other organisms. For example, the genes encoding for the proteins involved in silicate

polymerization, which is required for frustule synthesis, or plastid envelope transporters (Armbrust et al. 2004) have not been fully identified.

One of the striking surprises though arose from the genomic comparison of the centric (*T. pseudonana*) and the pennate diatom (*P. tricornutum*). Even though diatoms are a relatively young phylum, and pennates diverged from centric diatoms only 90 million years ago, they share only ~60 % of their genes (Bowler et al. 2008). Still puzzling is that many of the genes that are shared between centric and pennate diatoms are often differently regulated, potentially underlining the adaptability to their respective environmental niches (Allen et al. 2011; Hockin et al. 2012; Bender et al. 2014).

1.12 Studying the response to environmental factors in the era of 'OMICS'

Given the important role of diatoms in many processes affecting global biogeochemical cycles, the sequencing of the diatom genomes was awaited with keen anticipation. The first diatom to be sequenced was *T. pseudonana* (Armbrust et al. 2004). Thereafter, the field of diatom sequencing grew exponentially, with the genome of *P. tricornutum* completed in 2008 (Bowler et al. 2008), that of the open ocean *T. oceanica* (CCMP1005) in 2012 (Lommer et al. 2012), those of the two oleaginous diatoms *Fistulifera solaris* and *Cyclotella cryptic* in 2015 and 2016, respectively (Tanaka et al. 2015; Traller et al. 2016), and that of the pennate, cold-water adapted *Fragilariopsis cylindricus* in 2017 (Mock et al. 2017).

Though meaningful information can be retrieved from the genome of an organism, to elucidate cellular adaptations to certain environmental conditions, physiological, proteomic and transcriptomic data are crucial (Parker et al. 2008; Mock et al. 2008). The genome encodes all possible proteins of an organism to survive in an array of environmental conditions. However,

like a colour palette of an artist, not every colour is used for every picture. By subjecting the organism to a certain stress, one can monitor the cellular response (up- or down-regulation of proteins or genes) in comparison to a control. Two widely used approaches include monitoring either the proteomic content, e.g. via high-throughput mass spectrometric analysis (Washburn et al. 2001), or monitoring the genomic expression levels, e.g. via EST libraries (Maheswari et al. 2005) or genomic microarrays (Mock et al. 2008). All of these methods have advantages and disadvantages. For example, proteomic MS data is often biased towards abundant proteins and against membrane proteins (Ong and Mann 2005). Microarray data are highly dependent on the selected microarray and statistical analysis (Baldi and Long 2001).

To date, it is not possible to predict the regulation of all genes in a sequenced genome. For example, a whole-genome expression profiling for *T. pseudonana* generated extensive genomic microarray and EST data, as well as some differential proteomic data (Mock et al. 2008). This study found evidence for ~ 3,500 new genes which had not been predicted by the ~ 11,400 existing gene models originally used in the sequencing of the *T. pseudonana* genome (Armbrust et al. 2004). Of the new genes in Mock et al. (2008), 86% had no blast match, while 64% had EST support (with and without blast matches). Of the original gene models (Armbrust et al. 2004), only 28 % were predicted solely through homology searches, whereas the rest were supported by arrays and/or ESTs.

Studies examining acclimation strategies to metal limitation in diatoms have focussed on Fe limitation, with only two studies investigating physical and chemical parameter interactions, such as iron/light (Smith et al. 2016) or iron/temperature (Zhu et al. 2016b). Studies employed either transcriptomics (Mock et al. 2008; Allen et al. 2008), whole cell proteomics (Lommer et al. 2012; Nunn et al. 2013; Luo et al. 2014) or qRT-PCR of a limited set of genes of interest

(Kustka et al. 2007; Whitney et al. 2011; Chappell et al. 2014). When comparing results, it is imperative to be aware of the kind of Fe limitation that has been imposed, i.e. some studies investigate acute Fe limitation, most likely experienced in coastal areas (e.g. Lommer et al. 2012), whereas others grow acclimated cultures resembling a scenario more prevalent in open ocean environments (e.g. Nunn et al. 2013). Growing phytoplankton cultures with trace metal clean techniques, extracting DNA, RNA, or proteins and subjecting them further to down-stream analysis is a very time-consuming and costly process. Importantly, much more information can be obtained from whole-cell proteomic or transcriptomic data when it is complemented with a substantial and relevant set of whole-cell physiological parameters. Unfortunately, the standard physiological parameters supporting proteomic or transcriptomic data are usually limited to growth rate, F_v/F_m and maybe cell size and Chl*a* concentration, although Lommer et al. (2012) included additional information on chloroplast concentration and protein content. So far, Allen et al. (2008) have provided the most extensive list of physiological parameters (up to 13), including some enzyme essays and estimates of PSII, cytb_6f, and PSI concentration in their study of Fe limitation.

For the present study, we focused on the differential whole-cell proteomic responses of two strains of the open ocean, centric diatom *T. oceanica* (CCMP1003 and 1005), to trace metal limitation. This proteomic data was combined with an unprecedented array of physiological parameters, more than 20, including light response curves, carbon uptake, FRRF measurements of the photosynthetic apparatus, oxygen production, alternative oxidase enzymatic activity, cellular protein content, and the standard growth rate, cell size, and Chl*a* concentration measurements. Furthermore, we generated the first genomic information available for the *T. oceanica* strain CCMP1003, as an extensive EST library. Thus, we mapped our differential

proteomic peptide data to both the publicly available genome of *T. oceanica* (CCMP1005) and to our own transcriptomic data (CCMP1003).

1.13 Thesis objective

In my thesis I have two overarching questions to address: 1) what are the physiological and proteomic adaptations of open ocean diatoms to limiting concentrations of Cu and/or Fe, and 2) what are the differences in these adaptations between the two strains of *T. oceanica*, CCMP1003 and CCMP1005 (i.e. differential intraspecific responses to trace metal limitation)?

In order to answer these questions, I employed an integrative approach that combined measurements of a large number of physiological parameters with the most up-to-date molecular techniques (transcriptomics and proteomics), facilitated by the availability of a draft genome sequence of the *T. oceanica* strain CCMP1005 (Lommer et al. 2012).

In brief, I grew triplicate 10 L acclimated cultures for each of the two strains of *T. oceanica* (CCMP1003, referred to as TO03; and CCMP1005, referred to as TO05) under each of our 4 treatments (i.e. control; Cu-limiting, referred to as lowCu; Fe-limiting conditions, referred to as lowFe, and Fe-Cu co-limiting conditions, referred to as lowFeCu; see overview Figure 1.4). Slower growth rates were used as a proxy for their trace metal limited status. On the day of harvest, when the cultures were still in exponential phase, a part of the culture was used to extract proteins (both from the soluble and insoluble fractions). These protein extracts were the subject of differential proteomic analysis. The rest of the culture was used to investigate *in vivo* and *in vitro* physiological parameters such as cell size, Chl*a* content, rates of gross oxygen production, carbon uptake and electron transport in photosystem II (ETR_{PSII}), as well as photosynthesis *vs.* irradiance (PE) response curves, and activity of alternative oxidases. Having

concomitant proteomic and physiological data from the same cultures allowed me to draw conclusions regarding proteomic changes responsible for physiological adaptations to trace metal limitation. To this end, I was able to describe in detail very different adaptations by the two strains in response to low Cu. Furthermore, by comparing these different metal limitations (lowCu, lowFe, and lowFeCu), I was able to draw conclusions on physiological and proteomic responses to general cellular stress, versus those specific to trace metal limitation. My work furthers our knowledge on how diatoms adapt to metal limitation and opens up new avenues for future research.

1.14 Thesis structure

The physiological and proteomic datasets that I generated and analyzed for Chapters 3, 4, and 5 were derived through the same methodological approach, which I describe in the Method Chapter (Chapter 2). The importance of Fe limitation in controlling global primary productivity and therefore climate has been known for decades. Many phytoplankton adaptations to Fe limitation have been described using physiological, transcriptomic and proteomic approaches. However, the physiological interaction between Cu and Fe in open ocean diatoms, although known for about 10 years, has not received much attention. As little is known about Cu as a limiting nutrient and how marine phytoplankton respond to low Cu availability, I dedicated two chapters of my thesis to an in-depth description of the effects of low Cu on the photosynthetic apparatus (Chapter 3) and on the enzymes involved in the nitrogen, carbon, and oxidative stress metabolism (Chapter 4). In Chapter 5, I compare the effects of Cu and Fe limitation with each other and with co-limitation by both Cu and Fe on the photosynthetic apparatus. The challenges

of my research, the implications of my findings, as well as my outlook on future research are discussed in Chapter 6.

1.15 Tables and figures

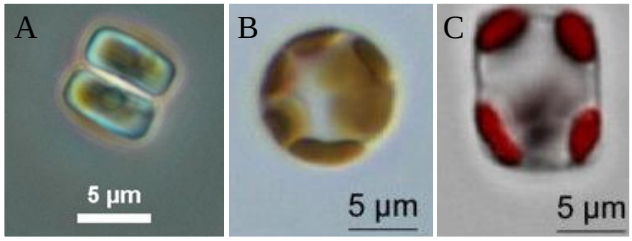

Figure 1.1: Light microscopy images of *Thalassiosira oceanica* (CCMP 1003 and CCMP 1005). A) CCMP 1003 in side (girdle) view (A. Hippmann); B) CCMP 1005 in top (valve) view; C) CCMP 1005 from side (girdle) view (Lommer et al. 2012). B and C from **(Lommer et al. 2012)**. Note that the chloroplasts are in their native brownish colour in A and B, and in red colour in C, from overlay of chlorophyll autofluorescence**.**

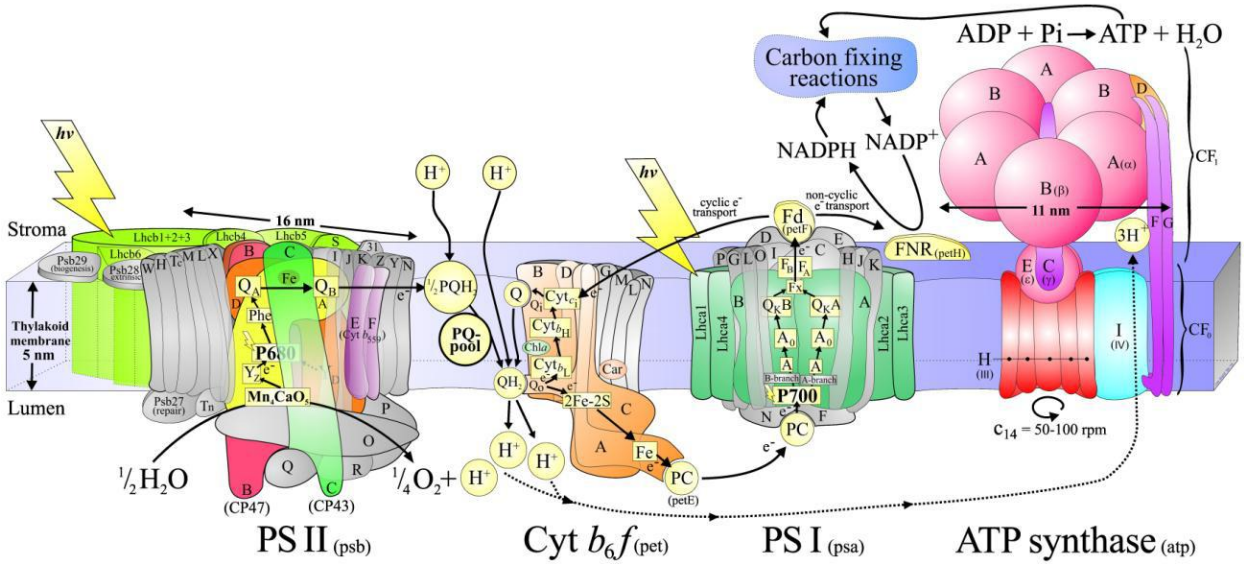

Figure 1.2: Schematic overview of the photosynthetic electron transport chain (ETC) in the chloroplast thylakoid membrane. Light energy is absorbed by light-harvesting complexes (LHCs) in the antenna and then channelled towards the reaction centres, PSII and PSI, respectively, where charge separation occurs and electrons are channelled through the electron transport chain (ETC) from PSII via plastoquinone (PQ Pool), cytochromeb_6f (cytb_6f) and plastocyanin (PC) to PSI, where electrons are used to reduce first ferredoxin (Fdx) and subsequently via ferredoxin:NADP+ reductase (FNR) $NADP^+$ to NAD(P)H. The electrons are replenished via the splitting of water (at PSII) into oxygen, electrons and H^+. Throughout the ETC, protons are pumped into the thylakoid lumen, thereby creating a proton gradient that is used to synthesise ATP. Figure used with permission from Dr Jon Nield, Queen Margaret University of London (for further information on all subunits see http://macromol.sbcs.qmul.ac.uk/).

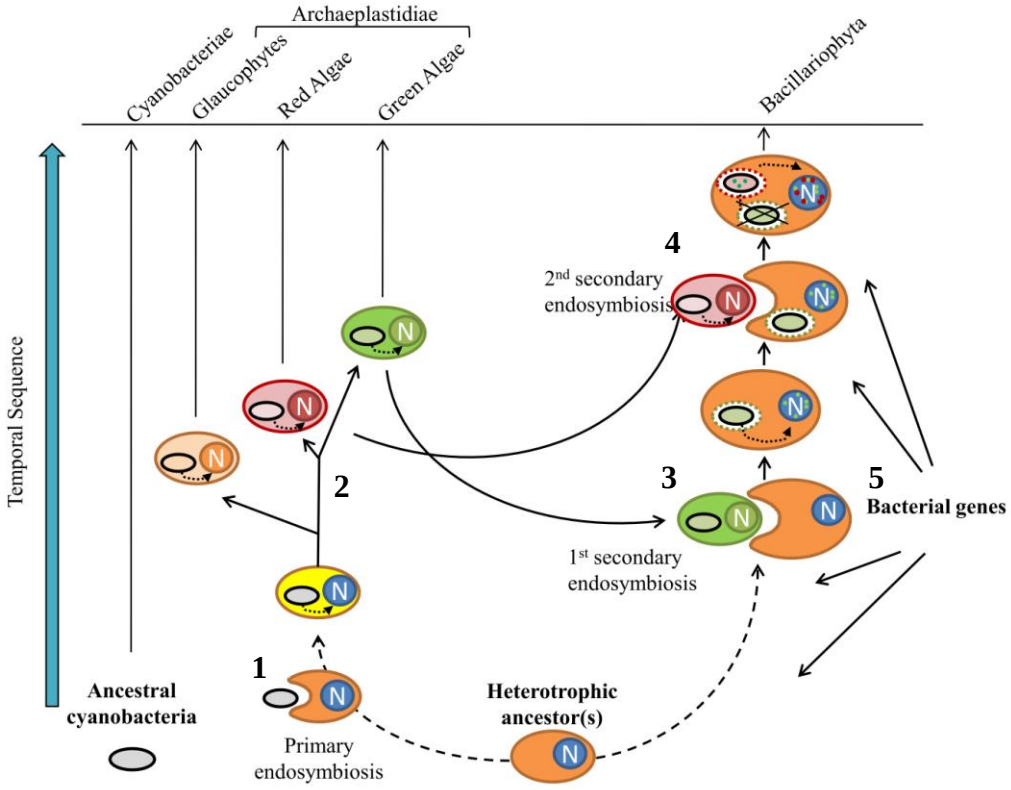

Figure 1.3 Schematic overview of the phylogenetic ancestry of diatoms. 1) in the primary endosymbiosis event an ancient cyanobacterium is engulfed by a heterotrophic eukaryote. **2)** three main algae lineages develop from this primary endosymbiosis; glaucophytes, red, and green algae. **3)** in a 1st secondary endosymbiosis, a green alga is engulfed by a heterotrophic eukaryote. Gene transfer occurs from the green algal nucleus and green algal chloroplast genome into the host nucleus. **4)** in a 2nd secondary endosymbiosis, the same organism from 3) engulfs a red alga. Subsequent gene transfer from the red algal nucleus and red algal chloroplast to the host nucleus and between the green and red algal chloroplasts takes place. Eventually, all remnants from the green algal cell including the plastid are lost. 5) throughout diatom history, bacterial gene transfers have occurred (based on Finazzi et al. 2010).

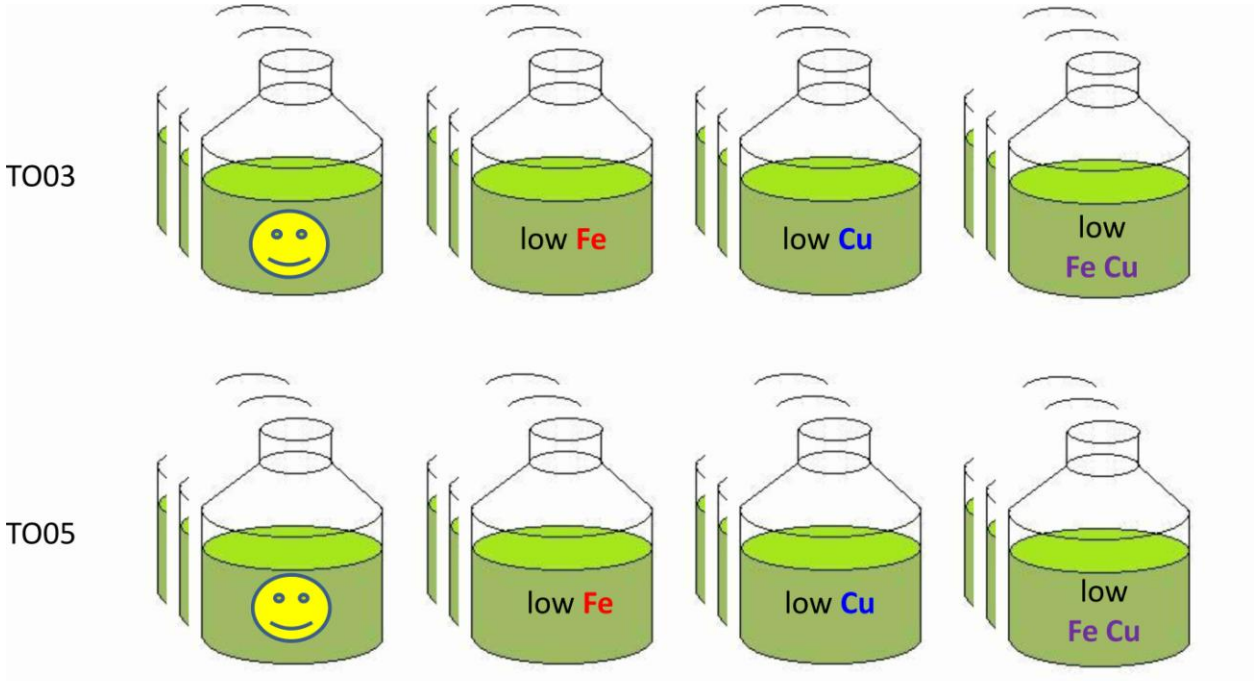
TO03
low Fe
low Cu
low
Fe Cu
TO05
low Fe
low Cu
low
Fe Cu

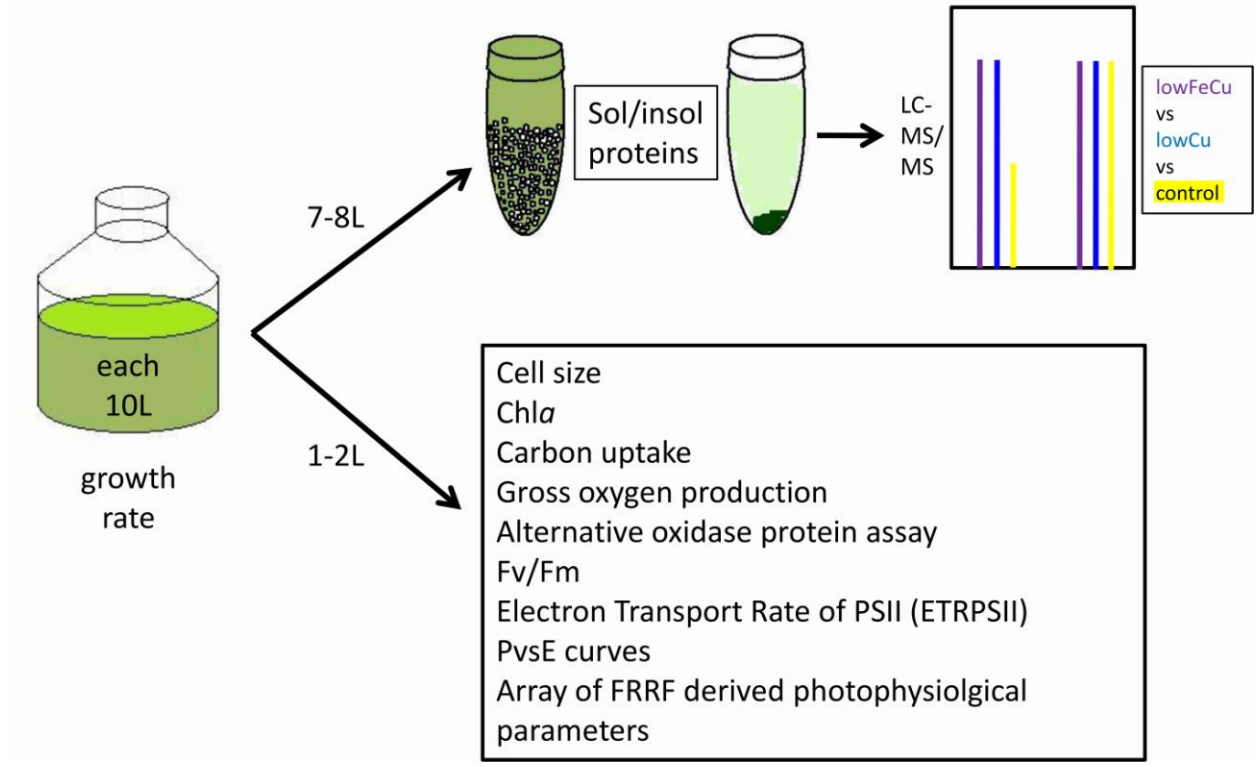
each
10L
growth
rate
7-8L
1-2L
Sol/insol
proteins
LC-
MS/
MS
lowFeCu
vs
lowCu
vs
control
Cell size
Chl*a*
Carbon uptake
Gross oxygen production
Alternative oxidase protein assay
Fv/Fm
Electron Transport Rate of PSII (ETRPSII)
PvsE curves
Array of FRRF derived photophysiolgical
parameters

Figure 1.4 Overview of experimental set-up. Triplicate 10 L cultures were grown in 4 different trace metal regimes (control, replete trace metal conditions; Fe-limiting conditions, lowFe; Cu-limiting conditions, lowCu; and Fe-Cu co-limiting conditions, lowFeCu) for 2 strains of *T. oceanica* (CCMP1003, TO03; and CCMP1005, TO05). While still in exponential growth phase, each 10 L culture was divided into 7-8 L for differential proteomic analysis and 1-2 L for the determination of an array of *in vivo* and *in vitro* physiological parameters. For a more in-depth description of the stable-isotope labeling used for our differential proteomics, please see (Chapter 2, Figure 2.1).

Chapter 2: Methods

2.1 General

Experimental set-up and analysis for all three data chapters were identical. Different subsets of the data are discussed in each data chapter, with some overlap in Chapters 3 and 5 (i.e. the low Cu photosynthetic protein response).

2.1.1 Study organism

Two strains of the centric diatom species *Thalassiosira oceanica* were used in this investigation, CCMP 1003 and CCMP 1005. Species and strain were confirmed based on the ITS region sequence (encompassing the ITS1–5.8S – ITS2, (Moniz and Kaczmarska 2009, 2010); Figure A.2). All isolates were obtained from the Provasoli-Guillard Center for Culture of Marine Phytoplankton, now National Centre for Marine Algae and Biota (NCMA) at Bigelow Laboratory for Ocean Sciences.

2.1.2 ITS region

For DNA extraction, the DNeasy® Plant Mini Kit (cat. nos. 69104 and 69106) from QIAGEN was used following its manual with one modification: cells from 40 mL of late exponential culture were concentrated via centrifugation, then mixed with 400 µL AP buffer, 2 µL RNase and 100 µL 0.2-0.5mm silica microbeads. The microbeads increase the DNA yield by breaking open the silica frustules. The 700bp long ITS fragment, comprised of ITS1, 5.8S rDNA gene and part of ITS2, as described by Moniz and Kaszmarska (Moniz and Kaczmarska 2009), was amplified using primers ITS1 and ITS5 and a PCR reaction mix as described by White et al.

(White et al. 1990) with an amplification regime as per Amato et al. (Amato et al. 2007). PCR products were visualized on a 1.5% agarose gel (Figure A.1). For PCR product cleanup, Promega Wizard ® SV Gel and PCR Clean-Up System (#A9282) was used. Sequencing was conducted by Genewiz© (Seattle, USA), following their standard procedure. The resulting sequences were aligned with other published *Thalassiosira* ITS regions using the multiple sequence alignment algorithm MAFFT (Katoh and Standley 2013, 2016) to create a phylogenetic tree (see 2.5.2).

2.1.3 Culture media and growth conditions

Cultures were grown in the artificial seawater medium Aquil (Price et al. 1988), which consists of a salt mixture (synthetic ocean water, SOW) at pH 8.2, enriched with standard additions of nitrate (300 µmol L^{-1} NO_3^-), phosphate (10 µmol L^{-1} PO_4^{3-}), and silicic acid (100 µmol L^{-1} SiO_3^{2-}), as well as vitamins. The trace elements Mn, Zn, Co, Mo, and Se were added bound to EDTA to attain a final EDTA concentration of 100 µmol L^{-1} in the growth medium (Maldonado and Price 1996). Iron and Cu were added separately as a premixed FeEDTA or CuEDTA complex (1:1.05) (for an overview of the Fe and Cu concentrations used in our media, see Table 2.1). Iron was added at a total concentration of 1.37 µmol L^{-1} (pFe 19) (speciation calculated using MINEQL) (Westall et al. 1976). Copper was added to give total concentrations of 10.2 nmol L^{-1} (pCu 14) and 14.32 nmol L^{-1} (pCu 13.5) in the Cu-sufficient media for TO03 and TO05, respectively. Copper-limited media had just background Cu contamination for TO03 and was enriched with 6.08 nmol L^{-1} for TO05. For the Fe- and Fe-Cu limiting media, Fe was added at a total concentration of 12.5 nmol L^{-1} (pFe 20.5) for both strains. In the Fe-Cu co-limiting media, Cu, however, was added at a total concentration of 1.96 nmol L^{-1} (pCu 15) for TO03 and 6.08 nmol L^{-1} (pCu 14.5) for TO05. Background Cu contamination in the media was <1 nmol L^{-1}

and was determined in parallel medium preparations by chemiluminescence detection using a flow injection analysis system (Zamzow et al. 1998; Semeniuk 2014)**.** Sterile, trace metal-clean techniques were used during all manipulations, and the metal-EDTA reactions in the media were allowed to equilibrate overnight.

2.2 Whole cell physiology

2.2.1 Growth measurements

Both strains were cultured in 28 mL acid-cleaned polycarbonate tubes at 19 ±1°C in continuous light (ca. 155 µmol quanta m^{-2} s^{-1}). Growth was monitored by daily measurements of in vivo Chl*a* fluorescence using a Turner10-AU Fluorometer, and cultures were kept in exponential growth phase using semi-continuous batch culturing (Brand et al. 1983). The cultures were considered acclimated when growth rates during approximately 40 cell divisions (five successive transfers), varied by <15% (Brand et al. 1983). Acclimated, exponentially growing cells were used to inoculate triplicate 10 L cultures grown in polycarbonate carboys with gentle stirring. Growth in the 10 L cultures was determined by monitoring cell density with a Coulter Counter (model Z2). During early to mid-exponential phase, each biological replicate culture was sampled in duplicate for Chl*a* concentration, total cellular protein, oxygen evolution, Fe uptake, ^{14}C uptake, ^{14}C light response (P*vs*E, PE) curves, electron transport rate in the reaction centre of PSII (ETR_{RCII}) -PE curves and other FRRF derived parameters, as described below. The remainder of the culture (7 – 8 L) was used for differential proteomic analyses. Sterile, trace metal clean techniques were used at all times.

2.2.2 Chla measurements

Duplicate 10 mL subsamples of the 10 L cultures were filtered onto a 25 mm glass fibre filter (GF/F, pore size 3 µm), flash-frozen in liquid N_2 and stored at -20°C until analysis. Chlorophyll was extracted overnight in 8 mL ice-cold 90% acetone and the Chl*a* concentration was determined fluorometrically following the method of Arar and Collins (Arar and Collins 1997).

2.2.3 Cellular protein concentration

Cellular protein concentration was measured following a method adapted from Lommer et al. (2012). Briefly, 1.5 x 10^6 cells were concentrated by filtering 10-20 mL of culture onto a 25 mm, 3 µm pore-sized polycarbonate (PC) filter. Filters were flash frozen in liquid N_2 and stored at -80°C until analysis. For protein determination, cells were resuspended and lysed in 250 µL SDS/CO_3 buffer [4% w/v SDS, 68mM Na_2CO_3, Halt™ protease inhibitor cocktail (Thermo Fisher Scientific, Waltham, MA, USA, #78430)] with application of ultrasonication. Cell debris was pelleted via centrifugation at 16,000 x g, at room temperature, for 4 min; protein concentration was determined with technical duplicates for each of the three biological replicates, using 50 µl of the supernatant in a bicinchoninic acid (BCA) protein assay (Thermo Fisher Scientific, Waltham, MA, USA, # 23227).

2.2.4 Oxygen evolution, respiration and alternative oxidase (AOX) assay

Oxygen evolution was measured using a Clark-type oxygen electrode (Hansatech). Before each experiment, the electrode was calibrated with sterile SOW bubbled with filtered compressed air or N_2 gas for O_2 saturated and O_2 zero standard, respectively. Cells were concentrated 15-fold via gentle filtration onto a 3 µm pore-sized PC filter, resuspended in fresh media, and duplicate

subsamples from each biological replicate were introduced to the sample chamber. Samples were briefly bubbled with N_2 before illumination at growth irradiance while O_2 evolution was recorded. Subsequently, samples were exposed to complete darkness, in order to record the rate of respiration. Rates of oxygen evolution and respiration were derived from the slope of the linear increase and decrease of dissolved dioxygen (O_2) over time. The raw data were analyzed using the software Oxypeak supplied by the manufacturer.

Alternative oxidase (AOX) is an enzyme that can oxidize NADH to NAD^+ instead of the usual cytochrome *c* oxidase (COX) in the mitochondrial respiratory electron transport chain. Both enzymes transfer electrons to oxygen, thereby producing H_2O. However, in contrast to COX, AOX does not contribute to the proton gradient, thus it does not increase ATP production. However, AOX has been shown to be wildly used in both plants and some phytoplankton species to counteract an overreduction of the mitochondrial electron transport chain (Eriksen and Lewitus 1999; Allen et al. 2008; Zhang et al. 2012).

In order to test the activity of AOX *vs* COX, two inhibitors were used. After 30-60 sec of recording the rate of respiration, in one subsample, the AOX inhibitor SHAM (salicylhydroxamic acid) was added into the sample chamber at a final concentration of 0.1 mM. The resulting change in respiration rate was due to the decrease in AOX activity. Accordingly, in the second subsample, the COX inhibitor Antimycin A was added at a final concentration of 1 mM. Here, the change in respiration rate was due to the decrease in COX activity.

2.2.5 Chl*a* fluorescence parameters and ETR_{RCII} using Fast Repetition Rate fluorometry (FRRf)

A bench-top FRRf instrument (Soliense Inc.) was used for all active chlorophyll fluorescence (ChlF) measurements as described in detail in Schuback et al. (Schuback et al. 2015). Briefly, a single turnover (ST) protocol was designed and used to derive the ChlF yields F_o and F_m in the dark-regulated state, as well as F' and F_m' in the light-regulated state while subjected to 10 'background' irradiances ranging from 0 to 1,000 µmol quanta m^{-2} s^{-1}. F_o' was calculated as $F_o' = F_o/ (F_v/F_m + F_o/F_m')$ (Oxborough and Baker 1997). The five ChlF yields, F_o, F_m, F', F_m' and F_o' were used to calculate ChlF parameters following Kitajima and Butler (1975), as described in detail in Schuback et al. (2015).

For the dark-regulated state, we derived the commonly used F_v/F_m ratio as $F_v/F_m = (F_m-F_o) / F_m$ (Kolber and Falkowski 1993). Furthermore, for each 'background' light level we derived: (1) The photochemical quenching of variable fluorescence, $Fq'/Fv' = (Fm'-F') / (Fm'-Fo')$, which quantifies the fraction of functional RCII in the open state (i.e. primary quinone acceptor Q_A in the oxidized state); (2) The maximum quantum yield of PSII photochemistry, $Fv'/Fm' = (Fm'-Fo') / Fm'$, which can be used to quantify the extent to which photochemistry in PSII is limited by competition with thermal decay of excitation energy (Oxborough and Baker 1997); (3) The overall quantum efficiency of photochemical energy conversion in PSII at a given light intensity $Fq'/Fm' = (Fm'-F') / Fm' = \Phi_{PSII}'$ (the product of Fq'/Fv' and Fv'/Fm'). The functional absorption cross section of PSII, σ_{PSII} ($Å^2$ $RCII^{-1}$), was derived from the rate of closure of RCII in the dark-regulated and at each light-regulated state (Kolber and Falkowski 1993; Kolber et al. 1998). Rates of charge separation (ETR_{RCII}) in functional RCII (mol e^- mol $RCII^{-1}$ s^{-1}) were estimated as the product of incident irradiance (E, µmol quanta m^{-2} s^{-1}), the

fraction of irradiance absorbed by PSII ($\sigma_{PSII,}$ $Å^2$ $RCII^{-1}$) and the efficiency with which charge separation occurs in RCII (Fq′/Fv′):

$$ETR_{RCII} = E \times \sigma_{PSII}' \times Fq'/\mathrm{Fv}' \times 6.022 \times 10^{-3} \quad (1)$$

The number 6.022 x 10^{-3} converts μmol quanta to quanta, $Å^2$ to m^2, and RC to mol RC.

Non-photochemical quenching (NPQ) at each light level was estimated as the normalized Stern-Volmer quenching coefficient, defined as $NPQ_{NSV} = (F_m'/F_v') - 1 = F_o'/F_v'$ (McKew et al. 2013; Schuback et al. 2015, 2016).

2.2.6 ^{14}C carbon assimilation

Light response curves (photosynthesis, P *vs.* irradiance, E: PE curves) for C fixation were generated by measuring rates of carbon assimilation at various light intensities as described in Schuback et al. (2015), using a custom built photosynthetron (Lewis and Smith 1983). A photosynthetron is a temperature controlled apparatus in which small aliquots of the same culture are subjected to different light intensities simultaneously. Briefly, on the day of harvest, an 80 mL subsample of exponentially growing culture was spiked with 40 μCi $NaH^{14}CO_3$ and 3 mL aliquots were incubated in glass vials in the photosynthetron for 60 minutes. Each subsample was subjected to a different light intensity provided by high power light emitting diodes (LEDs) located under each glass vial. Each PE curve consisted of 11 light levels spanning intensities from 2 to 700 μmol quanta m^{-2} s^{-1}. Actual light intensities were measured before and after each

experiment using a 4π quantum sensor (QSL-2100, Biospherical Instruments) immersed in water inside a scintillation vial. The temperature was kept within 1°C of growth temperature by circulating water from a water-bath through an aluminium cooling jacket. Duplicate curves were measured for each sample. The incubation was terminated by adding 1 mL of 1 M HCl to each vial. The samples were then completely dried, and subsequently re-suspended in 1 mL MilliQ water.

2.2.7 PE curves

Measurements of CO_2-assimilation and ETR_{RCII} were plotted against irradiance, and the model of Jassby and Platt (1976) was fit to the data using the 'phytotool' package (Silsbe and Malkin 2015) in R and RStudio (R Core Team 2013; RStudio Team 2015). For both rates of productivity, we derived the light utilization efficiency α [ETR_α = (mol e^- $RCII^-$) / (µmol quanta $m^{-2}s^{-1}$); $^{14}C_\alpha$ = (g C g Chl*a*$^{-1}$ h^{-1}) / (µmol quanta m^{-2} s^{-1})], the light-saturated maximum rate P_{max} (ETR_{Pmax} = mol e^- $RCII^-$; $^{14}C_{Pmax}$ = g C g Chl*a*$^{-1}$ h^{-1}), and the light saturation point E_k (µmol quanta m^{-2} s^{-1}). When photoinhibition was observed at high irradiances, the data points were excluded from the fitting procedure.

2.2.8 Derivation of conversion factor

Because we derived ETR_{RCII} in units of mol e^- mol $RCII^{-1}$ s^{-1} and CO_2-assimilation in units of mol C mol Chl*a*$^{-1}$ s^{-1}, the conversion factor between the two rates accounts for changes in Chl*a* functionally associated with each RCII ($1/n_{PSII}$, mol Chl*a* mol $RCII^{-1}$) and the number of charge separations in RCII needed per CO_2-assimilated into organic carbon products ($\Phi_{e:C}$, mol e^- mol C^{-1}).

$$\frac{\mathrm{ETR_{RCII}}\ (\mathrm{mol\ e^-\ mol\ RC^{-1}s^{-1}})}{\mathrm{CO_2\ assimilation}\ \ (\mathrm{mol\ C\ mol\ Chl}\ a^{-1}\mathrm{s^{-1}})} = \Phi_{\mathrm{e:C}}\left(\frac{\mathrm{mol\ e^-}}{\mathrm{mol\ C}}\right) \times \frac{1}{\mathrm{n_{PSII}}}\left(\frac{\mathrm{mol\ Chl}\ a}{\mathrm{mol\ RCII}}\right)$$

(2)

In this approach, we attribute the observed decoupling between ETR_{RCII} and CO_2-assimilation to changes in both $1/n_{PSII}$ and $\Phi_{e:C}$.

2.2.9 Statistical analysis of physiological experiments

Statistical analysis to test for significant and interacting effects was done on the complete dataset, even for Chapters 3 and 4 where only lowCu *vs.* control was discussed. This is to decrease the number of false positives that would ensue when examining each of the three treatment pairs separately (ctrl *vs.* low Cu, ctrl *vs.* low Fe, ctrl *vs.* low FeCu). The three main factors included in the linear model were: 1) Strain (TO03 *vs.* TO05), 2) Fe level (high *vs.* low), and 3) Cu level (high *vs.* low). We used the phia package (De Rosario-Martinez 2015) in R and RStudio (R Core Team 2013; RStudio Team 2015) to fit the linear model (including all three main effects) as well as for the post-hoc analysis of interactions (phia) in the factorial ANOVA. To focus the analysis on the low Cu data presented in Chapters 3 and 4, we then tested simple main effects for interactions, which consisted of evaluating contrasts across the levels of one factor, while the values of the other interaction factors were fixed at certain levels. For example, to test if the low Cu response in TO03 is significantly different from the control treatment, we set the fixed factors "Strain" = TO03, and "Fe level" = high. The variable factor to be tested would be "Cu level" (high *vs.* low). To test for differences between strains under low Cu, the factors of variable "Strain" (contrasts of TO03 *vs.* TO05) would be evaluated with fixed "Fe level" = high and "Cu level" = low.

2.3 Transcriptomics

2.3.1 RNA-Seq library preparation

Total RNA was purified from cell pellets using the Trizol reagent (Life Technologies; Carlsbad, CA), treated with DNase (Qiagen, Valencia, CA, USA), and cleaned with the RNeasy MinElute Kit (Qiagen, Valencia, CA, USA). RNA-Seq libraries were constructed with TruSeq RNA Sample Preparation Kits (Illumina; San Diego, CA). 0.8 µg of total RNA was used as input followed by the manufacturer's TruSeq RNA Sample Preparation Low Throughput protocol. A high sensitivity DNA Assay chip was used to assess quality (Agilent; Santa Clara, CA, USA). The mean sizes of the libraries were around 430-480bp.

2.3.2 RNA-Seq data analysis

Transcriptomes were sequenced on the Illumina HiSeq. Reads were trimmed of primer sequences, and rRNA sequences removed using Ribopicker v.0.4.3 (Schmieder et al. 2012). Contigs were assembled *de novo* using CLC Assembly Cell (CLC Assembly Cell, Quiagen Bioinformatics; http://www.clcbio.com, version 3. 22.55708, accessed 2013). Putative open reading frames on the assembled contigs were called using FragGeneScan (Rho et al. 2010). Predicted protein sequences were annotated by hidden Markov models for Pfam and TIGRfam, and by Blastp against PhyloDB 1.06 with an E-value threshold of $1e^{-3}$. PhyloDB is a comprehensive in-house database at JCVI consisting of proteins from many public sequence databases, including KEGG (Kanehisa et al. 2012), Pfam (Punta et al. 2012), GenBank (Benson et al. 2013), Ensembl (Flicek et al. 2011) and several in-house assemblies of algal uniculture transcriptomic sequences. The database PhyloDB is available for download at the following

website: https://scripps. ucsd. edu/labs/aallen/data/ (accessed 2017). The RNA-seq data reported here have been deposited in the NCBI sequence read archive (https://www.ncbi.nlm.nih.gov/sra/; BioProject accession no. PRJNA382002; BioSample accession nos. SAMN06698917-SAMN06698931, accessed 2017).

2.3.3 T. oceanica strain comparison

Filtered transcriptome reads from TO03 (CCMP1003) were mapped to the following sources: predicted ORFs resulting from the *de novo* assembly of TO03, assembled contigs of the publicly available TO05 genome (CCMP 1005, https://www.ncbi.nlm. nih.gov/bioproject/PRJNA36595, downloaded 12/1/2015), nuclear genes of TO05, and chloroplast genes of TO05. Read mapping was performed using BWA MEM (Li 2013) with default parameters. Mapped reads from each sample were counted and reads per kilobase of transcript per million mapped reads (RPKM) values were calculated for all genes.

2.4 Proteomics

2.4.1 Protein purification

From the 10 L triplicate cultures, 7 – 8 L in early to mid-exponential growth phase were harvested via gentle filtration onto 47 mm, 3 µm pore-sized PC filters. Depending on cell density and culture treatment, filters clogged after varying amounts of culture volume and had to be replaced. Cells washed from all filters were combined and resuspended in 10 mL ice-cold SOW and concentrated via centrifugation at 2,500 x g for 10 min. The pellet was resuspended in 2 mL ice-cold SOW and spun at 13,000 x g for 2 min. The resulting cell pellet was flash frozen in liquid N_2 and stored at -80ºC until final processing. During protein extraction, all samples and

buffers were kept on ice. To disrupt the cells, approximately 0.8 g of glass beads (212 - 300 µm diameter, Sigma, #G1277-100g) were added to the cell pellet in the Eppendorf tube, as well as ~ 1.5 mL lysis buffer (0.05 M Hepes, 0.02 M KCl, 0.001 M EDTA, 0.0002 M DTT, 0.15 sorbitol plus freshly added Protease Inhibitor, one Roche® Tablet per 50 mL lysis buffer). Complete cell lysis was achieved with three 1 min vortexing intervals, interrupted by 1 min cooling periods on ice. The samples were then settled by 10 seconds centrifugation in a tabletop centrifuge and the supernatant was transferred to a new 2 mL Eppendorf tube. The remaining cell debris and beads were repeatedly washed with lysis buffer and the supernatants were combined until the wash steps resulted in an almost clear supernatant (approximately 5-10 times). To pellet any potentially contaminating cell debris or beads, the combined supernatant was centrifuged at 2,500 x g, at 4ºC, for 15 min. The resulting supernatant was transferred to 12 mL ultracentrifuge tubes. Soluble and insoluble protein fractions were separated by ultracentrifugation at 100,000 x g, at 4ºC, for 1 h.

2.4.2 Protein preparation for mass spectrometry

Proteins were reduced with dithiothreitol (1:50 ratio of dithiothreitol: protein), alkylated using iodoacetamide (1:10 ratio of iodoacetamide:protein) and Trypsin digested (1:50 ratio of enzyme: protein) as described in Foster et al. (2003). Digested peptides were purified and concentrated on C18 STAGE-tips (Rappsilber et al. 2003) and eluted in 80% acetonitrile, 0.5% acetic acid, and dried in a vacuum concentrator (Eppendorf). Dried peptides were resuspended in 100 mM triethylammonium bicarbonate and labelled via chemical dimethylation using light (CH_2O, for control treatment), medium (CD_2O, for low Cu treatment), and heavy ($^{13}CD_2O$ for low FeCu treatment) isotopologues of formaldehyde as described previously (Boersema et al. 2009).

Labeled samples were finally combined together in equal amounts for STAGE-tip purification and subsequently eluted in 80% acetonitrile, 0.5 % acetic acid. Eluted samples were dried and resuspended in 0.5% acetic acid for the TO03 set and 1% TFA for the TO05 set (Boersema et al. 2009) (Figure 2.1).

2.4.3 Liquid chromatography-tandem mass spectrometry – LC-MS/MS

TO03's purified peptides were analyzed on the linear-trapping quadrupole-Orbitrap mass spectrometer (LTQ-Orbitrap Velos; ThermoFisher Scientific) on-line coupled to an Agilent 1290 Series HPLC using a nanospray ionization source (ThermoFisher Scientific) including a 2 cm long, 100 μm-inner diameter fused silica trap column, 50 μm-inner diameter fused silica fritted analytical column and a 20 μm-inner diameter fused silica gold coated spray tip (6 μm-diameter opening, pulled on a P-2000 laser puller from Sutter Instruments, coated on Leica EM SCD005 Super Cool Sputtering Device). The trap column was packed with 5 μm-diameter Aqua C-18 beads (Phenomenex, www.phenomenex.com, accessed 2015) while the analytical column was packed with 3 μm-diameter Reprosil-Pur C-18-AQ beads (Dr Maisch, www.Dr-Maisch.com, accessed 2015). Buffer A consisted of 0.5% aqueous acetic acid, and buffer B consisted of 0.5% acetic acid and 80% acetonitrile in water. Samples were run on a gradient method where buffer B was from 10% to 25% over 120 min, from 25% to 60% over 20 min, from 60% to 100% B over 7 min, kept at 100% for 2.5 min and then the column was reconditioned for 20 min with buffer A. The HPLC system included Agilent 1290 series Pump and Autosampler with Thermostat set at 6°C. The sample was loaded onto the trap column at 5 μL min^{-1} and the analysis was performed at 0.1 μL min^{-1}. The LTQ-Orbitrap was set to acquire a full-range scan at 60,000 resolution from 350 to 1600 Th in the Orbitrap to simultaneously fragment the top fifteen peptide

ions by CID in each cycle in the LTQ (minimum intensity 200 counts). Parent ions were then excluded from MS/MS for the next 30 sec. Singly charged ions were excluded since in ESI mode peptides usually carry multiple charges. The Orbitrap was continuously recalibrated using the lock-mass function. The mass error measurement was typically within 5 ppm and was not allowed to exceed 10 ppm.

TO05's purified peptides were analyzed using a quadrupole – time of flight mass spectrometer (Impact II; Bruker Daltonics) on-line coupled to an Easy nano LC 1000 HPLC (ThermoFisher Scientific) using a Captive nanospray ionization source (Bruker Daltonics) including a column setup identical to that for TO03. Buffer A consisted of 0.1% aqueous formic acid, and buffer B consisted of 0.1% formic acid and 80% acetonitrile in water. Samples were run on a gradient method where buffer B was from 5% to 20% over 45 min, from 20% to 40% over 45 min then to 100% over 2 min, held at 100% for 15 min. Re-equilibration back to 5% buffer B was done separately by the LC automatically. The LC thermostat temperature was set at 7°C. The sample was loaded onto the trap column at 800 Bar and the analysis was performed at 0.25 μL min^{-1}. The Impact II was set to acquire in a data-dependent auto-MS/MS mode fragmenting the 17 most abundant ions (one at the time) after each full-range scan from m/z 200 Th to m/z 2000 Th. The isolation window for MS/MS was 2 to 3 Th depending on parent ion mass to charge ratio. Parent ions were then excluded from MS/MS for the next 0.4 min. Singly charged ions were excluded since in ESI mode peptides usually carry multiple charges. The error of mass measurement was typically within 5 ppm and was not allowed to exceed 10 ppm.

2.4.4 Analysis of mass spectrometry data

Analysis of mass spectrometry data was performed using MaxQuant 1.5.1.0. Originally, the search was performed against a database comprised of the protein sequences from the source organism (TO05, publicly available) plus common contaminants using the default MaxQuant parameters with match between run and re-quantification options turned on. Only those peptides exceeding the individually calculated 99% confidence limit (as opposed to the average limit for the whole experiment) were considered as accurately identified. Another search was performed with identical search parameters but against a larger database that combined protein sequences from both the TO05 genome and our own TO03 transcriptome (predicted proteins on assembled EST contigs). If not noted otherwise, differential expression data is given from the original search. Tables that include both differential expression data from the original and the EST mapped search are found in the respective supplementary tables. The mass spectrometry proteomics data have been deposited to the ProteomeXchange Consortium via the PRIDE (Vizcaíno et al. 2016) partner repository with the dataset identifier PXD006237.

2.4.5 Statistical analysis of proteomic differential expression

As described above (Protein preparation for mass spectrometry), peptides were labelled with different isotopologues of formaldehyde depending on their growth regime (i.e. control, lowCu, lowFeCu). Once the peptides of the three treatments were labelled, they were mixed together in a 1:1:1 ratio and analyzed by LC-MS/MS. The differential expression of proteins is then derived from the ratio of the intensities (area under the curve) of the light, medium and heavy peaks for each peptide (for a schematic of the method see Figure 2.1).

For the published manuscript (Hippmann et al. 2017), we set the criteria to determine statistical significance in the differential expression of a protein as: 1) an observed differential expression ratio in at least two of the three biological replicates (see Figure 2.2 legend for details); 2) an average of the ratios > ±2-fold for significantly up- and down-regulated proteins; and 3) a *p*-value of <0.05 ($p<0.05$) for the z.test, determining significant difference of the average ratios between treatments, taking the variance into account. Additionally, any protein that had a ratio of >10 (up-regulated) or <0.1 (down-regulated) in at least one biological replicate was also considered to be an all-or-nothing response and was included in the 'significantly changed' set. For Chapters 4 and 5, we also included in the 'significantly changed' set, proteins that were more moderately regulated with average ratios between ±1.3- to 2-fold, as long as they fulfilled the other criteria (i.e. the protein was detected in at least two of the three biological replicates and $p<0.05$).

Separating the proteins into soluble and insoluble fractions has both advantages (e.g. deeper probing of the proteome), and disadvantages (e.g. more complex results when differential expression values are in disagreement between the two fractions). The expression values of the soluble and insoluble proteins are given in the respective tables. However, for the interpretation of the results, only one of them was discussed. For many proteins, the dominant cellular fraction (e.g. soluble or insoluble) where the protein should be found is known; in this case, the respective value is used. Some proteins, however, are loosely associated with the membrane and thus are more likely than others to be detected in both the soluble and insoluble fractions. For these, the following strategy was used: 1) if one is not significantly regulated and the other one is significantly regulated, the significant value is discussed; 2) if both are diametrically, but

significantly regulated, the one in the most likely fraction was discussed. For example, the usually membrane-bound LHC, THAOC_05777 (a TpFCP10 homolog) had a -2.24-fold change in the soluble fraction and +2.28 in the insoluble fraction, therefore, I discussed the +2.28-fold change observed in the insoluble fraction (Table 5.2), but data for both fractions was reported in the summary table (Table C.5).

2.4.6 Protein annotation

Predicted proteins from both the publicly available genome of TO05 (CCMP 1005) and our transcriptome of TO03 (CCMP 1003) were searched against the JCVI in-house curated database PhyloDB for functional annotation using BlastP. To determine gene localization for proteins involved in photosynthesis, three strategies were followed: 1) sequences of candidate genes were compared to the publicly available chloroplast genomes of *T. oceanica* (CCMP 1005) (Lommer et al. 2010) and *T. pseudonana* (Armbrust et al. 2004; Oudot-Le Secq et al. 2007), 2) the diatom-specific chloroplast targeting sequence software ASAFind (Gruber et al. 2015) was used in conjunction with SignalP (Petersen et al. 2011) to find nuclear encoded, chloroplast targeted proteins, and 3) the remaining proteins were blasted against NCBI to find the closest homologs.

2.5 Phylogenetic trees

2.5.1 Light harvesting complex (LHC)

Blasting of the publicly available genome of TO05 against the JCVI in-house curated database PhyloDB resulted in 68 predicted proteins containing Chl*a* binding sites typical for family members. Alignment with other known heterokont LHCs showed that 48 of these predicted *T. oceanica* LHCs had both the expected three trans-membrane helices as well as eight conserved

residues (Green and Durnford 1996; Green 2003; Liu et al. 2004). For phylogenetic tree analysis, the amino acid sequences of these 48 predicted *T. oceanica* gene models were aligned with 33 *T. pseudonana* gene models using the multiple sequence alignment algorithm MAFFT (Katoh and Standley 2013, 2016). Alignments were edited using the software package Bioedit (Hall 2013) resulting in 81 aligned sequences consisting of 118 characters, including 23 gaps. The phylogenetic tree was inferred using PhyML 3.0 (100 bootstrap replicates) (Guindon et al. 2010). Branch support was determined by three different methods: SH-aLRT, aBayes and standard bootstrap (Anisimova et al. 2011). The phylogenetic tree was visualized using TreeView (Page 1996, 2001, 2002).

2.5.2 ITS region

The ITS sequences of my diatoms (CCMP1003 and CCMP1005) were aligned with the publicly available sequences of 12 other diatoms (8 other *T. oceanica*, 2 *T. pseudonana*, 2 *T. weisfloggii*, see Table A.1) using the multiple sequence alignment algorithm MAFFT(Katoh and Standley 2013, 2016). Alignments were edited using the software package Bioedit (Hall 2013) resulting in 14 aligned sequences consisting of 640 characters, including 7 gaps. The phylogenetic tree was inferred using PhyML 3.0 (100 bootstrap replicates) (Guindon et al. 2010). Branch support was determined by standard bootstrap (Anisimova et al. 2011). The phylogenetic tree was visualized using TreeView (Page 1996, 2001, 2002).

2.6 Tables and figures

Table 2.1: Overview of the $Fe_{[total]}$ and $Cu_{[total]}$ concentrations added to our media for each *T.oceanica* strain.

Treatment	TO03		TO05	
	$Fe_{[total]}$	**$Cu_{[total]}$**	**$Fe_{[total]}$**	**$Cu_{[total]}$**
control	1.37 µM	10.2 nM	1.37 µM	14.32nM
lowCu	1.37 µM	<1 nM	1.37 µM	6.08 nM
lowFe	12.5 nM	10.2 nM	12.5 nM	14.32 nM
lowFeCu	12.5 nM	1.96 nM	12.5 nM	6.08 nM

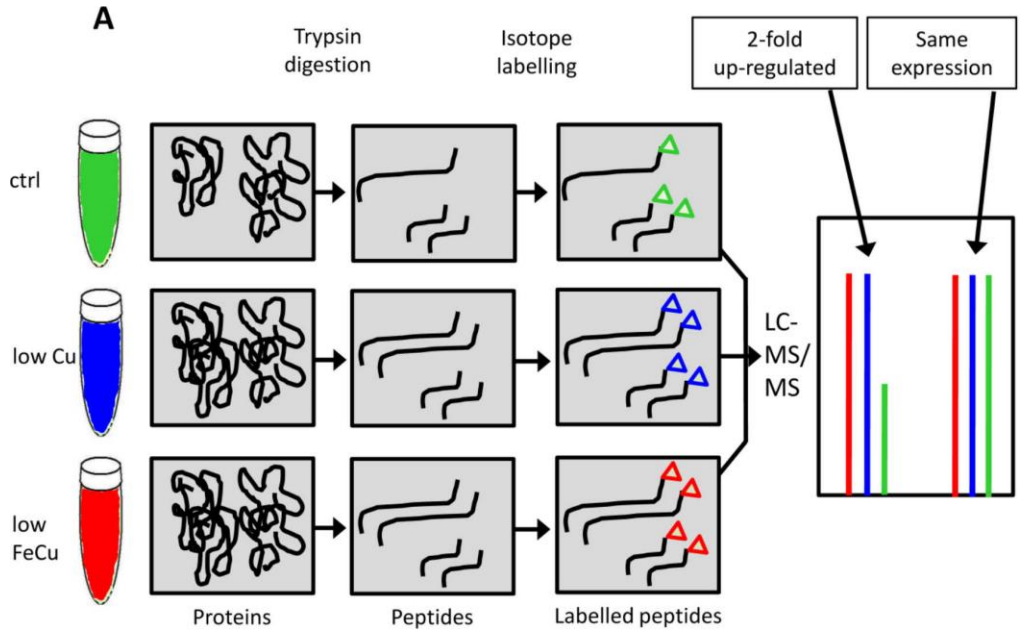

B

Treatment (label)	Biological Replicate		
Control (low)	1	2	3
lowCu (medium)	1	2	3
lowFeCu (heavy)	1	2	3
	↓	↓	↓
1:1:1 mix of labelled samples	1	2	3

Figure 2.1: Overview of Proteomic Method. A) Workflow: First the extracted proteins are trypsin digested. The resulting peptides are then labelled via chemical dimethylation using light (CH_2O, for control treatment; green), medium (CD_2O, for low Cu treatment; blue), and heavy ($^{13}CD_2O$ for low FeCu treatment; red) isotopologues of formaldehyde as described previously (Boersema et al. 2009). After peptides of the respective treatments are labelled, they are mixed together in a 1:1:1 ratio and then analyzed together by LC-MS/MS. The differential expression of proteins is then derived from the ratio of the intensities (area under the curve, here depicted as the height of bars) of the light (green), medium (blue) and heavy (red) peaks for each peptide**. B) Table of preparation and mixing of samples analyzed by LC-MS/MS.** Each biological replicate (three per treatment) is labelled

individually. Then one labelled sample of each treatment is mixed together in a 1:1:1 ratio, resulting in three separate biological replicate mixes to be analyzed by LC-MS/MS. Each of these three biological replicate mixes was then analyzed in technical duplicates (TO03) or triplicates (TO05).

Treatment (label)	Biological Replicate		
Control (low)	1	2	3
lowCu (medium)	1	2	3
lowFeCu (heavy)	1	2	3
	↓	↓	↓
1:1:1 mix of labelled samples	1	2	3

A

Treatment (label)	Protein A		
Control (low)	found	found	--
lowCu (medium)	found	--	found
lowFeCu (heavy)	found	--	--
	↓	↓	↓
lowCu differential expression ratio	yes	no	no
lowFeCu diff. expr. ratio	yes	no	no

Diff. expr. ratio?	*pval*?
yes	no
yes	no

B

Treatment (label)	Protein B		
Control (low)	--	found	found
lowCu (medium)	--	found	found
lowFeCu (heavy)	found	--	--
	↓	↓	↓
lowCu diff. expr. ratio	no	yes	yes
lowFeCu diff. expr. ratio	no	no	no

Diff. expr. ratio?	*pval*?
yes	yes
no	no

C

Treatment (label)	Protein C		
Control (low)	found	found	found
lowCu (medium)	found	found	found
lowFeCu (heavy)	found	found	--
	↓	↓	↓
lowCu diff. expr. ratio	yes	yes	yes
lowFeCu diff. expr. ratio	yes	yes	no

Diff. expr. ratio?	*pval*?
yes	yes
Yes	yes

Figure 2.2 Diagram, illustrating how the differential proteomic data were analyzed. If a protein was only detected in one treatment but not in another, it would not be part of the differential expression data set (e.g. Protein A: replicate 2, lowCu data). Furthermore, if only one of the three biological replicates resulted in a differential expression ratio, the protein would be part of the dataset, but the expression ratio would not have a statistical measure (*p*val) associated with it (e.g.Protein A: only detected in replicate 1, part of both lowCu and lowFeCu differnetial expression data sets). If two or three differential expression ratios were detected, the protein would be part of the dataset, this time with an associated *p*val (e.g. Protein B: lowCu differential expression data, replicate 2 and 3; Protein C: lowCu data, replicate 1, 2, and 3; Protein C: lowFeCu data, replicate 1 and 2).

Chapter 3: Contrasting Effects of Copper Limitation on the Photosynthetic Apparatus in Two Strains of the Open Ocean Diatom *Thalassiosira oceanica*

3.1 Summary

There is an intricate interaction between iron (Fe) and copper (Cu) physiology in diatoms. However, strategies to cope with low Cu are largely unknown. This study unveils the comprehensive restructuring of the photosynthetic apparatus in the diatom *Thalassiosira oceanica* (CCMP1003) in response to low Cu, at the physiological and proteomic level. The restructuring results in a shift from light harvesting for photochemistry —and ultimately for carbon fixation—to photoprotection, reducing carbon fixation and oxygen evolution. The observed decreases in the physiological parameters F_v/F_m, carbon fixation, and oxygen evolution, concomitant with increases in the antennae absorption cross section (σ_{PSII}), non-photochemical quenching (NPQ) and the conversion factor ($\varphi_{e:C}/\eta_{PSII}$) are in agreement with well-documented cellular responses to low Fe. However, the underlying proteomic changes due to low Cu are very different from those elicited by low Fe. Low Cu induces a significant four-fold reduction in the Cu-containing photosynthetic electron carrier plastocyanin. The decrease in plastocyanin causes a bottleneck within the photosynthetic electron transport chain (ETC), ultimately leading to substantial stoichiometric changes. Namely, a 2-fold reduction in both cytochrome b_6f complex (cytb_6f) and photosystem II (PSII), no change in the Fe-rich PSI and a 40- and a 2-fold increase in proteins potentially involved in detoxification of reactive oxygen species (ferredoxin and ferredoxin: $NADP^+$ reductase, respectively). Furthermore, we identify 48 light-harvesting complex (LHC) proteins in the publicly available genome of *T. oceanica* and provide proteomic

evidence for 33 of these. The change in the LHC composition within the antennae in response to low Cu underlines the shift from photochemistry to photoprotection in *T. oceanica* (CCMP1003). Interestingly, we also reveal very significant intra-specific strain differences. Another strain of *T. oceanica* (CCMP 1005) requires significantly higher Cu concentrations to sustain both its maximal and minimal growth rate compared to CCMP 1003. Under low Cu, CCMP 1005 decreases its growth rate, cell size, Chl*a* and total protein per cell. We argue that the reduction in protein per cell is the main strategy to decrease its cellular Cu requirement, as none of the other parameters tested are affected. Differences between the two strains, as well as differences between the well-documented responses to low Fe and those presented here in response to low Cu, are discussed.

3.2 Introduction

Diatoms account for almost a quarter of global primary productivity, thus contributing significantly to the transfer of CO_2 from the atmosphere to the ocean interior (Nelson et al. 1995; Field et al. 1998; Raven and Waite 2004). Yet in large oceanic regions, optimal growth of diatoms is constrained by iron (Fe) supply (Moore et al. 2004). However, in these low Fe regions, diatoms and other phytoplankton persist, and have evolved unique physiological strategies to grow at chronically low Fe levels (Maldonado and Price 1999, 2001; Strzepek and Harrison 2004; Maldonado et al. 2006; Allen et al. 2008; Zhu et al. 2010), even though they also respond rapidly to sporadic Fe inputs (Jickells et al. 2005; Marchetti et al. 2009a). In phytoplankton, the process of photosynthesis has the highest requirement for Fe. Therefore, some of the underlying cellular adaptations to low Fe include a) reducing the number of

chloroplasts, and the volume of individual chloroplasts (Lommer et al. 2012), b) restructuring the photosynthetic apparatus, such that the Fe intensive PSI is down-regulated relative to PSII (Strzepek and Harrison 2004), and c) replacing the electron carrier ferredoxin with the non-metal equivalent flavodoxin (LaRoche et al. 1996). In addition to these physiological adaptations under low Fe, open ocean diatoms enhance their demand for copper (Cu) — another essential redox active metal — by eliminating the Fe-containing cytc_6 in photosynthesis and replacing it with plastocyanin, a Cu-containing counterpart (Peers and Price 2006), and by up-regulating a high-affinity Fe uptake system (HAFeT) that depends on a multi-Cu oxidase (Peers et al. 2005; Maldonado et al. 2006). These physiological adaptations result in a higher Cu demand in Fe-limited than in Fe-sufficient diatoms and suggest an intricate link between Fe and Cu physiology (Annett et al. 2008).

Open ocean Fe concentrations are significantly lower (average ~0.6 nM) than those at the coast (average ~ 2nM) (Moore and Braucher 2008). Diatoms in oligotrophic regions, such as the Sargasso Sea, although not primarily chronically Fe limited, often may experience low Fe availability (surface waters $[Fe]_{diss}$ ranging from 0.2-0.8 nM (Wu and Boyle 2002), relative to the average half-saturation constant for growth for Fe (K_u) for field populations, 0.32 nM Fe (Marchetti and Maldonado 2016) in addition to macronutrient limitation and might, as a result, exhibit the physiological adaptations mentioned above. Indeed, several laboratory and field studies have shown that open ocean phytoplankton usually have higher Cu:C demands and thus are more easily limited by low Cu than their coastal counterparts (Peers et al. 2005; Annett et al. 2008; Guo et al. 2012).

The literature on adaptations of phytoplankton to cope with Cu limitation is scarce. In the model freshwater green alga *Chlamydomonas reinhardtii*, Cu limitation induces a tight

transcriptional regulatory mechanism (Kropat et al. 2005; Castruita et al. 2011). Most notably, it uses the Cu-containing electron carrier plastocyanin when grown under Cu replete conditions and switches to the Fe-containing cytc_6 under Cu limiting conditions (Merchant and Bogorad 1986; Merchant et al. 1991). This decreases its cellular photosynthetic Cu demand and enables adequate Cu supply to cytochrome oxidase in respiration (Kropat et al. 2015). An increase in unsaturated fatty acids in the thylakoid membrane also occurs in response to Cu limitation (Castruita et al. 2011). Changes in thylakoid fatty acid composition can have far-reaching consequences in a photosynthetic cell (Kern et al. 2009; Goss et al. 2009; Gao et al. 2014). An increase in the fatty acid MGDG (monogalactosyldiacylglycerol) might result in an increase in non-photochemical quenching (NPQ, an estimate of how much excess excitation energy is dissipated as heat) by facilitating both recruitment of diadinoxanthin and its interaction with light-harvesting complexes (LHCs) (Goss et al. 2005, 2007, 2009). One study examined the effects of low Cu on the photosynthetic apparatus of the prymnesiophyte *Phaeocystis*. Photosystem II reaction centres seemed to be damaged but no effects were observed downstream in the electron transport chain (Lombardi and Maldonado 2011).

In addition to photosynthesis, Cu limitation affects diatom physiology by a) inducing a high-affinity Cu uptake system, which has different characteristics and regulation in oceanic and coastal centric species (Guo et al. 2010), and b) increasing the cellular Chl*a* and lipid content in pennate diatoms (Lelong et al. 2013). Most recently, the genes encoding various Cu transporters and chaperones have been identified *in silico* in the genome of the diatom *T. pseudonana* (Guo et al. 2015).

Many of the physiological adaptations to Fe limitation described above were investigated using the model open ocean centric diatom, *T. oceanica*, strain CCMP 1003 (hereafter referred to

as TO03), whose genome has not been sequenced. However, recently, the genome of a different strain of *T. oceanica* (CCMP 1005; here TO05) was sequenced (Lommer et al. 2012). Given the importance of Cu nutrition for *T. oceanica* (Peers et al. 2005; Peers and Price 2006; Annett et al. 2008; Guo et al. 2010, 2012), we aimed to investigate the physiological and proteomic response to Cu limitation in both strains. Since TO03 has not been sequenced, we grew this strain under various Cu conditions and used transcriptomics to create an expressed sequence tag (EST) library with assembled contigs. Our preliminary growth experiments showed very contrasting Cu demands between TO05 and TO03 and inspired further comparative investigations. The present study focuses on the physiological and proteomic response of the photosynthetic apparatus to Cu limitation in both strains. Here, we also discuss similarities and differences between the well-known photosynthetic response of diatoms to low Fe and their understudied response to low Cu.

3.3 Results

The two strains of the oceanic diatom *T. oceanica* studied were both isolated from the Sargasso Sea, twenty-seven years apart (TO05 in 1958, TO03 in 1985). Despite being the same species, they have exceptionally different Cu requirements. The data presented below illustrate the contrasting physiology of these strains in response to Cu limitation. We structure our results in four sections; first, we describe the effects of Cu limitation on whole cell physiology, followed by a more focused description of the effects on photophysiology. We then present a brief overview of the two proteomic datasets. We conclude with a portrayal of the nature and expression patterns of the underlying light-harvesting complexes and proteins involved in photosynthesis, responsible for the changes we see in the photophysiological results.

3.3.1 Effect of chronic copper limitation on whole cell physiological parameters

TO03 achieved a maximum specific growth rate (μ_{max}) of 1.05 per day (d^{-1}) in the presence of 10.2 nM $[Cu]_{total}$ (Figure 3.1). The background Cu concentration in the media (<1 nM $[Cu]_{total}$) allowed TO03 to sustain a growth rate of 0.51 d^{-1}, equivalent to 48% of μ_{max} (± 6.45% std error). In contrast, TO05 could not survive at this lowCu level (<1 nM $[Cu]_{total}$) and achieved its maximum growth rate (1.26 d^{-1}) at higher Cu concentrations (14.3 nM $[Cu]_{total}$) than TO03. In TO05, Cu limitation was induced at 6.08 nM $[Cu]_{total}$ (0.82 d^{-1}, or 65% μ_{max}). Even though the absolute growth rates under Cu replete and deplete conditions are statistically different for the two strains, their relative Cu-limited growth rates (μ/μ_{max}) are indistinguishable ($p>0.1$, Figure 3.2A, Table A.2). Therefore, comparing the effect of Cu limitation between the strains is appropriate.

Cell diameter decreased 10% in both strains in response to low Cu (Figure 3.2B, Table A.2). Chl*a* concentration per cell was constant in TO03, while it decreased somewhat in TO05 (Figure 3.2C). However, as cell diameter decreased in both strains, when normalized to cell volume, Chl*a* concentration increased in response to low Cu in TO03 (4.3±0.1 to 7.4 ±0.5 fg Chl*a* fL^{-1}, $p<0.001$) and stayed the same in TO05 (4.3±0.8 and 3.8 ±0.4 fg Chl*a* fL^{-1}, Table A.2). Cellular protein content remained constant in TO03. However, TO05 significantly decreased its cellular protein content in response to low Cu by 50% (Figure 3.2O). Gross oxygen production decreased in TO03 in response to Cu limitation, regardless of the parameter used to normalize the rates (Table A.2): normalized to Chl*a*, it decreased by 72% (Figure 3.2D), and normalized to cell, it decreased by 70% (123±11.5 to 36 ±4.3 fmol O_2 $cell^{-1}$ h^{-1}, $p<0.001$). In contrast, in TO05, O_2 production was only significantly decreased when normalized to cell (139±10.4 to 69.4 ±2.0 fmol O_2 $cell^{-1}$ h^{-1}, $p<0.01$, Table A.2) but not when normalized to Chl*a*. Respiration, on the other

hand, was not affected by Cu concentration in either of the two strains, independent of normalization (Table A.2).

3.3.2 Effects of Cu limitation on photophysiology, ETR_{RCII} and C-assimilation

Chronic Cu limitation had profound effects on the photophysiology of TO03, but not TO05. In fact, none of the following photophysiological, ETR_{RCII}, or C-assimilation parameters changed in TO05 in response to low Cu. In TO03, Cu limitation resulted in a decrease of F_v/F_m from 0.6±0.01 to 0.3±0.01 A.U., $p<0.001$ (Figure 3.2E). The functional absorption cross-section of PSII (σ_{PSII}) increased by 30% (Figure 3.2F) and the plastoquinone (PQ) pool size increased by 37% (4.3 ±0.5 to 6.0±0.4 PQ mol Q_B^{-1}, $p<0.1$) (Table A.2).

To gain more insight into photophysiological changes, we generated PE curves for short-term C-assimilation and ETR_{RCII}. From these curves, we derived the respective photosynthetic parameters P_{max}, α, and E_k. For short-term C-assimilation, normalized to Chl*a*, all three parameters decreased in TO03: P_{max} decreased by 75%, α decreased by 63% and E_k decreased by 54% (Figure 3.2G-1). For ETR_{RCII} normalized to RC (Figure 3.2J-L), α increased by 18% in response to low Cu, while P_{max} remained constant and E_k decreased by 25%. For both strains, the light saturation point E_k was higher for carbon fixation than ETR_{RCII} (Figure 3.2I, L), implying that ETR_{RCII} saturated at lower light intensities than carbon fixation. At the growth irradiance (155 µmol quanta m^{-2} s^{-1}), the rates of ETR_{RCII} relative to those of C-assimilation (i.e. the conversion factor $\varphi_{e:C}/\eta_{PSII}$) increased two-fold in response to low Cu in TO03 (Table 3.2M). In line with the study by Schuback et al. (2015), we examined FRRF derived parameters at the growth irradiance to further elucidate the photophysiological mechanisms. The following parameters changed only in TO03 and not in TO05. Low Cu decreased the efficiency of

excitation energy capture by the fraction of open RCII **(**F_v'/F_m') by 53% in TO03 (0.6±0.01 to 0.3±0.01 A.U., p<0.0001, Table A.2). In line with the decrease in F_v'/F_m', we observed a four-fold increase in non-photochemical quenching, estimated as the normalized Stern Vollmer NPQ_{NSV} (Figure 3.2N). The overall quantum efficiency of photochemical energy conversion in PSII (F_q'/F_m', φ'_{PSII}) decreased by 63% in response to low Cu (0.4±0.03 to 0.2±0.01 A.U., p<0.001, Table A.2). In contrast, photochemical quenching (F_q'/F_v'), an indicator of the efficiency of charge separation in functional RCII was only slightly reduced by 17% (0.7 ±0.04 to 0.6±0.02 A.U., p<0.05, Table A.2).

3.3.3 Overview of the two proteomic datasets for the two strains – original *vs.* EST included

For each strain, we mapped the peptides generated by the LC-MS/MS to two databases (see methods). In the original search (thereafter called 'original'), peptides were mapped to proteins from the TO05 genome. To ensure that we did not miss any important information regarding the unique response of TO03 due to possible genomic differences between the two strains, we added the second search (thereafter called 'plusEST'), were the same peptides were mapped to a larger database composed of the original protein sequences of the TO05 genome plus the protein sequences of our own TO03 transcriptome. The 'plusEST' search leads to a moderate increase of identified proteins in both strains when comparing the results with the respective original search (15.6% in TO03 and 13.4 % in TO05, see Table A.6). As illustrated in Figure 3.3, the distribution of the identified proteins in both strains is as follows: approximately 83% of all identified proteins had best hits in the TO05 genome part and 17% (e. g. TO03: 139 ESTs) in the EST part of the database. Examining these 139 hits, we also observe a similar proportion of EST

sub-groups represented in both strains: 75% of these ESTs can themselves be mapped to predicted proteins of the TO05 genome, a little over 19% map to putatively non-coding regions of the TO05 genome, and 1.25% map to the chloroplast genome, whereas 6% do not map anywhere on the TO05 genome.

3.3.4 Proteomic shift in the antennae and photosynthetic transport chain

3.3.4.1 Identity and expression of LHC proteins

In silico probing of the publicly available genome of *Thalassiosira oceanica* (CCMP 1005) for proteins containing a predicted Chl*a/b* binding site, revealed 69 potential candidate genes coding for light harvesting complex (LHC) proteins. Aligning the predicted protein sequences with those of 41 predicted LHCs from the closely related diatom *Thalassiosira pseudonana* (CCMP 1335) revealed that only 48 LHCs from *T. oceanica* feature all three helices with conserved residues deemed essential for their proper functioning (Figure 3.4, Table A.3) (Green and Durnford 1996; Green 2003; Liu et al. 2004). Of the 48 predicted proteins in *T. oceanica*, 33 LHCs (69%) were identified at the protein level in this study (Figure 3.5, Table 3.1). The overall expressed inventory of LHCs was very similar between the two strains.

Of the 48 predicted gene models, we found evidence at the protein level for 33 LHCs (29 found in both, 1 only in TO03, and 3 only in TO05, Table A.3). Note that the number of proteins expressed per LHC clade is similar between the two strains. Considerable numbers of significantly differentially expressed LHCs are only found in TO03 with 9 up- and 7 down-regulated, whereas there is only one up-regulated in TO05 (Group III, Table 3.1, Table 3.2). Phylogenetic analysis of these 48 putative LHCs in *T. oceanica* (CCMP 1005) led to their classification into the four previously described clades (Figure 3.5, Table 3.1, Table A.4)

(Lefebvre et al. 2010; Goss and Lepetit 2015; Mock et al. 2017): the main Chl*a/c* Lhcf (26 predicted proteins), the red algal-like Lhcr (10 predicted proteins), the related clade Lhcz (3 predicted proteins), and the LI818-like clade Lhcx (8 predicted proteins). The additional clade around Tp17531 has been added, given that at least 5 different diatoms have a protein that clusters here (Mock et al. 2017), including *T. oceanica* (this study). Furthermore, the Lhcf clade can be divided into three subclades: Lhcf- Group I-III.

Of the 33 LHCs identified at the protein level, 88% (29 LHCs) are expressed in both strains. However, whereas TO05 has only one up-regulated LHC in response to low Cu concentrations (THAOC_08587, Lhcf-group III, TpFCP7 homolog) and none down-regulated, TO03 demonstrates a well-orchestrated response (Figure 3.5, Table 3.2). Approximately 55% of its expressed LHCs were significantly regulated in response to Cu limitation. Eight LHCs were down-regulated: four proteins in the Lhcf- Group I, one in the Lhcf – Group III and two in the Lhcr clade. Nine LHCs were up-regulated: one protein in the diatom-specific Lhcf- Group II, four in Lhcf - Group III, one in the Lhcr clade and three in the Lhcx clade.

3.3.4.2 Proteomic shift within the chloroplast electron transport chain (ETC)

In both strains, many of the proteins involved in the photosynthetic electron transport chain (ETC) were identified (23 in TO03, 24 in TO05) (Table 3.3); 17 of these were shared, whereas five and six were only found in TO03 and TO05, respectively. Acclimation to low Cu has a profound impact on the stoichiometry of the complexes involved in the ETC in strain TO03. Here, protein levels of PSII (psbC, psbD, psbE, psbQ), cytb_6f (petB), and the Cu-containing electron carrier plastocyanin (petE) are all significantly reduced (2-fold, 2-fold, and 4-fold, respectively) (Table 3). Protein levels for PSI are unchanged in response to low Cu (psaA, psaB,

psaC, psaD, psaF) whereas ferredoxin (petF) and FNR (petH) are both induced (40-fold and 2.4-fold, respectively). TO05 shows no significant differential expression of any of the proteins involved in the photosynthetic ETC. The EST mapped data support these findings (see Table A.4). We present a model of the photosynthetic electron transport chain in TO03, visualizing the stoichiometric changes of its major components in response to chronic Cu limitation (Figure 3.6).

3.4 Discussion

Low copper (Cu) concentrations in the media elicited a remarkably different cellular response in the two strains of the oceanic diatom *T. oceanica* (CCMP 1003 and CCMP 1005). This in itself is striking and will be discussed below. However, the main body of the discussion will focus on the effect of low Cu on TO03 (*T. oceanica*, CCMP 1003), showing an extensive restructuring of the photosynthetic apparatus, shifting from a primarily light harvesting to a photoprotective role. This restructuring is reflected in a) the composition of the light-harvesting antennae, b) the stoichiometry of components of the photosynthetic electron transport chain, and c) the difference in the ratio of electron transport and carbon fixation rate. Differences between the well-documented response to low Fe and that to low Cu presented here are discussed.

3.4.1 Differences between *T. oceanica* CCMP 1003 and CCMP 1005

The two strains of the open ocean diatom *T. oceanica*, CCMP 1003 (TO03) and CCMP 1005 (TO05), were isolated from the Sargasso Sea 27 years apart, and are considered the same species based on morphology. In our study, the species identity of the two *T. oceanica* strains was confirmed, using the comparison of the diatom barcoding region encompassing the ITS1–5.8S –

ITS2 (Moniz and Kaczmarska 2009, 2010). The phylogenetic tree of 14 *Thalassiosira* ITS sequences, including the sequences of the two *T.oceanica* strains used in this study (CCMP1003 and CCMP1005) plus the publicly available ITS sequences of eight other *T. oceanica* strains, two *T. pseudonana* strains and two *T. weisfloggii* strains, clearly supports the assumption that these are indeed strains of the same species (Fig A.3, p235). Aligning the ITS region of both strains (Figure A.2) shows a 99.66% identical overlap in their ITS sequence. Further evidence of their close genomic relationship is given when we compare the additional proteomic datasets of TO03 (EST) and TO05 (EST) (Figure 3.3). In both strains, peptides were mapped to a combined database comprised of predicted protein sequences derived from the TO05 genome and our TO03 transcriptome. We predicted that TO03 would have a higher proportion of identified proteins coming from the mapping of the peptides to its own transcriptome relative to mapping them to the TO05 genome. In contrast, for TO05 we predicted the opposite: a higher proportion of identified proteins coming from the mapping of the peptides to its own genome. However, the distribution of identified proteins using the TO05 genome plus TO03 transcriptome database is practically the same in both strains. Furthermore, even the fraction of EST subsets is the same in both strains (Figure 3.3). Thus, even though these two strains are the same species, have been isolated from the same oceanic region, and have a similar genomic makeup, it is striking that their physiological responses to Cu limitation are so different (Figure 3.1 and Figure 3.2, Table A.2).

Strain TO03 was able to sustain growth at a Cu concentration ($[Cu]_{total}$) of <1 nM, whereas strain TO05 required 6 times more Cu ($[Cu]_{total}$ = 6.08 nM). Moreover, to achieve maximal growth rate, TO03 required only 10.2 nM $[Cu]_{total}$, while TO05 required 40% more Cu (14.32 nM Cu; Figure 3.1, Table A.2). Although different Cu concentrations were used for the

two strains to reach their respective μ_{max} and Cu-limited growth rate, they achieved identical relative growth rate reduction under low Cu (~55% μ_{max}), allowing comparison between their respective physiological and proteomic responses (Figure 3.2A, Table A.2).

In addition to their matching growth rate reduction (Figure 3.2A), both also decreased their cell size by 10% (Figure 3.2B). Cell size reduction is a common strategy in unicellular organisms in response to nutrient limitation. Decreasing cell size increases surface-area-to-volume ratio, allowing a greater number of nutrient transporters at the cell surface, relative to the cellular nutrient demand, which is proportional to cell volume. Furthermore, smaller cells have a thinner surface boundary layer, facilitating the diffusion of nutrients to the cell membrane (Marchetti and Maldonado 2016). Interestingly, of the 23 parameters presented here, TO05 changed only four significantly, whereas TO03 adjusted 18.

Nutrient limitation usually results in chlorosis, a decrease in cellular Chl*a* concentration (Collier and Grossman 1992; Geider et al. 1993). This common strategy is only seen in TO05 but not in TO03 (Figure 3.2C). As described in more detail below, TO03 restructured its whole photosynthetic apparatus under low Cu, changing its Chl*a* content (normalized to cell volume, it actually increases, Table A.2), σ_{PSII}, F_v/F_m, NPQ_{NSV}, ETR, and ^{14}C uptake. TO05 did not vary any of these parameters ($p > 0.05$) (Figure 3.2, Table A.2). Furthermore, of the most prominent cellular Cu-containing proteins (i.e. plastocyanin, cytochrome *c* oxidase), none are down-regulated in TO05.

We speculate that the dominant strategy used by TO05 to deal with Cu limitation is a reduction in cell size (Figure 3.2B) and overall protein content (Figure 3.2O). A comparable decrease has been seen in this strain in response to low Fe (Lommer et al. 2012). An overall reduction in protein content could be expected to result in a decrease in growth rate. However, as

the majority of proteins are reduced to the same extent, this would not be detected in our proteomic analysis, because we mixed equal absolute amounts of protein (5 ng control: 5 ng low Cu) independent of changes in cellular protein content. Even though we did not measure Cu quotas, TO05, just by decreasing its overall cellular protein content by 50%, will decrease its Cu-containing proteins by 50%. Strikingly, this agrees well with the 57% decrease in $[Cu]_{total}$ concentration in the media and the resulting 45% decrease in growth rate we observed for TO05.

The gross oxygen production data provide additional evidence for the singular strategy of TO05 to reduce its protein content by 50%. Gross oxygen production, when normalized to cell, decreased by 50% (Table A.2), while when normalized to Chl*a* (Figure 3.2D) stays constant. This indicates that the photosynthetic unit itself in TO05 was not compromised, while it was greatly affected in TO03. Theoretically, when Cu is extremely low in the medium, the cell would be forced to decrease the proportion of Cu-containing proteins, as we observed for plastocyanin in TO03. However, it seems that TO05 is unable to decrease the Cu-containing proteins (i.e. plastocyanin) relative to other proteins, and thus is unable to grow at extremely low Cu. It is possible that TO05 has lost (or TO03 has gained) a Cu responsive transcription factor able to orchestrate a broad response when Cu concentrations are declining, similar to the one identified in *Chlamydomonas* (Sommer et al. 2010). TO03 is able to decrease plastocyanin significantly relative to other proteins and has to cope with potentially increased electron pressure and reactive oxygen species. As discussed below, TO03 rearranges its whole photosynthetic apparatus, and consequently, is able to sustain a decent growth rate (~0.5 d^{-1}) at extremely low $[Cu]_{total}$ concentrations (<1 nM Cu).

In recent years, multiple intra-specific physiological variations have been demonstrated in various phytoplankton taxa, such as the harmful algal bloom (HAB) forming raphidophyte

Heterosigma (Fredrickson et al. 2011; Lebret et al. 2012; Harvey et al. 2015), and diatoms such as *Skeletonema* (Kremp et al. 2012), *Ditylum* (Rynearson et al. 2006), *Thalassiosira rotula* (Chen and Rynearson 2016) and the HAB forming *Pseudo-nitzschia* (Orsini et al. 2004; Kim et al. 2015). These intra-specific differences can manifest themselves in spatial and/or temporal distinct occurrences of one strain over the other. However, four distinct strains of *T. rotula* co-existed in the North Atlantic spring bloom in 2008 (Chen and Rynearson 2016). This co-existence of various strains over large periods of time might facilitate niche-adaptations (Menden-Deuer and Rowlett 2014).

However, bearing in mind that diatoms are one of the faster-evolving phytoplankton phyla (Bowler et al. 2008), we must still consider the possibility of changes in the genome or epigenome of organisms kept in long-term culture collections. For example, the green alga *C. reinhardtii* took less than 500 generations in nutrient-rich media to lose its ability to synthesize cobalamin (Vit B_{12}) (Helliwell et al. 2015). To address this issue, we contacted the curator at NCMA; their culture transfer regime (every 2-3 weeks for >20 years without inverting the tubes) would indeed allow the cells to experience nutrient rich and limiting conditions during each transfer cycle, hopefully preventing changes in genome and epigenome. In support of this, all the studies investigating trace metal requirements of open ocean and coastal species have used isolates that had been in culture for over 20 years, under trace metal replete conditions. These studies still revealed striking differences in the metal requirements in the open ocean and coastal isolates (Sunda et al. 1991; Sunda and Huntsman 1995; Annett et al. 2008; Guo et al. 2010). We believe that the responses of TO05 (i.e. decrease of the whole complement of proteome to decrease Cu requirement) and TO03 (i.e. differential expression of proteins) are both viable, but represent very different strategies to cope with Cu limitation.

3.4.2 Proteomic shift within the photosynthetic apparatus in TO03: electron transport chain and antennae

3.4.2.1 Electron transport chain - ETC

In the plant photosynthetic electron transport chain (ETC), electrons are channelled from PSII via the PQ pool to cytb_6f, then via the small Cu-containing plastocyanin to PSI, from where they are transferred by way of ferredoxin (petF, Fdx) and FNR to NADP+, thereby producing the reducing equivalent NAD(P)H (Nelson and Ben-Shem 2004). In addition to the supply of reducing equivalents as NAD(P)H, the ETC generates a proton gradient across the thylakoid membrane ultimately resulting in ATP synthesis. Both ATP and NAD(P)H are needed in the carbon fixing Calvin-Benson-Bassham cycle. Since more ATP is needed for carbon fixation than the amount of ATP that can be generated via the proton gradient generated by this linear electron transport (LET) chain (Allen 2002, 2003), additional protons can be pumped into the lumen via cyclic electron transport (CET) either around PSII (Prasil et al. 1996; Lavaud et al. 2002; Ruban et al. 2004) or PSI (Yamori and Shikanai 2016). Keeping an adequate ATP/ NAD(P)H ratio is imperative for any cell to maximize growth and minimize cell damage. As shown by Bailleul et al. (2015), in diatoms, additional ATP and NAD(P)H can also be supplied to the chloroplast by the mitochondria.

Acclimation to low Cu has a profound impact on the stoichiometry of the complexes involved in the ETC in strain TO03 (Table 3). Changes in ETC stoichiometry have also been observed in TO03 in response to low Fe (Strzepek and Harrison 2004), when Fe-rich complexes, such as PSI and cytb_6f, are significantly reduced. However, low Cu concentrations induce a

different change in stoichiometry, such that the concentrations of some of the proteins associated with photosystem II, and with the photosynthetic electron transport chain (cytb_6f, and plastocyanin) are significantly reduced (Table 3.3, Figure 3.6). Protein levels for PSI, however, are unchanged in response to low Cu. The reduction in plastocyanin is expected given that this protein is thought to be the dominant Cu pool in *T. oceanica* (Peers and Price 2006). Indeed, our proteomic data showed a significant down-regulation of plastocyanin (4-fold) —a mandatory component in the ETC in *T. oceanica*—in response to low Cu (Table 3). This is accompanied by the 2-fold reduction of upstream components of the ETC (i.e. cytb_6f and PSII), thus avoiding over reduction and ensuing photodamage of PSII. In contrast to the low Fe response, the Fe-rich PSI complex located down-stream of plastocyanin is not affected by Cu limitation. Furthermore, ferredoxin and FNR are both induced under low Cu (Table 3.3). FNR is up-regulated by 2.4-fold and has been shown to increase the ability to deal with oxidative stress in tobacco plants (Rodriguez et al. 2007). Ferredoxin (Fdx, petF) is the most up-regulated protein in our dataset (>40-fold). In the green alga *Chlamydomonas*, one of six different ferredoxin genes is also strongly up-regulated under low Cu and might facilitate chlorophyll biosynthesis (Terauchi et al. 2009). However, Lin et al. (2013), using transgenic cell lines overexpressing petF, showed an increased ability to deal with reactive oxygen species (ROS) in heat stressed chloroplasts, most likely due to ferredoxin's ability to donate electrons in ascorbate-mediated ROS scavenging mechanisms. In stark contrast to the proteomic response to low Cu in TO03, TO05 shows no significant differential expression of any of the proteins involved in the photosynthetic ETC (Table 3.3). Considering that TO03 can grow relatively well at <1 nM Cu, while TO05 cannot even survive at 2 nM Cu, our results seem to indicate that TO05 is unable to restructure its photosynthetic apparatus to deal with low Cu.

3.4.2.2 Antennae

Under low Cu, strain TO03 exhibits another striking shift within the light-harvesting antennae. While cellular Chl*a* significantly increased when normalized to cell volume (Table A.2), the functional absorption cross section of PSII, σ_{PSII} ($Å^2$ $RCII^{-1}$) also increased by 30% (Figure 3.2F). An increase in σ_{PSII} has also been observed in cultures acclimated to low Fe (Petrou et al. 2014; Schuback et al. 2015), which is believed to compensate for decreased Chl*a* content and/or PSII abundance. I hypothesize that the unexpected trend of an increase in cellular Chl*a* ($p<0.1$) under low Cu could be associated with disconnected LHCs (DLHCs). DLHCs are not energetically connected to photosystems, hence they elevate F_o without changing F_m, thereby decreasing the apparent F_v/F_m (see review by Behrenfeld and Milligan (2013) and references therein). They may provide a fast pigment pool in the early stages of Fe recovery. Furthermore, DLHCs have been proclaimed to play a vital role in non-photochemical quenching (Miloslavina et al. 2009; Goss and Lepetit 2015). In summary, the proposed presence of DLHCs in TO03 in response to low Cu can explain increased Chl*a* per cell volume (Table A.2), decreased F_v/F_m and increased NPQ_{NSV} (Figure 3.2E, N).

The restructuring of the light-harvesting antenna of PSII is further reflected in changes of protein composition in TO03 (Table 3.1, Table 3.2). Indeed, the protein abundance of 55% of the 29 LHCs changed significantly under low Cu (Table 3.1, Table 3.2). As shown in the phylogenetic tree (Figure 3.5, summarized in Table 2), the down-regulated proteins are phylogenetically related to known LHCs that are particularly involved in light harvesting reactions in both PSII (Nagao et al. 2013) and PSI (Grouneva et al. 2011; Ikeda et al. 2013). Of the nine up-regulated LHCs, four are part of Lhcf-group III, which is most closely related to the

major Lhcf cluster in the haptophyte *Emiliania* (McKew et al. 2013). To our knowledge, this group has not been associated with stress response in diatoms in any other study and was actually down-regulated by high light stress in *Emiliania*. One up-regulated LHC is part of the diatom-specific Lhcf-group II. The most notable set of up-regulated LHCs are the Lhcx homologs. Lhcx1, in particular, has been shown to play an important role in stress responses by maintaining thylakoid membrane stability (Zhu and Green 2010) and supporting the antenna's ability for NPQ (Miloslavina et al. 2009; Zhu et al. 2010; Goss and Lepetit 2015; Taddei et al. 2016). This rearrangement supports a general switch within the antennae from light harvesting (for photochemistry) to photoprotection in TO03. This switch is not seen in TO05 which only regulated one LHC (TpFCP7 homolog THAOC_08587: up-regulated).

3.4.3 P*vs*E curves (ETR_{PSII} & ^{14}C), conversion factor

For decades, PE curves have played a central role in elucidating strategies of photoacclimation in different photosynthetically active organisms (Richardson et al. 1983; Zhu et al. 2016a). Various parameters can be derived to obtain a measure of change in photosynthesis (P) per incident light (E, µmol quanta m^{-2} s^{-1}). The initial slope of the curve, α, quantifies the linear light-dependent increase of the rate of photosynthesis under sub-saturating light conditions (Jassby and Platt 1976). When irradiance increases beyond the light saturation point, E_k, photosynthesis starts to become light-saturated until the cell reaches its maximum photosynthetic rate P_{max}. In our study, we generated PE curves for both short-term C assimilation normalized to Chl*a* and electron transport rate in PSII [ETR_{RCII}, normalized to reaction centres (RC)]. The two curves respond differently to Cu limitation, demonstrating that low Cu decouples these two rates of photosynthesis.

3.4.3.1 PvsE curve – ETR_{RCII} and carbon uptake

At growth irradiance, in response to low Cu, TO03 reduced CO_2 uptake per chlorophyll by 68%. Furthermore, all PE parameters significantly decreased in response to low Cu: α^{14C} by 63%, $E_k{}^{14C}$ by 32%, and $P_{max}{}^{14C}$ by 75% (Figure 3.2G-I). This indicates that under the same irradiance, Cu limited cells cannot provide the necessary amount of ATP and/or NAD(P)H to sustain the same rate of carbon fixation as the Cu replete cultures.

Counter-intuitively—considering the 68% decrease in carbon uptake—the rate of charge separation per reaction centre in PSII (ETR_{RCII}) is not impacted by low Cu. However, as the number of reaction centres in the cell decreases by 50% under low Cu (as per 2-fold decrease in PSII proteins), the overall cellular ETC performance is impaired. Under Cu limitation, the functional absorption cross section of PSII (σ_{PSII}) increased by 30%, whereas PSII concentration decreased 2-fold (Table 3.3, Figure 3.6). These changes result in more efficient light harvesting per RCII at low light levels, reflected in both an increase in α^{ETR} and a decrease in the light saturation point $E_k{}^{ETR}$ (Figure 3.2J, L). $E_k{}^{ETR}$ is reduced to such an extent that cells were effectively growing under light saturating conditions (lowCu $E_k{}^{ETR}$ = 105 µmol quanta m^{-2} s^{-1} *vs.* growth irradiance = 155 µmol quanta m^{-2} s^{-1}). Maintaining the same maximal rate of charge separation per functional RC, even under severe Cu limitation, assists in preventing accumulation of excess excitation energy which could result in an increase in ROS. Even though protein levels of both PSII and cytb_6f decreased to the same extent (~2x), plastocyanin levels decreased even more (>4x) in response to low Cu (Table 3.3). This disproportionate decrease of a key electron carrier downstream of PSII ultimately restricts the flow of electrons away from PSII. This bottleneck in the linear electron transport chain, if not safely dissipated, could

ultimately lead to a built-up of excitation energy and photoinhibition. The increased PQ pool size (mol PQ mol Q_B^{-1}) (Table A.2, Figure 3.6) is an indication of its needed buffer function. Furthermore, numerous alternative electron sinks have been suggested to alleviate excess excitation pressure. Of these alternative electron sinks, the Mehler reaction (Claquin et al. 2004), photorespiration (Parker and Armbrust 2005), nitrate reduction (Lomas and Glibert 2000) and cyclic electron transport around PSI (CET_{PSI}) occur after plastocyanin, whereas the short water-water cycle involving plastoquinone terminal oxidase (PTOX) (Bailey et al. 2008; Mackey et al. 2008) channels electrons away from the linear electron transport chain before plastocyanin. Cyclic electron transport around PSII (CET_{PSII})(Prasil et al. 1996; Lavaud et al. 2002; Ruban et al. 2004) could also reduce electron pressure. In CET_{PSII}, the e^- in RC_{PSII} that has been injected into the ETC, is resupplied by a recycled e^- from the reduced plastoquinone pool, thus no additional new e^- from the oxygen-evolving complex (OEC) is added. This could also explain, in part, the decreased O_2 production in TO03 in response to low Cu (Table A.2). We identified putative candidate genes involved in these alternative electron flow pathways in the *T. oceanica* genome (i.e. the two PTOX homologues THAOC_16363, THAOC_20783). However, none of these were found expressed in any of the four proteomic datasets (2x TO03, 2x TO05). It is possible that these proteins are present but at a concentration below the detection limit of our method. If this is the case in only one of the two treatments, the protein would not be seen in our dataset (see method section). For example, the abundance of PTOX in a non-stressed cell is as low as 1 per 100 PSII complexes (Lennon et al. 2003).

In summary, up to 50% of the decrease in both carbon uptake and oxygen production in TO03 can be explained by the overall cellular reduction of PSII reaction centres (as seen in the proteomic data), as the ETR in each of those reaction centres is not impaired. The extra reduction

(17%) in carbon uptake could be due to the diversion of electrons away from the Calvin-Benson-Bassham cycle as suggested above. Cyclic electron transport around PSII, in particular, could rationalize the additional decrease in oxygen production (extra 5%).

3.4.3.2 Conversion factor

The conversion factor (mol e^- mol $RCII^{-1}$ / mol C mol Chl*a*$^{-1}$) as a measure of how many charge separations occur per RC_{PSII} in the light reaction of photosynthesis per carbon fixed per Chl*a* in the dark reaction of photosynthesis, has recently been shown to increase in response to low Fe in both natural phytoplankton assemblages and monoclonal *T. oceanica* (CCMP1003) cultures (Schuback et al. 2015). This factor is of particular interest to oceanographers estimating global primary productivity using fluorescence data (Jassby and Platt 1976; Schuback et al. 2015). However, whereas the low Fe-mediated increase is due to an increase in ETR_{RCII} compared to a stable Chl*a* normalized C-assimilation, the low Cu-mediated increase is due to a stable ETR_{RCII} coupled to a substantially decreased Chl*a* normalized C-assimilation rate (Figure 3.2M, Table A.2). Why is carbon fixation so impaired in TO03, if cellular Chl*a* and rates of initial charge separation (ETR_{RCII}) are not affected by Cu limitation? The answer to this question has multiple components: first, the ETR per reaction centre (ETR_{RCII}) is not impaired, but given that the overall concentration of PSII decreases 2-fold, overall cellular ETR_{RCII} also decreases; second, a higher fraction of absorbed light energy is dissipated as heat, as suggested by a) the 4-fold increase in NPQ_{NSV} (as an estimate of how much excess excitation energy is dissipated as heat, ultimately relieving excitation energy from PSII), b) the 53% decrease in the efficiency of excitation energy capture by the fraction of open RCII (F_v'/F_m') and c) the 63% decrease in overall quantum efficiency of photochemical energy conversion in PSII (Fq'/Fm', $\varphi'_{PSII,}$ is the

fraction of the primary stable electron acceptor Q_A in the oxidized state, hence ready to participate directly in ETR) (Table A.2). So even though the abundance of cellular RC_{PSII} is decreased, the cells are able to modulate the amount of excitation energy reaching the functional RC_{PSII} in a way that ETR_{RCII} is not greatly impaired. The slight 17% reduction in photochemical quenching (Fq′/Fv′) indicates a small increase in the reduction level of the photosynthetic electron transport chain, pointing towards the potential of increased ROS production and the need for other electron sinks (as discussed above). In summary, this suggests that TO03 copes with low Cu by dissipating an increased fraction of the absorbed light as heat, thus modulating the amount of excitation energy reaching functional RCII, such that the ETR_{RCII} is not greatly impaired.

3.5 Conclusion

The physiological adaptations of diatoms to cope with Cu limitation are largely unknown. In the present study, we investigated the response to Cu limitation in two strains of the model open ocean diatom *T. oceanica* (CCMP 1003 and CCMP 1005), focusing on physiological and proteomic changes in the photosynthetic apparatus. Our results show remarkable differences between the adaptations of TO05 and TO03 to low Cu, highlighting significant intraspecific variations. In essence, TO03 seems to be able to grow more efficiently under extremely low Cu by decreasing its most abundant Cu-containing protein, plastocyanin, an essential electron carrier between its PSII and PSI. However, decreasing plastocyanin levels promotes a bottleneck in the linear electron transport between PSII and PSI, which increases excitation energy in the pigment antennae and enhances susceptibility to photodamage by the production of ROS. The increased susceptibility to photodamage is counteracted by a) reconstructing the light harvesting antennae

(i.e. increasing the ability for photoprotective heat dissipation of absorbed light energy in the pigment antenna), b) decreasing the ETC components prior to plastocyanin (i.e. PSII, cytb_6f) to balance the flow of electrons through the ETC, c) increasing the ETC components counteracting ROS (i.e. Fdx, FNR), and d) using other sinks and pathways for excess e^- (i.e. CET_{PSII}, PTOX, photorespiration). Together, these biochemical shifts explain the observed changes in physiology, such as a) decreased oxygen evolution, carbon fixation, photosynthetic quotient, F_v/F_m and b) increased cellular Chl*a*, σ_{PSII}, and the conversion factor between ETR_{PSII} and carbon fixation. Therefore, even though the physiological response of TO03 (*e.g.* C-fixation rate or growth rate) to low Fe is similar to that of low Cu, this study shows that the underlying restructuring of the photosynthetic apparatus is markedly different for diatoms exposed to low Cu versus low Fe.

One has to be cautious, though, when trying to draw conclusions from one diatom to all. As presented here, a different strain of the same species, TO05, has a vastly different response to low Cu: it reduces its cellular protein content by half, without changing the relative concentration of certain expected proteins, such as the Cu-containing ones. Thus, TO05 seems unable to modulate a concerted response to low Cu and is unable to grow at Cu concentrations where TO03 thrives.

Strong evidence for Cu limitation of phytoplankton in the ocean is presently lacking. However, based on our data, the concentrations of Cu in some oceanic regions are sufficiently low (e.g. 0.5 nM in the North Pacific Bruland and Franks 1983) to result in sporadic Cu limitation of phytoplankton growth. For example, in regions with Cu concentrations less than 1 nM, large phytoplankton may experience Cu limitation (due to their low surface area to volume ratio). In addition, phytoplankton in Fe limited regions may experience co-limitation by Fe and

Cu, as shown by Semeniuk et al. (2009). Given our results, similarly to Fe, Cu limitation is likely to negatively affect C export to the ocean interior. Additionally, in response to low Cu, the potentially significant increase in the proposed DLHC, which do not participate in energy capture for carbon fixation, might bias global estimates of primary productivity based on satellite-derived Chl*a* fluorescence.

3.6 Tables and figures

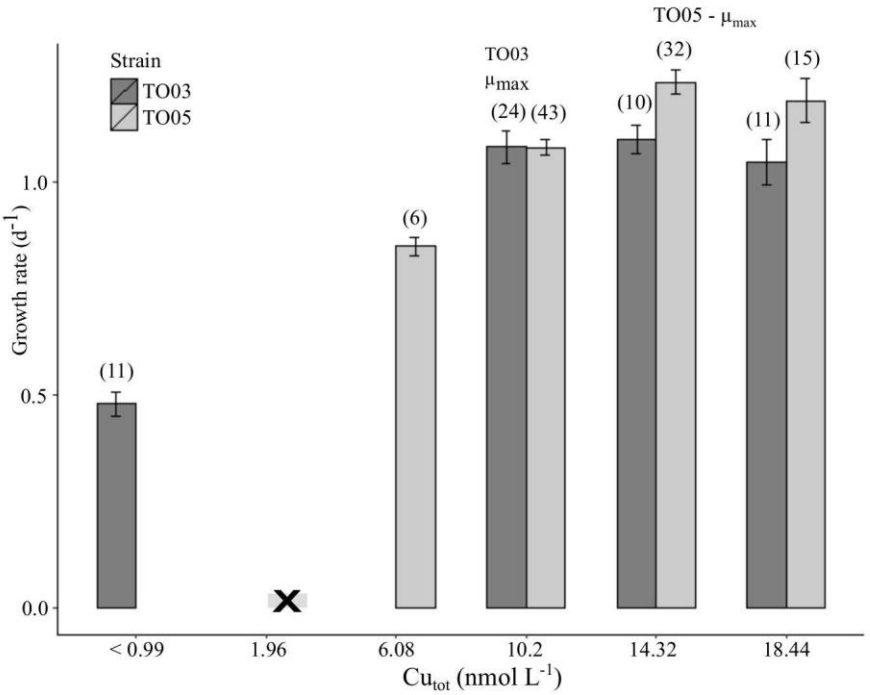

Figure 3.1. Copper-dependent growth rates of *Thalassiosira oceanica* TO03 and TO05. Mean values ± standard error are shown; numbers of biological replicates (n) are indicated in brackets. Note that TO05 was not able to grow under 1.96 nM Cu in the medium (indicated by X in the graph). Given the scope of this study, TO03 was not grown under 1.96 nM or 6.08 nM, as it was able to grow under Cu concentrations <1 nM.

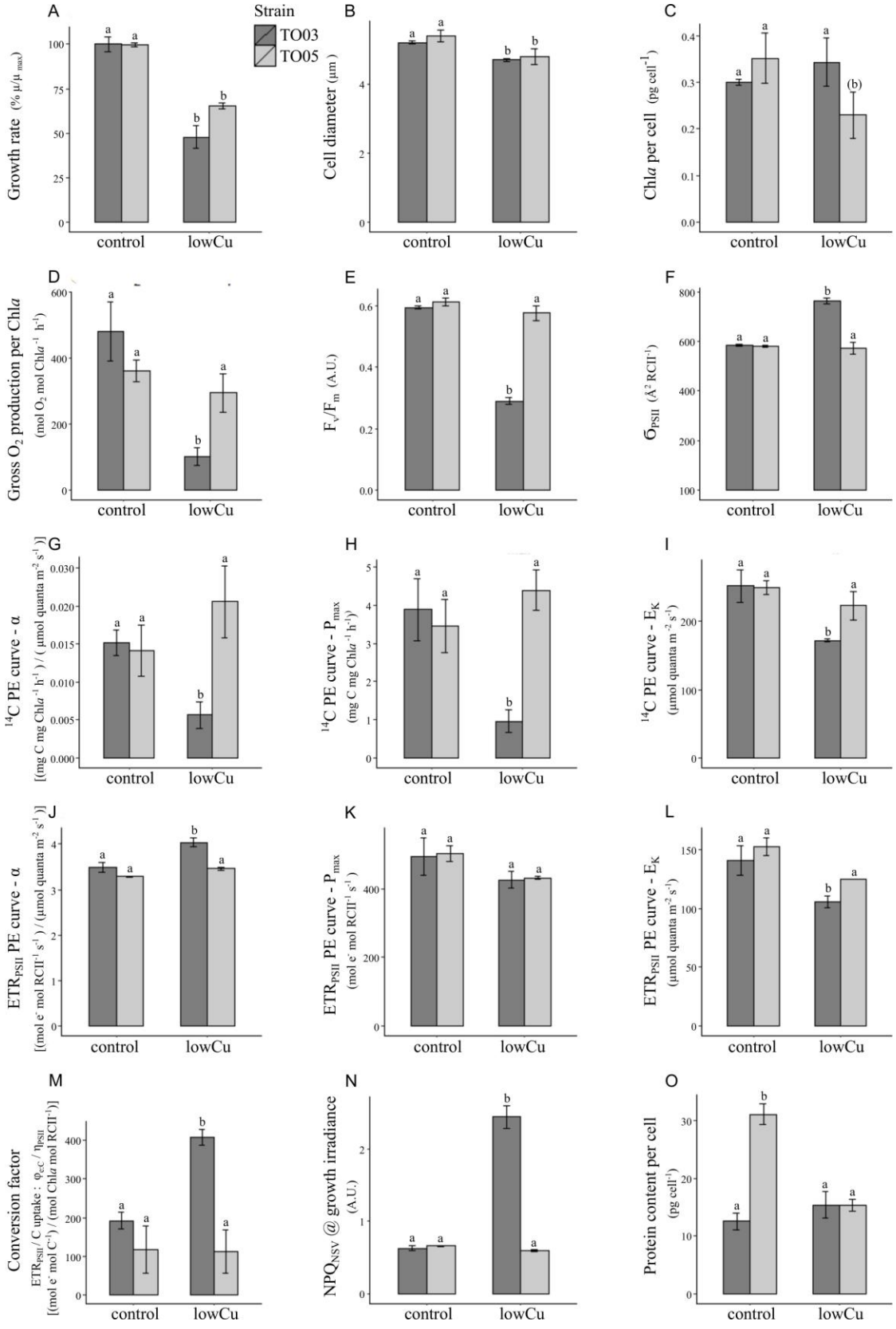
A
Strain
TO03
TO05
Growth rate (% μ/μ_{max})
B
Cell diameter (µm)
C
Chl*a* per cell (pg cell^{-1})
D
Gross O_2 production per Chl*a* (mol O_2 mol Chl*a*$^{-1}$ h^{-1})
E
F_v/F_m (A.U.)
F
σ_{PSII} (Å^2 RCII^{-1})
G
^{14}C PE curve - α [(mg C mg Chl*a*$^{-1}$ h^{-1}) / (µmol quanta m^{-2} s^{-1})]
H
^{14}C PE curve - P_{max} (mg C mg Chl*a*$^{-1}$ h^{-1})
I
^{14}C PE curve - E_K (µmol quanta m^{-2} s^{-1})
J
ETR_{PSII} PE curve - α [(mol e$^-$ mol RCII^{-1} s^{-1}) / (µmol quanta m^{-2} s^{-1})]
K
ETR_{PSII} PE curve - P_{max} (mol e$^-$ mol RCII^{-1} s^{-1})
L
ETR_{PSII} PE curve - E_K (µmol quanta m^{-2} s^{-1})
M
Conversion factor ETR_{PSII} / C uptake : $\varphi_{e:C}$ / η_{PSII} [(mol e$^-$ mol C^{-1}) / (mol Chl*a* mol RCII^{-1})]
N
NPQ_{NSV} @ growth irradiance (A.U.)
O
Protein content per cell (pg cell^{-1})
control
lowCu

Figure 3.2. The effects of Cu limitation on growth rate, cell diameter, protein content and a series of photophysiological parameters in two strains of *T. oceanica*. 2A-C, growth rate, cell diameter, and Chl*a* per cell, respectively; **2D-F**, gross oxygen production, F_v/F_m, and the absorption cross section of PS II antennae, respectively; **2G-I,** 14C PE curve parameters α, P_{max}, and E_K, respectively; **2J-L**, ETR_{PSII} PE curve parameters α, P_{max}, and E_K, respectively; **2M-O**, conversion factor, NPQ_{NSV}, and cellular protein content, respectively. The values are mean ± std. error of three biological replicates. Differing letters above bars represent statistically significant changes (p<0.05) using a 2-way ANOVA with post-hoc interaction analysis (see methods for details). Note that both strains have the same physiological responses under metal replete conditions. Under low Cu conditions, only growth rate and cell size are significantly reduced in the same manner in both strains.

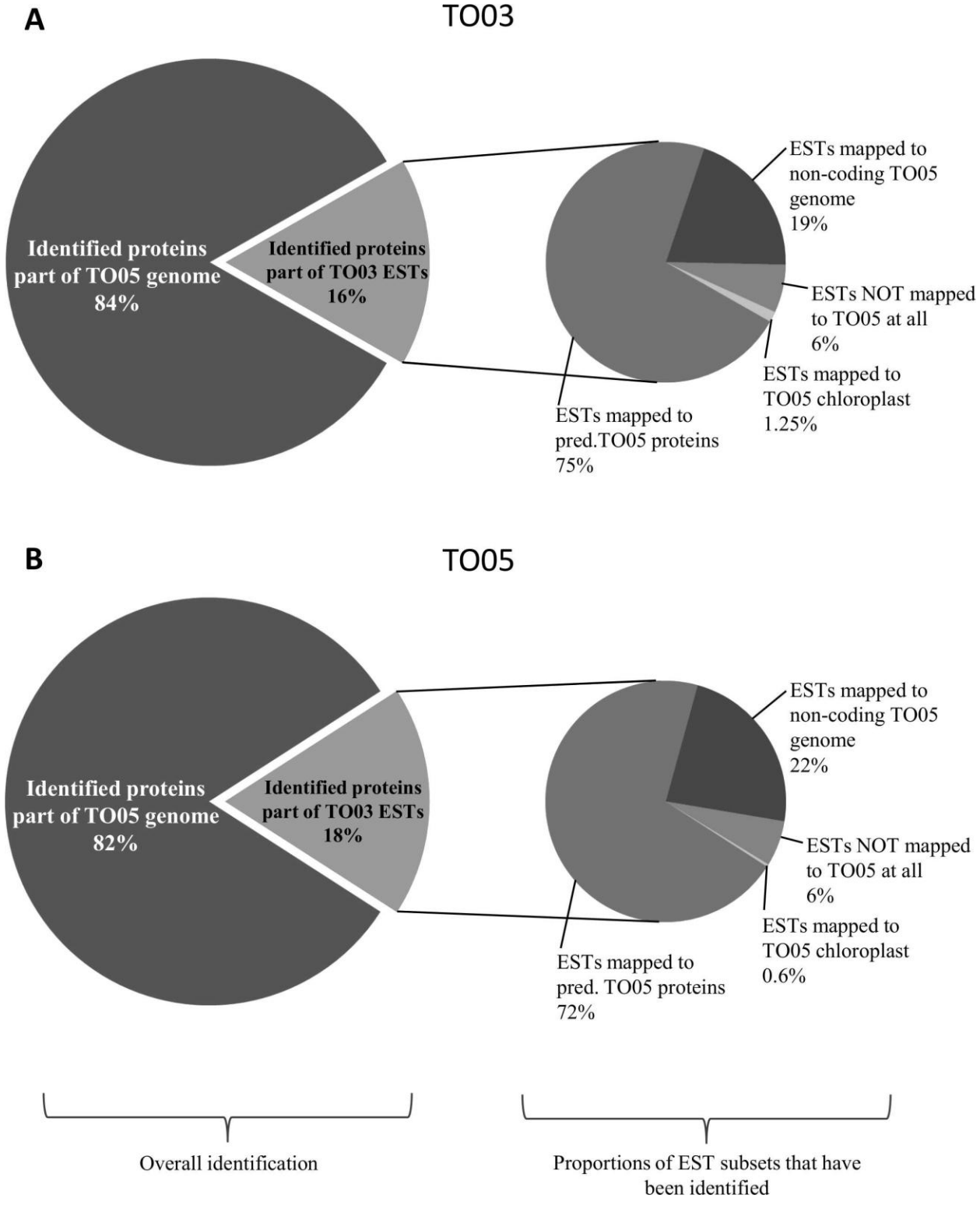
A
TO03
Identified proteins part of TO05 genome 84%
Identified proteins part of TO03 ESTs 16%
ESTs mapped to non-coding TO05 genome 19%
ESTs NOT mapped to TO05 at all 6%
ESTs mapped to TO05 chloroplast 1.25%
ESTs mapped to pred.TO05 proteins 75%
B
TO05
Identified proteins part of TO05 genome 82%
Identified proteins part of TO03 ESTs 18%
ESTs mapped to non-coding TO05 genome 22%
ESTs NOT mapped to TO05 at all 6%
ESTs mapped to TO05 chloroplast 0.6%
ESTs mapped to pred. TO05 proteins 72%
Overall identification
Proportions of EST subsets that have been identified

Figure 3.3. Comparison between EST-mapped proteomics datasets of TO03 and TO05, emphasizing the similarity in their genomes. A) Results for TO03 (plusEST). B) Results for TO05 (plusEST). The left side of the panel shows the proportion of identified predicted proteins coming from the TO05 genome *vs.* the TO03 transcriptome (ESTs). The right side of the panel shows the proportion of the different types of ESTs that have been mapped by the peptides coming from the LC-MS/MS. Even though we used the combined database including all known TO05 and TO03 predicted proteins, neither strain shows bias towards its own subset of proteins.

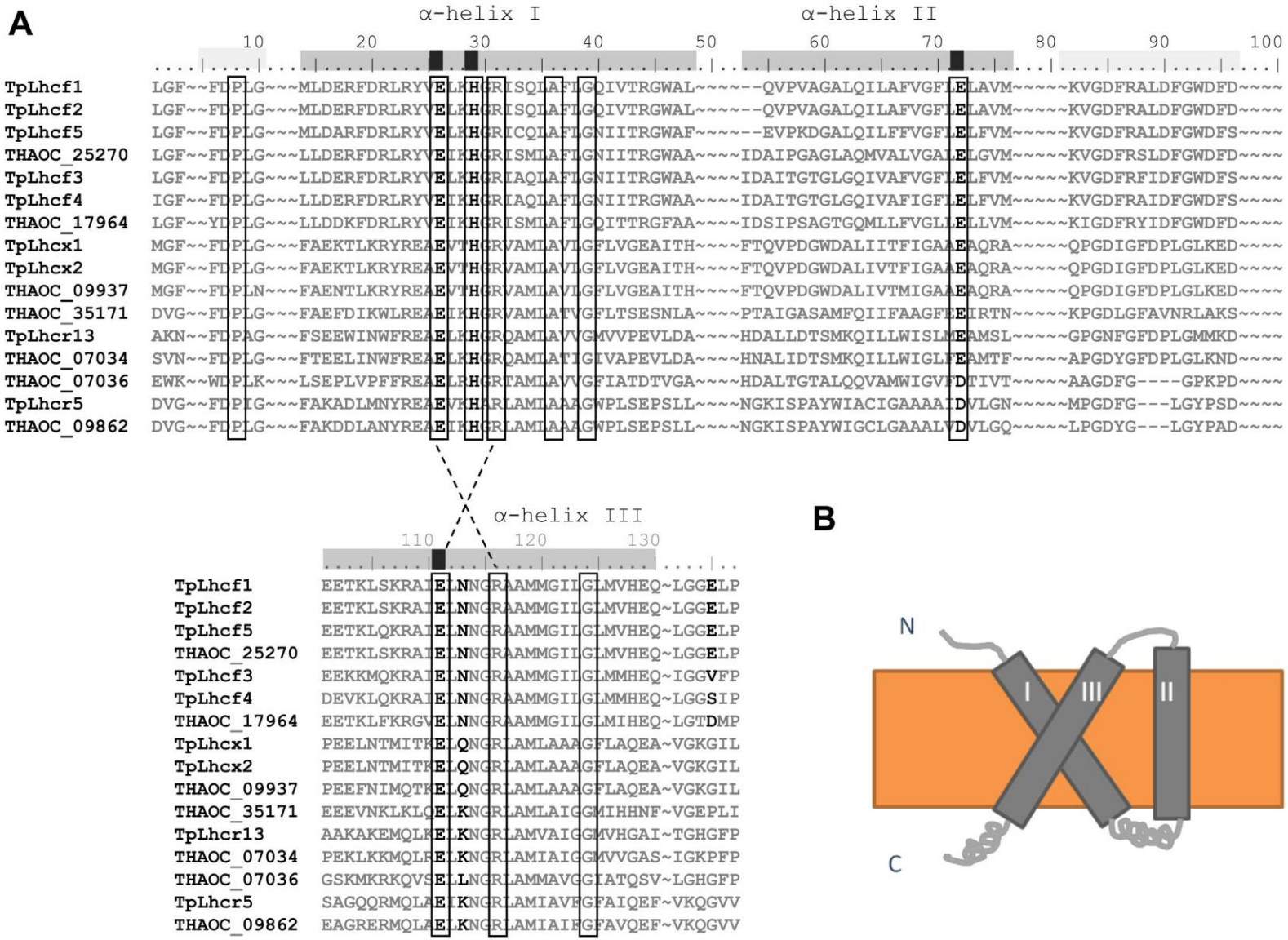
A
α-helix I
α-helix II
α-helix III
TpLhcf1
TpLhcf2
TpLhcf5
THAOC_25270
TpLhcf3
TpLhcf4
THAOC_17964
TpLhcx1
TpLhcx2
THAOC_09937
THAOC_35171
TpLhcr13
THAOC_07034
THAOC_07036
TpLhcr5
THAOC_09862
B
N
C
I
III
II

Figure 3.4. A) Representative sequence alignment of predicted LHCs from *Thalassiosira oceanica* (THAOC, CCMP 1005) and *T. pseudonana* (Tp, CCMP 1335): boxes indicate conserved residues; dotted lines show linkage between helix I and III; bold residues are predicted binding sites for Chl molecules. **B) Cartoon of the predicted general LHC structure** (grey) comprised of three membrane-spanning helices within the thylakoid membrane (orange) and the lumenal N-terminus and stromal C-terminus (Liu et al. 2004).

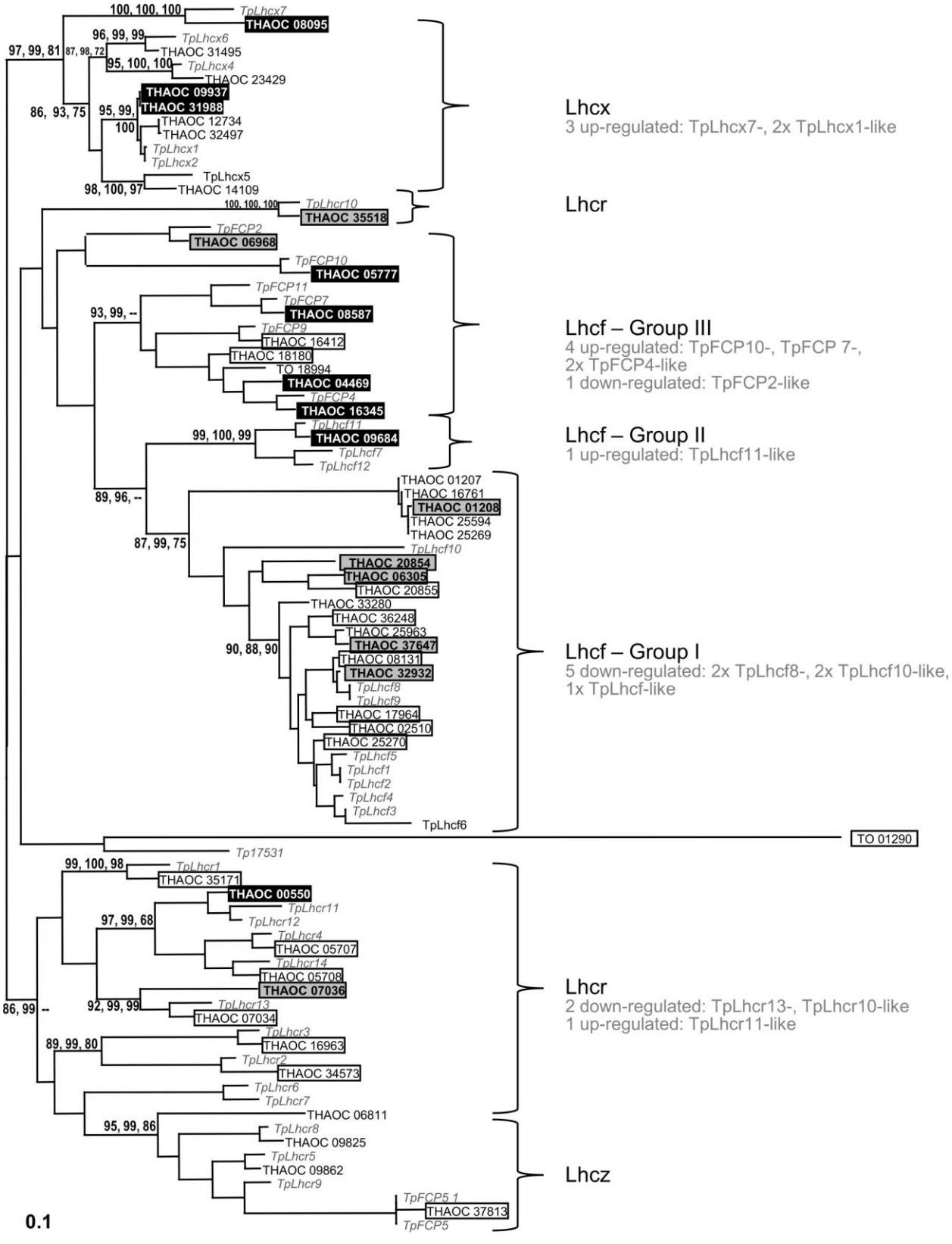
100, 100, 100
TpLhcx7
THAOC 08095
96, 99, 99
TpLhcx6
97, 99, 81
87, 98, 72
THAOC 31495
95, 100, 100
TpLhcx4
THAOC 23429
THAOC 09937
86, 93, 75
95, 99,
THAOC 31988
THAOC 12734
100
THAOC 32497
TpLhcx1
TpLhcx2
TpLhcx5
98, 100, 97
THAOC 14109
Lhcx
3 up-regulated: TpLhcx7-, 2x TpLhcx1-like
100, 100, 100
TpLhcr10
THAOC 35518
Lhcr
TpFCP2
THAOC 06968
TpFCP10
THAOC 05777
TpFCP11
TpFCP7
93, 99, --
THAOC 08587
TpFCP9
THAOC 16412
THAOC 18180
TO 18994
THAOC 04469
TpFCP4
THAOC 16345
Lhcf – Group III
4 up-regulated: TpFCP10-, TpFCP 7-,
2x TpFCP4-like
1 down-regulated: TpFCP2-like
TpLhcf11
99, 100, 99
THAOC 09684
TpLhcf7
TpLhcf12
Lhcf – Group II
1 up-regulated: TpLhcf11-like
THAOC 01207
THAOC 16761
89, 96, --
THAOC 01208
THAOC 25594
THAOC 25269
87, 99, 75
TpLhcf10
THAOC 20854
THAOC 06305
THAOC 20855
THAOC 33280
THAOC 36248
THAOC 25963
90, 88, 90
THAOC 37647
THAOC 08131
THAOC 32932
TpLhcf8
TpLhcf9
THAOC 17964
THAOC 02510
THAOC 25270
TpLhcf5
TpLhcf1
TpLhcf2
TpLhcf4
TpLhcf3
TpLhcf6
Lhcf – Group I
5 down-regulated: 2x TpLhcf8-, 2x TpLhcf10-like,
1x TpLhcf-like
TO 01290
Tp17531
99, 100, 98
TpLhcr1
THAOC 35171
THAOC 00550
TpLhcr11
97, 99, 68
TpLhcr12
TpLhcr4
THAOC 05707
TpLhcr14
THAOC 05708
THAOC 07036
86, 99 --
92, 99, 99
TpLhcr13
THAOC 07034
TpLhcr3
89, 99, 80
THAOC 16963
TpLhcr2
THAOC 34573
TpLhcr6
TpLhcr7
THAOC 06811
95, 99, 86
TpLhcr8
THAOC 09825
TpLhcr5
THAOC 09862
TpLhcr9
Lhcr
2 down-regulated: TpLhcr13-, TpLhcr10-like
1 up-regulated: TpLhcr11-like
TpFCP5.1
THAOC 37813
TpFCP5
Lhcz
0.1

Figure 3.5. Phylogenetic tree of 48 predicted LHCs from the *T. oceanica* genome (CCMP 1005) aligned with 41 LHCs from *T. pseudonana* (CCMP 1335). Boxed THAOC LHCs have been identified at the protein level in this study. LHCs in grey shaded boxes with bold, black letters are significantly down-regulated and those in black shaded boxes with bold, white letters are significantly up-regulated in response to low Cu in TO03. The only significantly regulated LHC in TO05 is THAOC_08587 (up), which aligns closest to TpFCP7 (Table 2). Numbers on nodes are based on PhyML alertSH, aBayes, and standard bootstrap (100 replicates) and are expressed as percentages. Bootstrap values below 65% are not shown.

Table 3.1. Overview of expression of all putative LHCs in both strains of *T. oceanica.*

clade	predicted	TO03 expressed[b]	TO05 expressed[b]	TO03 up[c]	TO03 down[c]
All	48	30	32	9	8
Lhcf - Group I	17	10	10	-	5
Lhcf - Group II	1	1	1	1	-
Lhcf - Group III	9	7	8	4	1
Lhcr	10	9	9	1	2
Lhcx	8	3	3	3	-
Lhcz	2	-	-	-	-
17531	1	-	1	-	-

[a]clade assignment as per phylogenetic tree (Figure 3.5)

[b]for full list of expressed LHCs see Table A.3

[c]up/down refers to significant differential expression as defined in methods

Table 3.2. Significantly differentially expressed LHCs under chronic low Cu conditions.

clade[a]	gene name (NCBI)	closest homolog in Tp[a]	TO03 sig regulated[b]	TO05 sig regulated[b]	Evidence for role in other diatoms
Lhcf - Group I	THAOC_06305	TpLhcf	-10. 34[c]		light harvesting
	THAOC_20854	TpLhcf	-5. 56		light harvesting
	THAOC_01208	TpLhcf	-2. 79		
	THAOC_32932	TpLhcf8	-2. 12		light harvesting, trimers, oligomers[d]
	THAOC_37647	TpLhcf	-2. 04		
Lhcf - Group II	THAOC_09684	TpLhcf11	4. 83		
Lhcf - Group III	THAOC_06968	TpFCP2	-2.52		in TP tightly bound to PSI[e]
	THAOC_04469	TpFCP4	2. 06		
	THAOC_05777	TpFCP10	2. 40		
	THAOC_16345	TpFCP4	2. 68		
	THAOC_08587	TpFCP7	2. 79	2. 07	close to haptophyte LHCs[e]
Lhcr	THAOC_07036	TpLhcr13	-6. 57		PS I light harvesting[f, g, h]
	THAOC_35518	TpLhcr10	-2.55		PS I light harvesting[g, i]
	THAOC_00550	TpLhcr11	2. 39[c]		PS I light harvesting[g, i]
Lhcx	THAOC_08095	TpLhcx7	2. 76[c]		
	THAOC_09937	TpLhcx1	3. 29		photoprotection, stress response, associated with both PSI + II, FCP trimers, oligo, or only loosely associated with the membrane, facilitates NPQ [g, i, j, k, l]
	THAOC_31988	TpLhcx1	3. 29		

Tp, *Thalassiosira pseudonana*

[a]as per phylogenetic tree (Figure 3.5)

[b]significant differential expression in original dataset as defined in methods, given in fold-change

[c]significant differential expression in EST dataset as defined in methods, for Table showing all expressed LHCs and including differential expression in both original and EST datasets, see Table A.3

[d](Nagao et al. 2013)

[e](Hoffman et al. 2011)

[f](Zhu and Green 2010)

[g](Grouneva et al. 2011)

[h](Ikeda et al. 2013)

[i](Gundermann and Büchel 2014)

[j](Zhu and Green 2010)

[k](Green 2007)

[l](Koziol et al. 2007)

Table 3.3. Differential expression of proteins involved in the photosynthetic electron transport chain (ETC) in response to chronic Cu limitation in *T. oceanica*.

			differential expression[a,b]		
Part of	**gene name (NCBI)[a]**	**Protein Description[a]**	**TO03**	**TO05**	**where encoded**
PS II	THAOC_34020	psb27-like, involved in Mn cluster formation	1. 73	1	Nuc
	psbA	psbA, photosystem II protein D1	-1. 92	-1. 03	C
	psbB	psbB, photosystem II CP47 reaction center protein	-1. 61	-1. 1	C
	psbC, THAOC_26185	**psbC, photosystem II CP43 reaction centre protein**	**-2. 1**	1. 05	C
	psbD, THAOC_24371	**psbD, photosystem II D2 protein**	**-2. 1**	-1. 01	C
	psbE, THAOC_24363	**psbE, cytochrome b559 subunit alpha**	**-2. 25**	-1. 21	C
	psbH	psbH, photosystem II reaction centre protein H		-1. 49	C
	THAOC_03193	psbO, Mn-stabilizing protein	-1. 41		Nuc
	THAOC_15373	psbP, oxygen-evolving enhancer protein 2 (OEE2)		-1. 03	Nuc
	THAOC_08500	**psbQ, oxygen-evolving enhancer protein 3 (OEE3)**	**-2. 96**		Nuc
	THAOC_09685	psbU-like, small extrinsic protein	1. 62	1. 32	Nuc
	psbV, THAOC_30541	psbV, cytochrome c-550	1. 07	1. 18	C
	psbY	psbY, photosystem II protein Y		-1. 11	C
PET	petA	petA, cytochrome f	-1. 63	-1. 11	C
	petB, THAOC_26188	**petB, cytochrome b6**	**-2. 33**		C
	THAOC_33417	petC, Fe-S subunit (Rieske protein)	-1. 51		Nuc
	petD, THAOC_24366	petD, cytochrome b6-f complex subunit 4		1. 1	C
	THAOC_29732	**petE, plastocyanin**	**-4. 41**	1. 31	Nuc
PS I	psaA	psaA, photosystem I P700 chlorophyll *a* apoprotein A1	-1. 21	1. 14	C
	psaB	psaB, photosystem I P700 chlorophyll *a* apoprotein A2	1. 11	1. 01	C

			differential expression[a,b]		
Part of	**gene name (NCBI)[a]**	**Protein Description[a]**	**TO03**	**TO05**	**where encoded**
	psaC	psaC, photosystem I iron-sulfur center	-1. 18	1. 2	C
	psaD, THAOC_24369	psaD, photosystem I reaction centre subunit II	1. 2	1	C
	psaF	psaF, photosystem I reaction centre subunit III	-1. 2	1. 04	C
	THAOC_24361	psaL, photosystem I reaction centre subunit XI	-1. 56	-1. 02	C
PET	**THAOC_25559**	**petF, ferredoxin**	**43. 79**	-1. 1	Nuc
	THAOC_36724	**petH, FNR - ferredoxin--NADP+ reductase**	**2. 47**		Nuc
	THAOC_06509	petH - FNR - ferredoxin--NADP+ reductase		-1. 13	Nuc

PSII, photosystem II; PET, photosynthetic electron transport; PSI, photosystem I, Nuc, nucleus; C, chloroplast

[a]content in bold indicates significantly differentially expressed proteins in TO03, as defined in methods

[b]differential expression given in fold-change of the original dataset; for Table including differential expression in EST dataset, see Table A.4

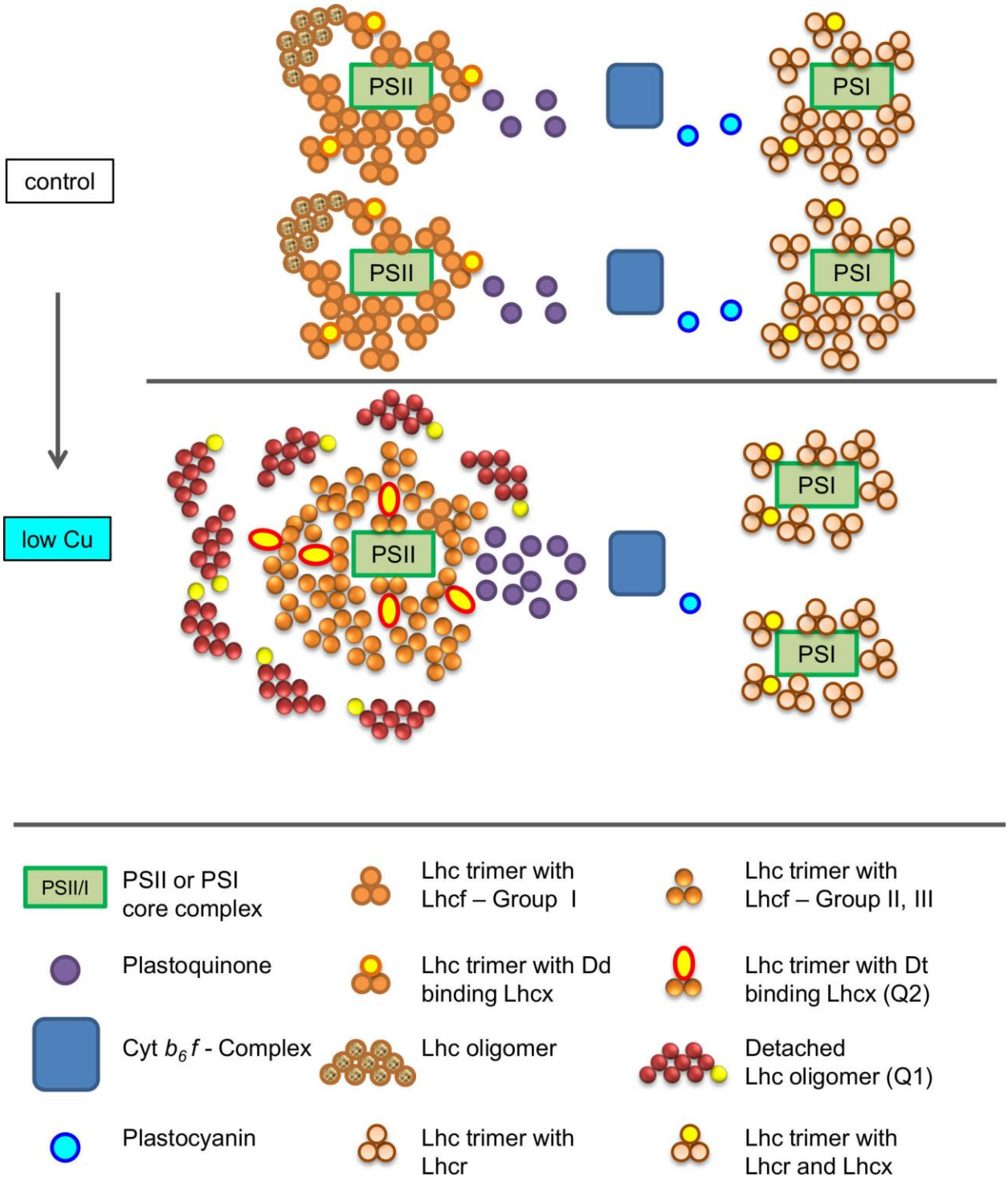
control
low Cu
PSII
PSI
PSII
PSI
PSII
PSI
PSI
PSII/I
PSII or PSI
core complex
Plastoquinone
Cyt b_6f - Complex
Plastocyanin
Lhc trimer with
Lhcf – Group I
Lhc trimer with Dd
binding Lhcx
Lhc oligomer
Lhc trimer with
Lhcr
Lhc trimer with
Lhcf – Group II, III
Lhc trimer with Dt
binding Lhcx (Q2)
Detached
Lhc oligomer (Q1)
Lhc trimer with
Lhcr and Lhcx

Figure 3.6. Model of the changes of the photosynthetic apparatus in *T. oceanica* (CCMP 1003) in response to growth in the presence of low Cu compared to optimal Cu levels (control). In the process of acclimation to low Cu concentration, several structural rearrangements take place in the photosynthetic apparatus allowing maximal photosynthetic efficiency and minimal photoinhibition. In our model, the represented changes in the numbers of LHCs, protein complexes and electron carriers are a reflection of the changes we observed in the proteomic data (see Figure 3.3 for details): Overall cellular concentrations of proteins associated with PSII, and the photosynthetic electron transport chain (PSII, cytb_6f complex and plastocyanin) decrease, whereas those associated with PSI, remain unchanged, and the size of the plastoquinone pool increases. In general, cellular Chl*a* concentration stays constant with an increase in the absorption cross section σ_{PSII}. NPQ_{NSV} increases dramatically as reflected in both a) quenching sites Q1 and Q2 located in detached oligomers (DLHCs) and b) trimers with diatoxanthin (Dt) binding Lhcx that are bound to PSII, respectively (NPQ response adapted from Goss and Lepetit 2015). Approximate pigment content per LHC monomer is 8 Fucoxanthin, 4-6 Chla, 2 Chl*c* (as per Premvardhan et al. 2010). For more details see "3.4.2 Proteomic shift within the photosynthetic apparatus in TO03" in the discussion.

Chapter 4: Proteomic Analysis Revealed the Intricate Interaction Between the Carbon and Nitrogen Metabolisms in Copper-Limited *T. oceanica*

4.1 Summary

Diatoms are one of the most successful phytoplankton groups in our oceans. Their phylogenetic history lead to a chimaeric genome with genes derived from the green lineage, red lineage, bacteria and heterotrophs. Furthermore, the sequential endosymbiosis events lead to an increased set of isoenzymes that can be regulated in very distinct ways and that are targeted to either the same or different cellular compartments. It gave also rise to novel interactions between metabolic pathways. In Chapter 3, I presented how Cu limitation affected the photosynthetic apparatus in *T. oceanica* (CCMP 1003), leading to the up-regulation of ferredoxin (Fdx) and ferredoxin:$NAD(P)^+$ reductase (FNR) and to a potential overreduction of the photosynthetic electron transport chain. In order to elucidate how the rest of the cellular metabolism changes to help alleviate the stresses incurred by low Cu (i.e. overreduction and the potentially ensuing reactive oxygen species), I probed the proteomic datasets and identified proteins involved in various carbon, nitrogen and stress-related metabolic pathways. Furthermore, due to the high amount of isoenzymes, I predicted their respective cellular localization by a combination of a) their homologies to known proteins in other diatoms and b) the use of various targeting softwares. I created metabolic pathway maps illustrating changes in their regulation and highlighting their integrated response to Cu limitation, including 1) nitrogen metabolism – photosynthesis: preferential up-regulation of ferredoxin-dependent isoenzymes in nitrogen metabolism; 2) nitrogen metabolism – reactive oxygen species (ROS) fighting: up-regulation of glutamate and cysteine synthase to support glutathione production to counteract ROS; 3)

photosynthesis – malate shunt: up-regulation of the malate-shunt to channel excess electrons from the chloroplast to the mitochondria; 4) photosynthesis – glycolysis: differential regulation of glycolytic enzymes to channel electrons from the chloroplast to the mitochondria and increase ATP levels in the chloroplast; and 5) malate shunt – citrate cycle – urea cycle – glycolysis: the interconnectedness among these metabolic pathways is enhanced under lowCu, whereby carbon skeletons and reducing equivalents are channeled in a directed manner to meet the cellular needs. Differences between the two strains and other published nutrient limitations are discussed.

4.2 Introduction

Diatoms form an integral part of our oceans, influencing nutrient cycling and productivity of many marine food webs (Armbrust 2009). Annually, marine diatoms fix as much carbon dioxide through photosynthesis as all terrestrial rainforests combined (Nelson et al. 1995; Field et al. 1998), thus having a significant impact on atmospheric CO_2 levels and global climate. Diatoms have a complex evolutionary history, resulting in a mosaic genome with genes derived from the original heterotrophic eukaryotic host cell, the engulfed green and red algal endosymbionts, as well as genes from bacterial horizontal gene transfer (Armbrust et al. 2004; Bowler et al. 2008; Finazzi et al. 2010). Their complex genomic make-up is reflected in several key features, including four membranes surrounding their chloroplast and having multiple isoenzymes in various metabolic pathways, especially in their carbon metabolism (Kroth et al. 2008; Gruber et al. 2009; Smith et al. 2012; Gruber and Kroth 2014). It is not yet well understood how the gene products of the acquired genes from various organisms are targeted into the various cellular compartments of the new host cell, especially for those targeted to the chloroplast with its four membranes.

In diatoms, multiple isoenzymes have also led to new locations for these enzymes and novel interactions among metabolic pathways, compared to green algal and animal ancestors (Allen et al. 2011; Gruber and Kroth 2017). For example, in animals, the complete set of proteins involved in glycolysis is located in the cytosol, whereas in green algae, the first half of glycolysis (glucose to glyceraldehyde-3-phosphate, GAP) is located in the chloroplast and the second half (GAP to pyruvate) in the cytosol. In diatoms, an almost complete set of glycolytic proteins is found in both the cytosol and the chloroplast, with an additional set of proteins from the second half of glycolysis located in the mitochondria (Kroth et al. 2008; Smith et al. 2012). Furthermore,

proteins involved in the ancient Entner-Dourodoff pathway, which is predominantly restricted to prokaryotes and catabolizes glucose to pyruvate using distinct enzymes, have also been identified in diatom genomes and are targeted to the mitochondria (Fabris et al. 2012). The expanded repertoire of isoenzymes in diatoms, both within one and/or across compartments, enables them to meet their metabolic needs (Allen et al. 2012; Smith et al. 2012; Gruber and Kroth 2014).

Underlining the mosaic nature of diatom genomes, Allen et al. (2012) showed that the genome of *P. tricornutum* encodes no less than five different fructose-bisphosphate aldolase (FBA) isoenzymes (three targeted to the chloroplast and two to the cytosol). Each FBA has its own phylogenetic history and is potentially involved in either carbon fixation in the Calvin-Benson-Bassham cycle or glycolysis. These FBAs are derived from a) their green and red algal ancestors, as well as the heterotrophic eukaryotic host cell, b) from bacteria through horizontal gene transfer, and c) from a chromalveolate-specific gene duplication event (Allen et al. 2012). The expression pattern of these five isoenzymes changes depending on the nutritional status of the cell.

One of the most surprising revelations from the sequencing of diatom genomes was the discovery of a complete set of proteins involved in the urea cycle (Armbrust et al. 2004; Allen et al. 2011). In contrast to the catabolic nature of the urea cycle in animals, in diatoms, it is an anabolic process. The urea cycle is an integral part of cellular metabolism and a hub of nitrogen and carbon redistribution within the cell. It is involved in amino acid synthesis, cell wall formation, carbon and nitrogen recycling, and interacts with the citric acid cycle (Armbrust et al. 2004; Allen et al. 2011).

Proteins and/or transcripts of genes involved in nitrogen and carbon metabolism are often differentially regulated under nutrient limitation. So far, studies have focused on adaptations to macronutrient limitation, such as nitrogen, phosphate or the essential micronutrient Fe. In 50% of the ocean, diatoms are limited by nitrate (Moore et al. 2002). However, in over 30% of the ocean, Fe is the limiting resource for phytoplankton (Moore et al. 2004). An intricate relationship between Fe and Cu physiology in diatoms has been shown (Maldonado et al. 2002; Peers and Price 2006; Maldonado et al. 2006; Annett et al. 2008; Guo et al. 2012, Semeniuk et al. 2015) and the possibility of Fe-Cu co-limitation of *in situ* diatoms in low Fe regions has been suggested (Coale 1991; Peers et al. 2005). Despite the importance of Cu in Fe-limited diatoms, our understanding of physiological adaptations to low Cu is limited to a handful of studies (Semeniuk et al. 2015), Semeniuk et al. 2015).

My recent comprehensive investigation on the physiological and proteomic changes to the photosynthetic apparatus in response to chronic Cu limitation in *T. oceanica* revealed both similar and inherently different strategies compared to those observed in response to low Fe (Chapter 3). To better understand how carbon and nitrogen metabolisms are affected and may interact when Cu is limiting, we expanded our probing, using both of our proteomic datasets, as well as the publicly available *T. oceanica* genome. I identified proteins involved in various carbon and nitrogen metabolic pathways (e.g. Calvin-Benson-Bassham cycle, glycolysis, nitrogen acquisition and assimilation, urea cycle, malate shunt, glutathione metabolism), predicted their targeted cellular compartments, and created respective metabolic pathway maps documenting their differential protein expression. In this chapter, I show a striking interaction between carbon and nitrogen metabolisms that potentially alleviates detrimental effects in the photosynthetic apparatus imposed by Cu limitation. This interaction is mediated by the

differential expression of isoenzymes both within and across cellular compartments, ensuring that excess, and possibly damaging, reducing equivalents in the chloroplast are safely removed and/or oxidized.

4.3 Results

I present a brief overview of the two original proteomic datasets (original TO03 and original TO05, as per methods), in which the peptides derived from the mass spectrometry were mapped against the TO05 genome. In order to elucidate the effect of Cu limitation on the carbon and nitrogen metabolisms, I then present all detected proteins involved in the respective key metabolic pathways: Calvin Benson Bassham cycle, glycolysis, citrate cycle, and nitrogen uptake and metabolism, including the urea cycle and proteins involved in glutathione metabolism, redox sensing and protection against ROS. Furthermore, I present data on proteins involved in the putative malate shunt, as well as an overview of the proteins directly involved in pyruvate metabolism and respiration. In line with the effects of Cu limitation on the photosynthetic apparatus described in Chapter 3, TO03 exhibits a far more comprehensive response in carbon and nitrogen metabolism compared with that in TO05. Thus, if not otherwise noted, I will focus on the visualization and description of the TO03 results. Tables will give the information on all relevant proteins across both strains (TO03, TO05), both proteomic searches (original and +EST, as per methods), as well as soluble and insoluble cellular fractions. When referring to proteins, either the official gene names are given, or the organism prefix "THAOC_" is abbreviated to "To". For example, the mitochondrial malate dehydrogenase (MDH) protein, THAOC_03405, will be referred to as To03405. All differential expression data discussed in the text are significantly up- or down-regulated ($p<0.05$), unless otherwise noted.

4.3.1 Overview of proteomic datasets

The proteomic dataset of TO03 encompasses 724 distinctive proteins, whereas in TO05 1,431 were identified. As seen in Figure 4.1**,** 644 proteins were identified in the datasets of both strains. *T. oceanica* (TO03) has three times as many significantly up-regulated proteins (78) than TO05 (28), of which four are shared. *T. oceanica* (TO03) has 45 proteins significantly down-regulated, whereas TO05 has only 5, of which one is shared.

Of the 724 distinctive proteins in TO03, 525 have associated Kegg Orthology (KO) identifiers (Figure 4.2). Overall, half of these (52%) are related to metabolism, 30% to genetic information processing, 10% cellular processes, and 8% to environmental information processing (Figure 4.2A). The proteins involved in metabolism are particularly affected by Cu limitation (Figure 4.2B and C). The general trend of down-regulation of energy metabolism, up-regulation of carbohydrate metabolism, and regulation of amino acid metabolism is illustrated in Figure 4.2D.

4.3.2 Calvin Benson Bassham cycle

Twelve proteins involved in the carbon fixing Calvin Benson Bassham cycle in the chloroplast were identified (Figure 4.3, Table B.1). Glyceraldehyde 3-phosphate dehydrogenase (GAPDH, To13085) and the essential Rubisco activator protein cbbX (To24360) were the only proteins that were down-regulated under Cu limitation (4.7- and 2.3-fold, respectively). In contrast, the Rubisco subunits were not affected (rbcS, rbcL). Similarly, fructose-bisphosphate aldolase, class I (FBA I, To02112), ribose 5-phosphate isomerase (RPI, To31290) and ribulose 5-phosphate epimerase (RPE, To09031) were unaffected. Five proteins were up-regulated: phosphoglycerate

kinase (PGK, To07617) by 6.8-fold, the three triose phosphate isomerase proteins (TPI, To02438, To35826, To32006) by 3.3-, 1.9- and 1.5-fold, respectively, and fructose-bisphosphate aldolase, class II (FBA II, To12069) by 2-fold. In TO05, cbbX and rbcS were 1.3- and 1.6-fold down-regulated, respectively, and only PGK was up-regulated by 3-fold.

4.3.3 Glycolysis

In diatoms, proteins involved in glycolysis are found in all three major cellular compartments. Of the 21 glycolytic proteins identified, seven are cytosolic, nine are targeted to the chloroplast, and five are targeted to the mitochondria (Figure 4.4**,** Table B.3). As described earlier (see methods), targeting was predicted via a combination of targeting software programs (TargetP, ASAFind) and the predicted targeting of the closest diatom homologous proteins (i.e. *T. pseudonana*, Tp; *P. tricornutum*, Pt; and/or *F. cylindricus*, Fc). Of the seven expressed cytosolic proteins, four were not affected by Cu limitation: glucose-6-phosphate isomerase (GPI, To25871), fructose-1,6-bisphosphatase (F2BP, To05494), triose phosphate isomerase (TPI, To21096), and fructose-bisphosphate aldolase, class II (FBA II, To24977). Three proteins were down-regulated: phosphoglucomutase (PGM, To06412) by 3.2-fold, phosphofructokinase (PFK, To16559) by 1.8-fold, and fructose-bisphosphate aldolase, class I (FBA I, To24978) by 1.6-fold (or 2.7-fold considering expression of a contig associated with the same gene). The only cytosolic protein involved in glycolysis that was up-regulated was pyruvate kinase (PK, To34937, by 1.6-fold). In TO05, GPI was up-regulated by 1.5-fold, whereas FBA II and FBA I were down-regulated by 1.3- and 2.4-fold, respectively.

Of the nine expressed proteins targeted to the chloroplast, only fructose-bisphosphate aldolase, class I (FBA I, To02112) was not affected by Cu limitation. Two fructose-bisphosphate

aldolase, class II proteins were up-regulated by 1.4- and 2-fold (FBA II, To00388 and To12069), three triosephosphate isomerase isoenzymes were up-regulated by 3.3-, 1.9-, and 1.5-fold (TPI; To02438, To35926, and To32006, respectively), and phosphoglycerate kinase (PGK, To07617) was up-regulated by 6.9-fold. Glyceraldehyde-3-phosphate dehydrogenase (GAPDH, To13085) and phosphoglycerate mutase (PGAM, To21902) were both down-regulated, by 4- and 2.3-fold, respectively. The up-regulation of TPI combined with a down-regulation of GAPDH could lead to an increase in and subsequent export of triose-compounds out of the chloroplast. Probing the genome for gene models containing a triose phosphate transporter Pfam domain identified seven candidate genes (Table B.2) of which only two were found expressed in TO03 and four in TO05. Of all chloroplast targeted glycolytic proteins in TO05, only FBA I and PGAM were down-regulated by 1.4- and 1.5-fold, respectively, whereas PGK was up-regulated by 3-fold.

Five proteins involved in glycolysis were found to be targeted to the mitochondria. Glyceraldehyde-3-phosphate dehydrogenase (GAPDH, To33331) and enolase (ENO, To34936) were both up-regulated by 3.8- and 1.5-fold, respectively. Phosphoglycerate mutase (PGAM, To08963) was not affected, whereas pyruvate kinase (PK, To07097) was down-regulated by 1.3-fold. The mitochondrial aldolase involved in the ancient Entner-Dourodoff glycolytic pathway, 2-keto-3-deoxy phosphogluconate aldolase (EDA, To10009) was not affected. In TO05 GAPDH was 1.6-fold up-regulated.

4.3.4 Citrate (TCA) cycle

Nine expressed proteins involved in the citrate cycle in the mitochondria were identified (Figure 4.4, Table B.4). Citrate synthase (CS, To19912) abundance did not change in response to low Cu concentrations. Aconitase hydratase (ACO, To20545) and two isocitrate proteins (IDH,

To37807, To34595) were all down-regulated by 4.7-, 3.0-, and 1.6-fold, respectively. Oxoglutarate dehydrogenase E1 component (OGD1, To28027), succinate CoA synthetase (SUCLA, To13425), and fumarate hydratase (FH, To24310) were not affected, whereas malate dehydrogenase (MDH, To03405) was 1.6-fold up-regulated. In TO05, two proteins were up-regulated: IDH by 1.5-fold and SUCLA by 1.6-fold.

4.3.5 Nitrogen metabolism

Twenty-two proteins involved in the urea cycle, nitrogen acquisition and assimilation, as well as four membrane transporters were identified at the proteomic level (Figure 4.5, Table B.5). Of these four transporters, the expression of the formate/nitrate (NiRT, To00240) and the ammonium transporter (AMT, To07247), both putatively located in the chloroplast envelope, were not affected by Cu limitation. However, the urea (URT, To31656) and nitrate/nitrite transporters (NRT, To04919), at the plasma membrane, were both significantly up-regulated (6.9 and 11-fold, respectively). In TO05, both URT and NiRT were up-regulated by 1.3-fold. Interestingly and in contrast to TO03, TO05 had two different isoenzymes of NRT up-regulated in response to low Cu (To01055 and To01056, by 1.7- and 1.6-fold, respectively).

Within the chloroplast, three different nitrite reductases were identified. Of these, the NAD(P)H-dependent isoenzyme was not differentially expressed (NAD(P)H-NiR, To35252), whereas two proteins containing ferredoxin-dependent nitrite reductase domains (Fe-NiR, To00016 and To02363) were up-regulated by 1.3- and 2.6-fold, respectively. Glutamine (GSII, To31900) and glutamate synthases (GOGAT, To13288) were both up-regulated (3.8 and 1.6-fold, respectively). In contrast, aspartate aminotransferase (AAT, To16827) was the only down-

regulated (2.3-fold) protein directly involved in the core nitrogen metabolism within the chloroplast. In TO05, only GS was mildly up-regulated (by 1.3-fold).

In the mitochondria, glutamine synthase (GSIII, To06032) was 5.3-fold down-regulated while glutamate synthase (GOGAT, TO04828) expression did not change. The mitochondrial aspartate aminotransferase (AAT, To15049) was up-regulated by 3.6-fold. Glycine decarboxylase t- and p-proteins (GDCT/P, To17688 and To36273), involved in photorespiration, were not affected by Cu limitation. In TO05, GS was again mildly up-regulated (by 1.4-fold).

In the urea cycle, six proteins were expressed. Five of these were not affected by Cu limitation: carbamoyl phosphate synthase (unCPSIII, To01996), argininosuccinate synthase (AsuS, To37170), argininosuccinate ligase (AsL, To12984), ornithine cyclodeaminase (OCD, To04380), and aspartate carbamoyltransferase (ATCase, To22587). In contrast, ornithine carbamoyltransferase (OTC, To05385) was up-regulated by 1.7-fold. In TO05 AsuS was 1.4-fold up-regulated.

Cytosolic glutamate dehydrogenase (GDH, To06254) was up-regulated by 2.09-fold ($p = 0.05$) and nitrate reductase (NR, To34460) was up-regulated by 1.5-fold. In TO05, GDH was up-regulated by 1.5-fold, while NR was down-regulated by 1.4-fold.

4.3.6 Glutathione metabolism

Glutathione is a small tripeptide (Glu-Cys-Gly) that is involved in redox sensing and counteracting ROS. Twenty-one expressed proteins involved in glutathione metabolism and other antioxidant agents (eg. thioredoxins, glutaredoxins, and superoxide dismutases, SOD) were identified (Figure 4.6, Table B.6). Nine proteins are predicted to be targeted to the chloroplast. The only down-regulated proteins were two chloroplast glutaredoxins (GRX; To07269,

To18234; both by 1.3-fold). In contrast, two chloroplast isoenzymes for cysteine synthase were up-regulated (CYS, To27524 by 2.5-fold, To10442 by 1.5-fold). As mentioned above (section 4.3.5), chloroplast glutamate synthase (GOGAT, To13288) was also up-regulated (by 1.6-fold). Additionally, glutathione synthase (GSS, To04546), glutathione reductase (GR, To07268) and thioredoxin (TXN, To31425) were all up-regulated (by 1.5-, 2.5-, and 1.5-fold, respectively). In addition, the Mn-containing SOD was also up-regulated (MnSOD, To02860 by 1.8-fold). In TO05, only two CYS isoenzymes were up-regulated (To27524 by 1.4-fold; To10442 by 1.3-fold), as well as a TXN (To31425 by 1.6-fold).

Of the seven cytosolic proteins, glutathione-S-transferase (GST, To09062) and TXN (To05213) were significantly up-regulated (by 7.3- and 4.2-fold, respectively). One of the two nickel-dependent SOD isoenzymes was also up-regulated (NiSOD, To10112, by 1.4-fold). Glutamate-cysteine ligase (GCL, To2335) was only identified in one pairing of the biological triplicate, where a differential expression of 4.5-fold was observed. The expression of cytosolic CYS (To05931) did not change upon Cu limitation, whereas the expression of glutamate dehydrogenase (GDH, To06254) increased by 2.1-fold ($p=0.05$, see also section 4.3.5). Interestingly, in TO05, a different isoenzyme of glutathione-S-transferase was significantly up-regulated (GST, To24526, by 2.3-fold). The latter has homologs to other diatom GSTs, whereas the up-regulated GST in TO03 (To09062) has no homolog in diatoms, but closest homologs in the polyp *Hydra vulgaris*, the anemone *Nematostella*, and the brachiopod *Lingula*. Cytosolic TXN and GDH were also up-regulated in TO05 (1.4- and 1.5-fold, respectively).

Only two of the 18 expressed proteins involved in glutathione metabolism are predicted to be targeted to the mitochondria: GRX and TXN. Of these, GRX (To02323) was not differentially

expressed under Cu limitation in TO03, whereas TXN (To13864) was up-regulated by 1.8-fold. In TO05, neither was differentially expressed.

4.3.7 Malate shunt

Six proteins were expressed in TO03 that are involved in the putative malate shunt (Figure 4.7, Table B.7). Three of these are located in the chloroplast and were all differentially expressed in response to low Cu. Whereas both pyruvate carboxylase (PC, To31413) and malate dehydrogenase (MDH, To30817) were up-regulated by 2.6-fold, aspartate aminotransferase (AAT, To16827) was down-regulated by 2.3-fold. In the mitochondria, PC (To19570) was not differentially expressed. Both MDH (To03405) and AAT (To15049) were up-regulated by 1.6- and 3.6-fold, respectively. None of these six proteins were affected in TO05. In fact, neither chloroplast AAT nor mitochondrial MDH have been identified in TO05. However, two putative malate/2-oxoglutarate antiporters have been identified in the TO05 proteome (To27515, To25255) and not in that of TO03. Their expression was not affected by Cu limitation.

4.3.8 Pyruvate metabolism

Pyruvate is a key metabolite at the intersection of, among others, glycolysis/gluconeogenesis, the citrate cycle and fatty acid metabolism. Sixteen proteins involved in pyruvate metabolism were identified (Figure 4.8, Table B.8). In the chloroplast, pyruvate carboxylase (PC, To31413) and malate dehydrogenase (MDH, To30817) were both 2.6-fold up-regulated. Pyruvate dehydrogenase E1 (PDH-E1, To34740) as well dihydrolipoamide dehydrogenase (DLDH, To19934) were not affected by low Cu. None were affected in TO05.

In the cytosol, four of the six expressed proteins were not differentially expressed: PDH-E1 (To08200), PDH-E2 (TO03499), acetyl-CoA synthase (ACAS, To05626), and lactate dehydrogenase (LDH, To33506). Phosphoenolpyruvate carboxylase (PEPC, To00276) was down-regulated by 4.3-fold. Pyruvate kinase (PK, To34937) was up-regulated by 1.6-fold. None were affected in TO05.

In the mitochondria, PC (To19570), DLDH (To30825), and PEPC (To33731) were all unaffected. However, PK (To07097) was 1.3-fold down-regulated and MDH was 1.6-fold up-regulated. In TO05, mitochondrial PEPC (To33731) was the only differentially expressed protein involved in pyruvate metabolism (1.4-fold up-regulated).

4.3.9 Respiration

Five proteins involved in mitochondrial respiration were identified (Table B.9). In TO03, each one was only identified in one of the paired biological triplicates (low Cu / control mix, see Chapter 2) and thus did not result in a significant differential expression ratio (i.e. no *p*-value as illustrated in Figure 2.2). However, NAD(P)H dehydrogenase (NAD(P)H-DH), as well as the three subunits of cytochrome *c* oxidase (cyt*c*) had fold increases indicative of up-regulation: NAD(P)H-DH (To05862) by 1.9-fold, cyt*c* oxidase subunit IV (To04852) by 1.5-fold, the subunit Vb (To22544) by 2.6-fold, and the subunit VIb (To12811) by 4.0-fold. The latter three membrane-bound subunits were identified in the insoluble fraction, as expected. However, the subunits Vb and VIb were also found in the soluble fraction, albeit with down-regulated expression (by 2.2 and 1.2-fold, respectively). Ubiquinol-cyt$_c$ reductase, in the insoluble fraction, was down-regulated by 1.4-fold in the low Cu treatment.

In TO05, subunit IV and Vb were both significantly up-regulated (by 2.0- and 2.1-fold, respectively) in the insoluble fraction. Subunit VIb was only found in the soluble fraction in one of the paired biological triplicates and was not differentially regulated (-1.1-fold). NAD(P)H-DH was up-regulated by 1.4-fold ($p<0.05$) and ubiquinol-cyt*c* reductase by 1.2-fold ($p<0.05$).

4.4 Discussion

In Chapter 3, I presented data implying that in response to low Cu, *T. oceanica* (CCMP1003) restructures the proteins in its photosynthetic electron transport chain, which results in a decrease in carbon assimilation, and an overreduction of the photosynthetic apparatus. Evidence for overreduction of photosynthesis was seen in an increase of the PQ pool size, as well as a reduction in photochemical quenching (F_q'/F_v'). The latter, in particular, indicates an excess of reducing power in the photosynthetic electron transport chain, pointing towards a potential increase in reactive oxygen species (ROS) and the need for additional electron sinks. Furthermore, an ~40-fold increase in ferredoxin (Fd, petF) and 2.5-fold increase in ferredoxin:NAD(P)H oxidoreductase (FNR) was observed. These proteins are potentially important in detoxifying reactive oxygen species. Thus, these combined results suggest that under Cu limitation there is a surplus of both reduced ferredoxin (Fd^{red}) and reducing equivalents in the form of NAD(P)H within the chloroplast. In order for photosynthesis to proceed safely, the cell needs to find a way to re-oxidize these two compounds, as well as counteract the production of potentially harmful ROS.

In this chapter, I describe the interaction between various metabolic pathways and subcellular compartments to facilitate the re-oxidation of Fd^{red}, as well as NAD(P)H in the chloroplast. The interaction among metabolic pathways (e.g. nitrogen assimilation, glycolysis,

citrate and the urea cycle), and the sophisticated coordination between the chloroplast and the mitochondria in TO03, underlines a physiological versatility that is most likely responsible for the environmental success of this genera. At the end of the chapter, I will contrast the response of TO03 and TO05.

In this study, the cells were acclimated to low Cu concentrations for many generations. Hence, the acclimation strategies in their physiology and proteome are not sudden, short-lived stress responses, but rather another 'normal' state for the cell to sustain continual growth under low Cu conditions.

4.4.1 Carbon metabolism – the Calvin-Benson-Bassham cycle is down-regulated via its activase and the reactions of glycolysis are used to redistribute ATP and NAD(P)H within the cell

One of the striking features of diatom genomes is the number of isoenzymes, particularly those involved in carbon metabolism. The differential expression of these isoenzymes is thought to direct the carbon flow within the cell. In this section, I argue that the Calvin-Benson-Bassham cycle is indeed down-regulated, whereas glycolysis is modulated in TO03 to promote ATP and reducing equivalent redistribution among cellular compartments to overcome Cu limitation.

The three most thoroughly annotated diatom genomes to date [*T. pseudonana* (*Tp*), Armbrust et al., 2004; *P. tricornutum* (*Pt*), Bowler et al., 2008; *F. cylindricus* (*Fc*), Mock et al., 2017] revealed a high number of isoenzymes in their respective sequences. However, studies comparing carbon metabolisms among these diatoms have found (Kroth et al. 2008; Smith et al. 2012) that even though there is a big overlap of homologous isoenzymes among them, due to gene loss, duplication, and/or horizontal gene transfer, there are still a significant number of

proteins that are only found in *T. pseudonana* (7), *P. tricornutum* (8), or *F. cylindricus* (11), or are shared between only two of these diatoms (Smith et al. 2012). For example, in *T. pseudonana*, the glycolytic enzyme enolase (ENO) is found in both the mitochondria and the cytosol, whereas *P. tricornutum* and *F. cylindricus* have enolases targeted only to the mitochondria and chloroplasts. In my study, *T. oceanica* has also two enolases but I predicted that both are targeted to the mitochondria (To23624, To34936, Figure 4.4, Table B.3).

Within the chloroplast of diatoms, depending on the specific species, five of the 8-10 proteins involved in glycolysis are also part of the Calvin-Benson-Bassham cycle (Smith et al. 2012). Different isoenzymes might be preferentially involved in glycolysis over carbon fixation, thereby regulating carbon flow. For example, the three plastidial fructose-bisphosphate aldolases (FBAs) in *P. tricornutum* are regulated differently under low *vs.* high Fe conditions (Allen et al. 2012). Strikingly, these FBAs are also targeted to different parts of the chloroplast (Allen et al., 2012, Table 4.2). The two FBAs closely associated with the pyrenoid and β-carbonic anhydrase (FbaC1 and C5) are up-regulated under low Fe in *P. tricornutum.* It is not yet resolved how the segregation of parts of the Calvin Benson Bassham cycle to the pyrenoid is advantageous for the cells (Allen et al. 2012). The third plastidial FBA, FbaC2, on the other hand, is diffusely distributed throughout the chloroplast and is down-regulated (Allen et al. 2012). In contrast, in response to low Cu, the regulation of the three corresponding FBA homologs in TO03 unfolds differently: one of the pyrenoid-associated FBAs is only mildly up-regulated (1.4-fold, FbaC1 homolog, To00388), whereas the expression of the other one remains unchanged (FbaC5 homolog, To02112). On the other hand, the FBA found throughout the chloroplast (FbaC2 homolog, To12069) is up-regulated by 2-fold.

I propose that FbaC2 is preferentially involved in glycolysis over carbon assimilation. Four lines of evidence support this conclusion: (1) carbon assimilation decreased by 66% compared to that in the control conditions (Chapter 3, Table A.2), making it less likely for the proteins involved in this metabolic pathway to be up-regulated; (2) in line with this reasoning, each of the three significantly up-regulated proteins involved in the Calvin-Benson-Bassham cycle can also be part of glycolysis, i.e. PGK, TPI, and FBA; (3) none of the three proteins that are distinct Calvin-Benson-Bassham cycle proteins, i.e. Rubisco, RPI, and RPE, were differentially expressed; (4) the red algal-type Rubisco activase, cbbX, was down-regulated by 2.25-fold. Thus, due to the down-regulation of its activase, even though Rubisco levels are unchanged, half of the Rubisco proteins are not actively involved in carbon fixation (Mueller-Cajar et al. 2011). With a fraction of 2-6% of the total cellular protein content, Rubisco is one of the most abundant proteins in the cell (Losh et al. 2013). This physiological adaptation might seem as a waste of cellular resources. However, as the abundance of RPI and RPE remains constant, it can be expected that these Rubisco proteins have ribulose-bisphosphate already bound and are thereby poised to engage in carbon assimilation anytime. Thus, once nutrient concentrations are more favourable, only the activase, cbbX, needs to be up-regulated and carbon fixation can proceed immediately. This strategy might be advantageous to outcompete other organisms that need more time to respond, especially in environments that are usually nutrient limited and where nutrient-rich conditions are only sporadic and short-lived.

The Calvin-Benson-Bassham cycle is dependent on the balance of ATP/NAD(P)H within the chloroplast and is thus linked to the state of the photosynthetic apparatus. Under Cu limitation, there is a significant electron pressure in the photosynthetic electron transport chain, resulting in excess reducing equivalents in the form of NAD(P)H in the chloroplast. Due to its

dependence on a defined ATP/NAD(P)H ratio, these additional reducing equivalents cannot be re-oxidized in the Calvin cycle. However, I argue that the differential expression of proteins involved in glycolysis can help channel NAD(P)H away from the chloroplast to the mitochondria, while generating ATP in the chloroplast.

In animals, glycolysis is restricted to the cytosol, whereas in green algae, the first half is located in the chloroplast and the second half is found in the cytosol. Thus, finding a subset of glycolytic proteins targeted to the mitochondria in diatoms was unexpected (Bowler et al. 2008). To date, the only known eukaryotes to share this trait are non-photosynthetic, heterokont oomycetes. In general, most reactions facilitated by proteins in glycolysis can proceed in either direction, i.e. glycolysis or gluconeogenesis. Smith et al. (2012) suggested that gluconeogenesis prevails in the mitochondria. However, assuming that the required metabolite transporters are present in the mitochondria (e.g. aspartate/glutamate shuttle, malate/2–oxoglutarate shuttle, citrate/malate shuttle, and fumarate/succinate shuttle), modelling flux balances in *P. tricornutum* predicted that glycolysis would indeed be more favorable in the mitochondria than gluconeogenesis (Kim et al. 2016). Another surprising finding in diatoms was the discovery of the ancient glycolytic Entner-Dourodoff pathway (EDP) in *P. tricornutum* (Fabris et al. 2012). This pathway, predominantly restricted to prokaryotes, generates less ATP than the usual Embden-Meyerhof-Parnas glycolysis pathway (EMPP). But, the EDP requires only two enzymes. Thus, the metabolic cost to sustain this pathway is less than that of EMPP. The EDP pathway generates pyruvate and GAP. The latter can then be metabolized in the mitochondria via the lower part of EMPP glycolysis. One hypothesis is that having multiple glycolytic pathways enables the cells to adapt faster to changing energy status in response to varying nutrient conditions (Fabris et al. 2012). It is worth noting that the involved 2-keto-3-deoxy

phosphogluconate aldolase (EDA, To10009) in the EDP was expressed constitutively in *T. oceanica* (Table B.3) and thus might not be an active component in the adaptation to chronic Cu limitation.

In TO03, in each cellular compartment, different subsets of glycolytic proteins were up- or down-regulated (Figure 4.4). Focusing on the up-regulated proteins only (Figure 4.9A), a pattern emerges revealing a regulation that leads to ATP formation in the chloroplast and cytosol, as well as NAD(P)H release in the mitochondria. In TO03, under low Cu, I have shown that a decreased ATP/NAD(P)H ratio in the plastid is likely. By reducing chloroplast (To13085) and increasing mitochondrial GAPDH (To33331), reducing equivalents are generated in the mitochondria, whereas increasing PGK (To07617) in the chloroplast will increase ATP in this compartment. Interestingly, Hoeckin et al. (2012) postulated for *T. pseudonana* an overall increase in the glycolytic activity when exposed to acute nitrogen starvation. However, when I mapped the involved proteins in *T. pseudonana* to their cellular target compartments (Figure 4.9B), I revealed a targeted regulation of these isoenzymes similar to the response of TO03 grown under chronic Cu limitation (i.e. PK down-regulated in mitochondria and up-regulated in the cytosol). Thus, the coordinated regulation of particular isoenzymes within one metabolic pathway seems to be indeed a general trait in diatoms.

4.4.2 Nitrogen metabolism is essential for Fd^{red} oxidation and glutamate synthesis to fight ROS

Another striking feature in the response to Cu limitation in TO03 was the up-regulation of nitrogen acquisition and assimilation (nitrogen metabolism, Figure 4.5, Table B.5; general overview, Figure 4.10). In contrast, short-term Fe limitation in *P. tricornutum* induced down-

regulation of the transcript levels of various genes involved in nitrogen metabolism: cytosolic nitrate reductase (NR), chloroplast nitrite transporter, chloroplast nitrite reductase, NiR, and chloroplast glutamine synthase, GSII (Allen et al. 2008) and resulted in a 50-fold decrease in NR activity in *T. weissfloggii* (Milligan and Harrison 2000). Furthermore, it has been shown that most of the proteins involved in nitrogen assimilation are redox-sensitive and are down-regulated upon short-term nitrogen limitation.

In *Chlamydomonas*, NR has been shown to be redox-regulated in tandem with carbon fixation via the reductive state of the PQ-pool, with a higher reducing state of the PQ-pool linked to faster carbon and nitrogen assimilation (Giordano et al. 2005). However, the authors suggest that the redox-dependent activity of NR might be one of several components in the complex regulatory network of nitrate assimilation.

In plants, nitrogen assimilation is an important sink for excess reducing equivalents (Hoefnagel et al. 1998). I argue that the up-regulation of nitrate assimilation in TO03 helps the cell to alleviate the stress incurred by low Cu, namely by re-oxidizing Fd^{red} in the chloroplast. This is achieved via differential regulation of only those isoenzymes that use Fd^{red} as their cofactor: of the three chloroplast nitrite reductases (NiR), the expression of the NAD(P)H-dependent NiR abundance stayed constant (To35252), whereas the two Fd^{red} dependent-NiRs were up-regulated (To00016, To02363). Glutamine synthase (GSII, To31900) and the Fd^{red}-dependent glutamate synthase (GOGAT, To13288) were also up-regulated, thereby easing the electron pressure in the chloroplast. The importance of this strategy for TO03 is further emphasized by the fact that both the urea (To31656) and nitrate (To 04919) transporters at the cell membrane are part of the 15 highest up-regulated proteins in our dataset (6.9- and 11.0-fold, respectively). In light of the decrease in carbon fixation (^{14}C data) and proposed increase in

nitrogen assimilation (proteomic data) in TO03, a decrease in the cellular C:N ratio would be expected. However, we did not measure particulate organic carbon or nitrogen. Interestingly, in TO05, based on unchanged carbon uptake rates and only a mild increase in nitrogen assimilation, we would assume no change, or only a slight change in its C:N ratio. This is in line with the constant carbon:nitrogen ratio documented for TO05 under Cu limitation by Kim and Price (2017).

4.4.2.1 Counteracting reactive oxygen species – glutathione, thioredoxin, and superoxide dismutases

An additional benefit of enhanced nitrogen assimilation is an increase of cellular glutamate levels. Glutamate and its aminated form, glutamine, may 1) play a central role in amino acid biosynthesis and metabolism (Bromke 2013); 2) be decarboxylated into the signaling molecule γ-aminobutyric acid (GABA) (Allen et al. 2006; Port et al. 2013); 3) be deaminated to 2-oxoglutarate, thus supplying carbon skeletons to the TCA; and 4) be incorporated into glutathione (GSH). Glutathione is a small sulphur containing tripeptide (γ-L-glutamyl-L-cysteine-glycine) able to detoxify ROS via either direct scavenging or the ascorbate-glutathione cycle (Foyer and Noctor 2011). Furthermore, it is involved in redox signaling, modulating gene expression and enzymatic activity (see review Noctor et al. 2012). Two proteins are involved in glutathione biosynthesis: (1) glutamate cysteine ligase (GCL, also known as γ-glutamylcysteine synthase, GCS) which combines glutamate and cysteine to γ-glutamylcysteine and (2) glutathione synthase (GSS) which adds glycine. Both genes are present in single copies in *T. pseudonana, P. tricornutum* and *T. oceanica*. Glutamate cysteine ligase is a cytosolic enzyme, while GSS is targeted to the chloroplast. Both proteins were up-regulated under Cu limitation in

TO03, but only in one pairing of the biological triplicates (GCL up by 4.5-fold and GSS up by 1.48-fold, no *p*-value). Interestingly, in plants, the rate-limiting process for glutathione production is cysteine biosynthesis (Zechmann 2014). In TO03, two chloroplast cysteine synthase isoenzymes were up-regulated (CS, To27524 and To10442, by 1.6- and 2.5-fold, respectively; Figure 4.6, Table B.6) indicating an increase in glutathione production. Furthermore, glutathione-S-transferase is one of the most highly up-regulated proteins in our dataset (GST, To09062, by 7.3-fold). It can add glutathione to nucleophilic groups as part of the cellular detoxification system, which might be related to oxidative stress (Gallogly and Mieyal 2007). Strikingly, of the six GSTs identified in the *T. oceanica* genome, the one that is significantly up-regulated in TO03 (To09062) has no homologs in the three other diatoms (*T.pseudonana, P. tricornutum* and *F. cylindricus*), but its three closest homologs are found in multicellular organisms (e.g. the polyp *Hydra vulgaris,* the anemone *Nematostella,* and the brachiopod *Lingula*). In contrast, in TO05 a different GST is significantly up-regulated (To24526, by 2.3-fold) with homologs in all three other diatoms. Further evidence supporting that glutathione is used by TO03 to counteract ROS is the up-regulation of glutathione reductase (GR, To07268, by 2.5-fold). Over-expressing glutathione reductase has the additional advantage of oxidizing the over-abundant NAD(P)H in the chloroplast.

Nevertheless, it was not possible to establish whether the glutathione-ascorbate cycle is up-regulated under Cu limitation, given that two of the required enzymes were not identified in our dataset (chloroplast dehydroascorbate reductase, DHAR; chloroplast ascorbate peroxidase, APX). However, two APX isoenzymes were constitutively expressed in the cytosol (To29696 and To37364).

Thioredoxins (TXN) are important redox regulators in plants, specifically in the chloroplast (Balmer et al. 2003), although their role in diatoms is still elusive (Weber et al. 2009). In TO03, three thioredoxins were up-regulated, and each one was targeted to either the chloroplast (TXN, To31425 by 1.5-fold), the cytosol (To05213 by 4.2-fold), or the mitochondria (To31425 by 1.5-fold). The *P. tricornutum* chloroplast TXN homolog (Pt46280) has been suggested to be involved in the activation of pyrenoid β-carbonic anhydrase (β-CA), thus primarily regulating carbon acquisition instead of carbon fixation (Kikutani et al. 2012). However, it is problematic to translate this functional regulation to homologs in *Thalassiosirales*, as the cellular allocation of CAs in diatoms differs greatly between *Thalassiosirales* and *Naviculales* (e.g. *T. pseudonana* and *P. tricornutum)* ((Samukawa et al. 2014). Most importantly in this context, *T. pseudonana* lacks a pyrenoid associated CA. Hence, even though the Pt TXN homolog regulates pyrenoid β-CA (Kikutani et al. 2012), it is challenging to confidently predict the exact regulatory target of the corresponding To TXN homolog without any biochemical evidence.

Another defence mechanism against ROS is the production of superoxide dismutases (SOD). These proteins catalyze the conversion of superoxide radicals into hydrogen peroxide and oxygen. Of the three SODs identified in TO03 under Cu limitation, two were up-regulated: chloroplast Mn/Fe-SOD (To02860) by1.8-fold and cytosolic Ni-SOD (To10112) by 1.4-fold. Thus, under Cu limitation, TO03 is able to control ROS levels by increasing the expression of both glutathione and superoxide dismutases. The increase of thioredoxin isoenzymes in all three major cellular compartments (i.e. cytosol, chloroplast, and mitochondria), suggests that they may be involved in sensing the cellular redox state and regulating the cellular response to excessive reducing equivalents.

4.4.3 The malate shunt drains reducing equivalents from the chloroplast to the mitochondria, thus integrating the nitrogen and carbon metabolisms

The efficiency of photosynthesis (both electron transport and carbon fixation) relies on having an adequate supply of ATP/ADP and NAD(P)H/NAD(P)$^+$ (Allen 2002). In plants, the malate shunt channels excessive reducing equivalents from the chloroplast to other compartments in the cell, via the differential regulation of malate dehydrogenase (MDH) isoenzymes (Heineke et al. 1991; Scheibe 2004). In the chloroplast, NAD(P)H is used to reduce oxaloacetate to malate, a compound that can be transported across membranes and can be reoxidized, resulting in the production of NAD(P)H in the target compartment. Furthermore, NAD(P)H can be used in reactions such as nitrate reduction in the cytosol or ATP production in the mitochondria (e.g. through oxidative phosphorylation in respiration).

In circumstances where the mitochondrial cytochrome-dependent respiration is comprised, such as under Fe limitation, excessive NAD(P)H can be dissipated via the mitochondrial alternative oxidase (AOX) (Yoshida et al. 2007). In diatoms, the interaction between the chloroplast and the mitochondria has been suggested to be even more significant with possibly direct exchange of ATP/ADP and indirect exchange of reducing equivalents via the malate/aspartate shunt (Prihoda et al. 2012; Bailleul et al. 2015). Neither the suggested overlap of plastidial and mitochondrial membranes nor the targeting of potential transporters to this intersection (e.g. malate/2-oxoglutarate antiporter, glutamate/aspartate antiporter) has been conclusively proven to exist (Kroth et al. 2008; Bailleul et al. 2015; Kim et al. 2016). However, an increase of AOX in response to low Fe, as demonstrated by Yoshida in plants, has been documented in diatoms (Allen et al. 2008). Probing the *T. oceanica* genome, two homologs were

found to *T. pseudonana* mitochondrial AOX (AOX_1, To08807; AOX_2, To08808), and one homolog to an *F. cylindricus* mitochondrial AOX (AOX, To33762). However, these were not detected in our proteomic datasets (TO03, TO05, orig/+EST). Furthermore, our physiological data showed no changes in AOX activity due to Cu limitation (Chapter 3, Table A.2). This could be due to species-specific differences between *T. oceanica* and *P. tricornutum* (Allen et al. 2008 investigated *P. tricornutum*), or the fact that cyt*c* oxidase is not affected by low Cu concentrations in TO03 (Table B.9). The latter would imply that any additional NAD(P)H—resulting from channelling electrons from the chloroplast to the mitochondria via the malate/aspartate shunt—could be oxidized via cytochrome-dependent respiration. One line of evidence in support of excess reducing equivalents being channelled towards respiration, as opposed to being used in the Calvin-Benson-Bassham cycle, is that carbon fixation decreased by 66%, while respiration rates remained constant (Chapter 3, Table A.2)

Another indication for an activated malate/aspartate shunt in TO03 in response to low Cu is the up-regulation of chloroplast and mitochondrial MDH (To 30817, To03405), as well as mitochondrial aspartate aminotransferase (AAT, To15049) (malate shunt, Figure 4.7; complete overview, Figure 4.10). Chloroplast oxaloacetate (OAA) is reduced to malate via MDH. Malate is then transported into the mitochondria via a putative malate/2-oxoglutarate antiporter (Kim et al. 2016). Reducing equivalents in the form of NAD(P)H are released in the mitochondria via the re-oxidation of malate to OAA by mitochondrial MDH. In turn, mitochondrial AAT transfers an amine group from glutamate to OAA, thereby releasing aspartate and 2-oxoglutarate into the mitochondria. To close the cycle, aspartate would be transported back, via a glutamate/aspartate antiporter, into the chloroplast where the plastidial AAT isoenzyme would resupply OAA. However, chloroplast AAT was significantly down-regulated. I suggest that chloroplast OAA,

the substrate for MDH, is resupplied in the chloroplast via the ATP-dependent carboxylation of pyruvate due to the significant up-regulation of pyruvate carboxylase (PC). This would lead to a net decrease of NAD(P)H in the chloroplast and a net increase of NAD(P)H in the mitochondria.

The increase in 2-oxoglutarate and aspartate in the mitochondria, as a result of the up-regulation of mitochondrial AAT, can be helpful for the cell in various ways. If the putative malate/2-oxoglutarate antiporter is indeed involved in the malate shunt, 2-oxoglutarate will be transported back into the chloroplast. As chloroplast AAT is down-regulated, 2-oxoglutarate can be used as a substrate for the up-regulated Fd-dependent glutamate synthase (GOGAT) in nitrogen assimilation (see 4.3.5 Nitrogen metabolism). Any surplus 2-oxoglutarate can feed into the citrate cycle. Fittingly, aconitase (To20545) and isocitrate dehydrogenase (To34595), the two proteins involved in the citrate cycle, immediately before 2-oxoglutarate, are both significantly down-regulated. Mitochondrial aspartate can be channelled into the urea cycle, where it will produce argininosuccinate, which can then be channelled back into the mitochondrial citrate cycle as fumarate via the aspartate/argininosuccinate shunt (Allen et al. 2008). Thus, even though two of the first three steps in the citrate cycle were down-regulated, the malate shunt, in combination with the urea cycle, ensures the continuation of this vital metabolic pathway by supplying it with essential carbon skeletons, i.e. 2-oxoglutarate and fumarate.

However, the involved antiporters were only identified in the TO05 proteomic data, and not in TO03. This might be due to the differential sequencing depth in the two strains, as TO03 had 50% less sequencing depth than TO05 (due to the different instruments utilized, see Chapter 2). Furthermore, membrane-bound proteins are generally less prominent in proteomic data. As a reminder, if a protein is not identified in one of the treatments, it will not be included in the differentially expressed protein dataset.

Recently, another shuttle system has been proposed in transferring excess reducing equivalents from the chloroplast to the mitochondria in *P. tricornutum;* the glutamine-ornithine shunt (Levering et al. 2016). However, none of the homologs involved in this newly proposed shunt were identified or up-regulated in *T. oceanica* under Cu limitation (e.g. n-acetyl-γ-glutamyl-phosphate reductase, AGRP, To01956, To25145, neither identified; n-acetylornithine aminotransferase, ACOAT, chloroplast, To09237, -1.4, $p<0.001$; cytosolic, To32466, -3.0, $p = 0.17$).

4.4.4 Contrasting adaptations to Cu limitation in TO03 *vs.* TO05

The response to Cu limitation is strikingly different between TO03 and TO05. *Thalassiosira oceanica* TO03 is able to decrease its Cu requirement drastically by restructuring its complete photosynthetic apparatus (Chapter 3) combined with complex changes in its carbon and nitrogen metabolism. These changes allow TO03 to alleviate ensued electron and ROS stress to sustain ongoing growth (this chapter). Strikingly, the main coping mechanism in TO05 to deal with Cu limitation lies in a 50% decrease of its entire proteome. Indeed, in response to low Cu, the only physiological parameters significantly affected in TO05 were growth rate, cell size and protein content (Chapter 3, Figure 3.2).

In contrast to the response in TO03, none of the proteins involved in nitrogen acquisition and assimilation were significantly up-regulated in TO05 **(**Figure 4.11). The only proteins that were somewhat up-regulated (between 1.3- and 2-fold with $p<0.5$) were the involved transporters (URT, NRT, NiRT) and glutamine synthases (GSII/GSII). As neither NAD(P)H, Fd^{red} oxidizing enzymes, or thioredoxins were up-regulated, it is unlikely that TO05 experienced any significant excess of reducing equivalents within the chloroplast, for which an enhanced

nitrogen metabolism would be helpful. At this point, it is unclear how a potential increase in glutamine (both chloroplast and mitochondrial glutamine synthase are up-regulated) would be beneficial for the cell. It is also puzzling, why the Calvin-Benson-Bassham cycle influencing Rubisco activase, cbbX, and Rubisco itself were both somewhat down-regulated. This differs from the unchanged carbon assimilation rate in Cu limited TO05. I acknowledge, though, that I have no information on metabolites in my study, so the hypothesis would be more robust if it were derived from combined results of significant changes in protein expressions and matching physiological data (e.g. inferred increased reduction state of chloroplast Fe^{red}/Fed^{ox} in TO03 under Cu limitation).

The malate shunt was not induced under low Cu in TO05. Two homologs of a putative malate/oxoglutarate antiporter were expressed constitutively. However, chloroplast ATT and mitochondrial MDH were not even identified, suggesting levels below detection in at least one treatment (see Chapter 2). The two only indications of an active response to Cu limitation in TO05 are the significant up-regulation of glutathione-S-transferase and two glycolytic enzymes.

The differential expression of various isozymes involved in glycolysis is a central strategy in TO03 to direct energy and reducing equivalent flow within the cell (Section 4.4.1 Carbon metabolism). TO05 does not exhibit the same level of sophistication in metabolic control. However, the only two significantly up-regulated proteins in carbon metabolism are chloroplast PGK and mitochondrial GAPDH, which would increase NADH in the mitochondria and ATP in the chloroplast. These two proteins might thus be the first line of defense in TO05 against small energy or reducing equivalent imbalances in the cell.

4.5 Conclusion

The success of diatoms in the modern ocean is due to their complex genomic makeup, and their successful integration and versatility of metabolic pathways among cellular compartments. This was exemplified in the acclimatization of *T. oceanica* (CCMP 1003) to severe Cu limiting growth conditions, where the interaction among metabolic pathways ensured their continuous growth. For example: (1) Photosynthesis – N metabolism (4.4.2 Nitrogen metabolism): the overreduced state of the photosynthetic apparatus resulted in a proposed increase in Fd^{red}, which was then oxidized by an N-assimilatory, Fd^{red} isoenzyme located in the chloroplast; (2) Nitrogen metabolism and ROS fighting (4.4.2 Nitrogen metabolism): the increase in glutamate and cysteine synthase, as well as other key proteins in the glutathione metabolism, ensures the ability to counteract ROS; (3) Photosynthesis and Malate Shunt (4.4.1 Malate Shunt): excess reducing equivalents generated by the photosynthetic apparatus are channeled from the chloroplast to the mitochondria via the malate shunt. (4) Photosynthesis – glycolysis – carbon fixation (4.4.1 Carbon Metabolism): to counteract the imbalance between ATP/NAD(P)H in the chloroplast, specific reactions in glycolysis occur in different compartments, where reducing equivalents or ATP are needed (i.e. NAD(P)H generation in mitochondria, ATP production in cytosol and chloroplast). (5) Malate shunt – urea cycle– citrate cycle – glycolysis (4.4.3 Malate Shunt, 4.4.2 Nitrogen Metabolism, 4.4.1 Carbon Metabolism): the products of the malate shunt can feed into the TCA cycle, and the master cellular C and N redistribution hub, the urea cycle. Furthermore, pyruvate can be carboxylated in the chloroplast to feed into the malate shunt, again transferring both reducing equivalents and carbon skeletons from the chloroplast to the mitochondria. The up-regulation of N assimilation in response to chronic low Cu in TO03 contrasts the response of

TO03 to acute Fe limitation, as well as the response of *P. tricornutum* to N limitation. Whether this is due to differences in species, nutrients or level of stress remains an intriguing question.

4.6 Tables and figures

Table 4.1: Comparison of cellular localization of various carbon metabolic pathways. (modified from Gruber and Kroth 2017)

Pathway	Function	*Chlamydomonas* (green lineage)	Diatoms	Animals	Comment regarding diatoms
Calvin Cycle (Reductive Pentose P Way)	Carbon fixation 3RuBisP + 3 CO_2 -> GAP	Plastid	Plastid	--	Rubsico has higher CO_2 affinity than other organisms
Oxidative Pentose P way	NAD(P)H, ribose (C5 sugars) for nt/ FA, AA	Plastid, Cytosol	Cytosol only (Kroth et al. 2008)	Cytosol	Cytosol only -> needed re-import of nts into plastid -> lots of nt transporters
Glycolysis 1st half (GAP)	Glucose -> GAP	Plastid	Plastid, Cytosol	Cytosol	
Glycolysis 2nd half (pyruvate)	GAP -> pyruvate	Cytosol (Johnson and Alric 2013)	Plastid, Cytosol, Mitochondria	Cytosol	Maybe also in mito to use Entner-Douderoff pathway generated pyruvate?
Entner-Douderoff pathway	6PG ->pyruvate + GAP	--	Mitochondria	--	Fewer proteins involved (cost for cell), but also less ATP generated, but then again, faster as well, another tool to be adaptable to fast changing environment
Phosphoketolase pathway	Fructose-6-P -> acetyl-phosphate and GAP	--	-- (only in *Phaeodactylum*)	--	
Citrate Cycle	Carbon hub, reducing equivalents for respiration	Mitochondria	Mitochondria	Mitochondria	Integrated with urea cycle / Aspartate shunt
Urea Cycle	Animals: catabolic nitrogen excretion Diatoms: anabolic nitrogen/carbon redistribution hub	--	Mitochondria Cytosol	Mitochondria	Incorporation of recycled N and C; in combination with bacterial HGT proteins, production of polyamines involved in cell wall formation and the osmolyte proline
Malate Shunt	Redistribution of reducing equivalents and C4/5-compounds	Plastid, Mitochondria	Plastid, Mitochondria	Mitochondria	Often mentioned/proclaimed as part of cross-talk between chloroplast and Mitochondria; no proteins found so far in Tp, only Mitochondrial membrane proteins from Oxaloacetate transporter in Pt.
Pyrimidine biosynthesis		Plastid	Cytosol	Cytosol	They need to be transported across all four membranes
Carbon Storage		Plastid, starch	Vacuole, Chrysolaminaran, lipids	Cytosol, lipid droplets (triglyceride)	

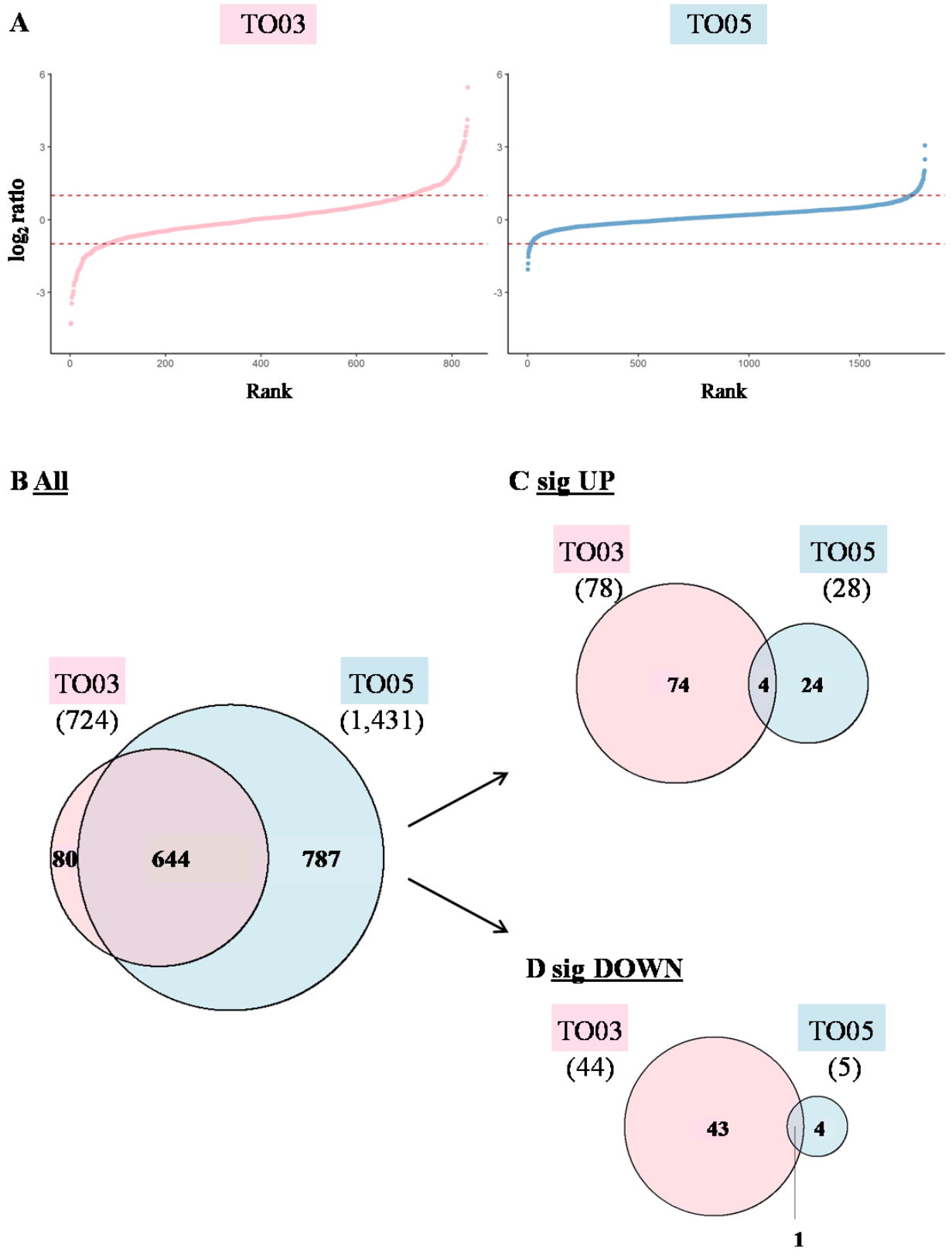
A
TO03
TO05
log2 ratio
Rank
Rank
B All
TO03
(724)
TO05
(1,431)
80
644
787
C sig UP
TO03
(78)
TO05
(28)
74
4
24
D sig DOWN
TO03
(44)
TO05
(5)
43
4
1

Figure 4.1: A) Overview of original proteomics data for *T. oceanica* CCMP 1003 (TO03, pink) and 1005 (TO05, blue) grown in Cu-limiting conditions. Dotted red lines indicate the significance threshold of two-fold difference. **B-D) Venn diagrams of distinct identified proteins in the original datasets of TO03 and TO05:** B) All proteins found; C) significantly up-regulated proteins; D) significantly down-regulated proteins. Note that even though only 50% of the proteins identified in TO05 were identified in TO03, in TO03 there were three times more significantly up-regulated proteins and five times more significantly down-regulated proteins than in TO05.

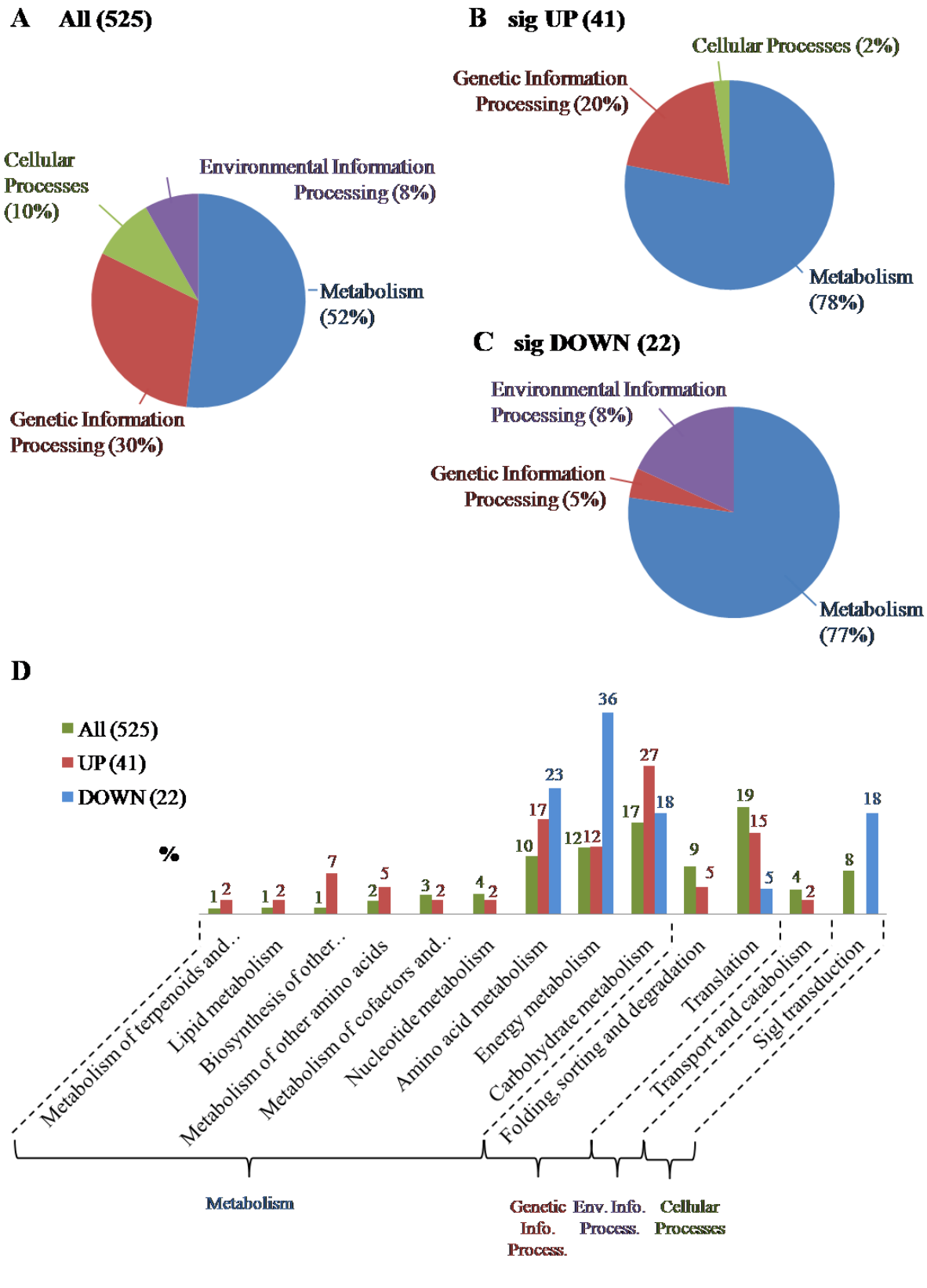
A All (525)
Cellular Processes (10%)
Environmental Information Processing (8%)
Metabolism (52%)
Genetic Information Processing (30%)
B sig UP (41)
Cellular Processes (2%)
Genetic Information Processing (20%)
Metabolism (78%)
C sig DOWN (22)
Environmental Information Processing (8%)
Genetic Information Processing (5%)
Metabolism (77%)
D
All (525)
UP (41)
DOWN (22)
%
Metabolism of terpenoids and..
Lipid metabolism
Biosynthesis of other..
Metabolism of other amino acids
Metabolism of cofactors and..
Nucleotide metabolism
Amino acid metabolism
Energy metabolism
Carbohydrate metabolism
Folding, sorting and degradation
Translation
Transport and catabolism
Sigl transduction
Metabolism
Genetic Info. Process.
Env. Info. Process.
Cellular Processes

Figure 4.2: Pie charts of the first level KeggOrthology (KO) identifiers associated with proteins identified in the original *T. oceanica* CCMP 1003 (TO03) proteomic dataset: A) All proteins found; B) significantly up-regulated proteins; C) significantly down-regulated proteins. D) Bar chart of second level KO identifiers associated with proteins in the original TO03 dataset, comparing proportions between all proteins and those that are significantly up- or down-regulated. Numbers in brackets indicate absolute protein numbers in each subset. Note that proteins involved in metabolism seem to be the most highly affected: those involved in energy metabolism seemed down-regulated, those in carbohydrate metabolism seem to be mainly up-regulated, whereas those involved in amino acid metabolism are both up- and down-regulated.

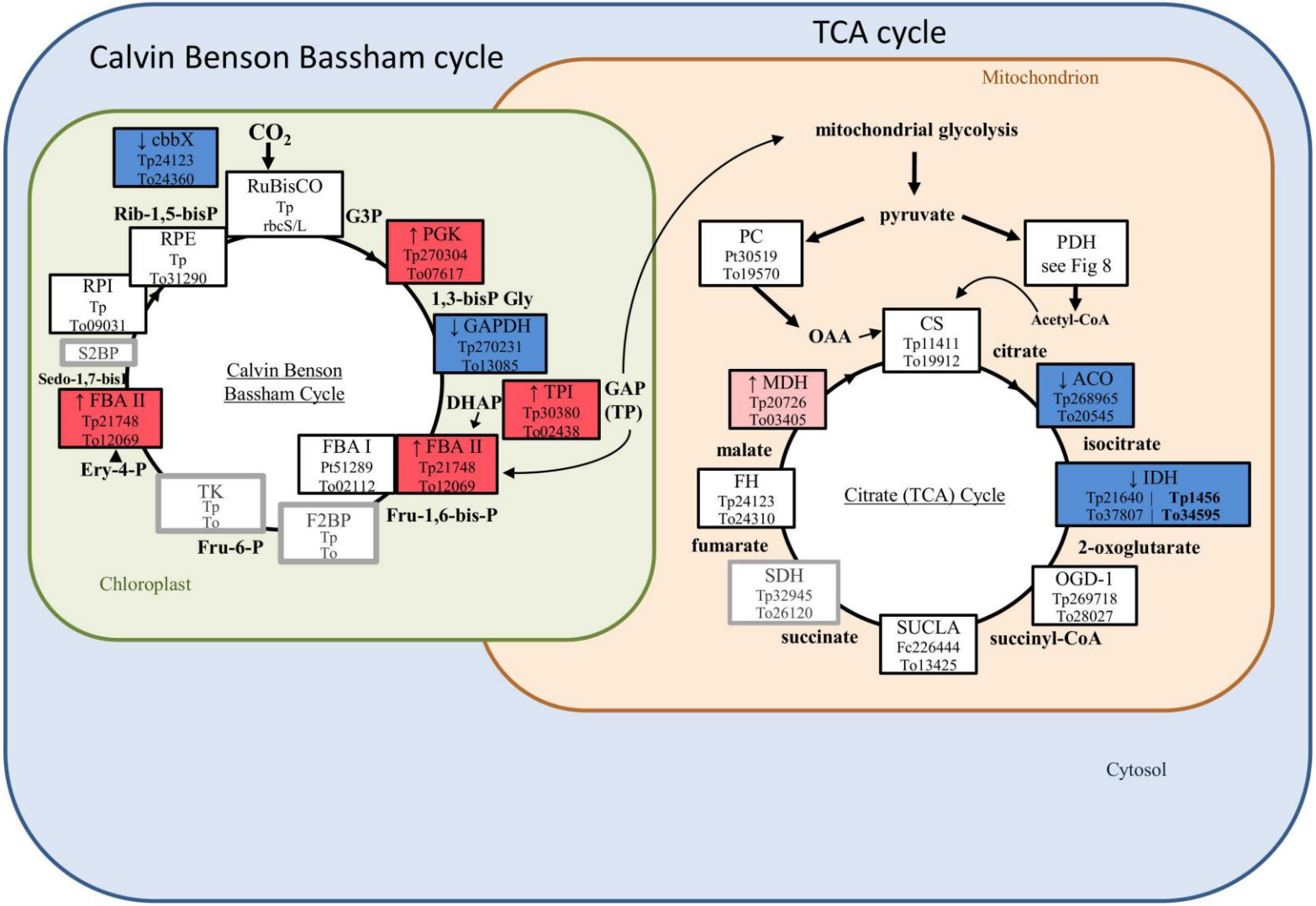
Calvin Benson Bassham cycle
TCA cycle
Mitochondrion
Chloroplast
Cytosol
↓ cbbX
Tp24123
To24360
CO2
RuBisCO
Tp
rbcS/L
Rib-1,5-bisP
G3P
RPE
Tp
To31290
↑ PGK
Tp270304
To07617
RPI
Tp
To09031
1,3-bisP Gly
↓ GAPDH
Tp270231
To13085
S2BP
Sedo-1,7-bisP
Calvin Benson
Bassham Cycle
↑ FBA II
Tp21748
To12069
DHAP
↑ TPI
Tp30380
To02438
GAP
(TP)
FBA I
Pt51289
To02112
↑ FBA II
Tp21748
To12069
Ery-4-P
TK
Tp
To
F2BP
Tp
To
Fru-1,6-bis-P
Fru-6-P
mitochondrial glycolysis
pyruvate
PC
Pt30519
To19570
PDH
see Fig 8
Acetyl-CoA
OAA
CS
Tp11411
To19912
citrate
↑ MDH
Tp20726
To03405
↓ ACO
Tp268965
To20545
isocitrate
malate
FH
Tp24123
To24310
Citrate (TCA) Cycle
↓ IDH
Tp21640 | Tp1456
To37807 | To34595
2-oxoglutarate
fumarate
SDH
Tp32945
To26120
OGD-1
Tp269718
To28027
succinate
SUCLA
Fc226444
To13425
succinyl-CoA

Figure 4.3: Diagram of proteins involved in the Calvin Benson Bassham cycle and citrate (TCA) cycle. Boxes indicate proteins with their abbreviated name and known *T. pseudonana* (Tp) and *T. oceanica* (To) homologs. The colors of the boxes indicate expression in TO03 under low Cu: dark red, highly up-regulated (>2-fold, $p<0.05$); light pink, up-regulated by 1.3 to 2-fold ($p<0.05$); dark blue, highly down-regulated (>2-fold, $p<0.05$); light blue, down-regulated by 1.3 to 2-fold ($p<0.05$); white, expressed in TO03; grey border around box, found in *T. oceanica* genome but not expressed in TO03 proteomic data; grey.

Protein abbreviations: ACO, aconitase hydratase; cbbX, rubisco expression protein; CS, citrate synthase; DLDH, dihydrolipoamide dehydrogenase; FBA I, fructose-bisphosphate aldolase class-I; FBA II, fructose-bisphosphate aldolase class-II; FH, fumarate hydratase; GAPDH, glyceraldehyde 3-phosphate dehydrogenase; GPI, glucose-6-phosphate isomerase; IDH, isocitrate dehydrogenase; MDH, malate dehydrogenase; OGD, 2-oxoglutarate dehydrogenase; PC, pyruvate carboxylase; PDH, pyruvate dehydrogenase; PFK, phosphofructokinase; PGAM, phosphoglycerate mutase; PGK, phosphoglycerate kinase; PGM, phosphoglucomutasePK, pyruvate kinase; rbcL, ribulose-bisphosphate carboxylase large chain; rbcS, ribulose-bisphosphate carboxylase small chain; RPE, ribulose-5-phosphate epimerase; RPI, ribose-5-Phosphate-isomerase; SUCLA, succinate CoA synthetase; TPI, triose-phosphate isomerase;

Compound abbreviations: 1,3- bisPG, 1,3-bisphosphateglycerate; G3P, glucose-3-phosphate; Ery-4-P, erythrose 4 phosphate; Sedo-1,7-bisP, sedoheptulose 1 7-bisphosphate; Rib-1,5-bisP, ribulose-1,5-bisphosphate; DHAP, dihydroxyacetone phosphate; Fru-1,6-bis-P, fructose 1,6-bisphosphate; Fru-6-P, fructose 6-phosphate; GAP, glyceraldehyde 3-phosphate; HCO_3^-, bicarbonate; OAA, oxaloacetate; TP, triose phosphate

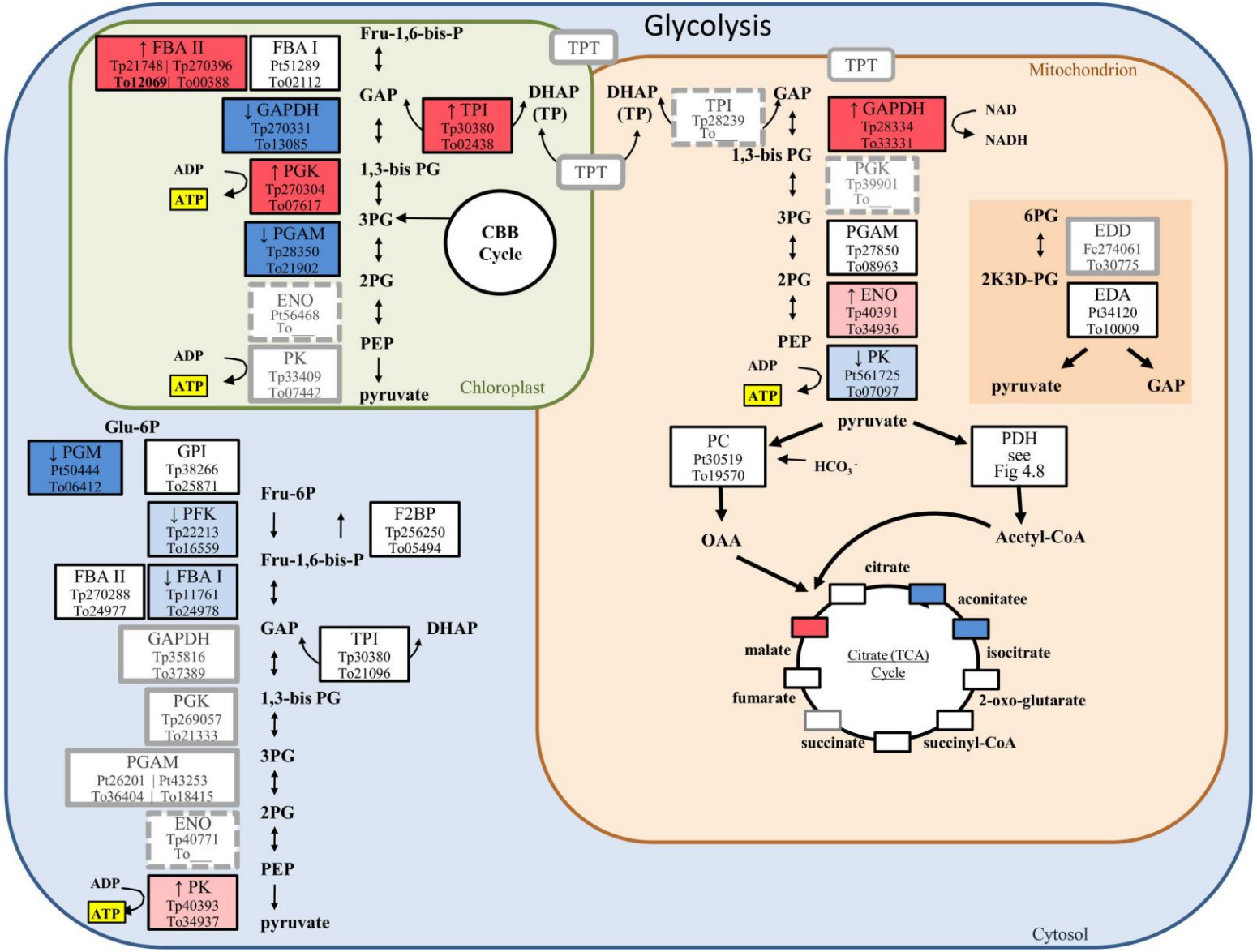
Glycolysis
Chloroplast
Mitochondrion
Cytosol
TPT
↑ FBA II
Tp21748 | Tp270396
To12069 | To00388
FBA I
Pt51289
To02112
Fru-1,6-bis-P
↓ GAPDH
Tp270331
To13085
GAP
↑ TPI
Tp30380
To02438
DHAP (TP)
ADP
ATP
↑ PGK
Tp270304
To07617
1,3-bis PG
↓ PGAM
Tp28350
To21902
3PG
CBB Cycle
ENO
Pt56468
To___
2PG
PEP
ADP
ATP
PK
Tp33409
To07442
pyruvate
TPT
DHAP (TP)
TPI
Tp28239
To___
GAP
↑ GAPDH
Tp28334
To33331
NAD
NADH
1,3-bis PG
PGK
Tp39901
To___
3PG
PGAM
Tp27850
To08963
2PG
↑ ENO
Tp40391
To34936
PEP
ADP
ATP
↓ PK
Pt561725
To07097
6PG
EDD
Fc274061
To30775
2K3D-PG
EDA
Pt34120
To10009
pyruvate
GAP
pyruvate
PC
Pt30519
To19570
HCO3-
PDH
see
Fig 4.8
OAA
Acetyl-CoA
citrate
aconitatee
malate
isocitrate
Citrate (TCA) Cycle
fumarate
2-oxo-glutarate
succinate
succinyl-CoA
Glu-6P
↓ PGM
Pt50444
To06412
GPI
Tp38266
To25871
Fru-6P
↓ PFK
Tp22213
To16559
F2BP
Tp256250
To05494
Fru-1,6-bis-P
FBA II
Tp270288
To24977
↓ FBA I
Tp11761
To24978
GAP
TPI
Tp30380
To21096
DHAP
GAPDH
Tp35816
To37389
1,3-bis PG
PGK
Tp269057
To21333
3PG
PGAM
Pt26201 | Pt43253
To36404 | To18415
2PG
ENO
Tp40771
To___
PEP
ADP
ATP
↑ PK
Tp40393
To34937
pyruvate

Figure 4.4: Diagram of proteins involved in glycolysis in the three compartments (chloroplast, mitochondrion, cytosol), including Entner-Dourdoroff pathway. Boxes indicate proteins with their abbreviated name and known *T. pseudonana* (Tp) and *T. oceanica* (To) homologs. The colors of the boxes indicate expression in TO03 under low Cu: dark red, highly up-regulated (>2-fold, $p<0.05$); light pink, up-regulated by 1.3 to 2-fold ($p<0.05$); dark blue, highly down-regulated (>2-fold, $p<0.05$); light blue, down-regulated by 1.3 to 2-fold ($p<0.05$); white, expressed in TO03; grey border around box, found in *T. oceanica* genome but not expressed in TO03 proteomic data; grey, dashed border around box, no putative homologs in the *T. oceanica* genome.

Protein abbreviations: CBB cycle, Calvin Benson Bassham cycle, EDA, 2-keto-3-deoxy phosphogluconate aldolase; EDD, 6-phosphogluconate dehydratase; ENO, enolase; F2BP, fructose-1-6-bisphosphatase; FBA I, fructose-bisphosphate aldolase class-I; FBA II, fructose-bisphosphate aldolase class-II; GAPDH, glyceraldehyde 3-phosphate dehydrogenase; GPI, glucose-6-phosphate isomerase; PC, pyruvate carboxylase; PDH, pyruvate dehydrogenase; PFK, phosphofructokinase; PGAM, phosphoglycerate mutase; PGK, phosphoglycerate kinase; PGM, phosphoglucomutase; PK, pyruvate kinase; TCA, tricarboxylic acid cycle;TP, triose phosphate; TPI, triose-phosphate isomerase, TPT, triose phosphate transporter

Compound abbreviations: 1,3- bisPG, 1,3-bisphosphateglycerate; 2K3D-PG, 2-keto-3-deoxyphosphogluconate; 2PG, 2-phosphoglycerate; 3PG, 3-phosphoglycerate; 6PG, 6-phosphogluconate; DHAP, dihydroxyacetone phosphate; Fru-1,6-bis-P, fructose 1,6-bisphosphate; Fru-6P, fructose 6-phosphate; GAP, glyceraldehyde 3-phosphate; Glu 6-P, glucose 6-phosphate; HCO_3^-, bicarbonate; OAA, oxaloacetate; PEP, phosphoenolpyruvate;

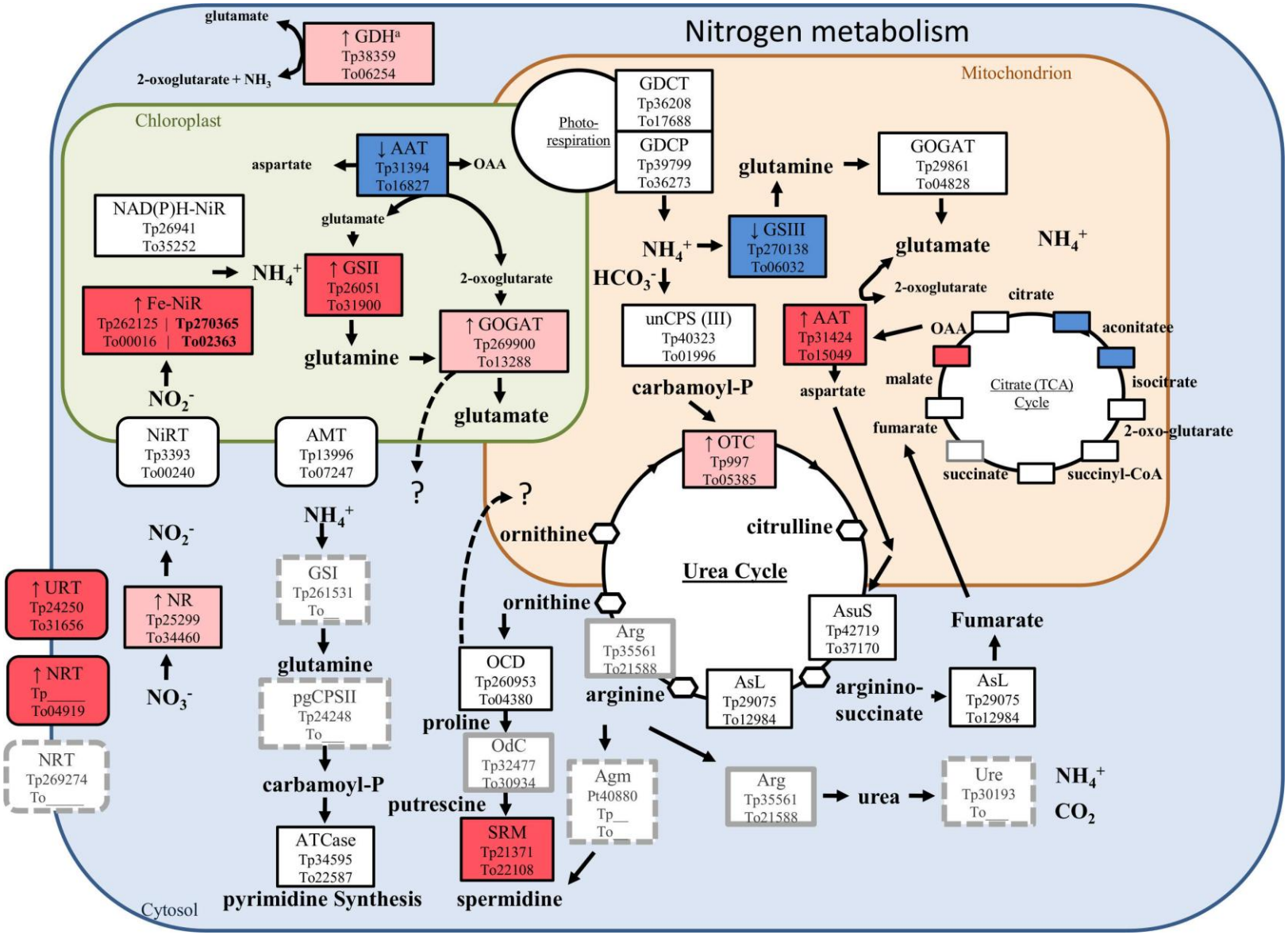
Nitrogen metabolism
glutamate
2-oxoglutarate + NH3
↑ GDHa
Tp38359
To06254
Chloroplast
Mitochondrion
Photo-respiration
GDCT
Tp36208
To17688
GDCP
Tp39799
To36273
↓ AAT
Tp31394
To16827
aspartate
OAA
NAD(P)H-NiR
Tp26941
To35252
glutamate
NH4+
↑ GSII
Tp26051
To31900
2-oxoglutarate
↑ Fe-NiR
Tp262125 | Tp270365
To00016 | To02363
glutamine
↑ GOGAT
Tp269900
To13288
NO2-
glutamate
NiRT
Tp3393
To00240
AMT
Tp13996
To07247
?
?
NH4+
HCO3-
↓ GSIII
Tp270138
To06032
glutamine
GOGAT
Tp29861
To04828
glutamate
NH4+
2-oxoglutarate
unCPS (III)
Tp40323
To01996
↑ AAT
Tp31424
To15049
citrate
OAA
aconitatee
malate
Citrate (TCA) Cycle
isocitrate
fumarate
2-oxo-glutarate
succinate
succinyl-CoA
carbamoyl-P
aspartate
↑ OTC
Tp997
To05385
ornithine
citrulline
Urea Cycle
NO2-
NH4+
↑ URT
Tp24250
To31656
↑ NR
Tp25299
To34460
GSI
Tp261531
To__
ornithine
Arg
Tp35561
To21588
AsuS
Tp42719
To37170
Fumarate
↑ NRT
Tp____
To04919
NO3-
glutamine
pgCPSII
Tp24248
To__
OCD
Tp260953
To04380
arginine
AsL
Tp29075
To12984
arginino-succinate
AsL
Tp29075
To12984
NRT
Tp269274
To_____
proline
OdC
Tp32477
To30934
Agm
Pt40880
Tp__
To__
Arg
Tp35561
To21588
urea
Ure
Tp30193
To__
NH4+
CO2
carbamoyl-P
putrescine
SRM
Tp21371
To22108
ATCase
Tp34595
To22587
pyrimidine Synthesis
spermidine
Cytosol

Figure 4.5: Diagram of proteins involved in nitrogen metabolism. Boxes indicate proteins with their abbreviated name and known *T. pseudonana* (Tp) and *T. oceanica* (To) homologs. The colours of the boxes indicate expression in TO03 under low Cu: dark red, highly up-regulated (>2-fold, $p<0.05$); light pink, up-regulated by 1.3 to 2-fold ($p<0.05$); dark blue, highly down-regulated (>2-fold, $p<0.05$); light blue, down-regulated by 1.3 to 2-fold ($p<0.05$); white, expressed in TO03; grey border around box, found in *T. oceanica* genome but not expressed in TO03 proteomic data; grey, dashed border around box, no putative homologs in the *T. oceanica* genome.

Protein abbreviations: AAT, aspartate aminotransferase; Agm, agmatinase; AMT, ammonium transporter; Arg, arginase; argD, n-acetylornithine aminotransferase; AsL, argininosuccinate lyase; AsuS, argininosuccinate synthase; ATCase, aspartate carbamoyltransferase; Fe-NiR, nitrite reductase (ferredoxin-dependent); GDCP, glycine decarboxylase p-protein; GDCT, glycine decarboxylase t-protein; GDH, glutamate dehydrogenase; GOGAT, glutamate synthase; GSI, glutamine synthase; GSII, glutamine synthetase; GSIII, glutamine synthetase; NAD(P)H-NiR, nitrite reductase (NAD(P)H dependent); NiRT, formate/nitrite transporter; NR, nitrate reductase; NRT, nitrate/nitrite transporter; OCD, ornithine cyclodeaminase; OdC, ornithine decarboxylase; OTC, ornithine carbamoyltransferase; pgCPSII, carbamoyl-phosphate synthase II; unCPS (CPSase III), carbamoyl-phosphate synthase; Ure, urease; URT, Na/urea-polyamine transporter.

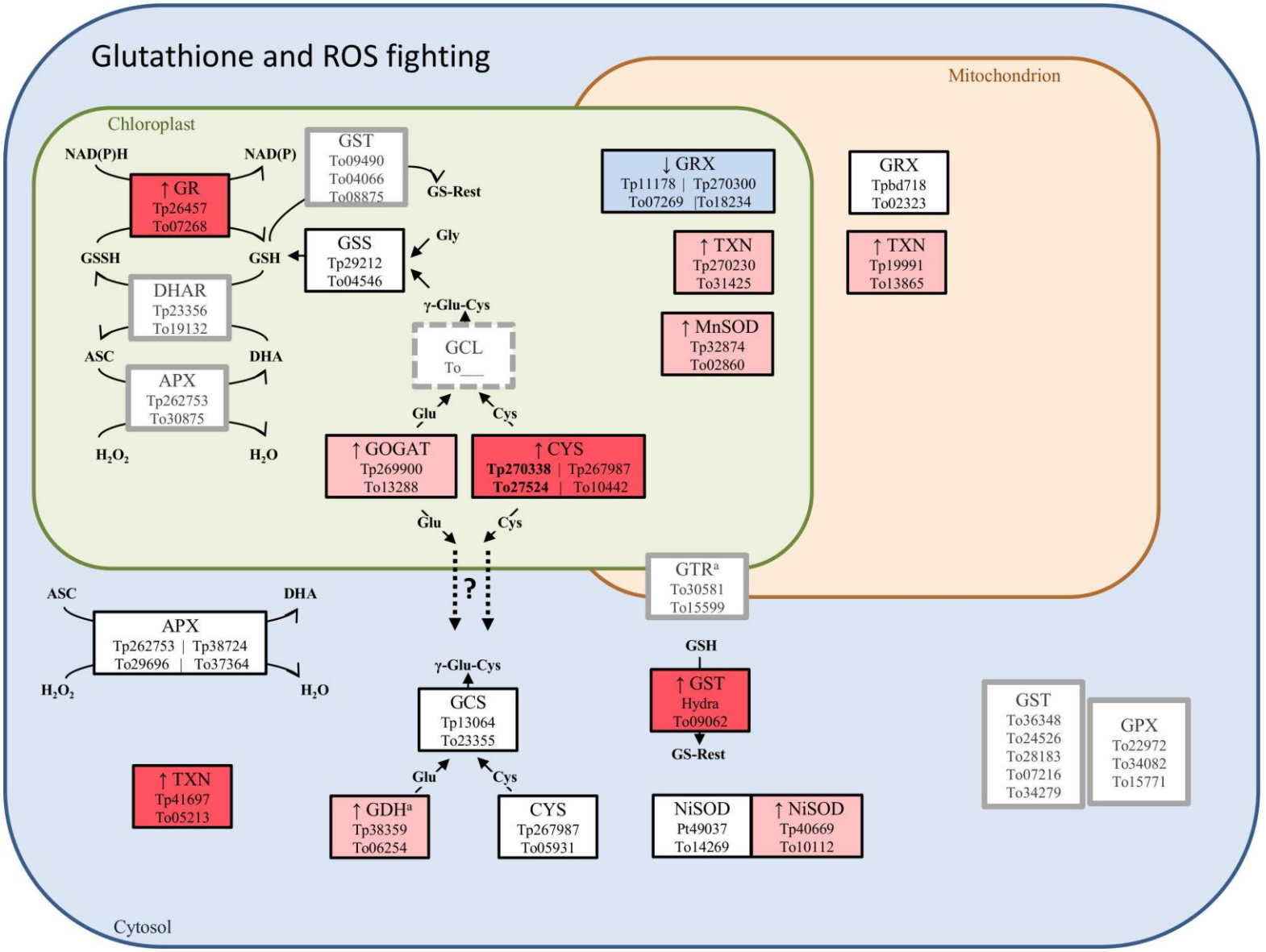
Glutathione and ROS fighting
Mitochondrion
Chloroplast
NAD(P)H
NAD(P)
↑ GR
Tp26457
To07268
GST
To09490
To04066
To08875
GS-Rest
GSSH
GSH
GSS
Tp29212
To04546
Gly
DHAR
Tp23356
To19132
ASC
DHA
APX
Tp262753
To30875
H2O2
H2O
γ-Glu-Cys
GCL
To___
Glu
Cys
↑ GOGAT
Tp269900
To13288
↑ CYS
Tp270338 | Tp267987
To27524 | To10442
↓ GRX
Tp11178 | Tp270300
To07269 | To18234
↑ TXN
Tp270230
To31425
↑ MnSOD
Tp32874
To02860
GRX
Tpbd718
To02323
↑ TXN
Tp19991
To13865
GTRa
To30581
To15599
?
ASC
DHA
APX
Tp262753 | Tp38724
To29696 | To37364
H2O2
H2O
γ-Glu-Cys
GCS
Tp13064
To23355
Glu
Cys
↑ GDHa
Tp38359
To06254
CYS
Tp267987
To05931
GSH
↑ GST
Hydra
To09062
GS-Rest
NiSOD
Pt49037
To14269
↑ NiSOD
Tp40669
To10112
↑ TXN
Tp41697
To05213
GST
To36348
To24526
To28183
To07216
To34279
GPX
To22972
To34082
To15771
Cytosol

Figure 4.6 Diagram of proteins involved in glutathione metabolism. Boxes indicate proteins with their abbreviated name and known *T. pseudonana* (Tp) and *T. oceanica* (To) homologs. The colors of the boxes indicate expression in TO03 under low Cu: dark red, highly up-regulated (>2-fold, $p<0.05$); light pink, up-regulated by 1.3 to 2-fold ($p<0.05$); dark blue, highly down-regulated (>2-fold, $p<0.05$); light blue, down-regulated by 1.3 to 2-fold ($p<0.05$); white, expressed in TO03; grey border around box, found in *T. oceanica* genome but not expressed in TO03 proteomic data; grey, dashed border around box, no putative homologs in the *T. oceanica* genome.

Protein and compound abbreviations: APX, ascorbate peroxidase; Cys, cysteine; CYS, cysteine synthase; DHAR, dehydroascorbate reductase; γ-glu-cys, γ-glutamylcysteine; GCL, glutamate cysteine ligase; GDH, glutamate dehydrogenase, glu, glutamate; NADP dependent; GOGAT, glutamate synthase; GR, glutathione reductase; GRX, glutaredoxin; GSS, glutathione synthetase; GTR, glutathione transporter; TXN, thioredoxin

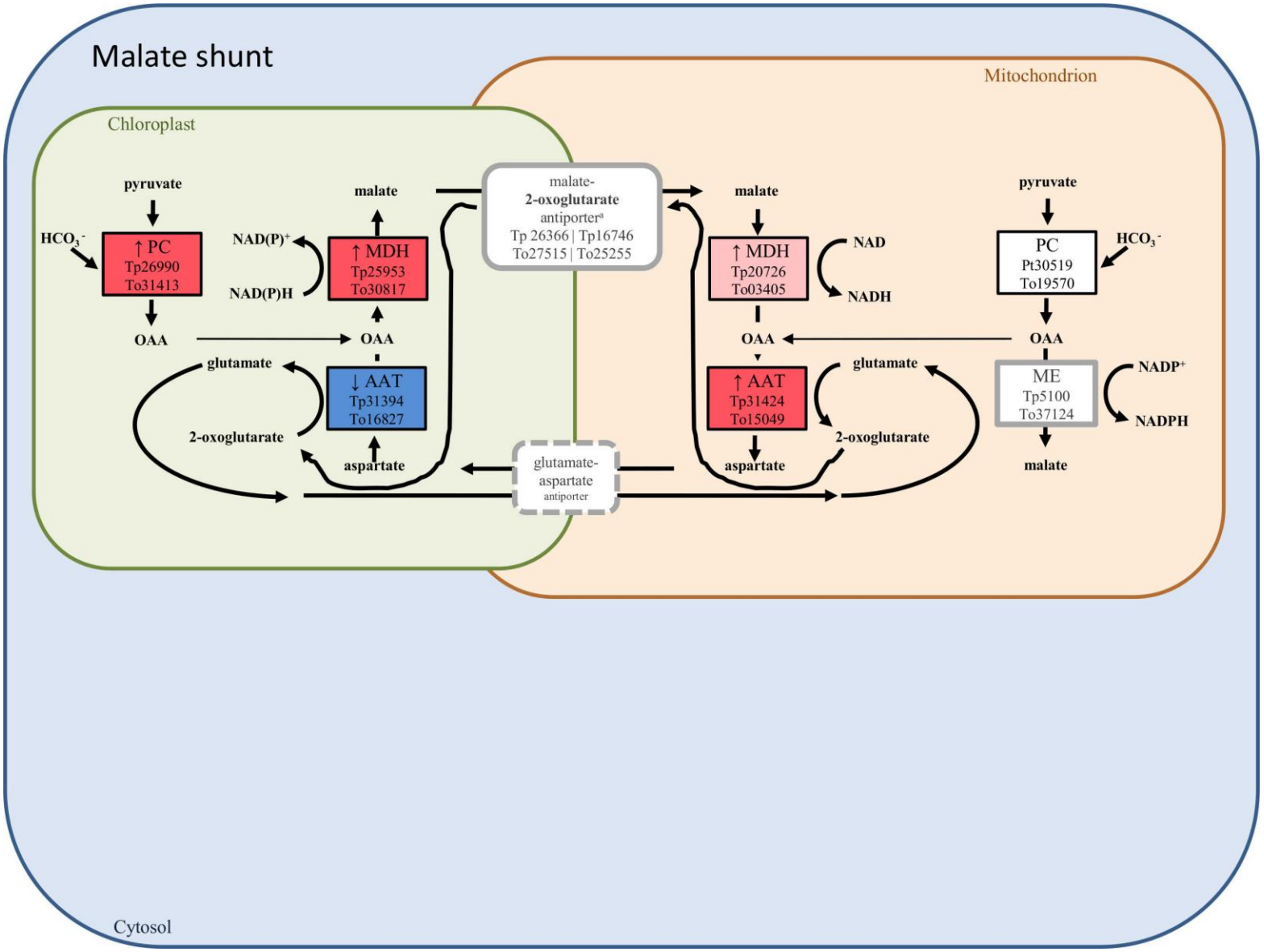
Malate shunt
Mitochondrion
Chloroplast
pyruvate
HCO3-
↑ PC
Tp26990
To31413
OAA
malate
NAD(P)+
NAD(P)H
↑ MDH
Tp25953
To30817
OAA
glutamate
2-oxoglutarate
↓ AAT
Tp31394
To16827
aspartate
malate-
2-oxoglutarate
antiporter[a]
Tp 26366 | Tp16746
To27515 | To25255
glutamate-
aspartate
antiporter
malate
↑ MDH
Tp20726
To03405
NAD
NADH
OAA
↑ AAT
Tp31424
To15049
glutamate
2-oxoglutarate
aspartate
pyruvate
PC
Pt30519
To19570
HCO3-
OAA
ME
Tp5100
To37124
NADP+
NADPH
malate
Cytosol

Figure 4.7: Diagram of proteins involved in the malate shunt. Boxes indicate proteins with their abbreviated name and known *T. pseudonana* (Tp) and *T. oceanica* (To) homologs. The colors of the boxes indicate expression in TO03 under low Cu: dark red, highly up-regulated (>2-fold, $p<0.05$); light pink, up-regulated by 1.3 to 2-fold ($p<0.05$); dark blue, highly down-regulated (>2-fold, $p<0.05$); light blue, down-regulated by 1.3 to 2-fold ($p<0.05$); white, expressed in TO03; grey border around box, found in *T. oceanica* genome but not expressed in TO03 proteomic data; grey, dashed border around box, no putative homologs in the *T. oceanica* genome.

Abbreviations: AAT, aspartate aminotransferase; MDH, malate dehydrogenase; ME, malic enzyme; OAA, oxaloacetate; PC, pyruvate carboxylase; PK, pyruvate kinase

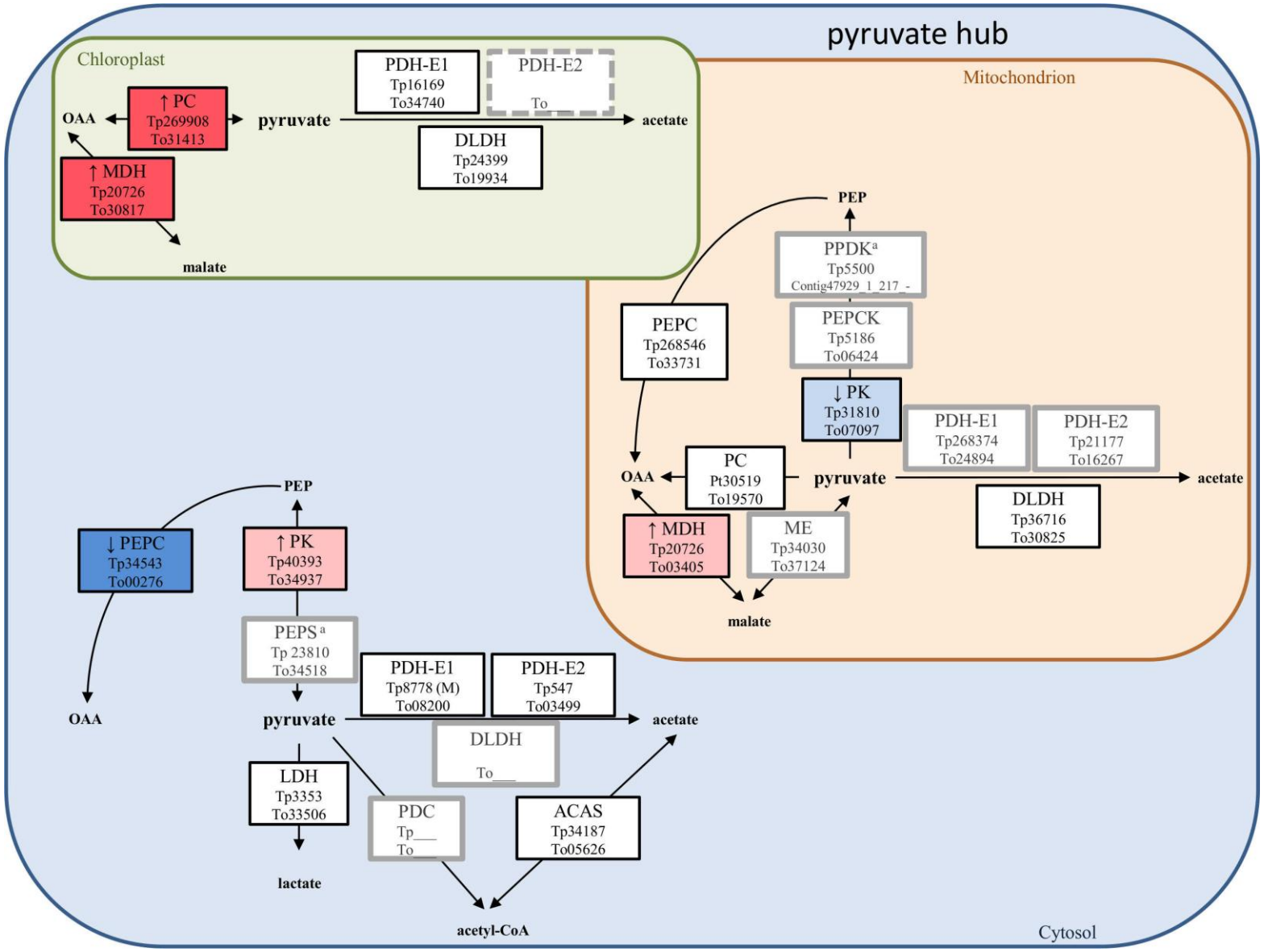
pyruvate hub
Chloroplast
Mitochondrion
Cytosol
PDH-E1
Tp16169
To34740
PDH-E2
To___
↑ PC
Tp269908
To31413
OAA
pyruvate
acetate
DLDH
Tp24399
To19934
↑ MDH
Tp20726
To30817
malate
PEP
PPDK[a]
Tp5500
Contig47929_1_217_-
PEPC
Tp268546
To33731
PEPCK
Tp5186
To06424
↓ PK
Tp31810
To07097
PDH-E1
Tp268374
To24894
PDH-E2
Tp21177
To16267
PC
Pt30519
To19570
DLDH
Tp36716
To30825
↑ MDH
Tp20726
To03405
ME
Tp34030
To37124
↓ PEPC
Tp34543
To00276
↑ PK
Tp40393
To34937
PEPS[a]
Tp 23810
To34518
PDH-E1
Tp8778 (M)
To08200
PDH-E2
Tp547
To03499
DLDH
To___
LDH
Tp3353
To33506
PDC
Tp___
To___
ACAS
Tp34187
To05626
lactate
acetyl-CoA

Figure 4.8: Diagram of proteins involved in pyruvate metabolism. Boxes indicate proteins with their abbreviated name and known *T. pseudonana* (Tp) and *T. oceanica* (To) homologs. The colours of the boxes indicate expression in TO03 under low Cu: dark red, highly up-regulated (>2-fold, $p<0.05$); light pink, up-regulated by 1.3 to 2-fold ($p<0.05$); dark blue, highly down-regulated (>2-fold, $p<0.05$); light blue, down-regulated by 1.3 to 2-fold ($p<0.05$); white, expressed in TO03; grey border around box, found in *T. oceanica* genome but not expressed in TO03 proteomic data; grey, dashed border around box, no putative homologs in the *T. oceanica* genome.

[a]Tp and To model are not homologs

Abbreviations: ACAS, acetyl-CoA synthase; ACC, acetyl-CoA carboxylase; DLDH, dihydrolipoamide dehydrogenase; LDH, L-lactate dehydrogenase; MDH, malate dehydrogenase; ME, malic enzyme; PC, pyruvate carboxylase; PDH-E1, pyruvate dehydrogenase-E1 component; PDH-E2, pyruvate dehydrogenase E2 component (dihydrolipoamide acetyltransferase); PEPC, phosphoenolpyruvate carboxylase; PEPCK, phosphoenolpyruvate carboxykinase; PEPS, phosphoenolpyruvate synthase; PK, pyruvate kinase; PPDK, pyruvate, phosphate dikinase.

Table 4.2: Fructose-bisphosphate aldolase (FBA) isoenzymes in *P. tricornutum* (Pt) and homologs in *T. oceanica* (To, CCMP 1003). Information on *P. tricornutum* as per Allen et al. (2012).

Gene name (Pt)[a]	FBA class[b]	Phylogenetic ancestry[c]	Location in Pt[d]	Pt id[e]	Pt mRNA lowFe[f]	To homolog[g]	protein ratio lowCu[h]
FbaC1	Class II	Chromalveolate specific gene duplication of FbaC2 prior to diversification	Chloroplast, Pyrenoid	Bd825	↑ >25	To00388	↑ (1.4)
FbaC2	Class II	Endosymbiotic gene transfer from prasinophyte-like green algal ancestor	Chloroplast, diffuse	Pt22993	↓ <20	To12069	↑ (2.0)
Fba3	Class II	Heterokont host of secondary endosymbiosis	Cytosol	Pt29014	↑ >10	To24977	±
Fba4	Class I	Bacterial like (unknown in non-diatom eukaryotes)	Cytosol, putative cytoskeletal interaction	Pt42447	~1	To24978	↓ (-2.8)
FbaC5	Class I	Endosymbiotic gene transfer from red algal ancestor (with selective gene loss in some centric diatoms)	Chloroplast, Pyrenoid	Pt51289	↑ >80	To02112	±

[a]as per Allen et al. (2012)
[b]Class I uses a metal co-factor, Class II uses a Schiff base
[c]as per Allen et al. (2012)
[d]as per Allen et al. (2012) using GFP-fusion proteins
[e]NCBI identifier
[f]fold-change of mRNA transcript levels in acute Fe limited *vs.* Fe replete cultures; arrows indicating up- and down-regulation
[g]as per blastP search
[h]fold change of protein levels in chronic Cu limited *vs.* Cu replete cultures
FBA, fructose-bisphosphate aldolase; Pt, *Phaeodactylum tricornutum*; To, *Thalassiosira oceanica*

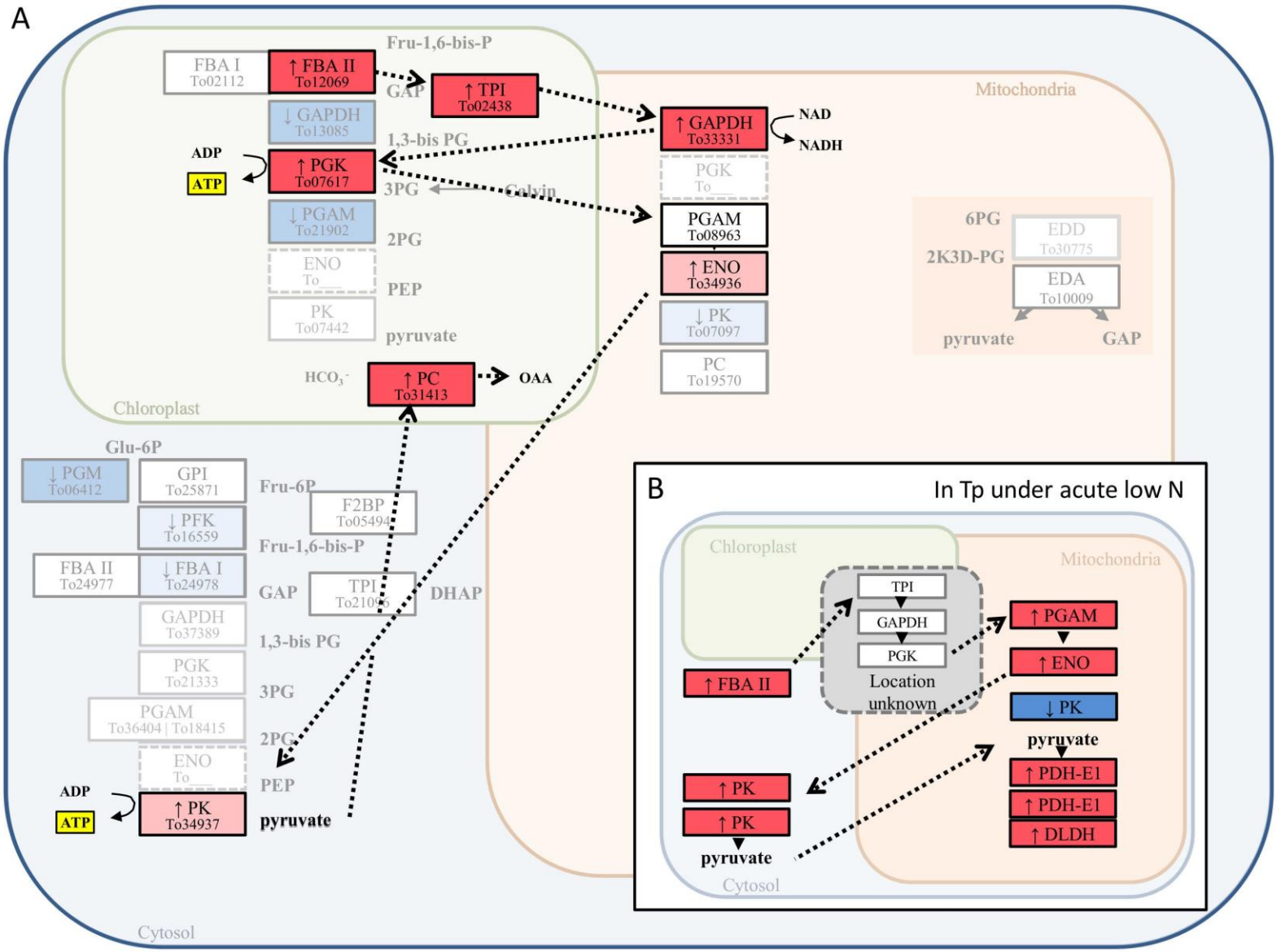
A
Fru-1,6-bis-P
FBA I
To02112
↑ FBA II
To12069
GAP
↑ TPI
To02438
↓ GAPDH
To13085
1,3-bis PG
ADP
ATP
↑ PGK
To07617
3PG
Calvin
↓ PGAM
To21902
2PG
ENO
To___
PEP
PK
To07442
pyruvate
HCO3-
↑ PC
To31413
OAA
Chloroplast
Mitochondria
↑ GAPDH
To33331
NAD
NADH
PGK
To___
PGAM
To08963
↑ ENO
To34936
↓ PK
To07097
PC
To19570
6PG
2K3D-PG
EDD
To30775
EDA
To10009
pyruvate
GAP
Glu-6P
↓ PGM
To06412
GPI
To25871
Fru-6P
F2BP
To05494
↓ PFK
To16559
Fru-1,6-bis-P
FBA II
To24977
↓ FBA I
To24978
GAP
TPI
To21096
DHAP
GAPDH
To37389
1,3-bis PG
PGK
To21333
3PG
PGAM
To36404 | To18415
2PG
ENO
To___
PEP
ADP
ATP
↑ PK
To34937
pyruvate
Cytosol
B
In Tp under acute low N
Chloroplast
Mitochondria
TPI
GAPDH
PGK
Location
unknown
↑ FBA II
↑ PGAM
↑ ENO
↓ PK
pyruvate
↑ PDH-E1
↑ PDH-E1
↑ DLDH
↑ PK
↑ PK
pyruvate
Cytosol

Figure 4.9. The regulated proteins involved in glycolysis. A) Up-regulated proteins in TO03 under Cu limitation. B) significantly regulated proteins in *T. pseudonana* under acute N limitation (Hockin et al. 2012)**.** Dark red boxes indicate highly up-regulated proteins (TO03: > 2-fold, $p<0.05$; Tp: as per Hockin et al. 2012), light red boxes indicate 1.3- to 2-fold up-regulated proteins ($p<0.05$), white boxes indicate no significant regulation, dark blue boxes indicate highly down-regulated proteins (TO03: > 2-fold, $p<0.05$; Tp: as per Hockin et al. 2012), light blue boxes indicate 1.3 to 2-fold down-regulated proteins ($p<0.05$). **Abbreviations:** EDA, 2-keto-3-deoxy phosphogluconate aldolase; EDD, 6-phosphogluconate dehydratase; ENO, enolase; F2BP, fructose-1-6-bisphosphatase; FBA I, fructose-bisphosphate aldolase class-I; FBA II, fructose-bisphosphate aldolase class-II; GAPDH, glyceraldehyde 3-phosphate dehydrogenase; GPI, glucose-6-phosphate isomerase; PFK, phosphofructokinase; PGAM, phosphoglycerate mutase; PGK, phosphoglycerate kinase; PGM, phosphoglucomutase; PK, pyruvate kinase; TPI, triose-phosphate isomerase.

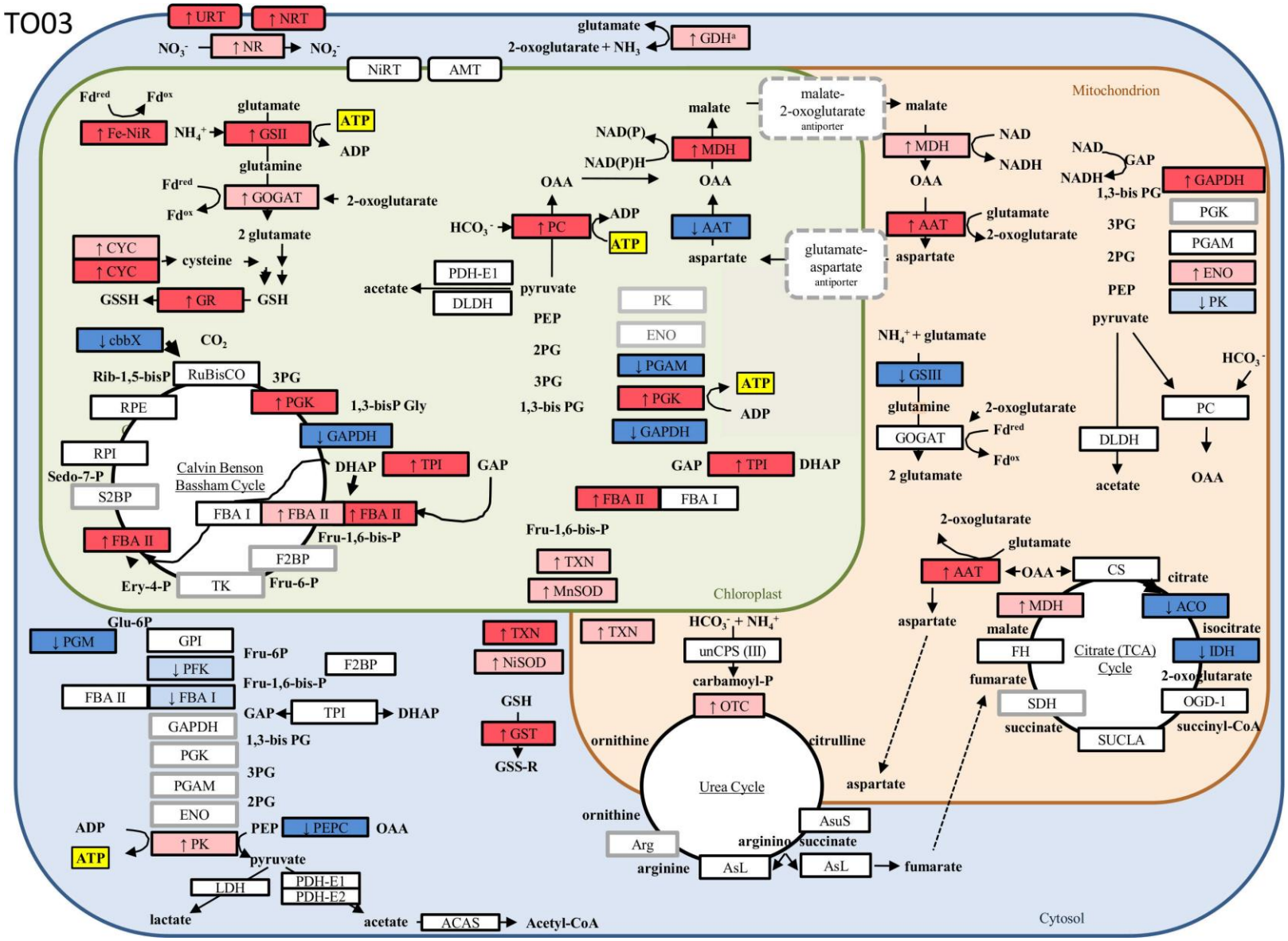
TO03
↑ URT
↑ NRT
NO_3^-
↑ NR
NO_2^-
NiRT
AMT
glutamate
↑ GDH[a]
2-oxoglutarate + NH_3
Chloroplast
Mitochondrion
Cytosol
Fd^{red}
Fd^{ox}
↑ Fe-NiR
NH_4^+
↑ GSII
ATP
ADP
glutamine
↑ GOGAT
2-oxoglutarate
2 glutamate
↑ CYC
↑ CYC
cysteine
GSSH
↑ GR
GSH
↓ cbbX
CO_2
Rib-1,5-bisP
RuBisCO
3PG
↑ PGK
1,3-bisP Gly
RPE
↓ GAPDH
RPI
Sedo-7-P
Calvin Benson
Bassham Cycle
DHAP
↑ TPI
GAP
S2BP
FBA I
↑ FBA II
↑ FBA II
Fru-1,6-bis-P
↑ FBA II
F2BP
Ery-4-P
TK
Fru-6-P
malate
NAD(P)
NAD(P)H
↑ MDH
OAA
HCO_3^-
↑ PC
ADP
ATP
↓ AAT
aspartate
acetate
PDH-E1
DLDH
pyruvate
PEP
2PG
3PG
1,3-bis PG
PK
ENO
↓ PGAM
↑ PGK
ATP
ADP
↓ GAPDH
GAP
↑ TPI
DHAP
↑ FBA II
FBA I
Fru-1,6-bis-P
malate-
2-oxoglutarate
antiporter
malate
↑ MDH
NAD
NADH
OAA
↑ AAT
glutamate
2-oxoglutarate
aspartate
glutamate-
aspartate
antiporter
NAD
GAP
NADH
1,3-bis PG
↑ GAPDH
3PG
PGK
2PG
PGAM
PEP
↑ ENO
pyruvate
↓ PK
NH_4^+ + glutamate
↓ GSIII
glutamine
2-oxoglutarate
GOGAT
Fd^{red}
Fd^{ox}
2 glutamate
DLDH
acetate
HCO_3^-
PC
OAA
2-oxoglutarate
glutamate
↑ AAT
OAA
CS
citrate
aspartate
↑ MDH
↓ ACO
malate
isocitrate
FH
Citrate (TCA)
Cycle
↓ IDH
fumarate
2-oxoglutarate
SDH
OGD-1
succinate
SUCLA
succinyl-CoA
Glu-6P
↓ PGM
GPI
Fru-6P
↓ PFK
F2BP
Fru-1,6-bis-P
FBA II
↓ FBA I
GAP
TPI
DHAP
GAPDH
1,3-bis PG
PGK
3PG
PGAM
2PG
ENO
ADP
PEP
↓ PEPC
OAA
ATP
↑ PK
pyruvate
LDH
PDH-E1
PDH-E2
lactate
acetate
ACAS
Acetyl-CoA
↑ TXN
↑ NiSOD
GSH
↑ GST
GSS-R
↑ TXN
HCO_3^- + NH_4^+
unCPS (III)
carbamoyl-P
↑ OTC
ornithine
citrulline
Urea Cycle
aspartate
ornithine
Arg
arginine
AsL
AsuS
arginino-succinate
AsL
fumarate

Figure 4.10: An overview of the proteomic response in the nitrogen and carbon metabolisms in *T. oceanica* (CCMP 1003) grown under Cu-limiting conditions. Boxes indicate proteins with their abbreviated name. The colors of the boxes indicate expression in TO03 under low Cu: dark red, highly up-regulated (> 2-fold, $p<0.05$); light pink, up-regulated by 1.3 to 2-fold ($p<0.05$); dark blue, highly down-regulated (> 2-fold, $p<0.05$); light blue, down-regulated by 1.3 to 2-fold ($p<0.05$); white, expressed in TO03; grey border around box, found in *T. oceanica* genome but not detected in TO03 proteomic data; grey, dashed border around box, no putative homologs in the *T. oceanica* genome.

Abbreviations: AAT, aspartate aminotransferase; ACO, aconitase hydratase; Arg, Arginase; AsL, argininosuccinate lyase; AsuS, argininosuccinate synthase; cbbX, rubisco expression protein; CS, citrate synthase; DLDH, dihydrolipoamide dehydrogenase; EDA, 2-keto-3-deoxy phosphogluconate aldolase; EDD, 6-phosphogluconate dehydratase; ENO, Enolase; F2BP, Fructose-1-6-bisphosphatase; FBA I, fructose-bisphosphate aldolase class-I; FBA II, fructose-bisphosphate aldolase class-II; Fe-NiR, nitrite reductase (ferredoxin-dependent); FH, fumarate hydratase; GAPDH, glyceraldehyde 3-phosphate dehydrogenase; GDH, glutamate dehydrogenase; GOGAT, glutamate synthase; GPI, glucose-6-phosphate isomerase; GSII, glutamine synthetase; GSIII, glutamine synthetase; IDH, isocitrate dehydrogenase; MDH, malate dehydrogenase; NR, nitrate reductase; NRT, nitrate/nitrite transporter; OGD, 2-oxoglutarate dehydrogenase; OTC, ornithine carbamoyltransferase; PC, pyruvate carboxylase; PEPC, phosphoenolpyruvate carboxylase; PFK, phosphofructokinase; PGAM, phosphoglycerate mutase; PGK, phosphoglycerate kinase; PGM, phosphoglucomutase; PK, pyruvate kinase; RPE, ribulose-5-phosphate epimerase; RPI, ribose-5-Phosphate-isomerase; RuBisCO, ribulose-bisphosphate carboxylase; SUCLA, Succinate CoA synthetase; TPI, triose-phosphate isomerase; TPI, triose-phosphate isomerase; unCPS (CPSase III), carbamoyl-phosphate synthase; URT, Na/urea-polyamine transporter.

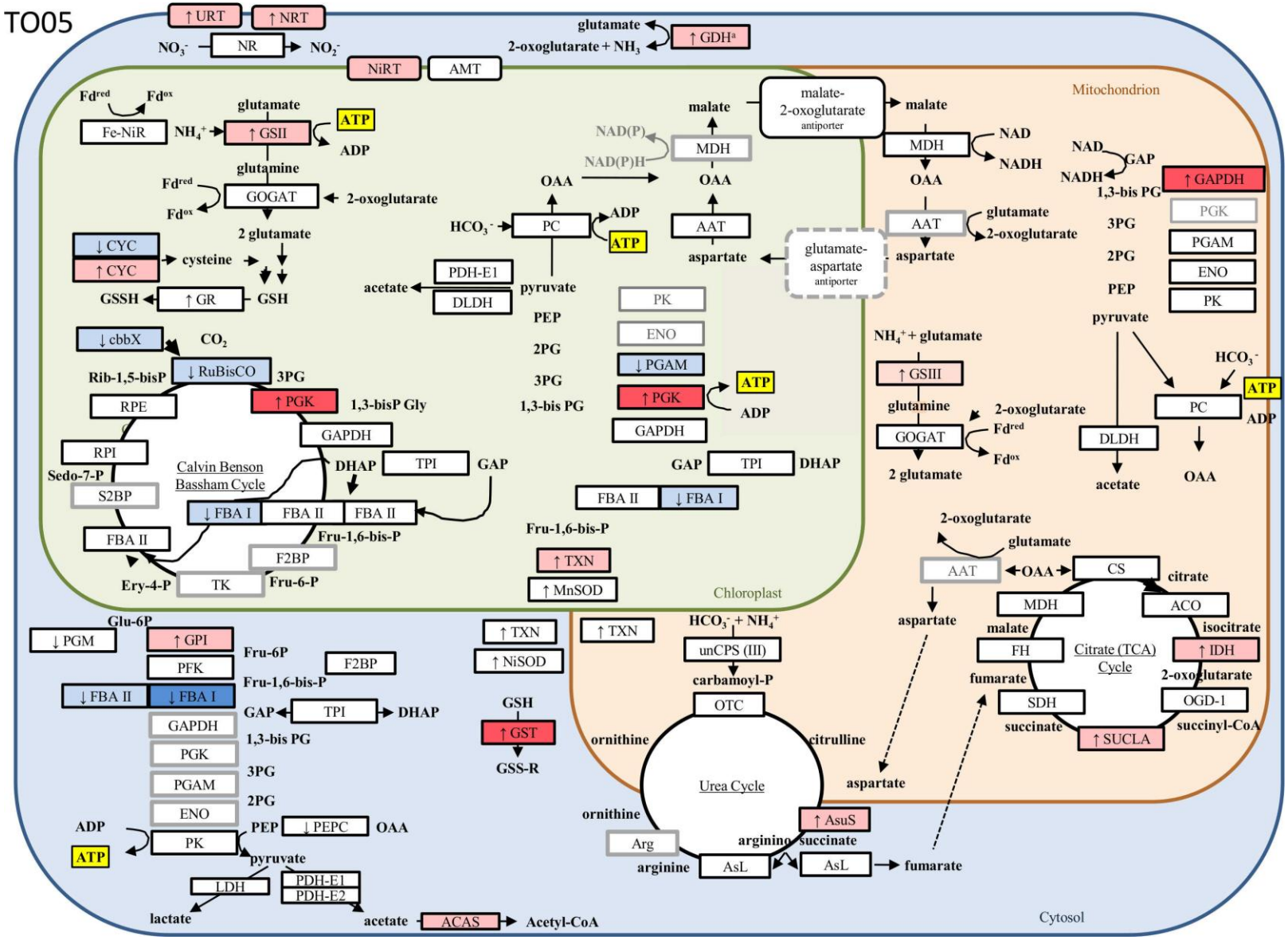
TO05
↑ URT
↑ NRT
NO3-
NR
NO2-
NiRT
AMT
glutamate
2-oxoglutarate + NH3
↑ GDHa
Fdred
Fdox
Fe-NiR
NH4+
↑ GSII
ATP
ADP
glutamine
GOGAT
2-oxoglutarate
2 glutamate
↓ CYC
↑ CYC
cysteine
GSSH
↑ GR
GSH
↓ cbbX
CO2
Rib-1,5-bisP
↓ RuBisCO
3PG
↑ PGK
1,3-bisP Gly
RPE
RPI
Sedo-7-P
S2BP
FBA II
Calvin Benson
Bassham Cycle
GAPDH
DHAP
TPI
GAP
↓ FBA I
FBA II
Fru-1,6-bis-P
F2BP
Ery-4-P
TK
Fru-6-P
malate
NAD(P)
NAD(P)H
MDH
OAA
HCO3-
PC
AAT
aspartate
PDH-E1
DLDH
acetate
pyruvate
PEP
2PG
3PG
1,3-bis PG
PK
ENO
↓ PGAM
malate-
2-oxoglutarate
antiporter
glutamate-
aspartate
antiporter
Chloroplast
↑ TXN
↑ MnSOD
Mitochondrion
NAD
NADH
NAD
GAP
NADH
↑ GAPDH
1,3-bis PG
PGK
3PG
PGAM
2PG
ENO
PEP
PK
pyruvate
NH4+ + glutamate
↑ GSIII
glutamine
2-oxoglutarate
GOGAT
Fdred
Fdox
2 glutamate
HCO3-
ATP
PC
ADP
DLDH
acetate
OAA
2-oxoglutarate
glutamate
AAT
OAA
CS
citrate
aspartate
MDH
ACO
isocitrate
malate
FH
Citrate (TCA)
Cycle
↑ IDH
fumarate
2-oxoglutarate
SDH
OGD-1
succinate
↑ SUCLA
succinyl-CoA
Glu-6P
↓ PGM
↑ GPI
Fru-6P
PFK
F2BP
Fru-1,6-bis-P
↓ FBA II
↓ FBA I
GAP
TPI
DHAP
GAPDH
1,3-bis PG
PGK
3PG
PGAM
2PG
ENO
ADP
ATP
PEP
↓ PEPC
OAA
PK
pyruvate
LDH
PDH-E1
PDH-E2
lactate
acetate
ACAS
Acetyl-CoA
↑ TXN
↑ NiSOD
GSH
↑ GST
GSS-R
↑ TXN
HCO3- + NH4+
unCPS (III)
carbamoyl-P
OTC
ornithine
citrulline
Urea Cycle
aspartate
ornithine
↑ AsuS
Arg
arginino-succinate
arginine
AsL
AsL
fumarate
Cytosol

Figure 4.11: An overview of the proteomic response in the nitrogen and carbon metabolisms in *T. oceanica* (CCMP 1005) grown under Cu-limiting conditions. Boxes indicate proteins with their abbreviated name. The colors of the boxes indicate expression in TO03 under low Cu: dark red, highly up-regulated (> 2-fold, $p<0.05$); light red, up-regulated by 1.3 to 2-fold ($p<0.05$); dark blue, highly down-regulated (> 2-fold, $p<0.05$); light blue, down-regulated by 1.3 to 2-fold ($p<0.05$); white, expressed in TO03; grey border around box, found in *T. oceanica* genome but not detected in TO03 proteomic data; grey, dashed border around box, no putative homologs in the *T. oceanica* genome.

Abbreviations: AAT, aspartate aminotransferase; ACO, aconitase hydratase; Arg, Arginase; AsL, argininosuccinate lyase; AsuS, argininosuccinate synthase; cbbX, rubisco expression protein; CS, citrate synthase; DLDH, dihydrolipoamide dehydrogenase; EDA, 2-keto-3-deoxy phosphogluconate aldolase; EDD, 6-phosphogluconate dehydratase; ENO, Enolase; F2BP, Fructose-1-6-bisphosphatase; FBA I, fructose-bisphosphate aldolase class-I; FBA II, fructose-bisphosphate aldolase class-II; Fe-NiR, nitrite reductase (ferredoxin-dependent); FH, fumarate hydratase; GAPDH, glyceraldehyde 3-phosphate dehydrogenase; GDH, glutamate dehydrogenase; GOGAT, glutamate synthase; GPI, glucose-6-phosphate isomerase; GSII, glutamine synthetase; GSIII, glutamine synthetase; IDH, isocitrate dehydrogenase; MDH, malate dehydrogenase; NR, nitrate reductase; NRT, nitrate/nitrite transporter; OGD, 2-oxoglutarate dehydrogenase; OTC, ornithine carbamoyltransferase; PC, pyruvate carboxylase; PEPC, phosphoenolpyruvate carboxylase; PFK, phosphofructokinase; PGAM, phosphoglycerate mutase; PGK, phosphoglycerate kinase; PGM, phosphoglucomutase; PK, pyruvate kinase; RPE, ribulose-5-phosphate epimerase; RPI, ribose-5-Phosphate-isomerase; RuBisCO, ribulose-bisphosphate carboxylase; SUCLA, Succinate CoA synthetase; TPI, triose-phosphate isomerase; TPI, triose-phosphate isomerase; unCPS (CPSase III), carbamoyl-phosphate synthase; URT, Na/urea-polyamine transporter.

Chapter 5: Comparative Proteomic Analysis of the Photosynthetic Apparatus of Copper and/or Iron Limited *T. oceanica*

5.1 Summary

Iron (Fe) and copper (Cu) are co-factors in proteins involved in photosynthesis, thus are essential micronutrients for photosynthetic organisms. Iron availability limits productivity in large oceanic regions and some studies have suggested the possibility of Fe-Cu co-limitation in these areas. Diatoms are responsible for almost half of the marine carbon fixation, are ubiquitous in Fe-limited regions, and are known to have interactive Fe and Cu physiologies. However, little is known about the underlying biochemical and proteomic changes in response to Cu- and Fe-Cu co-limitation. To gain a better understanding of the mechanics of low metal adaptation, I investigated and evaluated the physiological and proteomic response of two strains of the open ocean diatom *Thalassiosira oceanica* (CCMP1003 and CCMP1005) grown under three different limiting metal regimes: low Fe, low Cu and low Fe and Cu. Here, I show that the differential regulation of the photosynthetic components is both metal- and strain-dependent. Even though both strains were isolated from the oligotrophic Sargasso Sea, CCMP1003 seems to be better adapted to low metal concentrations than CCMP1005. Most strikingly, *T. oceanica* CCMP1003 modulated levels of the Cu-containing plastocyanin depending on the metal stress, i.e. decreasing it under low Cu, and to a lesser extent under low Fe and Cu, but increasing it under low Fe. Furthermore, TO03 up-regulated the expression of ferredoxin: $NADP^+$-reductase and an unknown flavodoxin isoform in response to all three metal limiting conditions. Both proteins are potentially important in detoxifying reactive oxygen species. Interestingly, in TO05 only the Fe-

responsive flavodoxin FldA was detected. Further differences and similarities between conditions and strains are discussed.

5.2 Introduction

Iron (Fe) and copper (Cu) are important trace metals for photosynthetic cells. Their redox potential makes them excellent co-factors in proteins involved in electron transfer reactions, such as the photosynthetic and respiratory electron transport chain in the chloroplast and mitochondria, respectively. Photosynthesis is particularly rich in Fe-containing proteins: PSII, 3-4 Fe atoms (depending on species); cytb_6f, 5 Fe atoms; PSI, 12 Fe atoms; and Fdx, 2 Fe atoms. Also depending on algal species, the electron carrier between cytb_6f and PSI may either be Fe-containing cytc_6, (1 Fe atom) or Cu-containing plastocyanin (1 Cu atom) (Raven et al. 1999). Even though these elements are only needed in trace amounts, Fe concentrations in the open ocean are so low that they limit primary productivity in 30-40% of the global ocean (Moore et al. 2004; Boyd et al. 2007). However, phytoplankton have partially adapted to these low Fe conditions by lowering their Fe requirements and increasing their ability for Fe uptake and storage. Strategies employed by some open ocean diatoms, like *Thalassiosira oceanica,* include lowering their PSII:PSI ratio and cytb_6f concentrations (Strzepek and Harrison 2004), substituting Fe-containing proteins with non-Fe-containing counterparts − such as Fdx with FldA (LaRoche et al. 1996; McKay et al. 1999) or cytc_6 with plastocyanin (Peers and Price 2006), and employing a high-affinity Fe uptake system (HAFeT) containing multi-Cu oxidases (MCO) (Maldonado et al. 2006).

The higher Cu requirements in some oceanic phytoplankton—specifically under low Fe—(Annett et al. 2008; Guo et al. 2012), and the identification of plastocyanin (Peers et al.

2005) and MCO (Peers et al. 2005; Maldonado et al. 2006; Guo et al. 2015) inspired further experiments to elucidate the interaction between Fe and Cu nutrition in diatoms. In the last 10 years, some open ocean diatoms (e.g. *T. oceanica*) were shown to have higher Cu:C quotas and faster steady-state Cu uptake rates than their coastal counterparts (e.g. *T. pseudonana*) (Annett et al. 2008; Guo et al. 2012). Furthermore, both *T. oceanica* and *T. pseudonana* have low- and high-affinity Cu uptake systems, but as expected, *T. oceanica* has a more efficient high-affinity Cu uptake system (Guo et al. 2010). Surprisingly, the high-affinity Cu transporters in *T. pseudonana* (*TpCTR* |9391 and *TpCTR* |24275) are up-regulated under low Fe, and down-regulated when Cu-limited cells are resupplied with Cu (Guo et al. 2015).

In summary, the complex interaction between Fe and Cu physiology in open ocean diatoms enables them to survive in low Fe environments. However, their higher Cu requirements might exceed supply in some Fe-limited open ocean settings, thus making diatoms susceptible to Fe-Cu co-limitation (Peers et al. 2005). Iron and Cu enrichment experiments in both the Bering Sea and the North East Pacific suggested that some phytoplankton groups could indeed experience Fe-Cu co-limitation *in situ* (Coale 1991; Peers et al. 2005).

Despite the potential importance of Fe and Cu nutrition in controlling primary productivity, little is known about biochemical changes in the cell in response to Cu or Fe-Cu co-limitation. To investigate the biological effects of these limiting trace metal conditions in diatoms, I grew two strains of the model open ocean diatom *T. oceanica* (TO03 and TO05) under low Cu conditions (Chapter 3), and also under low Fe and Fe-Cu co-limiting concentrations and evaluated cellular changes at the physiological and proteomic level. This Chapter focuses on the photosynthetic modifications, and compares the adaptive strategies a) of each strain to the three low metal conditions, and b) of both strains to each trace metal limiting treatment.

5.3 Results and discussion

In Chapter 3, I presented the contrasting effects of Cu limitation (lowCu) on the photosynthetic apparatus of both strains at the physiological and proteomic level. I analyzed the same parameters for two additional low metal treatments: Fe-limitation and Fe-Cu co-limitation, henceforth called lowFe, and lowFeCu, respectively. Below, I have focused the results and discussion on the most important differences elicited by lowFe, lowCu and lowFeCu in order to highlight a) the important interaction between Fe and Cu physiology in diatoms, and b) the intraspecific differences and similarities.

I will first discuss the trace metal limitation achieved in the different treatments and strains, in order to determine the comparability of the respective findings. Then I will present the changes to the photosynthetic apparatus, including the light-harvesting antennae, in each treatment. Finally, comparisons between the strains will be made and conclusions will be drawn.

Note, that the lowCu data presented here is a summary of Chapter 3. All up- and down-regulated proteins discussed in the present chapter are significantly regulated as defined in Chapter 2 (Methods) (i.e. highly up-regulated, ± 2-fold, $p<0.05$; up-regulated, ± 1.3- to 2-fold, $p<0.05$) unless otherwise noted.

5.3.1 Status of limitation

Before comparing proteomic and physiological responses to low metal availability between the strains, or different metal limitation responses in one strain, it is paramount to ensure that the comparisons are valid. For example, for comparisons between diatoms exposed to low trace metal conditions, either the degree of a trace metal limitation experienced is similar (Bucciarelli

et al. 2010), or the limiting trace metal concentration used is the same for all studied organisms (Strzepek and Harrison 2004). These two approaches are different but equally valid. Given the varying Fe and Cu requirements among diatoms (Annett et al. 2008), for comparisons among different trace metal limiting conditions within a given strain, the degree of limitation (relative decrease in growth rate relative to maximum growth rate, μ/μ_{max}) achieved in each treatment should be identified.

5.3.1.1 LowCu status

For both strains, we used the same Fe replete concentration (1.37 µM $Fe_{[total]}$) as that in previous studies from our laboratory (Maldonado et al. 2006; Guo et al. 2012). However, the Cu replete concentration used in these studies (10.2 nM $[Cu]_{total}$) only supported maximum growth rate for TO03. Hence, we increased the Cu replete concentration for TO05 to 14.3 nM $[Cu]_{total}$ thus enabling it to achieve its maximum growth rate under Fe replete concentration (for a more in-depth discussion of TO05 growth rates, see Chapter 3; for an overview of metal concentrations in our media, see Chapter 2, Table 2.1). Therefore, even though we used different Cu concentrations in the control media for TO03 and TO05, comparisons between the strains are valid, as both achieved maximal growth rates (μ_{max}) in the control treatment and statistically the same percentage of growth rate reduction under lowCu conditions (TO03, 48% of μ_{max}; TO05, 65% of μ_{max}; Figure 5.1A, Table C.1, Table C.2, Table C.3).

5.3.1.2 LowFe status

Under lowFe, we used their respective control Cu concentrations (TO03, 10.2 nM $[Cu]_{total}$; TO05, 14.3 nM $[Cu]_{total}$) but added the same lowFe concentration (12.5 nM $[Fe]_{total}$, as in Guo et

al. (2012). This low Fe level induced a significant growth rate reduction in both strains (Table 5.1): a 15% reduction of μ_{max} in TO03, and a 33% reduction of μ_{max} in TO05. Even though the % reduction of μ_{max} is greater for TO05, TO03 was also experiencing significant Fe limitation. Four lines of evidence support this conclusion.

Firstly, while the reduction in μ/μ_{max} in TO03 was not as severe as in TO05, the reduction was still significant (Figure 5.1). In addition, several well-established proxies of Fe-limitation were observed in low Fe TO03 cultures, including 1) lower F_v/F_m (reviewed by (Behrenfeld and Milligan 2013), 2) down-regulation of ferredoxin (Fdx) combined with an up-regulation of flavodoxin (FldA) (Ferreira and Straus 1994; LaRoche et al. 1996; McKay et al. 1999; Whitney et al. 2011), and 3) up-regulation of a set of iron starvation induced proteins (ISIPs) (Allen et al. 2008; Whitney et al. 2011; Lommer et al. 2012; Morrissey et al. 2015). Specifically, in TO03, each of these proxies behaved as expected for a Fe-limited culture: F_v/F_m was reduced from 0.6 to 0.35 (Figure 5.1 E), Fdx was down-regulated by 1.5-fold (no *p*-value), while FldA was up-regulated by 2.4-fold, and ISIP1A was up-regulated by 2.6-fold (Table 5.1, Table C.4). Thus, we can conclude that TO03 was indeed Fe limited. However, given that under identical Fe concentrations, TO05 achieved slower relative growth rates than TO03, the comparisons between strains should be restricted to adaptations to Fe limitation induced by this low Fe concentration.

Compared to the control, the growth rate of TO05 under lowFe was decreased to the same extent as that under lowCu. Thus, for TO05 comparisons between these two limiting trace metal conditions are sound.

5.3.1.3 LowFeCu status

Iron-Cu co-limitation is considered a Type III co-limitation (Saito et al. 2008), where uptake of one nutrient is dependent on sufficient cellular concentration of the other. To induce Fe-Cu co-limitation, we used the same lowFe concentration that was used to induce the lowFe response (12.5 nM $[Fe]_{total}$). In TO05, this lowFe concentration was combined with the same lowCu concentration that was used to induce its lowCu response (6.1 nM $[Cu]_{total}$), leading to a lowFeCu growth rate of 43% of μ_{max}. In contrast, the lowCu concentration supplied to TO03 (background Cu, <1 nM $[Cu]_{total}$) was insufficient to support growth when combined with the lowFe concentration. Thus, to induce measurable Fe-Cu co-limitation, TO03 had to be cultured with a higher Cu concentration (2.0 nM $[Cu]_{total}$) than its respective lowCu treatment (i.e. TO03: lowCu, <1.0 nM).

Relative to the growth rate achieved in the lowFe condition, the extra growth rate reduction due to Fe-Cu co-limitation was almost identical between the two strains (Figure 5.2, TO03, 67% of μ_{lowFe}; TO05, 63% of μ_{lowFe}). Thus, even though we used different Cu concentrations in the respective lowFeCu media, compared to their respective lowFe growth rate, their additional reduction in growth rate (~34% in both strains) in response to limiting levels of another metal, Cu, is practically the same between the two strains.

5.3.2 Changes in physiology

Chl*a* concentrations are often used as a proxy for phytoplankton biomass. However, the cellular pigment content can change depending on light and nutrient concentrations. Whereas TO03 decreased its cellular Chl*a* concentration drastically (50%) only under lowFeCu conditions, TO05 had the same reduction in cellular Chl*a* under lowFe and lowFeCu.

Furthermore, TO05 also decreased its Chl*a* concentration under lowCu (35% reduction, $p<0.1$) (Figure 5.1 B).

Carbon fixation (normalized to Chl*a*) in TO03 was decreased greatly by both lowCu treatments (lowCu and lowFeCu) (Figure 5.1C). In contrast, carbon fixation was unaffected by lowFe alone, as previously shown for this strain when severely Fe limited (growth rate = 32% of μ_{max}, 0.13 nM $[Fe]_{total}$, Schuback et al. 2015). Similarly, TO05 did not change its ability to fix carbon per Chl*a* under any metal limitation.

Gross oxygen production (normalized to Chl*a*) in TO03 was reduced most severely by lowCu (73%), followed by lowFe (by 42%), and then lowFeCu (by 30%, Figure 5.1D). The severe decrease in oxygen production under lowCu could be due to an increase of cyclic e^- transport around PSII (for further discussion see Chapter 3). TO05, on the other hand, did not modulate its gross oxygen production per Chl*a* in response to low metal availabilities.

F_v/F_m describes the maximum quantum yield of PSII photochemistry. It decreased significantly in all three metal limiting conditions in TO03 (Figure 5.1E). In TO05, F_v/F_m was only decreased in the two lowFe conditions (lowFe and lowFeCu). A constant F_v/F_m under Cu limitation has been previously documented for TO05 (supplementary data in Peers and Price 2006).

$NPQ_{(NSV)}$, non-photochemical quenching, usually increased under all low metal conditions. Relative to the control, TO03 increased $NPQ_{(NSV)}$ in lowCu and lowFeCu conditions (Figure 5.1G). Unfortunately, no results are available for our lowFe treatment. However, in Schuback et al. (2015), NPQ_{NSV} increased significantly in Fe-limited TO03. In TO05, NPQ_{NSV} increased to some extent in lowFe and lowFeCu ($p>0.05$), but remained constant under lowCu.

σ_{PSII}, the antennae absorption cross section in PSII, increased in TO03 by 30% in both lowCu treatments (lowCu and lowFeCu), but remained constant in lowFe (Figure 5.1F). Interestingly, under severe Fe limitation, Schuback et al. (2015) observed in TO03 an increase in σ_{PSII}, thus this parameter could be dependent on the degree of limitation experienced by TO03. In contrast, TO05 increased its antenna size by 20% in the two lowFe treatments (lowFe and lowFeCu) and kept it constant under lowCu, even though its growth rate was limited to a similar extent in the lowCu and lowFe treatments. This means that the degree of growth rate reduction alone is a poor predictor for σ_{PSII}. However, increasing σ_{PSII} may be one strategy of photoacclimation when PSII concentrations are decreased (Moore et al. 2006). In agreement, the treatments with increased σ_{PSII} are indeed the treatments where a decrease in PSII concentration was observed (see schematic visualization of all changes in photosynthetic electron transport chain in Figure 5.3).

Protein per cell concentrations in TO03 remained constant under lowCu but increased under lowFe (2-fold) and lowFeCu (2.5-fold) (Figure 5.1H). In contrast, TO05 protein content decreased when grown under all metal limitations: by 50% in the lowCu and by 75% in the lowFe and the lowFeCu treatments. In TO05, the decrease in overall protein content seems to be its main strategy to reduce its metal requirements (for further discussion Chapter 3).

5.3.3 Changes to the photosynthetic apparatus to balance maximum growth and minimal photodamage under low metal conditions

Limitation by Fe, Cu or Fe-Co poses different challenges for a photosynthetic cell. Trace metal(s) limitation is likely to alter the ideal stoichiometry of the electron transport chain (ETC). Changes in the ETC components will then require further adjustments to proteins up-stream (i.e.

antennae) and downstream (i.e. Fdx/FldA) of the ETC. Each of these changes, in turn, ensures that 1) sufficient light energy is absorbed to support maximal electron transport rates in PSII (ETR_{PSII}) while 2) maximum amounts of ATP and NAD(P)H are generated for cellular metabolism and growth and 3) these changes are finely tuned so that not too much light energy is absorbed, as this would lead to the production of harmful reactive oxygen species (ROS) (Nishiyama et al. 2006; Mackey et al. 2008).

As expected, stoichiometric changes to the ETC differ between strains and among the metal limitation imparted to the diatoms (Figure 5.3). However, it is worth noting that ETR_{PSII} rates did not vary among treatments or strains (Table C.1, Table C.2, Table C.3). This suggests that the acclimation strategies were efficient and allowed the photosystems to remain undamaged. In other words, the new stoichiometry of the electron transport chain was the new ideal under these trace metal limiting conditions. Changes in growth rate in these acclimated diatoms were due to decreases in the number of photosystems and/or alternative metabolic uses (e.g. fighting ROS) of photosynthetic reactants (ATP/NAD(P)H) besides carbon assimilation.

5.3.3.1 LowCu – changes to photosynthetic apparatus

In cyanobacteria and the green lineage of photosynthetic eukaryotes (i.e. chlorophytes, plants), Cu limitation leads to the substitution of the Cu-containing electron carrier plastocyanin with the equivalent Fe-containing cytc_6. Diatoms usually possess only cytc_6 (Groussman et al. 2015), but *T. oceanica* uses plastocyanin, potentially even constitutively (Peers and Price 2006). Even though its genome encodes two putative cytc_6 isoforms (cytc_6 isoformA, THAOC_06916; isoformB, THAOC_24412 (Lommer et al. 2012)), neither was detected in our proteomic dataset nor in any other published work (Strzepek and Harrison 2004; Lommer et al. 2012). It is possible

that cytc_6 was not detected in our data set because cytc_6 is generally only used under Cu limiting conditions (e.g. in *Chlamydomonas,* Quinn and Merchant 1998), thus cytc_6 levels in our control could have been below the detection limit (thus they would not be part of our dataset). The other published studies investigated responses to Fe limitation, making detection of the Fe-containing cytc_6 unlikely, given that plastocyanin is usually considered to be the preferred electron carrier in species that are able to express both (unless Cu is limiting) (Quinn and Merchant 1998).

Traditional PCR can be used to detect qualitatively if a gene of interest is present in the genome. To determine if for example cytc_6 encoding genes are actually transcribed under Cu limitation, reverse transcript PCR (RT-PCR, using mRNA as template) might be a suitable option. To see if the expression level of cytc_6 mRNA changes under varying metal concentrations, qualitative reverse transcript real-time PCR (RT-*q*PCR) would be used, in which a fluorescent dye is used to monitor the amplification reaction in real-time.

As discussed in detail in Chapter 3, the primary response of TO03 to lowCu is a decrease in plastocyanin, thereby generating an 'electron bottleneck' in the ETC just before PSI. In order to accommodate the observed 4-fold decrease in plastocyanin, complexes before plastocyanin were also down-regulated (cytb_6f, 2.3-fold; PSII, ~ 2-fold; Table 5.3**,** Figure 5.3). Even though F'q/F'v, an estimate of the open PSII (i.e. the fraction of oxidized primary electron acceptor Q_A), was decreased by 17%, electron transport rates in PSII (ETR_{PSII}) were not impaired (Table C.2). Indeed, LHC composition and antennae structure had changed successfully to channel an adequate amount of the absorbed light energy towards the PSII core for photochemistry while also dissipating enough excess energy as heat (see increase of NPQ_{NSV}, Figure 5.1G).

Differential expression of LHCs in response to lowCu further confirms my hypothesis [for an overview of highly regulated LHCs (> ±2-fold, $p<0.05$) see Table 5.4; for complete list,

see Table C.5]. Lhcf-Group I proteins are usually associated with light harvesting for photochemistry in PSII. Five of these proteins were strongly down-regulated. Furthermore, three of four known PSI LHCs were also down-regulated (TpFCP2-, TpLhcr10-, and TpLhcr13-homolog) (Grouneva et al. 2011). Energy channelled towards the reaction centres was thereby decreased. In addition, TpLhcf11 and TpLhcr11 were up-regulated. There is evidence that neither of these two LHCs is tightly associated with the thylakoid membrane in *T. pseudonana*, a closely related centric diatom (Grouneva et al. 2011), suggesting that TpLhcf11 and TpLhcr11 might be involved in energy dissipation. A set of four TpFCP homologs (Lhcf-Group III) were also up-regulated. This group is closely related to haptophyte LHCs which are down-regulated in *Emiliania* under high light conditions (McKew et al. 2013), implying a general involvement in stress response or an induction by an overreduction of the ETC. Our study is the first to show differential regulation of this group of LHCs in diatoms (Chapter 3, Hippmann et al. 2017). A well-anticipated LHC group to be up-regulated under stress is the Lhcx clade. Lhcx1 and Lhcx7 were the up-regulated representatives. Lhcx1, a well-studied protein, is often up-regulated under various nutritional stresses and is thought to be involved in increasing NPQ_{NSV} and giving further membrane stability (Green 2007; Koziol et al. 2007; Zhu and Green 2010; Grouneva et al. 2011; Gundermann and Büchel 2014). It can also be associated with both photosystems (Grouneva et al. 2011). Overall, in TO03 grown under lowCu, the antennae appear to decrease the amount of absorbed light energy channelled to photochemistry in exchange for an increase in the amount of absorbed light energy re-emitted as heat to diminish photodamage (see Chapter 3, overview model Figure 3.6).

At the downstream side of PSI, Fdx and FNR were up-regulated (Figure 5.3, Table 5.3). Both have been previously associated with alleviating stress related to ROS (Rodriguez et al.

2007; Lin et al. 2013). Interestingly, two isoforms of flavodoxin were also up-regulated: FldA (THAOC_31152), which is known to be Fe-responsive (LaRoche et al. 1996), by 1.5-fold and another Fld (THAOC_05010) by 3-fold. These two flavodoxins are likely up-regulated in addition to their Fe-containing counterpart Fdx, because of their ability to counteract a variety of cellular stresses. The stress response function of these proteins has been demonstrated in transgenic tobacco plants (Tognetti et al. 2006; Zurbriggen et al. 2008).

The changes to the photosynthetic components in TO05 were much more subtle. The growth rate reduction is mainly attributed to a decrease in overall protein content. Similarly, Chl*a* per cell decreased but so did the cellular volume. Furthermore, the absorption cross section of PSII, as well as the stoichiometry of almost all ETC components stayed constant (Figure 5.3, Table 5.3). Only FldA was up-regulated by 1.4-fold, and one putative stress-related LHC (TpFCP7) by 2.1-fold, thus mirroring the response in TO03 for these parameters. Surprisingly, one other protein was slightly up-regulated under Cu limitation: plastocyanin, by 1.3-fold. Counter-intuitively, this would not have increased cellular Cu levels, considering that the overall cellular protein decreased by 50% and plastocyanin being considered the main Cu-pool in *T. oceanica* (Peers and Price 2006). Thus cellular Cu requirements in TO05 would still be approximately 45% less in the lowCu treatment compared to those in the control. The only potentially down-regulated protein in the ETR in response to lowCu was FNR. No definite answer can be given, as there is only one data point (i.e. no *p*-value for lowCu). However, given that both lowFe and lowFeCu induced a decrease in FNR, this could also be the case under lowCu in TO05.

5.3.3.2 LowFe – changes to photosynthetic apparatus

Under lowFe, a decrease in Fe-containing proteins is expected, in addition to substitutions with non-Fe containing counterparts. Furthermore, proteins involved in Fe-uptake would be anticipated to be up-regulated (Maldonado and Price 1996; Lommer et al. 2010; Morrissey et al. 2015). Yet, neither Fe-transporters nor members of the high-affinity Fe transport systems (HAFeT) (e.g. multi-Cu containing oxidase) were readily identified in our dataset. This is not necessarily surprising, as these proteins a) are membrane-bound, which are notoriously underrepresented in proteomic datasets (Ong and Mann 2005), and b) may be expressed at very low levels, (i.e. below detection) under our control conditions. However, one putative membrane-associated iron-responsive protein (ISIP1A) was found in Fe-limited TO03. ISIP1A has been suggested to be involved in siderophore uptake, delivering the Fe-siderophore complex to the chloroplast (Bowler et al., *submitted*).

The Fe-containing proteins involved in the ETC stayed either constant (PSII and PSI) or were down-regulated: cytb_6f complex by 1.7-fold and Fdx potentially (i.e. one data point; no *p*-value) by 1.5-fold, thereby decreasing cellular Fe requirements. However, having the Fe-responsive FldA and ISIP1A up-regulated, suggests Fdx was likely, and truly down-regulated, as expected in a standard lowFe response. The abundance of both PSII and PSI stayed constant. This seems surprising at first, especially for PSI, being such a Fe-rich complex (with 12 Fe atoms). However, while coastal *Thalassiosira* species indeed lower their PSI:PSII ratio upon Fe limitation, the open ocean adapted *T. oceanica* has already a very low PSI: PSII ratio even under Fe replete conditions (Strzepek and Harrison 2004). I hypothesize that decreasing this ratio further might only be executed under severe Fe limitation. Under the present milder Fe limiting

conditions (85% μ/μ_{max}), a decrease in cytb_6f (5 Fe) and Fdx (1 Fe) seem to be sufficient to lower the photosynthetic Fe demand.

The non-Fe containing proteins in the ETC were all up-regulated. The Fe-responsive FldA, which is thought to act as a substitute for the Fe-containing Fdx, was up-regulated by 2.3-fold. Furthermore, the two proteins that are potentially involved in alleviating ROS and other stressors, FNR and the second Fld isoform (see lowCu response) were up-regulated by 2.7- and 2.3-fold, respectively. Interestingly, the Cu-containing plastocyanin was also up-regulated (by 2-fold). Usually, plastoquinone (PQ) pool oxidation is considered the rate-limiting step in the ETC. However, in barley, a 2- to 3-fold increase in plastocyanin has been shown to support electron flow under high light conditions; most likely due to a higher plastocyanin to PSI ratio (Burkey 1993). Maybe, in diatoms, the up-regulation of plastocyanin might help to ensure that cytb_6f complexes (now in lower abundance) stay oxidized, preventing an electron flow bottleneck in ETC, which would lead to the overreduction of the PQ pool. Unfortunately, we do not have the complete set of FRRF parameters that would allow us to verify changes in the PQ pool size or the oxidation state of the primary electron acceptor at PSII. Another scenario where increasing the plastocyanin content would be advantageous could be if the diffusional motion of PC is inhibited under lowFe and thus a higher pool of PC could buffer the slower movement. However, given our results, there is no obvious physiological explanation for the increased plastocyanin content under lowFe.

The functional absorption cross section (σ_{PSII}) stayed constant under lowFe. However, the LHC composition changed in a very similar fashion as that in lowCu (Table 5.4). Light harvesting for photochemistry in both PSII and PSI was down-regulated (5 Lhcf-Group I and 2 Lhcr LHCs were down-regulated), whereas known (Lhcx) and potentially stress-induced LHCs

(Lhcf-Group III, and the two less tightly membrane-associated TpLhcr11 and TpLhcf11homologs) were up-regulated. Interestingly, two more Lhcr were up-regulated (TpLhcr2, TpLhcr13) demonstrating a finely tuned differentiation between the various LHCs depending on cellular needs.

Contrary to its lowCu response, the Fe-limited TO05 showed a remarkable stoichiometric shift in its photosynthetic apparatus, resembling a textbook response to Fe limitation: all Fe-containing complexes were down-regulated (PSII, 1.5-fold; cytb_6f, 1.8-fold; PSI, 1.9-fold), whereas plastocyanin and FNR remained constant, and FldA was up-regulated by 8-fold. Changes in the regulation of Fdx were not definitive due to insufficient data, but the one single data point we have indicates the expected down-regulation (5.3-fold, no *p*-value).

The increased σ_{PSII} is also expected, given the lower abundance of PSII (Moore et al. 2006), and was accompanied by a lowering of F_v/F_m. Generally, most LHCs seemed to be uniformly down-regulated by 1.2- to 1.5-fold (see Table C.5, underlined expression values have an associated $p<0.05$). The three LHCs that were highly regulated ($> \pm$ 2-fold, $p<0.05$) were: another TpFCP4 homolog (up-regulated), TpFCP10 homolog (down-regulated), and TpLhcr13 homolog (down-regulated). The diatom-specific LHC (THAOC_Tp17531 homolog, 17531-clade) was down-regulated by 1.8-fold. The 17531-homolog in *P. tricornutum* has been found associated with PSI (Grouneva et al. 2011), but no putative role has been suggested for this elusive LHC. Surprisingly, no Lhcx was up-regulated.

5.3.3.3 LowFeCu – changes to the photosynthetic apparatus

Iron and Cu are important co-factors in a series of photosynthetic ETC proteins and thus the growth of open ocean diatoms might be affected by co-limitation of Fe and Cu. Both strains of *T.*

oceanica were Fe-Cu co-limited to a similar extent (as discussed in 5.3.1.3). When TO03 was grown in lowFeCu, all metal-containing components were down-regulated: PSII by 2.3-fold, cytb_6f by 3-fold, plastocyanin by 1.5-fold, PSI by 3-fold and Fdx by 11-fold. All three photosynthetic non-metal containing proteins were up-regulated: the Fe-responsive FldA by 218-fold, the supporting Fld isoform by 4-fold, and FNR by 2.9-fold.

As PSII decreased, σ_{PSII} increased again. The composition of LHCs changed drastically as well, but some unique features appeared compared to the single metal limitations: three of the four Lhcf-Group III LHCs that were up-regulated under single metal limitation were down-regulated under Fe-Cu co-limitation (two TpFCP4 and one TpFCP10 homologs). Maybe lowFeCu poses an even more severe over-reduction of the ETC, approaching a turning point to substitute for more suitable LHCs. In line with this hypothesis, the change in LHCs did dissipate enough energy to even increase the portion of open PSII (Fq/Fv) under lowFeCu. This adaptation suggests that the cells are extremely well equipped to dissipate excess energy as heat. Fittingly, NPQ_{NSV} was also highest under lowFeCu (Figure 5.1G). The Fe-responsive TpLhcr2 homolog that was up-regulated under lowFe was likewise up-regulated under lowFeCu. Curiously, TpLhcx7 homolog was down-regulated under lowFeCu, whereas it was up-regulated under lowCu.

Under lowFeCu, the regulation of the ETC components in TO05 was very similar to those in TO03. Specifically, all metal-containing proteins were down-regulated (PSII, 1.8-fold; cytb_6f, 2.1-fold; plastocyanin, 1.4-fold; PSI, 1.9-fold; Fdx, 1.9-fold). The Fe-responsive FldA was highly up-regulated, too (by 17-fold). However, FNR was down-regulated by 1.6-fold. Sigma and NPQ_{NSV}, on the other hand, followed the same trend as in TO03 (i.e. an increase in absorption cross section σPSII and NPQ_{NSV}). LHCs, however, were only down-regulated

(TpFCP4 homolog and two Lhcr homologs). Interestingly though, the same TpLhcr3 homolog was down-regulated under lowFeCu in TO05 and TO03. Under lowFeCu, a lower concentration of FNR and/or insufficient regulation of LHCs in TO05 may be responsible for a somewhat less efficient ETC compared with that in TO03, as indicated by a lower fraction of open PSII in TO05. However, as mentioned above, the maximal electron transport rate in PSII (ETR_{PSII}) was constant in both strains (Table C.1, Table C.2, Table C.3).

5.3.4 Comparisons of the changes to the photosynthetic apparatus between strains and among trace metal limiting treatments

Comparisons of the changes in the photosynthetic apparatus in response to lowCu, lowFe, and lowFeCu reveal trends and differences between strains and amongst treatments. Most importantly, under trace metal limitation(s), the diatoms changed their photosynthetic protein inventories to prevent photodamage while retaining maximal rates of electron transport in PSII.

There are two main themes that stand out regarding regulation of proteins in TO03: 1) metal-dependent modulation (i.e. protein regulation depends on the limiting metal) and 2) metal-independent modulation (i.e. regulation seems related to a more general stress response). I will discuss these first in TO03 and will proceed with comparing them with those in TO05.

Metal-dependent regulation. The regulation of certain proteins seemed to be determined by whether Fe or Cu concentrations were limiting growth. For example, under lowCu, PSII was decreased to accommodate lower levels of essential downstream PSII components, such as plastocyanin. In contrast, in lowFe, PSII remained constant, possibly because under mild Fe limitation a decrease in cytb_6f and Fdx was sufficient to lower cellular Fe requirements while

supporting optimal photosystem activity. However, under Fe-Cu co-limitation (lowFeCu), lower Cu concentrations might have caused slower rates of Fe transport, thus intensifying Fe limitation, and resulting in a need for reduction of all photosynthetic Fe-containing proteins. A similar chain of explanations is possible for PSI. However, in contrast to the lowCu induced down-regulation of PSII, PSI was unaffected by lowCu. This might be because PSI is down-stream of the electron transport bottleneck generated by a decrease in plastocyanin. Thus, regulation of PSII and PSI seems to vary depending on the unique stoichiometric pattern imposed by the distinct metal limitations.

The regulation of plastocyanin seems to be mainly Cu dependent. At the lowest Cu concentration, plastocyanin was down-regulated by 4-fold. Similarly, under lowFeCu (with slightly higher lowCu concentrations), it was decreased by 1.5-fold. Puzzlingly, lowFe induced up-regulation of plastocyanin by 2-fold. Whether plastocyanin might fulfil a similar buffer capacity for electrons between cytb_6f and PSI, as the plastoquinone pool between PSII and cytb_6f, remains to be seen.

Ferredoxin seems to be used to alleviate electron pressure under lowCu and was hence highly up-regulated (more on the use of Fdx to alleviate electron pressure, Chapter 4, 4.4.2). However, under both lowFe conditions, this Fe-containing carrier was replaced with the non-Fe-containing alternative FldA.

In general, TO05 only modulated its protein levels moderately. Plastocyanin levels, even though also changing in a metal-dependent manner, did so differently compared to TO03: it increased somewhat under lowCu (by 1.3-fold), stayed constant under lowFe and increased under lowFeCu (by 1.4-fold). As discussed under 5.3.3.1, the counter-intuitive slight increase under lowCu, would not impact cellular Cu levels greatly, but, taking the overall 50% decrease

in cellular protein content into account (Figure 5.1H), it would still result in an overall decrease in cellular Cu content of ~ 45%. Under lowFe, plastocyanin remains constant, whereas it is decreased under lowFeCu. The main strategy used by TO05 to decrease its cellular metal requirements was decreasing its overall proteome, by 50% in lowCu and by 75% in each lowFe and lowFeCu treatment (relative to the control). Additional modulation of ETC components occurred in TO05 only under lowFe and lowFeCu, in which Fe-containing proteins were down-regulated and FldA was up-regulated. Interestingly, the lowFeCu response of TO05 seems to be a more pronounced lowFe response (PSII from 1.5-fold down-regulation to 1.8-fold; cytb_6f from 1.8-fold to 2.1-fold; plastocyanin from 1 to 1.4-fold, PSI from 1.7-fold to 3-fold), thus underlining the Type III co-limitation in this strain.

Metal-independent regulation might be more closely connected to a holistic cellular stress-response, such as excess intracellular reducing equivalents or suboptimal pH. This was observed in TO03 in the expression of FNR and both Fld isoforms, where protein levels were enhanced in all trace metal limiting treatments. These proteins are generally associated with alleviating various cellular stresses (Rodriguez et al. 2007; Zurbriggen et al. 2008). Interestingly, TO05 did not express the second flavodoxin isoform. Furthermore, in contrast to TO03, the expression of FNR was either maintained or down-regulated. The inability to use the second isoform of Fld and increase FNR, both proteins potentially involved in alleviating ROS, might be one reason why TO05 is more susceptible to low metal concentrations compared to TO03.

5.3.4.1 Iron-Cu co-limitation in *T. oceanica* – more than just Type III

Co-limitation can occur in three theoretical forms (see Saito et al., 2008 and references therein). Type I co-limitation occurs when both nutrients are potentially limiting on their own, independent of each other (i.e. "independent" in the strict sense that they are neither dependent as described for Type II or Type III). In Type II, one nutrient can substitute for the other either through 1) direct substitution of co-factors in the same protein or 2) as co-factors of proteins that fulfil the same task (e.g. plastocyanin and cytc_6 in *Chlamydomonas*). In Type III, uptake of one nutrient is dependent on the other. Iron-Cu co-limitation has been deemed "Type III – biochemically dependent" as Cu is needed in the high-affinity uptake of Fe (Maldonado et al. 2006). However, given that in the open ocean diatom *T. oceanica*, plastocyanin accounts for the vast majority of its intracellular Cu-pool (Peers and Price 2006), the interaction between Fe and Cu in photosynthesis might be even more intriguing and interesting.

I propose an integrated Fe-Cu co-limitation in the form of a combined Type III and Type I limitation. Evidence for the classic Type III Fe-Cu co-limitation is observed in both strains: even though the same Fe concentration (42 nM Fe) was used for lowFe and lowFeCu media, all Fe-containing proteins were reduced further in the lowFeCu compared to the lowFe only media (Figure 5.3). When Cu concentration was decreased in the lowFeCu media to the lowCu-only concentration (i.e. no Cu added), TO03 could not survive. In a Type III co-limitation, this would be predominantly due to the need for Cu in Fe-uptake. My data suggest that this is only part of the story, as in TO03, Cu requirements are expected to be higher under low Fe because of the increase in plastocyanin (i.e. it is up-regulated by 2-fold under lowFe). Perhaps, the extra plastocyanin helps to compensate for the decrease in cytb_6f in maintaining electron flow in the ETC.

Thus, under lowFeCu, plastocyanin levels could not be down-regulated to the same extent as in lowCu (by 4-fold), but only by 1.5-fold. This decrease could be explained in two ways. First, the higher Cu concentration in lowFeCu (2 nM Cu) relative to that in lowCu (<1 nM Cu) will permit higher plastocyanin expression. Secondly, in the lowFe medium, the Cu concentrations (10.2 nM) might have been sufficient to support the higher plastocyanin levels observed in order to alleviate the stress incurred by lowFe, as well as the Cu required for the high-affinity Fe uptake system. In contrast, under lowFeCu, the Cu concentration was almost an order of magnitude lower (1.96 nM Cu) than that under lowFe, thus the cell would have had a much lower intracellular Cu pool to fulfil the Cu demand of both photosynthetic electron and cellular Fe transport. Without data on TO03 grown with 2 nM Cu under Fe replete conditions, or maybe even qPCR data on MCO expression under lowCu *vs.* lowFe *vs.* lowFeCu, it is speculative to select which scenario is correct. However, either one of these scenarios would further support a Type I Fe-Cu co-limitation.

It is possible that the ratio between cytb_6f and plastocyanin might play a bigger role in sustaining an efficient electron flow under Fe-limitation than previously thought. In Table 5.5, I normalized the differential expression of the four major ETC components (PSII, cytb_6f, plastocyanin, PSI) to the differential expression of cytb_6f. Under lowCu, cytb_6f: plastocyanin is 1:0.6, reflecting the 2.3-fold decrease in cytb_6f and the 4-fold decrease in plastocyanin. Under lowFe, the ratio is 1:3.5 (reflecting the 1.7-fold decrease in cytb_6f and the 2-fold increase is plastocyanin). As discussed above, the plastocyanin pool might have some electron buffering capacity to ensure that cytb_6f is oxidized at all times. Under lowFeCu, this putative buffer capacity would still be needed, thus the cytb_6f: plastocyanin ratio (1:2, reflecting the 3-fold

decrease in cytb_6f and the 1.5-fold decrease in plastocyanin) resembles more the lowFe response (1:3.5) than the lowCu one (1:0.6).

5.4 Conclusion

Overall, open ocean diatoms seem to be well equipped to adapt to chronic metal limitation (days/weeks), which they might experience often in their natural habitat (Behrenfeld and Milligan 2013). In general, TO03 is ultimately capable of withstanding lower Fe and Cu concentrations than TO05. Indeed, TO03 is able to make significant and complex changes to its light-harvesting components and photosynthetic ETC proteins, including plastocyanin, depending on the trace metal limitation experienced by the cell and its general needs. Furthermore, TO03 can enlist in the up-regulation of proteins potentially involved in the alleviation of ROS, such as FNR and two types of flavodoxins.

According to the results presented here, the interaction between Fe and Cu, as trace metals potentially limiting primary productivity, is synergistic. Importantly, this means that we cannot predict changes in the stoichiometry of proteins or their absolute levels by examining the response to a single metal limitation in the laboratory. Furthermore, the proteomic response to trace metal limitation(s) by these two closely related *T. oceanica* strains was extremely different. These differences couldn't have been inferred from genomic data. In general, intraspecific strain differences have become the focus of many recent investigations, both in natural assemblages and model species (Von Dassow et al. 2008; Kremp et al. 2012; Kim et al. 2015; Luxem et al. 2017; Hippmann et al. 2017). Ultimately, predicting which strain will be more successful in its original habitat will be difficult, as environmental conditions in the sea are very dynamic. However, a deeper understanding of the possible stoichiometries of a fully operational

photosynthetic apparatus under various trace metal limiting conditions is useful for interpreting *in situ* findings.

5.5 Tables and figures

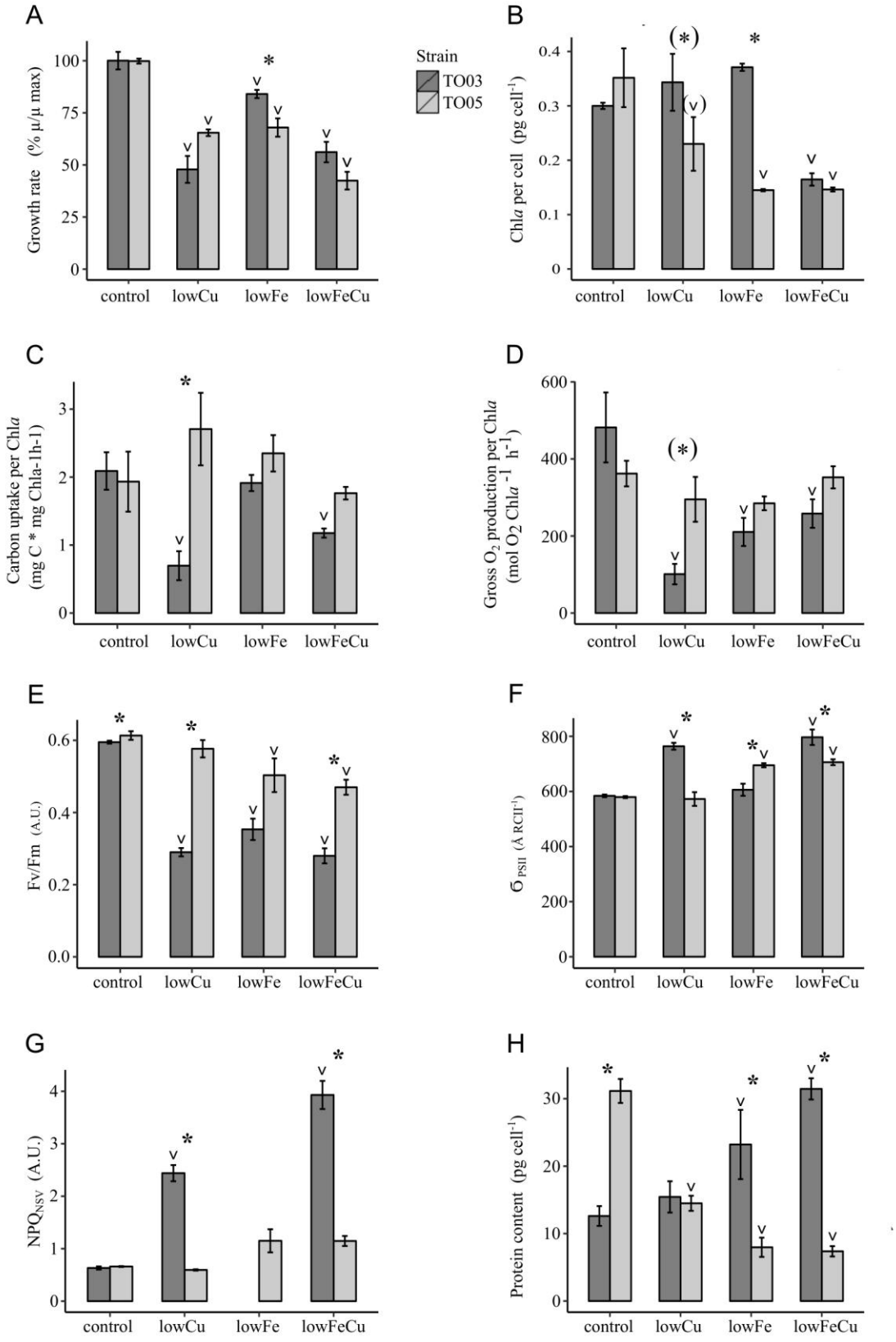
A
Growth rate (% μ/μ max)
100
75
50
25
0
control
lowCu
lowFe
lowFeCu
Strain
TO03
TO05
B
Chla per cell (pg cell-1)
0.4
0.3
0.2
0.1
0
C
Carbon uptake per Chla
(mg C * mg Chla-1h-1)
3
2
1
0
D
Gross O2 production per Chla
(mol O2 Chla -1 h-1)
600
400
200
0
E
Fv/Fm (A.U.)
0.6
0.4
0.2
0.0
F
σPSII (A RCII-1)
800
600
400
200
0
G
NPQNSV (A.U.)
4
3
2
1
0
H
Protein content (pg cell-1)
30
20
10
0

Figure 5.1 The effects of all three low metal treatments (lowCu, lowFe, lowFeCu) on various physiological parameters in two strains of *T. oceanica*, CCMP 1003 (TO03) and 1005 (TO05). A) relative growth rate, **B)** Chl*a* per cell, **C)** carbon uptake at growth irradiance, **D)** gross oxygen production, **E)** F_v/F_m, **F)** absorption cross section of PSII antennae, σ_{PSII}, **G)** NPQ_{NSV} at growth irradiance, **H)** cellular protein content. The values are means ± standard error of three biological replicates. Differing signs above columns indicate statistically significant changes ($p<0.05$) using a 2-way ANOVA with post-hoc interaction analysis (see methods for details): * indicates significant difference between strains in the same treatment (intraspecific), (*) indicates differences with $p<0.01$, ∨ indicates significant difference between one specific treatment of one strain *vs.* its respective control (e.g. TO03 lowFeCu *vs.*TO03 control).

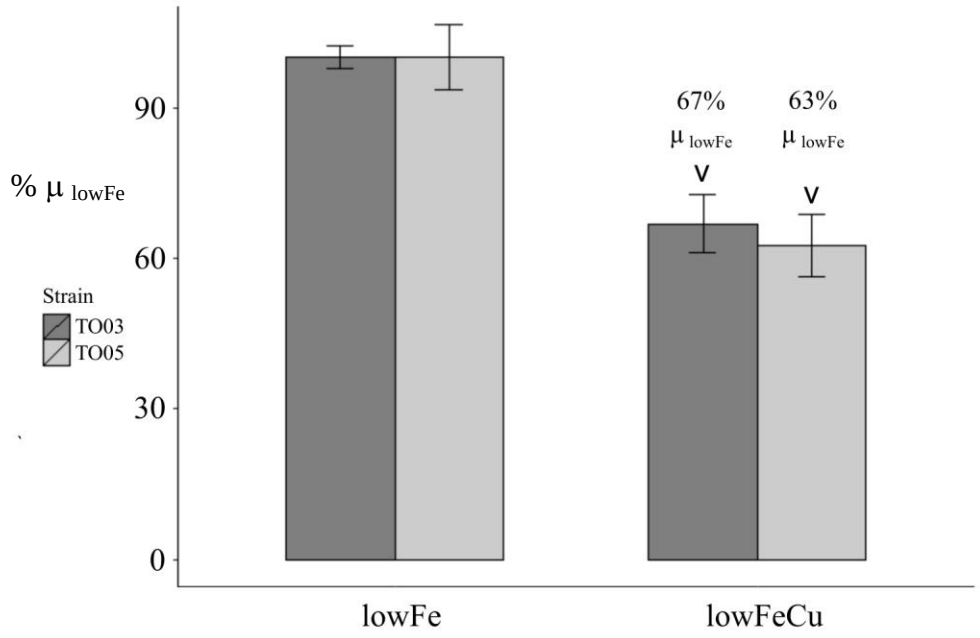

Figure 5.2 Percent growth rates for the Fe-Cu co-limited cultures (lowFeCu) of *T. oceanica* CCMP 1003 (TO03) and 1005 (TO05) relative to their respective Fe-limited growth rates (lowFe). The values are means ± standard error of three biological replicates.∨ indicates significant difference between lowFeCu and lowFe.

Table 5.1 Expression of iron-responsive proteins in two strains of *T. oceanica,* CCMP 1003 (TO03) and 1005 (TO05), grown under low Cu (lowCu), low Fe (lowFe), and low Fe and Cu conditions (lowFeCu).

		TO03 lowCu[a]		TO03 lowFe[a]		TO03 lowFeCu[a]		TO05 lowCu[a]		TO05 lowFe[a]		TO05 lowFeCu[a]	
Gene name	**Name**	sol	insol	sol	insol	sol	insol	sol	insol	sol	insol	sol	insol
ISIPS, iron starvation induced proteins													
THAOC_30995	ISIP1A, isoform A	1.56		**2.57**	1.52	**9.41**	**16.19**	*1.51*	1.41	**7.14**	**34.1**	**6.64**	**9.04**
THAOC_34758, contig_117647_681_1617_-	ISIP3							*1.01*	*1.37*	***18.3***	***19.2***	***15.33***	*18.94*
THAOC_36410	ISIP2A, isoform A								1		-1.37	-1.58	-1.15
ferredoxin													
THAOC_25559	petF	**43.79**		-1.46		**-11.02**		-1.48		*-5.31*		-1.21	-1.85
flavodoxin													
THAOC_05010	fld	**2.95**		**2.32**		**3.82**							
THAOC_31152	fldA, isoform A	1.44		**2.35**		**218.8**		1.4		**8.09**		**17.24**	**20.77**
FNR, ferredoxin-NADP+ reductase													
THAOC_06509	FNR	-1.46		-1.27		-1.05		-1.14	-1.14	1.27		1.34	1.35
THAOC_36724	FNR	**2.47**		**2.71**		**2.88**		-1.34		-1.32		-1.62	*-1.83*
THAOC_36724, contig_64183_1_637_+	FNR	***5.5***		***4.15***		***3.92***							

[a]expression of proteins given in fold-change as per original proteomic analysis (see methods for details); bold indicates highly differential expression (>± 2-fold, $p<0.05$); underlined indicates moderate differential expression (>±1.3- to 2-fold, $p<0.05$), italic indicates expression value is derived from EST proteomic analysis

Table 5.2 Significantly differentially expressed LHCs in two strains of *T. oceanica,* CCMP 1003 (TO03) and 1005 (TO05), grown under low Cu (lowCu), low Fe (lowFe), and low Fe and Cu conditions (lowFeCu).

Gene name[a]	closest homolog[b]	TO03 lowCu[c]	TO03 lowFe[c]	TO03 lowFeCu[c]	TO05 lowCu[c]	TO05 lowFe[c]	TO05 lowFeCu[c]	Evidence for role in other diatoms
Lhcf - Group I								
THAOC_01208	TpLhcf	**-2.79**						
THAOC_01927	TpLhcf	**-2.04**	**-2.04**					
THAOC_06305	TpLhcf	***-10.34***	**-8.21**	**-2.07**				light harvesting
THAOC_20854	TpLhcf	**-5.56**	**-5.1**	**-2.79**				light harvesting
THAOC_20855	TpLhcf			**-3.9**				
THAOC_25270, contig_123884_1_219_-	TpLhcf		***-2.23***					
THAOC_32932	TpLhcf8	**-2.12**	**-2.05**	**-2.23**				light harvesting, trimers, oligomers[d,e]
THAOC_36248	TpLhcf			**3.55**				
Lhcf - Group II								
THAOC_09684	TpLhcf11	**4.83**	**3.7**	**2.52**				
Lhcf - Group III								
THAOC_04469	TpFCP4	**2.06**	**2.09**	**-5.65**				
THAOC_05777	TpFCP10	**2.4**	**2.28**	**-2.22**		**-2.14**		
THAOC_06968	TpFCP2	**-2.52**		**-2.37**				in TP tightly bound to PSI[f,g]
THAOC_08587	TpFCP7	**2.79**	**2.54**	**-2.72**	**2.07**			close to haptophyte LHCs[f]
THAOC_16345	TpFCP4	**2.68**	**2.17**					
THAOC_18994	TpFCP4					**2.48**	***2.87***	

Gene name[a]	closest homolog[b]	TO03 lowCu[c]	TO03 lowFe[c]	TO03 lowFeCu[c]	TO05 lowCu[c]	TO05 lowFe[c]	TO05 lowFeCu[c]	Evidence for role in other diatoms
Lhcr								
THAOC_00550	TpLhcr11	***2.39***	***2.33***	**-6.64**				PS I light harvesting[g, h]
THAOC_05707	TpLhcr4		**-9.33**					
THAOC_05708	TpLhcr14			**-2.21**				
THAOC_07034	TpLhcr13		**2.08**					
THAOC_07036	TpLhcr13	**-6.57**	**-5.79**	**-2.75**		**-2.09**	**-2.18**	PS I light harvesting[g, h, i]
THAOC_16963	TpLhcr3			**-6.51**			**-2.23**	
THAOC_34573	TpLhcr2		**3.06**	**3.12**				
THAOC_35518	TpLhcr10	**-2.55**		**-4.93**				PS I light harvesting[g, h]
Lhcx								
THAOC_08095	TpLhcx7	***2.76***		**-2.78**				
THAOC_08095, contig_119183_41_788_+	TpLhcx7			***-2.39***				
THAOC_09937	TpLhcx1	**3.29**	**3.09**	**12.57**				photoprotection, stress response, associated with both PSI + II, FCP trimers, oligo, or only loosely associated with membrane, facilitates NPQ [g, h, i,j, k]
THAOC_31988	TpLhcx1	***3.29***	***3.14***	**12.41**				

[a]grouped into different LHC clades as per phylogenetic analysis (Chapter 3, Figure 3.5)

[b]closest homolog as per phylogenetic analysis (Chapter 3, Figure 3.5)

[c]expression of proteins given in fold-change as per original proteomic analysis (see methods for details); italic indicates that expression value is derived from EST proteomic analysis

[d](Ikeda et al. 2013)

[e](Nagao et al. 2013)

[f](Hoffman et al. 2011)

[g](Grouneva et al. 2011)

[h](Gundermann and Büchel 2014)

[i](Green 2007)

[j](Zhu and Green 2010)

[k](Koziol et al. 2007)

Table 5.3: Differential expression of proteins involved in the photosynthetic electron transport chain (ETC) in two strains of *T. oceanica,* CCMP 1003 (TO03) and 1005 (TO05), in response to chronic metal limitation induced by low Cu (lowCu), low Fe (lowFe), and low Fe and Cu concentrations (lowFeCu).

Gene name[a]	Protein name	TO03 lowCu[b] sol	TO03 lowCu[b] insol	TO03 lowFe[b] sol	TO03 lowFe[b] insol	TO03 lowFeCu[b] sol	TO03 lowFeCu[b] insol	TO05 lowCu[b] sol	TO05 lowCu[b] insol	TO05 lowFe[b] sol	TO05 lowFe[b] insol	TO05 lowFeCu[b] sol	TO05 lowFeCu[b] insol
PSII													
THAOC_34020	psb27-like, involved in Mn cluster formation	1.73	*1.13*	1.43		1.14	*1.84*	-1.21	1	-1.6	-1.4	-1.42	-1.51
psbA	psbA, PSII protein D1		-1.92		1.09		-1.63		-1.03		-1.41	-1.69	-1.71
psbA, contig_8044_1_175_+	psbA, PSII protein D1		***-2.45***		*-1.06*		***-2.05***		*-1.2*		*-1.61*		*-1.99*
psbB	psbB, PSII CP47 RC protein		-1.61		-1.28		**-2.18**	-1.61	-1.1		-1.43	-1.53	-1.43
psbC, THAOC_26185	psbC, PSII CP43 RC protein								1.05		-1.41	-1.53	-1.36
psbC, THAOC_26185	psbC, PSII CP43 RC protein		**-2.1**		-1.22		**-3**						
psbD, THAOC_24371	psbD, PSII D2 protein		***-2.01***		*-1.14*		***-2.48***						
psbD, THAOC_24371	psbD, PSII D2 protein		**-2.1**		-1.08		**-2.02**		-1.01		-1.34	-1.57	-1.39
psbE, THAOC_24363	psbE, cytb_{559} subunit alpha		***-2.28***		*-1.1*		***-2.21***		*-1.2*		*-1.42*		*-1.91*
psbE, THAOC_24363	psbE, cyt b_{559} subunit alpha		**-2.25**	*4.15*	-1.1	*4.38*	**-2.19**		-1.22		-1.38	-1.92	-1.71
psbH	psbH, PSII RC protein H				-1.23		-1.37		-1.61		-1.61	**-2.47**	**-2.77**
psbL	psbL, PSII reaction center protein L		-1.63		-1.48		**-2.97**		-1.12				*-2.62*
THAOC_03193	psbO, Mn-stabilizing protein	-1.41		1.15		-1.09		-1.27	-1.03	-1.42	-1.26	-1.18	-1.06
THAOC_15373	psbP, oxygen-evolving enhancer protein 2 (OEE2)							-1.06		-1.16		1.03	-1.26

Gene name[a]	Protein name	TO03 lowCu[b] sol	TO03 lowCu[b] insol	TO03 lowFe[b] sol	TO03 lowFe[b] insol	TO03 lowFeCu[b] sol	TO03 lowFeCu[b] insol	TO05 lowCu[b] sol	TO05 lowCu[b] insol	TO05 lowFe[b] sol	TO05 lowFe[b] insol	TO05 lowFeCu[b] sol	TO05 lowFeCu[b] insol
THAOC_08500	psbQ, oxygen-evolving enhancer protein 3 (OEE3)	-1.15	**-2.96**	1.34	1.06	-1.86	**-2.04**	-1.44	1.34	-1.71	-1.48	-1.66	**-2.13**
THAOC_09685	psbU-like, small extrinsic protein	1.62		3.14	-1.29	1.45	*-2.68*	-1.19	1.31	-1.22	-1.58	-1.19	-1.19
psbV, THAOC_30541	psbV, cytc_{550}		*1.56*	1.1		*-1.89*	*4.92*	*1.06*	*1.18*	*-1.2*	*1.6*	*-1.33*	*1.48*
psbV, THAOC_30541	psbV, cytc_{550}	1.07	1.56	1.11		-1.73	*4.92*	1.04	1.18	-1.26	1.6	1.09	1.13
psbY	psbY, PSII protein Y								-1.12		-1.33	-1.68	-1.87
PET													
petA	petA, cyt*f*		*-1.65*		*-1.49*		***-2.93***		-1.12		-1.99	**-2.02**	**-2.04**
petB, THAOC_26188	petB, cytb_6		**-2.33**		-1.92		***-4.69***		-1.16		-1.64	-1.91	**-2.15**
THAOC_33417	petC, Fe-S subunit (Rieske protein)		-1.51		-2.83		-3.97		*-1.48*		-1.93	**-2.15**	**-2.21**
THAOC_33417, contig_35113_1_741_+	petC, Fe-S subunit (Rieske protein)		*-1.01*				*-1.47*		-1.2				*-1.86*
petD, THAOC_24366	petD, cytb_6f complex subunit 4								*-1.15*		*-1.86*		***-2.27***
petD, THAOC_24366	petD, cytb_6f complex subunit 4								-1.1		-1.88	**-2.34**	**-2.01**
THAOC_06915, contig_97569_1_258_-	petE, plastocyanin							*-1.92*		*1.12*			
THAOC_29732	petE, plastocyanin	**-4.41**		**2.23**		-1.49		1.16	1.32	-1.46	-1.14	-1.3	-1.41
PS I													
psaA	psaA, PSI P700 chl*a* apoprotein A1		-1.21		-1.14		**-3.03**		1.14		-1.54	-1.74	-1.7
psaB	psaB, PSI P700 chl*a* apoprotein A2		1.11		-1.07		**-2.18**		1.01		-1.73	**-2.14**	**-2.08**
psaC	psaC, PSI Fe-S center		-1.18		-1.65		**-6.95**		1.2		-1.55	**-2.05**	-1.98
psaD, THAOC_24369	psaD, PSI RC subunit II		*1.2*		*1.12*		***-2.71***	*-1.02*	*-1.02*	*1.09*	*-1.83*	*1.02*	***-2.17***

Gene name[a]	Protein name	TO03 lowCu[b] sol	TO03 lowCu[b] insol	TO03 lowFe[b] sol	TO03 lowFe[b] insol	TO03 lowFeCu[b] sol	TO03 lowFeCu[b] insol	TO05 lowCu[b] sol	TO05 lowCu[b] insol	TO05 lowFe[b] sol	TO05 lowFe[b] insol	TO05 lowFeCu[b] sol	TO05 lowFeCu[b] insol
psaD, THAOC_24369	psaD, PSI RC subunit II		1.2		1.16		**-2.59**	1	-1.01	1.21	-1.88	-1.91	-1.95
psaF	psaF, PSI RC subunit III		-1.2		-1.03		**-2.3**		1.04		-1.7	-1.86	-1.75
psaL, THAOC_24361	psaL, PSI RC subunit XI		*-2.08*		*-1.56*		*-4.09*		*1.31*		*-1.56*		*-1.96*
psaL, THAOC_24361	psaL, PSI RC subunit XI		-1.56		-1.56				-1.05		-1.76	**-2.83**	**-2.23**
PET													
THAOC_05010	fld, flavodoxin	**2.95**		**2.32**		**3.82**							
THAOC_31152	fldA, isoform A	1.44		**2.35**		**218.8**		1.4		**8.09**		**7.36**	**20.77**
THAOC_25559	petF, ferredoxin	**43.79**		-1.46		**-11.02**		-1.48		*-5.31*		-1.21	-1.85
THAOC_36724	petH, FNR	**2.47**		**2.71**		**2.88**		-1.34		-1.32		-1.62	-1.83
THAOC_36724, contig_64183_1_637_+	petH, FNR			***4.15***		***3.92***							
THAOC_36724	FNR	**2.47**		**2.71**		**2.88**		-1.34		-1.32		-1.62	*-1.83*
THAOC_36724, contig_64183_1_637_+	FNR	***5.5***		***4.15***		***3.92***							
THAOC_06509	FNR	-1.46		-1.27		-1.05		-1.14	-1.14	1.27		1.3	1.35

[a]grouped into core photosynthetic protein complexes (PSII, PSI) and proteins involved in photosynthetic electron transfer (PET)
[b]expression of proteins given in fold-change as per original proteomic analysis unless in italics, then as per +EST dataset (see methods for details); bold indicates highly regulated changes in expression as defined in methods (>± 2-fold, $p<0.05$); underlined indicates moderately regulated changes in expression (>±1.3-fold $p<0.05$).
chl*a*, *c*hlorophyll*a*; cyt, cytochrome; FNR, ferredoxin: $NADP^+$ reductase; PS, photosystem; RC, reaction centre

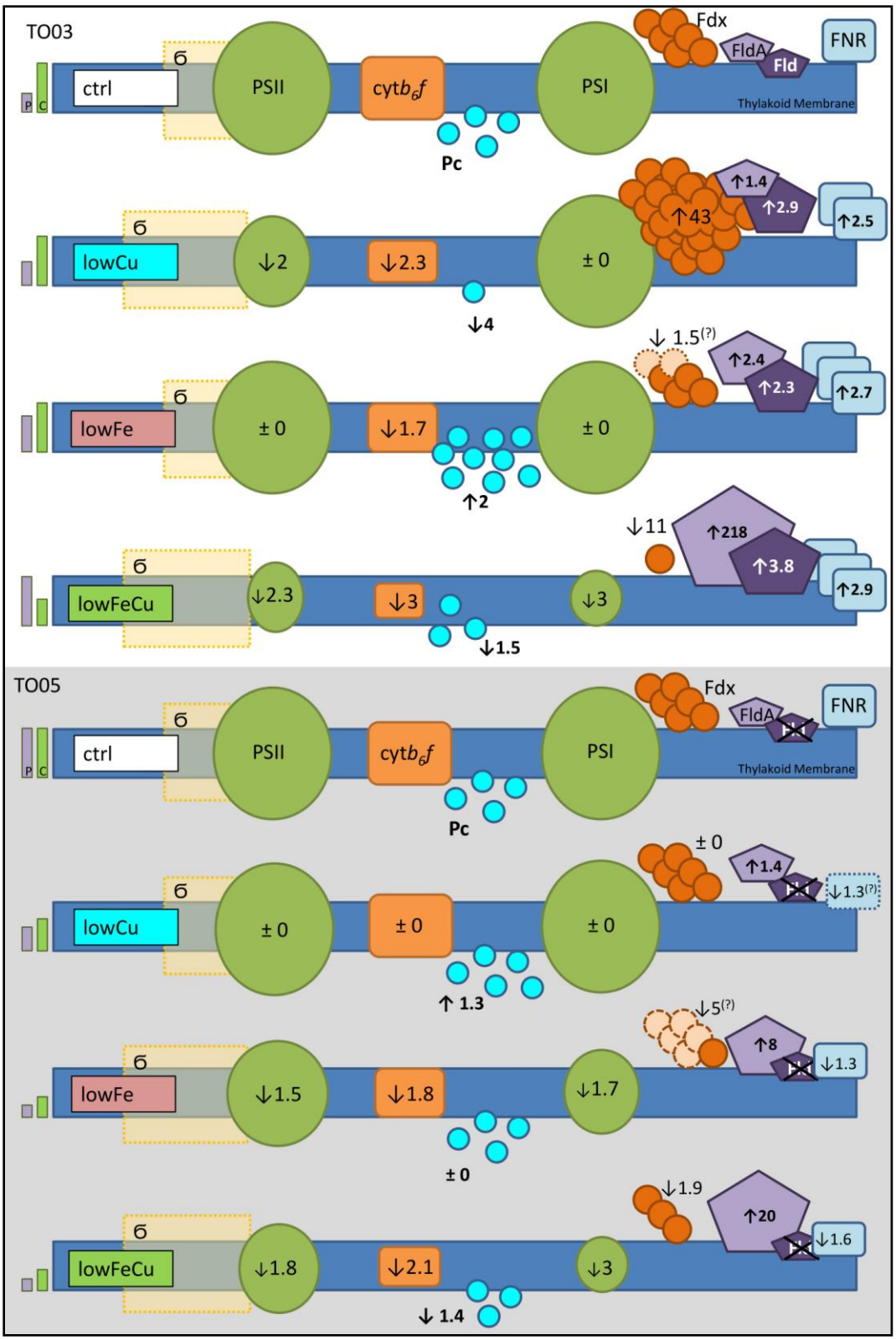
TO03
ctrl
PSII
cytb6f
PSI
Fdx
FldA
Fld
FNR
Thylakoid Membrane
Pc
lowCu
↓2
↓2.3
± 0
↑43
↑1.4
↑2.9
↑2.5
↓4
lowFe
± 0
↓1.7
± 0
↓ 1.5(?)
↑2.4
↑2.3
↑2.7
↑2
lowFeCu
↓2.3
↓3
↓3
↓11
↑218
↑3.8
↑2.9
↓1.5
TO05
ctrl
PSII
cytb6f
PSI
Fdx
FldA
FNR
Thylakoid Membrane
Pc
lowCu
± 0
± 0
± 0
± 0
↑1.4
↓1.3(?)
↑ 1.3
lowFe
↓1.5
↓1.8
↓1.7
↓5(?)
↑8
↓1.3
± 0
lowFeCu
↓1.8
↓2.1
↓3
↓1.9
↑20
↓1.6
↓ 1.4

Figure 5.3 Model of the proteomic and selected physiological changes observed in the photosynthetic electron transport chain (ETC) of two strains of *T. oceanica* (CCMP 1003, TO03, and 1005, TO05) in response to low Cu (lowCu), low Fe (lowFe), and low Fe and Cu conditions (lowFeCu) compared to optimal metal levels (control). Depending on the strain and the limiting metal(s) treatment, acclimation results in the up- and down-regulation of different components of the ETC. (?) indicates that this ratio was only detected in one of the three biological replicates, thus it has no *p*-value associated; C, Chla concentration per cell (Figure 5.1); Ctrl, control; cytb_6f, cytochromeb_6f complex; Fdx, ferredoxin; Fld, flavodoxin; FldA, flavodoxin isoform A; FNR, ferredoxin-$NADP^+$- reductase; P, Protein concentrations per cell (Figure 5.1); Pc, plastocyanin; PSI, photosystem I; PSII, photosystem II; σ, antenna absorption cross section of PSII, σPSII (Figure 5.1).

Table 5.4: Overview of all highly regulated LHC in two strains of *T. oceanica* (CCMP 1003, TO03, and 1005, TO05) in response to low Cu (lowCu), low Fe (lowFe), and low Fe and Cu conditions (lowFeCu).

Strain and Treatment	Lhcf – Group I[a]	Lhcf – Group II[a]	Lhcf – Group III[a]	Lhcr[a]	Lhcx[a]
TO03					
lowCu		**Lhcf11**-09684 ↑	**FCP4**-04469 ↑ **FCP4**-16345 **FCP7**-08587 **FCP10**-05777	**Lhcr11**-00550 ↑	**Lhcx1**-09937 ↑ **Lhcx1**-31988 **Lhcx7**-08095
	Lhcf8-32932 **Lhcf**-01208 **Lhcf**-01927 **Lhcf**-06305 **Lhcf**-20854 ↓		**FCP2**-06968 ↓	**Lhcr10**-35513 **Lhcr13**-07036 ↓	
lowFe		**Lhcf11**-09684 ↑	**FCP4**-04469 ↑ **FCP4**-16345 **FCP7**-08587 **FCP10**-05777	**Lhcr2**-34573 ↑ **Lhcr11**-00550 **Lhcr13**-07034	**Lhcx1**-09937 ↑ **Lhcx1**-31988
	Lhcf8-32932 **Lhcf**-01927 **Lhcf**-06305 **Lhcf**-20854 **Lhcf**-25270 ↓			**Lhcr4**-05707 **Lhcr13-07036** ↓	
lowFeCu	**Lhcf**-36248 ↑	**Lhcf11**-09684 ↑		**Lhcr2**-34573 ↑	**Lhcx1**-09937 ↑ **Lhcx1**-31988
	Lhcf8-32932 **Lhcf**-06305 **Lhcf**-20854 **Lhcf**-20855 ↓		**FCP2**-06968 **FCP4**-04469 **FCP4**-16345 **FCP10**-05777 ↓	**Lhcr3**-16963 **Lhcr10**-35513 **Lhcr11**-00550 **Lhcr14**-05708 ↓	**Lhcx7**-08095 ↓
TO05					
lowCu			**FCP7**-08587 ↑		
lowFe			**FCP4**-18994 ↑		
			FCP10-05777 ↓	**Lhcr13**-07036 ↓	
lowFeCu			**FCP4**-18994 ↓	**Lhcr3**-16963 **Lhcr13**-07036 ↓	

[a]bold: name of Tp homolog as per phylogenetic tree; number after name indicates THAOC_ gene model; arrows indicate up- or down-regulation (>±2-fold, $p<0.05$)

Table 5.5: Changes in stoichiometry in the ETC normalized to the change seen in cytb_6f in two strains of *T. oceanica* (CCMP 1003, TO03, and 1005, TO05) in response to low Cu (lowCu), low Fe (lowFe), and low Fe and Cu conditions (lowFeCu).

Treatment	PSII	**cytb_6f**	**plastocyanin**	PSI
TO03				
lowCu	1.2	**1**	**0.6**	2.3
lowFe	1.7	**1**	**3.5**	1.7
lowFeCu	1.3	**1**	**2**	1
TO05				
lowCu	1	**1**	**1.3**	1
lowFe	1.2	**1**	**1.8**	1
lowFeCu	1.2	**1**	**1.5**	0.7

Chapter 6: Conclusion

6.1 General thoughts on elemental limitation

Sabeeha Merchant's group has studied the interplay between nutrient demand and supply in the green alga *Chlamydomonas* extensively (Merchant et al. 2006; Glaesener et al. 2013; Blaby-Haas and Merchant 2014, 2017) and has coined the terms "metal sparing" and "metal economy". Metal sparing refers to the reduced use of the limiting nutrient. It may consist of repressing the synthesis of non-essential proteins or macromolecules containing the limiting nutrient, or substituting the protein or macromolecule for another one (Merchant and Helmann 2012). Metal economy (Figure 6.1 A and B) is related to the concept of metal homeostasis. There is only a very narrow set of circumstances in which nutrient demand and supply are equal. Most of the time, the supply is either lower or higher than the demand. The cell has numerous ways to counteract this imbalance. In case of a limiting supply, the cell can increase nutrient acquisition capacity via an increase in transporters or a change to high-affinity transporters (e.g. HAFeT in various phytoplankton including diatoms, Maldonado et al., 2006). Furthermore, internal stores can be released (e.g. Fe stored in ferritin in *Phaeodactylum* (Marchetti et al. 2009b)) or, in case of metals, other non-metal containing alternative proteins can be used (one form of metal sparing: e.g. flavodoxin for Fe- containing ferredoxin, LaRoche et al., 1995). In case of a surplus of nutrients, uptake can be decreased, efflux increased, or nutrients can be stored in vacuoles or specialized proteins for later consumption. With this metal economy, the cell is able to support its maximal growth rate over an extended nutrient concentration gradient and optimize it under nutrient limitation or toxicity.

When we investigate adaptations to limiting conditions, we need to be aware of the physiological state of our model species. This will help when we compare the different responses of various species to metal limiting conditions. For that reason, I made extensive physiological measurements in parallel with acquiring proteomics data.

6.2 My research

In this thesis, my main goal was to describe in detail the acclimation strategies used by two strains of *Thalassiosira oceanica* (CCMP1003 and CCMP1005) when grown under Cu-limiting conditions (Chapters 3 and 4). So far Cu-limitation in diatoms has received little attention. The uniqueness of my project is that I combined differential proteomic data with an array of physiological measurements. This enabled me to investigate the interplay between various metabolic pathways, as well as how changes in the stoichiometry of a given metabolic pathway affect cellular physiology. For example, in Cu-limited *T. oceanica* (CCMP 1003), I was able to document alterations in proteins within the photosynthetic apparatus, and concomitantly determine the resulting effects on photophysiology. I also revealed an intricate interaction between the N and C metabolisms, allowing *T. oceanica* (CCMP 1003) to counteract the excess of reducing power within the chloroplast. Namely, that nitrogen acquisition and assimilation are up-regulated with an emphasis on plastid-located, ferredoxin-dependent isoenzymes, thus helping to alleviate the proposed increased reduced plastidial ferredoxin pool. Furthermore, the differential expression of isoenzymes of both malate dehydrogenase and aspartate aminotransferase supports the previously proposed malate shunt (Prihoda et al. 2012; Bailleul et al. 2015), channelling both electrons and carbon skeletons from the chloroplast to the mitochondria. I also uncovered the modulation of glycolytic isoenzymes (located in the cytosol,

chloroplast and mitochondria), directing a) reducing equivalents to the mitochondria, and b) ATP as well as pyruvate (needed to resupply oxaloacetate involved in the malate shunt) to the chloroplast.

Hockin et al. (2012) showed that glycolysis is up-regulated under acute nitrogen limitation in *T. pseudonana*. When I mapped these up-regulated glycolytic proteins to their target locations in *T. pseudonana*, I revealed a close resemblance of the directed modulation seen in TO03 under chronic Cu limitation. This suggests that compartmentalized modulation of specific isoenzymes in glycolysis might be a general first line of defence in diatoms to redistribute reducing equivalents and ATP to meet their new cellular requirements.

When I compared the response of TO03 and TO05, I showed significant differences between the two strains (intraspecific differences) in their acclimation strategies to limiting metal conditions. As a result of these distinct acclimation strategies, TO05 has higher Cu requirements and lower tolerance to Cu limitation than TO03. The impaired capability of TO05 to deal with Cu-limitation stems from its inability to reduce plastocyanin content and/or to counteract excess reducing power in the photosynthetic ETC. Instead, TO05 decreases its Cu requirement mainly by a general 50% reduction of its overall proteome.

In addition, I collected the same set of physiological and differential proteomic data for *T. oceanica* cultures grown under Fe-limiting concentrations (a well-documented *in situ* environmental condition) as well as Fe-Cu co-limiting levels (a possible *in situ* condition in Fe-limited regions). Photosynthesis is the most important metabolic pathway in phytoplankton. Thus, I focused on comparing changes to the photosynthetic apparatus as the cells acclimated to the three metal limiting conditions. I uncovered specific metal-dependent changes in the photosynthetic apparatus and general stress-dependent ones.

The most important finding when comparing the three metal limiting conditions relates to the regulation of Fe- and Cu-containing proteins involved in the ETC in TO03. Namely, plastocyanin is down-regulated (by 4-fold) under lowCu, accompanied by the down-regulation of the up-stream cytb_6f and PSII but not the down-stream PSI. Under low Fe, an unforeseen up-regulation of plastocyanin (by 2-fold) seems to support the efficiency of the ETC under stoichiometric changes involving a decrease in the Fe-containing cytb_6f. Up-regulation of plastocyanin under these conditions was surprising as increased Cu requirements under low Fe have been attributed to increased activity of multi-Cu oxidases in the high-affinity Fe transport system (HAFeT, Maldonado et al. 2006). Given that plastocyanin is down-regulated under lowCu and up-regulated under lowFe, it is difficult to predict its regulation under lowFeCu. Based on our data, under lowFeCu, plastocyanin is somewhat down-regulated (by 1.5-fold), suggesting a dual effect of growth limitation by Cu and Fe on plastocyanin (decrease by 4-fold combined with an increase by 2-fold results in a decrease by ~ 2-fold). However, the actual down-regulation of plastocyanin under lowFeCu was slightly less (by 1.5 fold) than the expected 2-fold. This could be due to the slightly higher Cu concentrations in the lowFeCu media relative to that in lowCu (1.96 *vs.* < 1 nM Cu, respectively) or the process of Cu-sparing. In this process, the cell represses the synthesis of the least essential Cu-proteins (e.g. plastocyanin) and enhances the synthesis of the most essential ones (e.g. MCO). Therefore, in the lowFeCu case, we could predict an increased amount of Cu allocated to the HAFeT system to increase Fe uptake, and thus a limiting availability of Cu allocated to plastocyanin in the photosynthetic ETC.

6.3 Challenges of my research

The two *T. oceanica* strains have different Fe and Cu requirements. The differential trace metal demands made it challenging to determine comparable growth conditions for culturing them. In previous studies using *T. oceanica* CCMP 1003 and 1005, control (replete) concentrations ranged from 10.2 to 21.4 nM for Cu in both strains, 42 nM to 8.6 μM for Fe in TO03 and 1.29 μM to 1.37 μM for Fe in TO05 (Table 6.1). In my study, I determined that TO05 needed higher Cu concentrations (14.32 nM) to support its maximum growth rate than that in our laboratory's standard Cu-sufficient medium (10.2 nM Cu, Figure 6.1C). To deal with this problem, I first determined the Fe and Cu concentrations to support the maximum growth rate of TO03 and TO05, respectively. Secondly, I determined a Cu concentration that limited the growth of TO03. Thirdly, I established the comparable limiting Cu concentration for TO05, so that identical growth rate reductions were observed for TO05 and TO03 under the lowCu conditions (Figure 6.1D). To induce Fe limitation, I decided to use the same Fe concentration for both strains and focused on their response to this specific Fe-limiting condition (Figure 6.1E).

Culturing phytoplankton under trace metal limiting conditions is challenging, even though every precaution to avoid contamination is taken. Comparisons among published studies clearly show different growth responses to identical trace metal limiting conditions, or identical growth rate responses to different trace metal limiting conditions. This ultimately suggests different levels of trace metal contamination in each laboratory. For example, in three TO03 studies, Fe concentrations ranged from 4 to 42 nM Fe but resulted in the same relative growth rate of ~ 85 % μ_{max} (Table 6.1). Similarly, in the three TO03 studies using 42 nM Fe to induce Fe-limitation, the relative growth rates ranged from 58% μ_{max} to 100% μ_{max}. Kim and Price (2017) conceded that, even though Cu concentration in their media was below ICPMS detection,

Cu contamination was likely in their zero-Cu-media, as TO05 was able to grow. Thus, I suggest that it is critical to report growth rate reductions relative to μ_{max} to compare the results of studies investigating the responses of phytoplankton to metal limitation.

The remarkable intraspecific differences that I discovered questioned whether my two strains were truly the same species. I thus compared their ITS regions and confirmed that they were the same species. Specifically, the sequenced CCMP1003 ITS region was 99.66% identical to the sequence of CCMP1005. Further evidence of their overall matching genomes was found when I mapped their respective proteomes to both the sequenced TO05 genome and our TO03 EST database. There was no bias in either direction in either of the strains. At this point, there is no conclusive explanation for the underlying differential regulation of proteins in these two strains. Ongoing research into epigenomics and transcriptional regulation in diatoms points to transcriptional modulation strategies acquired from plants and animals, including RNA directed DNA methylation and posttranslational modifications of histones (see review by Tirichine et al. 2017). However, the exact mechanisms underlying the differential expression of proteins I observed in TO03 and TO05 remains elusive.

6.4 Implications of my findings

Plastocyanin concentration plays a more important role in *Thalassiosira oceanica's* response to Fe and Cu limitation than previously thought. Its up-regulation under low Fe was surprising, given the general assumption that the release of oxidized plastoquinone from the cytb_6f complex is the rate-limiting step in the ETC (Rochaix 2011). This opens up the interesting question: how could an increase in plastocyanin support more efficient photosynthetic electron transport? I hypothesized that the increase in plastocyanin might support rapid oxidation of cytb_6f in order to

(as suggested in barley, Burkey 1993) limit the possibility of cytb_6f becoming an ETC bottleneck due to its reduced state. Another possibility is that the ratio between plastocyanin and its downside partner, PSI, is the more important one. Here, again, the release of the electron carrier (plastocyanin from PSI) is thought to be the rate-limiting step. Monitoring the ratio of these three ETC components (cytb_6f, plastocyanin, PSI) across varying Fe, Cu and Fe-Cu co-limiting conditions might help to answer this question.

The intraspecific strain differences that I described here could not have been predicted from their genomic information. This means that caution should be exercised when gathering detailed information from only one strain and extrapolating the findings to an "open ocean population". Thus, we need to a) verify prediction through *in situ* experiments and b) broaden our laboratory experiments to include more than one strain of a species. The recent review on intraspecific strain differences in diatoms (Godhe and Rynearson 2017) also stressed the importance of including several strains in future experiments.

6.5 Outlook for future research

Copper physiology in diatoms, especially in the context of co-limitation, either with Fe (Wells et al. 2005; Lelong et al. 2013) or light (Kim and Price 2017) has been acknowledged to be relevant in the ocean in recent years. I hope that the results of this thesis will promote further investigations on the interacting effects of Fe and Cu on phytoplankton growth.

As a result of my work, a number of research questions remain to be addressed. I also have some recommendations for future work. For example, when investigating metal limitation in any species, it would be beneficial to generate a growth rate curve as a function of metal concentration, as seen for TO 1005 in Kim and Price (2017) for Cu and in Bucciarelli et al.

(2010) for Fe. This will provide valuable information on each strain's ability to adapt to low metal concentrations. Furthermore, this will allow better comparability between studies. For example, if we find a direct relationship between plastocyanin levels, Cu concentrations and growth rate reduction, the corresponding physiological data collected can be more easily used in other studies. However, depending on the species investigated, other metals might also be important contributors to growth rate modifications. Wells et al. (2005) had to decrease nickel concentrations in their control media to achieve higher growth rates when investigating Fe and Cu physiology in *Pseudo-nitzschia*.

For years, flavodoxin (FldA) alone or the expression ratio of ferredoxin / (ferredoxin + FldA) have been used as a proxy for Fe-limitation in diatoms both in the laboratory and *in situ* (Roche et al. 1995; LaRoche et al. 1996; McKay et al. 1999; Whitney et al. 2011; Suzuki et al. 2014; Chappell et al. 2014). A next goal would be to find a suitable proxy to determine the degree of Cu or even Fe-Cu co-limitation of laboratory and *in situ* phytoplankton. Several potential candidate proteins or protein ratios could be investigated. As a first step, I suggest investigating the relationship or metal sparing between plastocyanin, multicopper oxidase, chloroplast (ETC) cyt*c*, and mitochondrial cyt*c* oxidase. As neither MCO nor chloroplast cyt*c* were detected in our proteomic dataset, *q*PCR or an immunological approach could be useful to monitor the expression levels of these proteins. As I hypothesized that the ratio of plastocyanin: cytb_6f or plastocyanin:PSI could be relevant to ensure efficient electron transport in the ETC under lowFe and lowFeCu conditions, I would also monitor both cytb_6f and PSI levels. Uncovering a suitable proxy for Cu limitation might be a useful tool during *in situ* Cu amendment experiments to determine whether an increase in phytoplankton biomass is due to a

toxic Cu effect on the grazers of phytoplankton or a true response in phytoplankton biomass due to their Cu limiting conditions *in situ* (Coale 1991; Peers et al. 2005; Semeniuk et al. 2009).

There are large areas in the open ocean in which reported dissolved Cu concentrations are as low as those that are used to induce Cu limitation in the laboratory (e.g. Jacquot and Moffett 2015; Heller and Croot 2015; Roshan and Wu 2015). However, we do not expect to find exclusively Cu-limited phytoplankton in the open ocean. This hypothesis is based on two facts. First, dissolved Cu oncentrations in the open ocean are relatively high, ranging from 0.5-3 nM Cu (Jacquot and Moffett 2015), and thus are not expected to limit phytoplankton productivity. Second, even though a few numbers of studies have suggested that low inorganic Cu^{2+} levels may limit primary productivity in some oceanic regions (eg. Moffet and Dupont 2007), this hypothesis assumes that only inorganic Cu can be used by phytoplankton. Recent studies have demonstrated that Cu bound to model and *in situ* strong organic complexes is taken up by indigenous phytoplankton (Semeniuk et al. 2009, 2015). Thus, phytoplankton are not expected to be Cu limited as they are able to access Cu within strong organic ligands from a relatively large dissolved Cu pool.

I mainly envision the possibility of co-limitation of Cu and Fe in the open ocean—rather than Cu-limitation alone—given the higher Cu quotas of some oceanic phytoplankton and the higher Cu requirements documented for some Fe-limited phytoplankton (Annett et al. 2008; Guo et al. 2012), and the co-occuring low Fe concentrations in the open ocean. As suggested above, more *in situ* bottle, metal amendment experiments are needed to determine which phytoplankton groups might benefit from increased Cu concentrations in the ocean.

The projected increasing acidification and stratification of our global oceans due to climate change will alter Fe and Cu bioavailabilities. Thus, in order to predict how the phytoplankton community might react to these changing conditions, it is of importance to understand their Fe and Cu physiology. More research on a variety of phytoplankton species and strains will uncover unifying and unique phytoplankton responses to trace metal limitation that reflect genomic and metabolic diversity of the *in situ* population. This will be useful for understanding phytoplankton population dynamics in a changing ocean.

6.6 Tables and figures

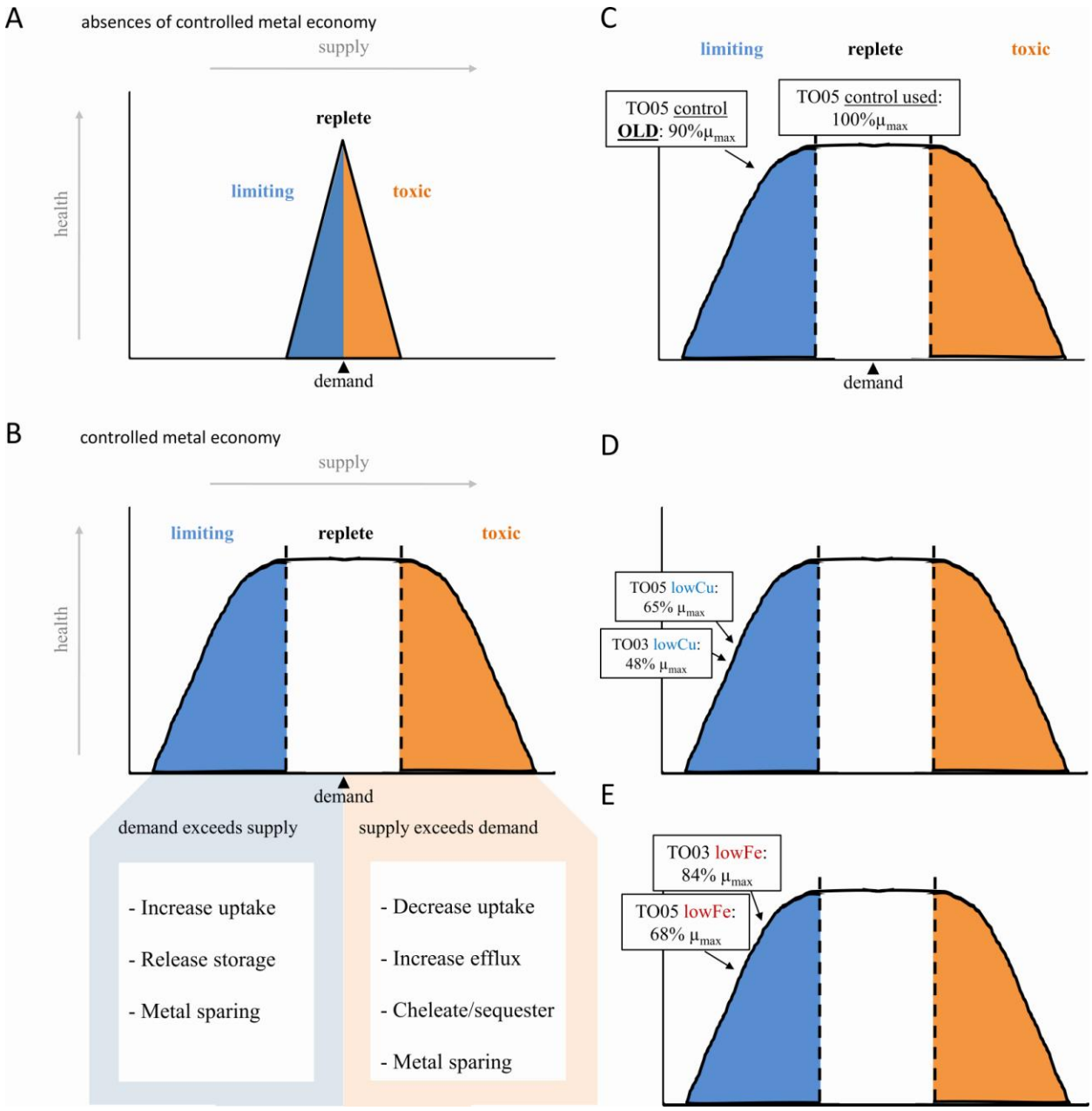

Figure 6.1: Concept of how metal homeostasis on cellular level helps increase resilience towards metal fluctuations. A) The absence of controlled metal economy. A cell can only achieve maximum growth if inner demand equals outer supply. **B) Controlled economy.** Cellular metabolism can accommodate fluctuation in metal supply to some extent**. C-E) Limitation status achieved in *T. oceanica* cultures.** "OLD" denotes the growth rate of

TO05 achieved in the standard Cu-concentration medium used in our lab (10.2 nM Cu), relative to the maximum growth rate achieved in my new control medium (14.3 nM Cu).

Table 6.1: Overview of Fe and Cu concentrations used in various studies on Fe and Cu physiology in *T. oceanica* and their induced changes in growth rate (%μ_{max})

	TO03			TO05				
Treatment	**$[Fe]_{total}$**	**$[Cu]_{total}$**	**μ/μ_{max}**	**$[Fe]_{total}$**	**$[Cu]_{total}$**	**μ/μ_{max}**	**Ref**	
Control	1.37 µM	10.2 nM		1.37µM	14.32 nM		(1)	Hippmann et al., 2017
	42 nM	10.2 nM					(2)	Schuback et al., 2015
	1.37µM	11.2 nM					(3)	Guo et al., 2010
	1.37 µM	10.2 nM		1.37µM	10.2 nM		(4)	Annett et al., 2008
	1.37µM	10.2 nM					(5)	Maldonado et al., 2006
				1.37 µM?	21.4 nM		(6)	Peers and Price, 2006
	1.29 µM	21.4 nM		1.29 µM	21.4 nM		(7)	Peers et al., 2005
	59 nM	10.2 nM ?					(8)	Strzepek and Harrison, 2004
	8.6 µM	10.2 nM ?					(9)	Maldonado and Price, 2001
lowCu	1.37µM	< 1.0 nM	48%	1.37 µM	6.08 nM	65%	(1)	Hippmann et al., 2017
				1.37 µM	1.96 nM	0%	(1)	Hippmann et al., 2017
	1.37 µM	1.0 nM	91%				(3)	Guo, 2010
	1.37 µM	1.96 nM					(4)	Annett et al., 2008
	1.37 µM	1.96 nM	49%				(5)	Maldonado et al., 2006
				1.37 µM	2.5 nM	58%	(6)	Peers and Price, 2006
				1.37 µM	1.0 nM	38%	(6)	Peers and Price, 2006
	1.29 µM	1.0 nM	65%	1.29 µM	1.0 nM	65%	(7)	Peers et al., 2005
lowFe	42 nM	10.2 nM	85%	42 nM	14.32 nM	68%	(1)	Hippmann et al., 2017
	0.13 nM	10.2 nM	32%				(2)	Schuback et al., 2015
	1.28 nM	11.2 nM	64%				(3)	Guo et al., 2010
	42 nM	10.2 nM	100%	42 nM	10.2 nM	100%	(4)	Annett et al., 2008
	4.2 nM	10.2 nM	62%				(4)	Annett et al., 2008
	42 nM	10.2 nM	58% (42-95%, n=6)				(5)	Maldonado et al., 2006
	4 nM	21.4 nM	82%	4 nM	21.4 nM	78%	(7)	Peers et al., 2005
	7.8 nM	10.2 nM ?	100%				(8)	Strzepek and Harrison, 2004
	4.7 nM	10.2 nM?	83%				(8)	Strzepek and Harrison, 2004
	12.9 nM	10.2 nM	1.27 - 1.8 dd-1 (n=5)				(9)	Maldonado and Price, 2001
lowFeCu	42 nM	1.96 nM	56%	42 nM	6.08 nM	43%	(1)	Hippmann et al., 2017
	42 nM	< 1.0 nM	0%				(1)	Hippmann et al., 2017
	1.28 nM	2.96 nM	60%				(3)	Guo, 2010
	42 nM	1.96 nM	82%	42 nM	1.96 nM	68%	(4)	Annett et al., 2008
	4.2 nM	1.96 nM	65%				(4)	Annett et al., 2008
	42 nM	1 nM	70%				(5)	Maldonado et al., 2006
	4 nM	1.0 nM	41%	40.8 nM	1.0 nM	66%	(7)	Peers et al., 2005
	4 nM	0.0 nM	0%	4 nM	1.0 nM	44%	(7)	Peers et al., 2005

References

Adhikari, U. K., and M. M. Rahman. 2017. Comparative analysis of amino acid composition in the active site of nirk gene encoding copper-containing nitrite reductase (CuNiR) in bacterial spp. Computational Biology and Chemistry **67**: 102–113. doi:10.1016/j.compbiolchem.2016.12.011

Allen, A. E., C. L. Dupont, M. Oborník, and others. 2011. Evolution and metabolic significance of the urea cycle in photosynthetic diatoms. Nature **473**: 203–207. doi:10.1038/nature10074

Allen, A. E., J. LaRoche, U. Maheswari, and others. 2008. Whole-cell response of the pennate diatom Phaeodactylum tricornutum to iron starvation. Proceedings of the National Academy of Sciences **105**: 10438–10443. doi:10.1073/pnas.0711370105

Allen, A. E., A. Moustafa, A. Montsant, A. Eckert, P. G. Kroth, and C. Bowler. 2012. Evolution and Functional Diversification of Fructose Bisphosphate Aldolase Genes in Photosynthetic Marine Diatoms. Mol Biol Evol **29**: 367–379. doi:10.1093/molbev/msr223

Allen, A. E., A. Vardi, and C. Bowler. 2006. An ecological and evolutionary context for integrated nitrogen metabolism and related signaling pathways in marine diatoms. Current Opinion in Plant Biology **9**: 264–273. doi:10.1016/j.pbi.2006.03.013

Allen, J. F. 2002. Photosynthesis of ATP—Electrons, Proton Pumps, Rotors, and Poise. Cell **110**: 273–276. doi:10.1016/S0092-8674(02)00870-X

Allen, J. F. 2003. Cyclic, pseudocyclic and noncyclic photophosphorylation: new links in the chain. Trends in Plant Science **8**: 15–19. doi:10.1016/S1360-1385(02)00006-7

Alscher, R. G., J. L. Donahue, and C. L. Cramer. 1997. Reactive oxygen species and antioxidants: Relationships in green cells. Physiologia Plantarum **100**: 224–233. doi:10.1111/j.1399-3054.1997.tb04778.x

Amato, A., W. H. C. F. Kooistra, J. H. Levialdi Ghiron, D. G. Mann, T. Pröschold, and M. Montresor. 2007. Reproductive Isolation among Sympatric Cryptic Species in Marine Diatoms. Protist **158**: 193–207. doi:10.1016/j.protis.2006.10.001

Anisimova, M., M. Gil, J.-F. Dufayard, C. Dessimoz, and O. Gascuel. 2011. Survey of Branch Support Methods Demonstrates Accuracy, Power, and Robustness of Fast Likelihood-based Approximation Schemes. Syst Biol syr041. doi:10.1093/sysbio/syr041

Annett, A. L., S. Lapi, T. J. Ruth, and M. T. Maldonado. 2008. The effects of Cu and Fe availability on the growth and Cu:C ratios of marine diatoms. Limnol. Oceanogr. **53**: 2451–2461. doi:10.4319/lo.2008.53.6.2451

Arar, E. J., and G. B. Collins. 1997. In Vitro Determination of Chlorophyll a and Pheophytin a in Marine and Freshwater Algae by Fluorescence US EPA Method 445.0. U.S. ENVIRONMENTAL PROTECTION AGENCY (EPA).

Archer, D. 2003. Biological Fluxes in the Ocean and Atmospheric pCO2. Treatise on Geochemistry **6**: 625. doi:10.1016/B0-08-043751-6/06156-9

Archibald, J. M. 2005. Jumping genes and shrinking genomes--probing the evolution of eukaryotic photosynthesis with genomics. IUBMB Life **57**: 539–547. doi:10.1080/15216540500167732

Archibald, J. M., and P. J. Keeling. 2002. Recycled plastids: a “green movement” in eukaryotic evolution. Trends Genet. **18**: 577–584.

Armbrust, E. V. 2009. The life of diatoms in the world's oceans. Nature **459**: 185–192. doi:10.1038/nature08057

Armbrust, E. V., J. A. Berges, C. Bowler, and others. 2004. The Genome of the Diatom Thalassiosira Pseudonana: Ecology, Evolution, and Metabolism. Science **306**: 79–86. doi:10.1126/science.1101156

Bailey, S., A. Melis, K. R. M. Mackey, and others. 2008. Alternative photosynthetic electron flow to oxygen in marine Synechococcus. Biochimica et Biophysica Acta (BBA) - Bioenergetics **1777**: 269–276. doi:10.1016/j.bbabio.2008.01.002

Bailleul, B., N. Berne, O. Murik, and others. 2015. Energetic coupling between plastids and mitochondria drives CO2 assimilation in diatoms. Nature **524**: 366–369. doi:10.1038/nature14599

Baldi, P., and A. D. Long. 2001. A Bayesian framework for the analysis of microarray expression data: regularized t -test and statistical inferences of gene changes. Bioinformatics **17**: 509–519.

Balmer, Y., A. Koller, G. del Val, W. Manieri, P. Schürmann, and B. B. Buchanan. 2003. Proteomics gives insight into the regulatory function of chloroplast thioredoxins. PNAS **100**: 370–375. doi:10.1073/pnas.232703799

Behrenfeld, M. J., and A. J. Milligan. 2013. Photophysiological Expressions of Iron Stress in Phytoplankton. Annu. Rev. Mar. Sci. **5**: 217–246. doi:10.1146/annurev-marine-121211-172356

Bekker, A., H. D. Holland, P.-L. Wang, D. Rumble, H. J. Stein, J. L. Hannah, L. L. Coetzee, and N. J. Beukes. 2004. Dating the rise of atmospheric oxygen. Nature **427**: 117–120. doi:10.1038/nature02260

Bender, S. J., C. A. Durkin, C. T. Berthiaume, R. L. Morales, and E. V. Armbrust. 2014. Transcriptional responses of three model diatoms to nitrate limitation of growth. Front. Mar. Sci **1**: 3. doi:10.3389/fmars.2014.00003

Benson, D. A., M. Cavanaugh, K. Clark, I. Karsch-Mizrachi, D. J. Lipman, J. Ostell, and E. W. Sayers. 2013. GenBank. Nucleic Acids Res **41**: D36–D42. doi:10.1093/nar/gks1195

Blaby-Haas, C. E., and S. S. Merchant. 2014. Lysosome-related Organelles as Mediators of Metal Homeostasis. J. Biol. Chem. **289**: 28129–28136. doi:10.1074/jbc.R114.592618

Blaby-Haas, C. E., and S. S. Merchant. 2017. Regulating cellular trace metal economy in algae. Curr. Opin. Plant Biol. **39**: 88–96. doi:10.1016/j.pbi.2017.06.005

Blaby-Haas, C. E., T. Padilla-Benavides, R. Stübe, J. M. Argüello, and S. S. Merchant. 2014. Evolution of a plant-specific copper chaperone family for chloroplast copper homeostasis. PNAS **111**: E5480–E5487. doi:10.1073/pnas.1421545111

Boersema, P. J., R. Raijmakers, S. Lemeer, S. Mohammed, and A. J. R. Heck. 2009. Multiplex peptide stable isotope dimethyl labeling for quantitative proteomics. Nat. Protocols **4**: 484–494. doi:10.1038/nprot.2009.21

Bowler, C., A. E. Allen, J. H. Badger, and others. 2008. The Phaeodactylum genome reveals the evolutionary history of diatom genomes. Nature **456**: 239–244. doi:10.1038/nature07410

Boyd, P. W., T. Jickells, C. S. Law, and others. 2007. Mesoscale Iron Enrichment Experiments 1993-2005: Synthesis and Future Directions. Science **315**: 612–617. doi:10.1126/science.1131669

Boyle, E. A., S. S. Huested, and S. P. Jones. 1981. On the distribution of copper, nickel, and cadmium in the surface waters of the North Atlantic and North Pacific Ocean. J. Geophys. Res. **86**: 8048–8066. doi:10.1029/JC086iC09p08048

Brand, L. E., W. G. Sunda, and R. R. L. Guillard. 1983. Limitation of marine phytoplankton reproductive rates by zinc, manganese, and iron1. Limnology and Oceanography **28**: 1182–1198. doi:10.4319/lo.1983.28.6.1182

Brand, L. E., W. G. Sunda, and R. R. L. Guillard. 1986. Reduction of marine phytoplankton reproduction rates by copper and cadmium. Journal of Experimental Marine Biology and Ecology **96**: 225–250. doi:10.1016/0022-0981(86)90205-4

Bromke, M. A. 2013. Amino Acid Biosynthesis Pathways in Diatoms. Metabolites **3**: 294–311. doi:10.3390/metabo3020294

Bruland, K. W. 1980. Oceanographic distributions of cadmium, zinc, nickel, and copper in the North Pacific. Earth and Planetary Science Letters **47**: 176–198. doi:10.1016/0012-821X(80)90035-7

Bruland, K. W., and R. P. Franks. 1983. Mn, Ni, Cu, Zn and Cd in the Western North Atlantic, p. 395–414. *In* C.S. Wong, E. Boyle, K.W. Bruland, J.D. Burton, and E.D. Goldberg [eds.], Trace Metals in Sea Water. Springer US.

Bucciarelli, E., P. Pondaven, and G. Sarthou. 2010. Effects of an iron-light co-limitation on the elemental composition (Si, C, N) of the marine diatoms Thalassiosira oceanica and Ditylum brightwellii. Biogeosciences **7**: 657–669. doi:10.5194/bg-7-657-2010

Burkey, K. O. 1993. Effect of growth irradiance on plastocyanin levels in barley. Photosynth Res **36**: 103–110. doi:10.1007/BF00016275

Burki, F., M. Kaplan, D. V. Tikhonenkov, and others. 2016. Untangling the early diversification of eukaryotes: a phylogenomic study of the evolutionary origins of Centrohelida, Haptophyta and Cryptista. Proc. Biol. Sci. **283**. doi:10.1098/rspb.2015.2802

Capozzi, F., S. Ciurli, and C. Luchinat. 1998. Coordination sphere versus protein environment as determinants of electronic and functional properties of iron-sulfur proteins. SpringerLink 127–160. doi:10.1007/3-540-62888-6_5

Castruita, M., D. Casero, S. J. Karpowicz, and others. 2011. Systems Biology Approach in Chlamydomonas Reveals Connections between Copper Nutrition and Multiple Metabolic Steps. Plant Cell **23**: 1273–1292. doi:10.1105/tpc.111.084400

Catling, D. C., and M. W. Claire. 2005. How Earth's atmosphere evolved to an oxic state: A status report. Earth and Planetary Science Letters **237**: 1–20. doi:10.1016/j.epsl.2005.06.013

Chappell, P. D., L. P. Whitney, J. R. Wallace, A. I. Darer, S. Jean-Charles, and B. D. Jenkins. 2014. Genetic indicators of iron limitation in wild populations of Thalassiosira oceanica from the northeast Pacific Ocean. ISME J. doi:10.1038/ismej.2014.171

Chen, G., and T. A. Rynearson. 2016. Genetically distinct populations of a diatom co-exist during the North Atlantic spring bloom. Limnol. Oceanogr. n/a-n/a. doi:10.1002/lno.10361

Claquin, P., J. C. Kromkamp, and V. Martin-Jezequel. 2004. Relationship between photosynthetic metabolism and cell cycle in a synchronized culture of the marine alga Cylindrotheca fusiformis (Bacillariophyceae). European Journal of Phycology **39**: 33–41. doi:10.1080/0967026032000157165

Coale, K. H. 1991. Effects of iron, manganese, copper, and zinc enrichments on productivity and biomass in the subarctic Pacific. Limnology and Oceanography **36**: 1851–1864.

Coale, K. H., and K. W. Bruland. 1988. Copper complexation in the Northeast Pacific. Limnol. Oceanogr. **33**: 1084–1101. doi:10.4319/lo.1988.33.5.1084

Collier, J. L., and A. R. Grossman. 1992. Chlorosis induced by nutrient deprivation in Synechococcus sp. strain PCC 7942: not all bleaching is the same. J Bacteriol **174**: 4718–4726.

Croot, P. L., J. W. Moffett, and L. E. Brand. 2000. Production of extracellular Cu complexing ligands by eucaryotic phytoplankton in response to Cu stress. Limnol. Oceanogr. **45**: 619–627. doi:10.4319/lo.2000.45.3.0619

Davis, A. K., M. Hildebrand, and B. Palenik. 2006. Gene Expression Induced by Copper Stress in the Diatom Thalassiosira pseudonana. Eukaryot Cell **5**: 1157–1168. doi:10.1128/EC.00042-06

De Rienzo, F., R. R. Gabdoulline, M. C. Menziani, and R. C. Wade. 2000. Blue copper proteins: a comparative analysis of their molecular interaction properties. Protein Sci **9**: 1439–1454.

De Rosario-Martinez, H. 2015. phia: Post-Hoc Interaction Analysis,.

Eriksen, N. T., and A. J. Lewitus. 1999. Cyanide-resistant respiration in diverse marine phytoplankton. Evidence for the widespread occurrence of the alternative oxidase. Aquat Microb Ecol **17**: 145–152. doi:10.3354/ame017145

Fabris, M., M. Matthijs, S. Rombauts, W. Vyverman, A. Goossens, and G. J. E. Baart. 2012. The metabolic blueprint of Phaeodactylum tricornutum reveals a eukaryotic Entner–Doudoroff glycolytic pathway. The Plant Journal **70**: 1004–1014. doi:10.1111/j.1365-313X.2012.04941.x

Falkowski, P. G., M. E. Katz, A. H. Knoll, A. Quigg, J. A. Raven, O. Schofield, and F. J. R. Taylor. 2004. The Evolution of Modern Eukaryotic Phytoplankton. Science **305**: 354–360. doi:10.1126/science.1095964

Ferreira, F., and N. A. Straus. 1994. Iron deprivation in cyanobacteria. J Appl Phycol **6**: 199–210. doi:10.1007/BF02186073

Fetherolf, M. M., S. D. Boyd, D. D. Winkler, and D. R. Winge. 2017. Oxygen-dependent activation of Cu,Zn-superoxide dismutase-1. Metallomics **9**: 1047–1059. doi:10.1039/C6MT00298F

Field, C. B., M. J. Behrenfeld, J. T. Randerson, and P. Falkowski. 1998. Primary Production of the Biosphere: Integrating Terrestrial and Oceanic Components. Science **281**: 237–240. doi:10.1126/science.281.5374.237

Finazzi, G., H. Moreau, and C. Bowler. 2010. Genomic insights into photosynthesis in eukaryotic phytoplankton. Trends in Plant Science **15**: 565–572. doi:10.1016/j.tplants.2010.07.004

Flicek, P., M. R. Amode, D. Barrell, and others. 2011. Ensembl 2011. Nucleic Acids Res **39**: D800–D806. doi:10.1093/nar/gkq1064

Foster, L. J., C. L. De Hoog, and M. Mann. 2003. Unbiased quantitative proteomics of lipid rafts reveals high specificity for signaling factors. Proc. Natl. Acad. Sci. U.S.A. **100**: 5813–5818. doi:10.1073/pnas.0631608100

Foyer, C. H., and G. Noctor. 2011. Ascorbate and Glutathione: The Heart of the Redox Hub. Plant Physiol. **155**: 2–18. doi:10.1104/pp.110.167569

Fredrickson, K. A., S. L. Strom, R. Crim, and K. J. Coyne. 2011. Interstrain Variability in Physiology and Genetics of Heterosigma Akashiwo (raphidophyceae) from the West Coast of North America1. Journal of Phycology **47**: 25–35. doi:10.1111/j.1529-8817.2010.00942.x

Gallogly, M. M., and J. J. Mieyal. 2007. Mechanisms of reversible protein glutathionylation in redox signaling and oxidative stress. Current Opinion in Pharmacology **7**: 381–391. doi:10.1016/j.coph.2007.06.003

Gao, Q., K. Yu, Y. Xia, M. B. Shine, C. Wang, D. Navarre, A. Kachroo, and P. Kachroo. 2014. Mono- and Digalactosyldiacylglycerol Lipids Function Nonredundantly to Regulate Systemic Acquired Resistance in Plants. Cell Reports **9**: 1681–1691. doi:10.1016/j.celrep.2014.10.069

Geider, R. J., J. La Roche, R. M. Greene, and M. Olaizola. 1993. Response of the Photosynthetic Apparatus of Phaeodactylum Tricornutum (bacillariophyceae) to Nitrate, Phosphate, or Iron Starvation1. Journal of Phycology **29**: 755–766. doi:10.1111/j.0022-3646.1993.00755.x

Giordano, M., Y.-B. Chen, M. Koblizek, and P. G. Falkowski. 2005. Regulation of nitrate reductase in Chlamydomonas reinhardtii by the redox state of the plastoquinone pool. European Journal of Phycology **40**: 345–352. doi:10.1080/09670260500334263

Glaesener, A. G., S. S. Merchant, and C. E. Blaby-Haas. 2013. Iron economy in Chlamydomonas reinhardtii. Front Plant Sci **4**. doi:10.3389/fpls.2013.00337

Godhe, A., and T. Rynearson. 2017. The role of intraspecific variation in the ecological and evolutionary success of diatoms in changing environments. Phil. Trans. R. Soc. B **372**: 20160399. doi:10.1098/rstb.2016.0399

Goss, R., D. Latowski, J. Grzyb, A. Vieler, M. Lohr, C. Wilhelm, and K. Strzalka. 2007. Lipid dependence of diadinoxanthin solubilization and de-epoxidation in artificial membrane systems resembling the lipid composition of the natural thylakoid membrane. Biochimica

et Biophysica Acta (BBA) - Biomembranes **1768**: 67–75. doi:10.1016/j.bbamem.2006.06.006

Goss, R., and B. Lepetit. 2015. Biodiversity of NPQ. Journal of Plant Physiology **172**: 13–32. doi:10.1016/j.jplph.2014.03.004

Goss, R., M. Lohr, D. Latowski, J. Grzyb, A. Vieler, C. Wilhelm, and K. Strzalka. 2005. Role of Hexagonal Structure-Forming Lipids in Diadinoxanthin and Violaxanthin Solubilization and De-Epoxidation. Biochemistry **44**: 4028–4036. doi:10.1021/bi047464k

Goss, R., J. Nerlich, B. Lepetit, S. Schaller, A. Vieler, and C. Wilhelm. 2009. The lipid dependence of diadinoxanthin de-epoxidation presents new evidence for a macrodomain organization of the diatom thylakoid membrane. Journal of Plant Physiology **166**: 1839–1854. doi:10.1016/j.jplph.2009.05.017

Green, B. R. 2003. The Evolution of Light-harvesting Antennas, p. 129–168. *In* B.R. Green and W.W. Parson [eds.], Light-Harvesting Antennas in Photosynthesis. Springer Netherlands.

Green, B. R. 2007. Evolution of Light-Harvesting Antennas in an Oxygen World, p. 37–53. *In* Evolution of Primary Producers in the Sea. Elsevier.

Green, B. R., and D. G. Durnford. 1996. The Chlorophyll-Carotenoid Proteins of Oxygenic Photosynthesis. Annual Review of Plant Physiology and Plant Molecular Biology **47**: 685–714. doi:10.1146/annurev.arplant.47.1.685

Grouneva, I., A. Rokka, and E.-M. Aro. 2011. The Thylakoid Membrane Proteome of Two Marine Diatoms Outlines Both Diatom-Specific and Species-Specific Features of the Photosynthetic Machinery. J. Proteome Res. **10**: 5338–5353. doi:10.1021/pr200600f

Groussman, R. D., M. S. Parker, and E. V. Armbrust. 2015. Diversity and Evolutionary History of Iron Metabolism Genes in Diatoms. PLOS ONE **10**: e0129081. doi:10.1371/journal.pone.0129081

Gruber, A., and P. G. Kroth. 2014. Deducing Intracellular Distributions of Metabolic Pathways from Genomic Data, p. 187–211. *In* G. Sriram [ed.], Plant Metabolism. Humana Press.

Gruber, A., and P. G. Kroth. 2017. Intracellular metabolic pathway distribution in diatoms and tools for genome-enabled experimental diatom research. Phil. Trans. R. Soc. B **372**: 20160402. doi:10.1098/rstb.2016.0402

Gruber, A., G. Rocap, P. G. Kroth, E. V. Armbrust, and T. Mock. 2015. Plastid proteome prediction for diatoms and other algae with secondary plastids of the red lineage. Plant J **81**: 519–528. doi:10.1111/tpj.12734

Gruber, A., T. Weber, C. R. Bártulos, S. Vugrinec, and P. G. Kroth. 2009. Intracellular distribution of the reductive and oxidative pentose phosphate pathways in two diatoms. J. Basic Microbiol. **49**: 58–72. doi:10.1002/jobm.200800339

Guillard, R. R., and J. H. Ryther. 1962. Studies of marine planktonic diatoms. I. Cyclotella nana Hustedt, and Detonula confervacea (cleve) Gran. Can. J. Microbiol. **8**: 229–239.

Guindon, S., J.-F. Dufayard, V. Lefort, M. Anisimova, W. Hordijk, and O. Gascuel. 2010. New Algorithms and Methods to Estimate Maximum-Likelihood Phylogenies: Assessing the Performance of PhyML 3.0. Syst Biol **59**: 307–321. doi:10.1093/sysbio/syq010

Gundermann, K., and C. Büchel. 2014. Structure and Functional Heterogeneity of Fucoxanthin-Chlorophyll Proteins in Diatoms, p. 21–37. *In* M.F. Hohmann-Marriott [ed.], The Structural Basis of Biological Energy Generation. Springer Netherlands.

Guo, J., A. L. Annett, R. L. Taylor, S. Lapi, T. J. Ruth, and M. T. Maldonado. 2010. Copper-Uptake Kinetics of Coastal and Oceanic Diatoms1. Journal of Phycology **46**: 1218–1228. doi:10.1111/j.1529-8817.2010.00911.x

Guo, J., B. R. Green, and M. T. Maldonado. 2015. Sequence Analysis and Gene Expression of Potential Components of Copper Transport and Homeostasis in Thalassiosira pseudonana. Protist **166**: 58–77. doi:10.1016/j.protis.2014.11.006

Guo, J., S. Lapi, T. J. Ruth, and M. T. Maldonado. 2012. The Effects of Iron and Copper Availability on the Copper Stoichiometry of Marine Phytoplankton1. Journal of Phycology **48**: 312–325. doi:10.1111/j.1529-8817.2012.01133.x

Hall, T. 2013. BioEdit, Biological Sequence alignment editor for Win95/98/NT/2K/XP/7, Ibis Biosciences.

Hanke, G., and P. Mulo. 2013. Plant type ferredoxins and ferredoxin-dependent metabolism. Plant Cell Environ **36**: 1071–1084. doi:10.1111/pce.12046

Harvey, E. L., S. Menden-Deuer, and T. A. Rynearson. 2015. Persistent Intra-Specific Variation in Genetic and Behavioral Traits in the Raphidophyte, Heterosigma akashiwo. Frontiers in Microbiology **6**. doi:10.3389/fmicb.2015.01277

Hasle, G. R. 1983. The Marine, Planktonic Diatoms Thalassiosira Oceanica Sp. Nov. and T. Partheneia1. Journal of Phycology **19**: 220–229. doi:10.1111/j.0022-3646.1983.00220.x

Heineke, D., B. Riens, H. Grosse, P. Hoferichter, U. Peter, U.-I. Flügge, and H. W. Heldt. 1991. Redox Transfer across the Inner Chloroplast Envelope Membrane. Plant Physiol. **95**: 1131–1137. doi:10.1104/pp.95.4.1131

Heller, M. I., and P. L. Croot. 2015. Copper speciation and distribution in the Atlantic sector of the Southern Ocean. Marine Chemistry **173**: 253–268. doi:10.1016/j.marchem.2014.09.017

Helliwell, K. E., S. Collins, E. Kazamia, S. Purton, G. L. Wheeler, and A. G. Smith. 2015. Fundamental shift in vitamin B12 eco-physiology of a model alga demonstrated by experimental evolution. ISME J **9**: 1446–1455. doi:10.1038/ismej.2014.230

Hermann, B., M. Kern, L. La Pietra, J. Simon, and O. Einsle. 2015. The octahaem MccA is a haem c-copper sulfite reductase. Nature **520**: 706–709. doi:10.1038/nature14109

Hippmann, A. A., N. Schuback, K.-M. Moon, J. P. McCrow, A. E. Allen, L. J. Foster, B. R. Green, and M. T. Maldonado. 2017. Contrasting effects of copper limitation on the photosynthetic apparatus in two strains of the open ocean diatom Thalassiosira oceanica P.A. Cobine [ed.]. PLOS ONE **12**: e0181753. doi:10.1371/journal.pone.0181753

Ho, T.-Y., A. Quigg, Z. V. Finkel, A. J. Milligan, K. Wyman, P. G. Falkowski, and F. M. M. Morel. 2003. The Elemental Composition of Some Marine Phytoplankton1. Journal of Phycology **39**: 1145–1159. doi:10.1111/j.0022-3646.2003.03-090.x

Hockin, N. L., T. Mock, F. Mulholland, S. Kopriva, and G. Malin. 2012. The Response of Diatom Central Carbon Metabolism to Nitrogen Starvation Is Different from That of Green Algae and Higher Plants1[W]. Plant Physiol **158**: 299–312. doi:10.1104/pp.111.184333

Hoefnagel, M. H. N., O. K. Atkin, and J. T. Wiskich. 1998. Interdependence between chloroplasts and mitochondria in the light and the dark. Biochimica et Biophysica Acta (BBA) - Bioenergetics **1366**: 235–255. doi:10.1016/S0005-2728(98)00126-1

Hoffman, G. E., M. V. Sanchez-Puerta, and C. F. Delwiche. 2011. Evolution of light-harvesting complex proteins from Chl c-containing algae. BMC Evolutionary Biology **11**: 101. doi:10.1186/1471-2148-11-101

Hunter, K. A., and P. W. Boyd. 2007. Iron-binding ligands and their role in the ocean biogeochemistry of iron. Environmental Chemistry **4**. doi:10.1071/EN07012

Ikeda, Y., A. Yamagishi, M. Komura, and others. 2013. Two types of fucoxanthin-chlorophyll-binding proteins I tightly bound to the photosystem I core complex in marine centric diatoms. Biochimica et Biophysica Acta (BBA) - Bioenergetics **1827**: 529–539. doi:10.1016/j.bbabio.2013.02.003

Jacquot, J. E., and J. W. Moffett. 2015. Copper distribution and speciation across the International GEOTRACES Section GA03. Deep Sea Research Part II: Topical Studies in Oceanography **116**: 187–207. doi:10.1016/j.dsr2.2014.11.013

Jassby, A. D., and T. Platt. 1976. Mathematical formulation of the relationship between photosynthesis and light for phytoplankton. Limnol. Oceanogr. **21**: 540–547. doi:10.4319/lo.1976.21.4.0540

Jickells, T. D., Z. S. An, K. K. Andersen, and others. 2005. Global Iron Connections between Desert Dust, Ocean Biogeochemistry, and Climate. Science **308**: 67–71.

Johnson, K. S., R. M. Gordon, and K. H. Coale. 1997. What controls dissolved iron concentrations in the world ocean? Marine Chemistry **57**: 137–161. doi:10.1016/S0304-4203(97)00043-1

Johnson, X., and J. Alric. 2013. Central Carbon Metabolism and Electron Transport in Chlamydomonas reinhardtii: Metabolic Constraints for Carbon Partitioning between Oil and Starch. Eukaryot Cell **12**: 776–793. doi:10.1128/EC.00318-12

Jordan, P. A., Y. Tang, A. J. Bradbury, A. J. Thomson, and J. R. Guest. 1999. Biochemical and spectroscopic characterization of Escherichia coli aconitases (AcnA and AcnB). Biochem J **344**: 739–746.

Kaim, W., and J. Rall. 1996. Copper—A "Modern" Bioelement. Angew. Chem. Int. Ed. Engl. **35**: 43–60. doi:10.1002/anie.199600431

Kanehisa, M., S. Goto, Y. Sato, M. Furumichi, and M. Tanabe. 2012. KEGG for integration and interpretation of large-scale molecular data sets. Nucleic Acids Res **40**: D109–D114. doi:10.1093/nar/gkr988

Katoh, K., and D. M. Standley. 2013. MAFFT Multiple Sequence Alignment Software Version 7: Improvements in Performance and Usability. Mol Biol Evol **30**: 772–780. doi:10.1093/molbev/mst010

Katoh, K., and D. M. Standley. 2016. A simple method to control over-alignment in the MAFFT multiple sequence alignment program. Bioinformatics **32**: 1933–1942. doi:10.1093/bioinformatics/btw108

Keeling, P. J. 2004. Diversity and evolutionary history of plastids and their hosts. Am. J. Bot. **91**: 1481–1493. doi:10.3732/ajb.91.10.1481

Kern, J., A. Zouni, A. Guskov, and N. Krauß. 2009. Lipids in the Structure of Photosystem I, Photosystem II and the Cytochrome b 6 f Complex, p. 203–242. *In* H. Wada and N. Murata [eds.], Lipids in Photosynthesis. Springer Netherlands.

Kikutani, S., R. Tanaka, Y. Yamazaki, S. Hara, T. Hisabori, P. G. Kroth, and Y. Matsuda. 2012. Redox Regulation of Carbonic Anhydrases via Thioredoxin in Chloroplast of the Marine Diatom Phaeodactylum tricornutum. J. Biol. Chem. **287**: 20689–20700. doi:10.1074/jbc.M111.322743

Kim, J., M. Fabris, G. Baart, M. K. Kim, A. Goossens, W. Vyverman, P. G. Falkowski, and D. S. Lun. 2016. Flux balance analysis of primary metabolism in the diatom Phaeodactylum tricornutum. Plant J **85**: 161–176. doi:10.1111/tpj.13081

Kim, J. H., B. S. Park, J.-H. Kim, P. Wang, and M.-S. Han. 2015. Intraspecific diversity and distribution of the cosmopolitan species Pseudo-nitzschia pungens (Bacillariophyceae): morphology, genetics, and ecophysiology of the three clades. J. Phycol. **51**: 159–172. doi:10.1111/jpy.12263

Kim, J.-W., and N. M. Price. 2017. The influence of light on copper-limited growth of an oceanic diatom, Thalassiosira oceanica (Coscinodiscophyceae). J. Phycol. n/a-n/a. doi:10.1111/jpy.12563

Kitajima, M., and W. Butler. 1975. Quenching of Chlorophyll Fluorescence and Primary Photochemistry in Chloroplasts by Dibromothymoquinone. Biochimica Et Biophysica Acta **376**: 105–115. doi:10.1016/0005-2728(75)90209-1

Knauert, S., and K. Knauer. 2008. The Role of Reactive Oxygen Species in Copper Toxicity to Two Freshwater Green Algae1. Journal of Phycology **44**: 311–319. doi:10.1111/j.1529-8817.2008.00471.x

Kolber, Z., and P. G. Falkowski. 1993. Use of active fluorescence to estimate phytoplankton photosynthesis in situ. Limnol. Oceanogr. **38**: 1646–1665. doi:10.4319/lo.1993.38.8.1646

Kolber, Z. S., O. Prášil, and P. G. Falkowski. 1998. Measurements of variable chlorophyll fluorescence using fast repetition rate techniques: defining methodology and experimental protocols. Biochimica et Biophysica Acta (BBA) - Bioenergetics **1367**: 88–106. doi:10.1016/S0005-2728(98)00135-2

Koziol, A. G., T. Borza, K.-I. Ishida, P. Keeling, R. W. Lee, and D. G. Durnford. 2007. Tracing the Evolution of the Light-Harvesting Antennae in Chlorophyll a/b-Containing Organisms. Plant Physiol **143**: 1802–1816. doi:10.1104/pp.106.092536

Kremp, A., A. Godhe, J. Egardt, S. Dupont, S. Suikkanen, S. Casabianca, and A. Penna. 2012. Intraspecific variability in the response of bloom-forming marine microalgae to changed climate conditions. Ecology and Evolution **2**: 1195–1207. doi:10.1002/ece3.245

Kropat, J., S. D. Gallaher, E. I. Urzica, S. S. Nakamoto, D. Strenkert, S. Tottey, A. Z. Mason, and S. S. Merchant. 2015. Copper economy in Chlamydomonas: Prioritized allocation and reallocation of copper to respiration vs. photosynthesis. Proc Natl Acad Sci U S A **112**: 2644–2651. doi:10.1073/pnas.1422492112

Kropat, J., S. Tottey, R. P. Birkenbihl, N. Depège, P. Huijser, and S. Merchant. 2005. A regulator of nutritional copper signaling in Chlamydomonas is an SBP domain protein that recognizes the GTAC core of copper response element. PNAS **102**: 18730–18735. doi:10.1073/pnas.0507693102

Kroth, P. G., A. Chiovitti, A. Gruber, and others. 2008. A Model for Carbohydrate Metabolism in the Diatom Phaeodactylum tricornutum Deduced from Comparative Whole Genome Analysis. PLOS ONE **3**: e1426. doi:10.1371/journal.pone.0001426

Kustka, A., A. Allen, F. Morel, and F. Morel. 2007. Sequence analysis and transcriptional regulation of iron acquisition genes in two marine diatoms1. Journal of Phycology **43**: 715–729. doi:10.1111/j.1529-8817.2007.00359.x

La Fontaine, S., J. M. Quinn, S. S. Nakamoto, M. D. Page, V. Göhre, J. L. Moseley, J. Kropat, and S. Merchant. 2002. Copper-Dependent Iron Assimilation Pathway in the Model

Photosynthetic Eukaryote Chlamydomonas reinhardtii. Eukaryot Cell **1**: 736–757. doi:10.1128/EC.1.5.736-757.2002

LaRoche, J., P. W. Boyd, R. M. L. McKay, and R. J. Geider. 1996. Flavodoxin as an in situ marker for iron stress in phytoplankton. Nature **382**: 802–805. doi:10.1038/382802a0

Lavaud, J., H. J. van Gorkom, and A.-L. Etienne. 2002. Photosystem II electron transfer cycle and chlororespiration in planktonic diatoms. Photosynthesis Research **74**: 51–59. doi:10.1023/A:1020890625141

Lebret, K., E. S. Kritzberg, R. Figueroa, and K. Rengefors. 2012. Genetic diversity within and genetic differentiation between blooms of a microalgal species. Environmental Microbiology **14**: 2395–2404. doi:10.1111/j.1462-2920.2012.02769.x

Lefebvre, S. C., G. Harris, R. Webster, N. Leonardos, R. J. Geider, C. A. Raines, B. A. Read, and J. L. Garrido. 2010. CHARACTERIZATION AND EXPRESSION ANALYSIS OF THE Lhcf GENE FAMILY IN EMILIANIA HUXLEYI (HAPTOPHYTA) REVEALS DIFFERENTIAL RESPONSES TO LIGHT AND CO21. Journal of Phycology **46**: 123–134. doi:10.1111/j.1529-8817.2009.00793.x

Lelong, A., E. Bucciarelli, H. Hégaret, and P. Soudant. 2013. Iron and copper limitations differently affect growth rates and photosynthetic and physiological parameters of the marine diatom Pseudo-nitzschia delicatissima. Limnol. Oceanogr. **58**: 613–623. doi:10.4319/lo.2013.58.2.0613

Lennon, A. M., P. Prommeenate, and P. J. Nixon. 2003. Location, expression and orientation of the putative chlororespiratory enzymes, Ndh and IMMUTANS, in higher-plant plastids. Planta **218**: 254–260. doi:10.1007/s00425-003-1111-7

Levering, J., J. Broddrick, C. L. Dupont, and others. 2016. Genome-Scale Model Reveals Metabolic Basis of Biomass Partitioning in a Model Diatom. PLOS ONE **11**: e0155038. doi:10.1371/journal.pone.0155038

Lewis, M., and J. Smith. 1983. A small volume, short-incubation-time method for measurement of photosynthesis as a function of incident irradiance. Marine Ecology Progress Series **13**: 99–102. doi:10.3354/meps013099

Li, H. 2013. Aligning sequence reads, clone sequences and assembly contigs with BWA-MEM. arXiv:1303.3997 [q-bio].

Lin, Y.-H., K.-Y. Pan, C.-H. Hung, H.-E. Huang, C.-L. Chen, T.-Y. Feng, and L.-F. Huang. 2013. Overexpression of Ferredoxin, PETF, Enhances Tolerance to Heat Stress in Chlamydomonas reinhardtii. Int J Mol Sci **14**: 20913–20929. doi:10.3390/ijms141020913

Liu, Z., H. Yan, K. Wang, T. Kuang, J. Zhang, L. Gui, X. An, and W. Chang. 2004. Crystal structure of spinach major light-harvesting complex at 2.72 Å resolution. Nature **428**: 287–292. doi:10.1038/nature02373

Lomas, M. W., and P. M. Glibert. 2000. Comparisons of Nitrate Uptake, Storage, and Reduction in Marine Diatoms and Flagellates. Journal of Phycology **36**: 903–913. doi:10.1046/j.1529-8817.2000.99029.x

Lombardi, A. T., and M. T. Maldonado. 2011. The effects of copper on the photosynthetic response of Phaeocystis cordata. Photosynth Res **108**: 77–87. doi:10.1007/s11120-011-9655-z

Lommer, M., A.-S. Roy, M. Schilhabel, S. Schreiber, P. Rosenstiel, and J. LaRoche. 2010. Recent transfer of an iron-regulated gene from the plastid to the nuclear genome in an

oceanic diatom adapted to chronic iron limitation. BMC Genomics **11**: 718. doi:10.1186/1471-2164-11-718

Lommer, M., M. Specht, A.-S. Roy, and others. 2012. Genome and low-iron response of an oceanic diatom adapted to chronic iron limitation. Genome Biol **13**: 1–21. doi:10.1186/gb-2012-13-7-r66

Longhurst, A. 1995. Seasonal cycles of pelagic production and consumption. Progress in Oceanography **36**: 77–167. doi:10.1016/0079-6611(95)00015-1

Losh, J. L., J. N. Young, and F. M. M. Morel. 2013. Rubisco is a small fraction of total protein in marine phytoplankton. New Phytol **198**: 52–58. doi:10.1111/nph.12143

Luo, C.-S., J.-R. Liang, Q. Lin, and others. 2014. Cellular Responses Associated with ROS Production and Cell Fate Decision in Early Stress Response to Iron Limitation in the Diatom Thalassiosira pseudonana. J. Proteome Res. **13**: 5510–5523. doi:10.1021/pr5004664

Luxem, K. E., M. J. Ellwood, and R. F. Strzepek. 2017. Intraspecific variability in Phaeocystis antarctica's response to iron and light stress. PLOS ONE **12**: e0179751. doi:10.1371/journal.pone.0179751

Mackey, K. R. M., A. Paytan, A. R. Grossman, and S. Bailey. 2008. A photosynthetic strategy for coping in a high-light, low-nutrient environment. Limnology and Oceanography **53**: 900–913. doi:10.4319/lo.2008.53.3.0900

Maheswari, U., A. Montsant, J. Goll, S. Krishnasamy, K. R. Rajyashri, V. M. Patell, and C. Bowler. 2005. The Diatom EST Database. Nucleic Acids Res **33**: D344–D347. doi:10.1093/nar/gki121

Maldonado, M. T., A. E. Allen, J. S. Chong, K. Lin, D. Leus, N. Karpenko, and S. L. Harris. 2006. Copper-dependent iron transport in coastal and oceanic diatoms. Limnol. Oceanogr. **51**: 1729–1743. doi:10.4319/lo.2006.51.4.1729

Maldonado, M. T., M. P. Hughes, E. L. Rue, and M. L. Wells. 2002. The effect of Fe and Cu on growth and domoic acid production by Pseudo-nitzschia multiseries and Pseudo-nitzschia australis. Limnol. Oceanogr. **47**: 515–526. doi:10.4319/lo.2002.47.2.0515

Maldonado, M. T., and N. M. Price. 1996. Influence of N substrate on Fe requirements of marine centric diatoms. Mar Ecol Prog Ser **141**: 161–172. doi:10.3354/meps141161

Maldonado, M. T., and N. M. Price. 1999. Utilization of iron bound to strong organic ligands by plankton communities in the subarctic Pacific Ocean. Deep Sea Research Part II: Topical Studies in Oceanography **46**: 2447–2473. doi:10.1016/S0967-0645(99)00071-5

Maldonado, M. T., and N. M. Price. 2001. Reduction and Transport of Organically Bound Iron by Thalassiosira Oceanica (bacillariophyceae). Journal of Phycology **37**: 298–310. doi:10.1046/j.1529-8817.2001.037002298.x

Marchetti, A., and M. T. Maldonado. 2016. Iron, p. 233–279. *In* M.A. Borowitzka, J. Beardall, and J.A. Raven [eds.], The Physiology of Microalgae. Springer International Publishing.

Marchetti, A., M. S. Parker, L. P. Moccia, and others. 2009a. Ferritin is used for iron storage in bloom-forming marine pennate diatoms. Nature **457**: 467–470. doi:10.1038/nature07539

Marchetti, A., M. S. Parker, L. P. Moccia, and others. 2009b. Ferritin is used for iron storage in bloom-forming marine pennate diatoms. Nature **457**: 467–470. doi:10.1038/nature07539

McFadden, G. I. 1999. Plastids and protein targeting. J. Eukaryot. Microbiol. **46**: 339–346.

McKay, R. M. L., J. La Roche, A. F. Yakunin, D. G. Durnford, and R. J. Geider. 1999. Accumulation of Ferredoxin and Flavodoxin in a Marine Diatom in Response to Fe. Journal of Phycology **35**: 510–519. doi:10.1046/j.1529-8817.1999.3530510.x

McKew, B. A., P. Davey, S. J. Finch, and others. 2013. The trade-off between the light-harvesting and photoprotective functions of fucoxanthin-chlorophyll proteins dominates light acclimation in Emiliania huxleyi (clone CCMP 1516). New Phytol **200**: 74–85. doi:10.1111/nph.12373

Menden-Deuer, S., and J. Rowlett. 2014. Many ways to stay in the game: individual variability maintains high biodiversity in planktonic microorganisms. Journal of The Royal Society Interface **11**: 20140031. doi:10.1098/rsif.2014.0031

Merchant, S., and L. Bogorad. 1986. Regulation by copper of the expression of plastocyanin and cytochrome c552 in Chlamydomonas reinhardi. Mol Cell Biol **6**: 462–469.

Merchant, S., K. Hill, and G. Howe. 1991. Dynamic interplay between two copper-titrating components in the transcriptional regulation of cyt c6. EMBO J **10**: 1383–1389.

Merchant, S. S., M. D. Allen, J. Kropat, J. L. Moseley, J. C. Long, S. Tottey, and A. M. Terauchi. 2006. Between a rock and a hard place: Trace element nutrition in Chlamydomonas. Biochimica et Biophysica Acta (BBA) - Molecular Cell Research **1763**: 578–594. doi:10.1016/j.bbamcr.2006.04.007

Merchant, S. S., and J. D. Helmann. 2012. Elemental Economy: microbial strategies for optimizing growth in the face of nutrient limitation. Adv Microb Physiol **60**: 91–210. doi:10.1016/B978-0-12-398264-3.00002-4

Messerschmidt, A. 1998. Metal sites in small blue copper proteins, blue copper oxidases and vanadium-containing enzymes. SpringerLink 37–68. doi:10.1007/3-540-62888-6_2

Millero, F. J. 1998. Solubility of Fe(III) in seawater. Earth and Planetary Science Letters **154**: 323–329. doi:10.1016/S0012-821X(97)00179-9

Milligan, A. J., and P. J. Harrison. 2000. Effects of non-steady-state iron limitation on nitrogen assimilatory enzymes in the marine diatom thalassiosira weissflogii (BACILLARIOPHYCEAE). Journal of Phycology **36**: 78–86. doi:10.1046/j.1529-8817.2000.99013.x

Miloslavina, Y., I. Grouneva, P. H. Lambrev, B. Lepetit, R. Goss, C. Wilhelm, and A. R. Holzwarth. 2009. Ultrafast fluorescence study on the location and mechanism of non-photochemical quenching in diatoms. Biochimica et Biophysica Acta (BBA) - Bioenergetics **1787**: 1189–1197. doi:10.1016/j.bbabio.2009.05.012

Mock, T., R. P. Otillar, J. Strauss, and others. 2017. Evolutionary genomics of the cold-adapted diatom Fragilariopsis cylindrus. Nature **advance online publication**: 1–5. doi:10.1038/nature20803

Mock, T., M. P. Samanta, V. Iverson, and others. 2008. Whole-genome expression profiling of the marine diatom Thalassiosira pseudonana identifies genes involved in silicon bioprocesses. PNAS **105**: 1579–1584. doi:10.1073/pnas.0707946105

Moffett, J. W., and L. E. Brand. 1996. Production of strong, extracellular Cu chelators by marine cyanobacteria in response to Cu stress. Limnol. Oceanogr. **41**: 388–395. doi:10.4319/lo.1996.41.3.0388

Moffett, J. W., L. E. Brand, P. L. Croot, and K. A. Barbeau. 1997. Cu speciation and cyanobacterial distribution in harbors subject to anthropogenic Cu inputs. Limnol. Oceanogr. **42**: 789–799. doi:10.4319/lo.1997.42.5.0789

Moffett, J. W., and R. G. Zika. 1983. Oxidation kinetics of Cu(I) in seawater: implications for its existence in the marine environment. Marine Chemistry **13**: 239–251. doi:10.1016/0304-4203(83)90017-8

Moniz, M. B. J., and I. Kaczmarska. 2009. Barcoding diatoms: Is there a good marker? Molecular Ecology Resources **9**: 65–74. doi:10.1111/j.1755-0998.2009.02633.x

Moniz, M. B. J., and I. Kaczmarska. 2010. Barcoding of Diatoms: Nuclear Encoded ITS Revisited. Protist **161**: 7–34. doi:10.1016/j.protis.2009.07.001

Moore, C. M., D. J. Suggett, A. E. Hickman, Y.-N. Kim, J. F. Tweddle, J. Sharples, R. J. Geider, and P. M. Holligan. 2006. Phytoplankton photoacclimation and photoadaptation in response to environmental gradients in a shelf sea. Limnol. Oceanogr. **51**: 936–949. doi:10.4319/lo.2006.51.2.0936

Moore, J. K., and O. Braucher. 2008. Sedimentary and mineral dust sources of dissolved iron to the world ocean. Biogeosciences **5**: 631–656. doi:10.5194/bg-5-631-2008

Moore, J. K., S. C. Doney, and K. Lindsay. 2004. Upper ocean ecosystem dynamics and iron cycling in a global three-dimensional model. Global Biogeochem. Cycles **18**: GB4028. doi:10.1029/2004GB002220

Morrissey, J., R. Sutak, J. Paz-Yepes, and others. 2015. A Novel Protein, Ubiquitous in Marine Phytoplankton, Concentrates Iron at the Cell Surface and Facilitates Uptake. Current Biology **25**: 364–371. doi:10.1016/j.cub.2014.12.004

Moustafa, A., B. Beszteri, U. G. Maier, C. Bowler, K. Valentin, and D. Bhattacharya. 2009. Genomic Footprints of a Cryptic Plastid Endosymbiosis in Diatoms. Science **324**: 1724–1726. doi:10.1126/science.1172983

Mueller-Cajar, O., M. Stotz, P. Wendler, F. U. Hartl, A. Bracher, and M. Hayer-Hartl. 2011. Structure and function of the AAA+ protein CbbX, a red-type Rubisco activase. Nature **479**: 194–199. doi:10.1038/nature10568

Nagao, R., S. Takahashi, T. Suzuki, N. Dohmae, K. Nakazato, and T. Tomo. 2013. Comparison of oligomeric states and polypeptide compositions of fucoxanthin chlorophyll a/c-binding protein complexes among various diatom species. Photosynth Res **117**: 281–288. doi:10.1007/s11120-013-9903-5

Navarro, J. A., M. Hervás, and M. A. D. la Rosa. 1997. Co-evolution of cytochrome c6 and plastocyanin, mobile proteins transferring electrons from cytochrome b6f to photosystem I. JBIC **2**: 11–22. doi:10.1007/s007750050101

Nelson, D. M., P. Tréguer, M. A. Brzezinski, A. Leynaert, and B. Quéguiner. 1995. Production and dissolution of biogenic silica in the ocean: Revised global estimates, comparison with regional data and relationship to biogenic sedimentation. Global Biogeochem. Cycles **9**: 359–372. doi:10.1029/95GB01070

Nelson, N., and A. Ben-Shem. 2004. The complex architecture of oxygenic photosynthesis. Nat Rev Mol Cell Biol **5**: 971–982. doi:10.1038/nrm1525

Nishiyama, Y., S. I. Allakhverdiev, and N. Murata. 2006. A new paradigm for the action of reactive oxygen species in the photoinhibition of photosystem II. Biochimica et Biophysica Acta (BBA) - Bioenergetics **1757**: 742–749. doi:10.1016/j.bbabio.2006.05.013

Noctor, G., A. Mhamdi, S. Chaouch, Y. Han, J. Neukermans, B. Marquez-Garcia, G. Queval, and C. H. Foyer. 2012. Glutathione in plants: an integrated overview. Plant, Cell & Environment **35**: 454–484. doi:10.1111/j.1365-3040.2011.02400.x

Nunn, B. L., J. F. Faux, A. A. Hippmann, M. T. Maldonado, H. R. Harvey, D. R. Goodlett, P. W. Boyd, and R. F. Strzepek. 2013. Diatom Proteomics Reveals Unique Acclimation Strategies to Mitigate Fe Limitation. PLoS ONE **8**: e75653. doi:10.1371/journal.pone.0075653

Oborník, M., and B. R. Green. 2005. Mosaic Origin of the Heme Biosynthesis Pathway in Photosynthetic Eukaryotes. Mol Biol Evol **22**: 2343–2353. doi:10.1093/molbev/msi230

Ong, S.-E., and M. Mann. 2005. Mass spectrometry–based proteomics turns quantitative. Nat Chem Biol **1**: 252–262. doi:10.1038/nchembio736

Orsini, L., G. Procaccini, D. Sarno, and M. Montresor. 2004. Multiple rDNA ITS-types within the diatom Pseudo-nitzschia delicatissima (Bacillariophyceae) and their relative abundances across a spring bloom in the Gulf of Naples. Mar Ecol Prog Ser **271**: 87–98. doi:10.3354/meps271087

Oudot-Le Secq, M.-P. O.-L., J. Grimwood, H. Shapiro, E. V. Armbrust, C. Bowler, and B. R. Green. 2007. Chloroplast genomes of the diatoms Phaeodactylum tricornutum and Thalassiosira pseudonana: comparison with other plastid genomes of the red lineage. Mol Genet Genomics **277**: 427–439. doi:10.1007/s00438-006-0199-4

Oxborough, K., and N. R. Baker. 1997. Resolving chlorophyll a fluorescence images of photosynthetic efficiency into photochemical and non-photochemical components – calculation of qP and Fv-/Fm-; without measuring Fo-; Photosynthesis Research **54**: 135–142. doi:10.1023/A:1005936823310

Page, R. D. 1996. TreeView: an application to display phylogenetic trees on personal computers. Comput. Appl. Biosci. **12**: 357–358.

Page, R. D. M. 2001. Treeview(Win32),.

Page, R. D. M. 2002. Visualizing phylogenetic trees using TreeView. Curr Protoc Bioinformatics **Chapter 6**: Unit 6.2. doi:10.1002/0471250953.bi0602s01

Parker, M. S., and E. V. Armbrust. 2005. Synergistic Effects of Light, Temperature, and Nitrogen Source on Transcription of Genes for Carbon and Nitrogen Metabolism in the Centric Diatom Thalassiosira Pseudonana (bacillariophyceae)1. Journal of Phycology **41**: 1142–1153. doi:10.1111/j.1529-8817.2005.00139.x

Parker, M. S., T. Mock, and E. V. Armbrust. 2008. Genomic Insights into Marine Microalgae. Annual Review of Genetics **42**: 619–645. doi:10.1146/annurev.genet.42.110807.091417

Peers, G., and N. M. Price. 2006. Copper-containing plastocyanin used for electron transport by an oceanic diatom. Nature **441**: 341–344. doi:10.1038/nature04630

Peers, G., S.-A. Quesnel, and N. M. Price. 2005. Copper requirements for iron acquisition and growth of coastal and oceanic diatoms. Limnol. Oceanogr. **50**: 1149–1158. doi:10.4319/lo.2005.50.4.1149

Petersen, T. N., S. Brunak, G. von Heijne, and H. Nielsen. 2011. SignalP 4.0: discriminating signal peptides from transmembrane regions. Nat Meth **8**: 785–786. doi:10.1038/nmeth.1701

Petrou, K., S. Trimborn, B. Rost, P. J. Ralph, and C. S. Hassler. 2014. The impact of iron limitation on the physiology of the Antarctic diatom Chaetoceros simplex. Mar Biol **161**: 925–937. doi:10.1007/s00227-014-2392-z

Port, J. A., M. S. Parker, R. B. Kodner, J. C. Wallace, E. V. Armbrust, and E. M. Faustman. 2013. Identification of G protein-coupled receptor signaling pathway proteins in marine diatoms using comparative genomics. BMC Genomics **14**: 503. doi:10.1186/1471-2164-14-503

Prasil, O., Z. Kolber, J. A. Berry, and P. G. Falkowski. 1996. Cyclic electron flow around Photosystem II in vivo. Photosynth Res **48**: 395–410. doi:10.1007/BF00029472

Premvardhan, L., B. Robert, A. Beer, and C. Büchel. 2010. Pigment organization in fucoxanthin chlorophyll a/c2 proteins (FCP) based on resonance Raman spectroscopy and sequence analysis. Biochimica et Biophysica Acta (BBA) - Bioenergetics **1797**: 1647–1656. doi:10.1016/j.bbabio.2010.05.002

Price, N. M., G. I. Harrison, J. G. Hering, R. J. Hudson, P. M. V. Nirel, B. Palenik, and F. M. M. Morel. 1988. Preparation and chemistry of the artificial algal culture medium Aquil. Biological Oceanography **6**: 443–461.

Prihoda, J., A. Tanaka, W. B. M. de Paula, J. F. Allen, L. Tirichine, and C. Bowler. 2012. Chloroplast-mitochondria cross-talk in diatoms. J. Exp. Bot. **63**: 1543–1557. doi:10.1093/jxb/err441

Punta, M., P. C. Coggill, R. Y. Eberhardt, and others. 2012. The Pfam protein families database. Nucleic Acids Res **40**: D290–D301. doi:10.1093/nar/gkr1065

Quinn, J. M., and S. Merchant. 1998. [18] Copper-responsive gene expression during adaptation to copper deficiency, p. 263–279. *In* Methods in Enzymology. Academic Press.

R Core Team. 2013. R: A Language and Environment for Statistical Computing, R Foundation for Statistical Computing.

Rae, T. D., P. J. Schmidt, R. A. Pufahl, V. C. Culotta, and T. V. O'Halloran. 1999. Undetectable Intracellular Free Copper: The Requirement of a Copper Chaperone for Superoxide Dismutase. Science **284**: 805–808. doi:10.1126/science.284.5415.805

Rappsilber, J., Y. Ishihama, and M. Mann. 2003. Stop and Go Extraction Tips for Matrix-Assisted Laser Desorption/Ionization, Nanoelectrospray, and LC/MS Sample Pretreatment in Proteomics. Anal. Chem. **75**: 663–670. doi:10.1021/ac026117i

Raven, J. A. 1988. The iron and molybdenum use efficiencies of plant growth with different energy, carbon and nitrogen sources. New Phytologist **109**: 279–287. doi:10.1111/j.1469-8137.1988.tb04196.x

Raven, J. A., M. C. W. Evans, and R. E. Korb. 1999. The role of trace metals in photosynthetic electron transport in O2-evolving organisms. Photosynthesis Research **60**: 111–150. doi:10.1023/A:1006282714942

Raven, J. A., and A. M. Waite. 2004. The evolution of silicification in diatoms: inescapable sinking and sinking as escape? New Phytologist **162**: 45–61. doi:10.1111/j.1469-8137.2004.01022.x

Redfield, A. C. 1934. On the Proportions of Organic Derivatives in Sea Water and Their Relation to the Composition of Plankton, p. 176–192. *In* James Johnstone Memorial Volume. University Press of Liverpool.

Redfield, A. C. 1958. The Biological Control of Chemical Factors in the Environment. American Scientist **46**: 230A–221.

Reyes-Prieto, A., A. P. M. Weber, and D. Bhattacharya. 2007. The Origin and Establishment of the Plastid in Algae and Plants. Annu. Rev. Genet. **41**: 147–168. doi:10.1146/annurev.genet.41.110306.130134

Rho, M., H. Tang, and Y. Ye. 2010. FragGeneScan: predicting genes in short and error-prone reads. Nucleic Acids Res **38**: e191. doi:10.1093/nar/gkq747

Richardson, K., J. Beardall, and J. A. Raven. 1983. Adaptation of Unicellular Algae to Irradiance: An Analysis of Strategies. New Phytologist **93**: 157–191. doi:10.1111/j.1469-8137.1983.tb03422.x

Rochaix, J.-D. 2011. Regulation of photosynthetic electron transport. Biochimica et Biophysica Acta (BBA) - Bioenergetics **1807**: 375–383. doi:10.1016/j.bbabio.2010.11.010

Roche, J. L., H. Murray, M. Orellana, and J. Newton. 1995. Flavodoxin Expression as an Indicator of Iron Limitation in Marine Diatoms1. Journal of Phycology **31**: 520–530. doi:10.1111/j.1529-8817.1995.tb02545.x

Rodriguez, R. E., A. Lodeyro, H. O. Poli, and others. 2007. Transgenic Tobacco Plants Overexpressing Chloroplastic Ferredoxin-NADP(H) Reductase Display Normal Rates of Photosynthesis and Increased Tolerance to Oxidative Stress. Plant Physiol **143**: 639–649. doi:10.1104/pp.106.090449

Rodríguez-Ezpeleta, N., H. Brinkmann, S. C. Burey, and others. 2005. Monophyly of Primary Photosynthetic Eukaryotes: Green Plants, Red Algae, and Glaucophytes. Current Biology **15**: 1325–1330. doi:10.1016/j.cub.2005.06.040

Roshan, S., and J. Wu. 2015. The distribution of dissolved copper in the tropical-subtropical north Atlantic across the GEOTRACES GA03 transect. Marine Chemistry **176**: 189–198. doi:10.1016/j.marchem.2015.09.006

RStudio Team. 2015. RStudio: Integrated Development Environment for R, RStudio, Inc.

Ruban, A., J. Lavaud, B. Rousseau, G. Guglielmi, P. Horton, and A.-L. Etienne. 2004. The super-excess energy dissipation in diatom algae: comparative analysis with higher plants. Photosynthesis Research **82**: 165. doi:10.1007/s11120-004-1456-1

Rue, E. L., and K. W. Bruland. 1995. Complexation of iron(III) by natural organic ligands in the Central North Pacific as determined by a new competitive ligand equilibration/adsorptive cathodic stripping voltammetric method. Marine Chemistry **50**: 117–138. doi:10.1016/0304-4203(95)00031-L

Rueter, J. G., J. J. McCarthy, and E. J. Carpenter. 1979. The toxic effect of copper on Oscillatoria (Trichodesmium) theibautii1. Limnol. Oceanogr. **24**: 558–562. doi:10.4319/lo.1979.24.3.0558

Rynearson, T. A., J. A. Newton, and E. V. Armbrust. 2006. Spring bloom development, genetic variation, and population succession in the planktonic diatom Ditylum brightwellii. Limnol. Oceanogr. **51**: 1249–1261. doi:10.4319/lo.2006.51.3.1249

Samukawa, M., C. Shen, B. M. Hopkinson, and Y. Matsuda. 2014. Localization of putative carbonic anhydrases in the marine diatom, Thalassiosira pseudonana. Photosynth Res **121**: 235–249. doi:10.1007/s11120-014-9967-x

Sandmann, G., and P. Böger. 1980. Copper-induced exchange of plastocyanin and cytochrome c-533 in cultures of Anabaena variabilis and Plectonema boryanum. Plant Science Letters **17**: 417–424. doi:10.1016/0304-4211(80)90128-5

Scheibe, R. 2004. Malate valves to balance cellular energy supply. Physiologia Plantarum **120**: 21–26. doi:10.1111/j.0031-9317.2004.0222.x

Schmidt, C. L., and L. Shaw. 2001. A Comprehensive Phylogenetic Analysis of Rieske and Rieske-Type Iron-Sulfur Proteins. J Bioenerg Biomembr **33**: 9–26. doi:10.1023/A:1005616505962

Schmieder, R., Y. W. Lim, and R. Edwards. 2012. Identification and removal of ribosomal RNA sequences from metatranscriptomes. Bioinformatics **28**: 433–435. doi:10.1093/bioinformatics/btr669

Schuback, N., M. Flecken, M. T. Maldonado, and P. D. Tortell. 2016. Diurnal variation in the coupling of photosynthetic electron transport and carbon fixation in iron-limited phytoplankton in the NE subarctic Pacific. Biogeosciences **13**: 1019–1035. doi:10.5194/bg-13-1019-2016

Schuback, N., C. Schallenberg, C. Duckham, M. T. Maldonado, and P. D. Tortell. 2015. Interacting Effects of Light and Iron Availability on the Coupling of Photosynthetic Electron Transport and CO2-Assimilation in Marine Phytoplankton. PLoS ONE **10**: e0133235. doi:10.1371/journal.pone.0133235

Semeniuk, D., R. Bundy, C. D. Payne, K. A. Barbeau, and M. Maldonado. 2015. Acquisition of organically complexed copper by marine phytoplankton and bacteria in the northeast subarctic Pacific Ocean,.

Semeniuk, D. M. 2014. Copper nutrition and transport mechanisms in plankton communities in the northeast Pacific Ocean. University of British Columbia.

Semeniuk, D. M., J. T. Cullen, W. K. Johnson, K. Gagnon, T. J. Ruth, and M. T. Maldonado. 2009. Plankton copper requirements and uptake in the subarctic Northeast Pacific Ocean. Deep Sea Research Part I: Oceanographic Research Papers **56**: 1130–1142. doi:10.1016/j.dsr.2009.03.003

Silsbe, G. M., and S. Y. Malkin. 2015. phytotools: Phytoplankton Production Tools,.

Smith, B. E. 1999. Structure, Function, and Biosynthesis of the Metallosulfur Clusters in Nitrogenases, p. 159–218. *In* A.G. Sykes [ed.], Advances in Inorganic Chemistry. Academic Press.

Smith, S. R., R. M. Abbriano, and M. Hildebrand. 2012. Comparative analysis of diatom genomes reveals substantial differences in the organization of carbon partitioning pathways. Algal Research **1**: 2–16. doi:10.1016/j.algal.2012.04.003

Smith, S. R., J. T. F. Gillard, A. B. Kustka, and others. 2016. Transcriptional Orchestration of the Global Cellular Response of a Model Pennate Diatom to Diel Light Cycling under Iron Limitation. PLOS Genetics **12**: e1006490. doi:10.1371/journal.pgen.1006490

Sommer, F., J. Kropat, D. Malasarn, N. E. Grossoehme, X. Chen, D. P. Giedroc, and S. S. Merchant. 2010. The CRR1 Nutritional Copper Sensor in Chlamydomonas Contains Two Distinct Metal-Responsive Domains. Plant Cell **22**: 4098–4113. doi:10.1105/tpc.110.080069

Strzepek, R. F., and P. J. Harrison. 2004. Photosynthetic architecture differs in coastal and oceanic diatoms. Nature **431**: 689–692. doi:10.1038/nature02954

Sunda, W. G., and S. A. Huntsman. 1995. Iron uptake and growth limitation in oceanic and coastal phytoplankton. Marine Chemistry **50**: 189–206. doi:10.1016/0304-4203(95)00035-P

Sunda, W. G., D. G. Swift, and S. A. Huntsman. 1991. Low iron requirement for growth in oceanic phytoplankton. Nature **351**: 55–57. doi:10.1038/351055a0

Suzuki, K., A. Hattori-Saito, Y. Sekiguchi, J. Nishioka, M. Shigemitsu, T. Isada, H. Liu, and R. M. L. McKay. 2014. Spatial variability in iron nutritional status of large diatoms in the

Sea of Okhotsk with special reference to the Amur River discharge. Biogeosciences **11**: 2503–2517. doi:https://doi.org/10.5194/bg-11-2503-2014

Taddei, L., G. R. Stella, A. Rogato, and others. 2016. Multisignal control of expression of the LHCX protein family in the marine diatom Phaeodactylum tricornutum. J. Exp. Bot. erw198. doi:10.1093/jxb/erw198

Tanaka, T., Y. Maeda, A. Veluchamy, and others. 2015. Oil Accumulation by the Oleaginous Diatom Fistulifera solaris as Revealed by the Genome and Transcriptome. The Plant Cell Online tpc.114.135194. doi:10.1105/tpc.114.135194

Terauchi, A. M., S.-F. Lu, M. Zaffagnini, and others. 2009. Pattern of Expression and Substrate Specificity of Chloroplast Ferredoxins from Chlamydomonas reinhardtii. J. Biol. Chem. **284**: 25867–25878. doi:10.1074/jbc.M109.023622

Tirichine, L., A. Rastogi, and C. Bowler. 2017. Recent progress in diatom genomics and epigenomics. Current Opinion in Plant Biology **36**: 46–55. doi:10.1016/j.pbi.2017.02.001

Tognetti, V. B., J. F. Palatnik, M. F. Fillat, M. Melzer, M.-R. Hajirezaei, E. M. Valle, and N. Carrillo. 2006. Functional Replacement of Ferredoxin by a Cyanobacterial Flavodoxin in Tobacco Confers Broad-Range Stress Tolerance. The Plant Cell Online **18**: 2035–2050. doi:10.1105/tpc.106.042424

Traller, J. C., S. J. Cokus, D. A. Lopez, and others. 2016. Genome and methylome of the oleaginous diatom Cyclotella cryptica reveal genetic flexibility toward a high lipid phenotype. Biotechnology for Biofuels **9**: 258. doi:10.1186/s13068-016-0670-3

Trick, C. G. 1989. Hydroxamate-siderophore production and utilization by marine eubacteria. Current Microbiology **18**: 375–378. doi:10.1007/BF01571131

Van Den Berg, C. M. G. 1984. Organic and inorganic speciation of copper in the Irish Sea. Marine Chemistry **14**: 201–212. doi:10.1016/0304-4203(84)90042-2

Vizcaíno, J. A., A. Csordas, N. del-Toro, and others. 2016. 2016 update of the PRIDE database and its related tools. Nucleic Acids Res. **44**: D447-456. doi:10.1093/nar/gkv1145

Von Dassow, P., T. W. Petersen, V. A. Chepurnov, and E. Virginia Armbrust. 2008. Inter- and Intraspecific Relationships Between Nuclear Dna Content and Cell Size in Selected Members of the Centric Diatom Genus Thalassiosira (bacillariophyceae)1. Journal of Phycology **44**: 335–349. doi:10.1111/j.1529-8817.2008.00476.x

Washburn, M. P., D. Wolters, and J. R. Yates. 2001. Large-scale analysis of the yeast proteome by multidimensional protein identification technology. Nat Biotech **19**: 242–247. doi:10.1038/85686

Weber, T., A. Gruber, and P. G. Kroth. 2009. The Presence and Localization of Thioredoxins in Diatoms, Unicellular Algae of Secondary Endosymbiotic Origin. Molecular Plant **2**: 468–477. doi:10.1093/mp/ssp010

Wells, M. L., C. G. Trick, W. P. Cochlan, M. P. Hughes, and V. L. Trainer. 2005. Domoic acid: The synergy of iron, copper, and the toxicity of diatoms. Limnol. Oceanogr. **50**: 1908–1917. doi:10.4319/lo.2005.50.6.1908

Westall, J. C., J. L. Zachary, and F. M. M. Morel. 1976. MINEQL, A Computer Program for the Calculation of Chemical Equilibrium Composition of Aqueous Systems. MIT Technical Note 18. MIT Technical Note 18.

White, T., T. Bruns, S. Lee, and J. Taylor. 1990. Amplification and direct sequencing of fungal ribosomal RNA genes for phylogenetics In: PCR Protocols: A Guide to Methods and

Applications, p. 315–322. *In* PCR Protocols: A Guide to Methods and Applications. Academic Press, Inc.

Whitney, L. P., J. J. Lins, P. D. Chappell, and B. D. Jenkins. 2011. Characterization of putative iron responsive genes as species-specific indicators of iron stress in Thalassiosiroid diatoms. Front. Microbio. **2**: 234. doi:10.3389/fmicb.2011.00234

Wu, J., and E. Boyle. 2002. Iron in the Sargasso Sea: Implications for the processes controlling dissolved Fe distribution in the ocean. Global Biogeochem. Cycles **16**: 1086. doi:10.1029/2001GB001453

Wu, J., and G. W. Luther III. 1995. Complexation of Fe(III) by natural organic ligands in the Northwest Atlantic Ocean by a competitive ligand equilibration method and a kinetic approach. Marine Chemistry **50**: 159–177. doi:10.1016/0304-4203(95)00033-N

Yamori, W., and T. Shikanai. 2016. Physiological Functions of Cyclic Electron Transport Around Photosystem I in Sustaining Photosynthesis and Plant Growth. Annual Review of Plant Biology **67**: 81–106. doi:10.1146/annurev-arplant-043015-112002

Yoshida, K., I. Terashima, and K. Noguchi. 2007. Up-Regulation of Mitochondrial Alternative Oxidase Concomitant with Chloroplast Over-Reduction by Excess Light. Plant Cell Physiol **48**: 606–614. doi:10.1093/pcp/pcm033

Zamzow, H., K. H. Coale, K. S. Johnson, and C. M. Sakamoto. 1998. Determination of copper complexation in seawater using flow injection analysis with chemiluminescence detection. Analytica Chimica Acta **377**: 133–144. doi:10.1016/S0003-2670(98)00618-7

Zechmann, B. 2014. Compartment-specific importance of glutathione during abiotic and biotic stress. Front Plant Sci **5**. doi:10.3389/fpls.2014.00566

Zhang, L.-T., Z.-S. Zhang, H.-Y. Gao, X.-L. Meng, C. Yang, J.-G. Liu, and Q.-W. Meng. 2012. The mitochondrial alternative oxidase pathway protects the photosynthetic apparatus against photodamage in Rumex K-1 leaves. BMC Plant Biol **12**: 40. doi:10.1186/1471-2229-12-40

Zhu, S.-H., and B. R. Green. 2010. Photoprotection in the diatom Thalassiosira pseudonana: Role of LI818-like proteins in response to high light stress. Biochimica et Biophysica Acta (BBA) - Bioenergetics **1797**: 1449–1457. doi:10.1016/j.bbabio.2010.04.003

Zhu, S.-H., J. Guo, M. T. Maldonado, and B. R. Green. 2010. Effects of Iron and Copper Deficiency on the Expression of Members of the Light-Harvesting Family in the Diatom Thalassiosira Pseudonana (bacillariophyceae)1. Journal of Phycology **46**: 974–981. doi:10.1111/j.1529-8817.2010.00884.x

Zhu, Y., J. Ishizaka, S. C. Tripathy, S. Wang, Y. Mino, T. Matsuno, and D. J. Suggett. 2016a. Variation of the photosynthetic electron transfer rate and electron requirement for daily net carbon fixation in Ariake Bay, Japan. J Oceanogr 1–16. doi:10.1007/s10872-016-0370-4

Zhu, Z., K. Xu, F. Fu, J. L. Spackeen, D. A. Bronk, and D. A. Hutchins. 2016b. A comparative study of iron and temperature interactive effects on diatoms and Phaeocystis antarctica from the Ross Sea, Antarctica. Marine Ecology Progress Series **550**: 39–51. doi:10.3354/meps11732

Zurbriggen, M. D., V. B. Tognetti, M. F. Fillat, M.-R. Hajirezaei, E. M. Valle, and N. Carrillo. 2008. Combating stress with flavodoxin: a promising route for crop improvement. Trends Biotechnol. **26**: 531–537. doi:10.1016/j.tibtech.2008.07.001

Appendices

Appendix A − Supplementary material for Chapter 3: Contrasting Effects of Copper Limitation on the Photosynthetic Apparatus in Two Strains of the Open Ocean Diatom *Thalassiosira oceanica*

A.1 ITS fragment visualization

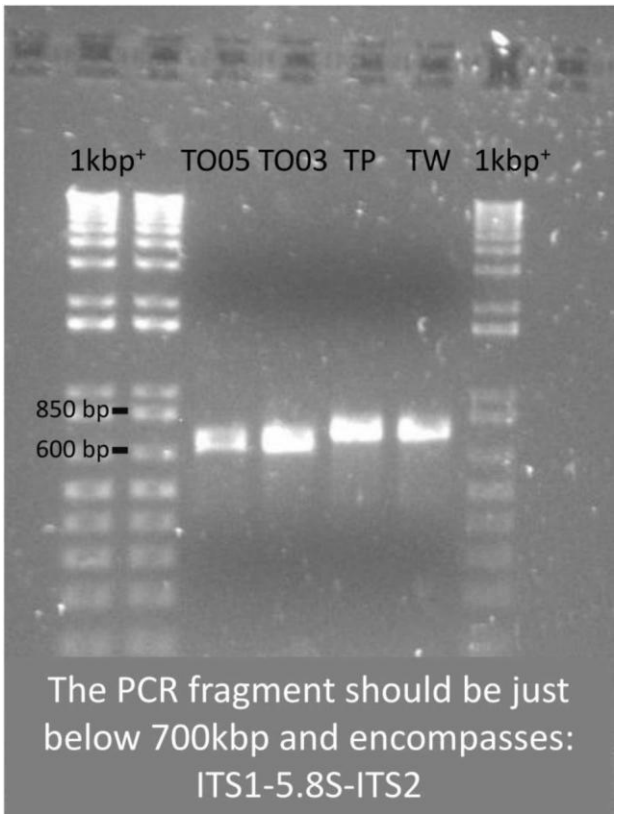

Figure A.1: ITS fragment visualization. Approximately 700bp long ITS fragment, comprised of ITS1, 5.8SrDNA gene and part of ITS2, 1.5% agarose gel. TO03, *T. oceanica* (CCMP1003); TO05, *T. oceanica* (CCMP1005); TP, *T. pseudonana*; TW, *T. weisfloggii*

A.2 ITS sequence alignment

```
TO1003          cggaaggatcatttcacaccatccaacttcatccccgggaaacgacgagcggagctcgag
TO1005          cggaaggatcatttcacaccatccaacttcatccccgggaaacgacgagcggagctcgag
                ************************************************************

TO1003          cgccgatacactggccgggcttgtcctcctaacataatcataaaaaacaaaaccaggtgc
TO1005          cgccgatacactggccgggcttgtcctcctaacataatcataaaaaacaaaaccaggtgc
                ************************************************************

TO1003          tactaccagcaatggatgtagtgccgcccaatactaagtgacaaaataactgaacataac
TO1005          tactaccagcaatggatgtagtgccgcccaatactaagtgacaaaataactgaacataac
                ************************************************************

TO1003          ggtctcttggagcgagagctcctctaggctgcacaattatttacaactttcagcaatgga
TO1005          ggtctcttggagcgagagctcctctaggctgcacaattatttacaactttcagcaatgga
                ************************************************************

TO1003          tgtcttggatcccacaacgatgaagaacgcagcgaactgcgatacgtaatacgaactgca
TO1005          tgtcttggatcccacaacgatgaagaacgcagcgaactgcgatacgtaatacgaactgca
                ************************************************************

TO1003          gaacctcgtgaatcatcaaaattttgaacgcacattgcgcttttgggtaattcccaagag
TO1005          gaacctcgtgaatcatcaaaattttgaacgcacattgcgcttttgggtaattcccaagag
                ************************************************************

TO1003          catgcttatctgagtgtccctgaaccccactcagccactgctgcggttgcaagaccccgg
TO1005          catgcttatctgagtgtccctgaaccccactcagccactgctgcggttgcaagactccgg
                ************************************************************.****

TO1003          agtgagctggactgtgacggtgcaaggccctgccgagctccgttcaaatggttagcctgt
TO1005          agtgagctggactgtgacggtgcaaggccctgccgagctccgttcaaatggttagcctgt
                ************************************************************

TO1003          gcactgacccctcctggtgagcgcagtgatggacttggtagatgcactgatgtgtgtttg
TO1005          gcactgacccctcctggtgagcgcagtgatggacttggtagatgcactgatgtgtgtttg
                ************************************************************

TO1003          agtcttgacccgtgcgagcctaggtaggacggtgcctcatggtgcatgccgtgtgcatgc
TO1005          agtcttgacccgtgcgagcctaggtaggacggtgcctcatggtgcatgccgtgtgtatgc
                ************************************************************.****

TO1003          ccatccaatcctatacttggatctcagatta
TO1005          ccatccaatcctatacttggatctcagatta
                ******************************
```

Figure A.2: CLUSTAL format alignment by MAFFT (v7.372) of the two T. oceanica ITS sequences (CCMP 1003 and CCMP 1005). Of the 597 nucleotides, only two (yellow) are different (99.66% identical)

A.3 ITS phylogenetic tree

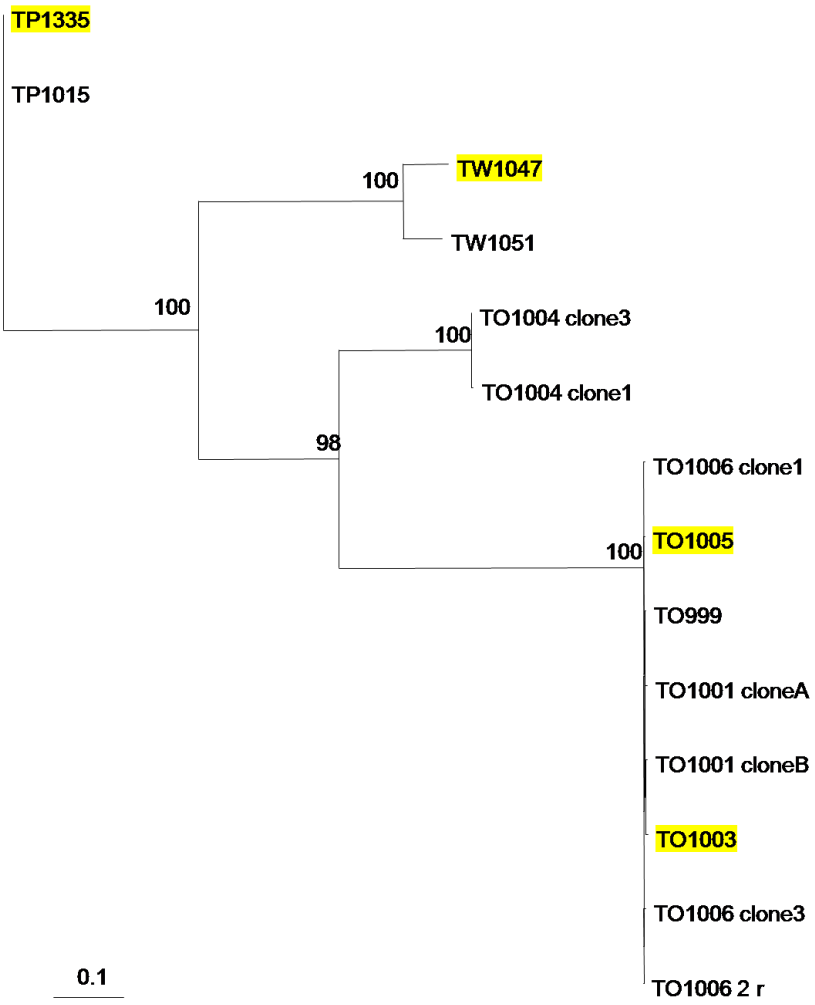

Figure A.3: Phylogenetic tree of 14 diatom ITS regions (10 *Thalassiosira oceanica*, 2 *T. pseudonana*, and 2 *T. weisfloggii*), supporting the close genetic relationship between the *T. oceanica* strains used in this thesis (CCMP1003 and CCMP1005). Only bootstrap values (100 replicates) above 90 are shown.

A.4 ITS sequences used for phylogenetic tree

Table A.1: Sequence information used to generate phylogenetic tree of various diatom ITS sequences

Strain abbreviation	genbank ITS sequence accession number
TO999	EF134953.1
TO1001 clone A	EF134955.1
TO1001 clone B	EF134954.1
TO1004 clone1	EF208794.1
TO1004 clone3	EF208795.1
TO1006 clone1	EF362631.1
TO1006 clone2	EF362632.1
TO1006 clone3	EF362633.1
TP1015	EF208792.1
TP1335	EF208793.1
TW1047	EF208779.1
TW1051	EF208787.1

A.5 Summary table of effects of low Cu on physiological parameters in *Thalassiosira oceanica* (CCMP 1003 and CCMP 1005)

Table A.2: Effect of chronic copper limitation on physiology in two strains of the open ocean diatom Thalassiosira oceanica: CCMP 1003 and CCMP 1005 abbreviated to TO03 and TO05, respectively. Arrows indicate if the response to low Cu statistically increases ↑ or decreases ↓. Shown are means with standard errors for parameters derived from three biological replicates (^ indicates measurements have only been done on two of the three biological triplicates, see raw data in Table A.2). Low Cu results in bold indicate statistically significant differences compared to the respective control treatment. Stars (*, **, ***) indicate the level of significance of a 2-way ANOVA with post-hoc interaction analysis (see methods for details). The right panel indicates whether the physiological response differs between the two strains; ↓ and ↑ mean the result is significantly lower or higher in TO03 compared to TO05. Note that there is hardly any difference in their physiology under their respective replete metal concentrations. However, when Cu limited, roughly half of the tested parameters show significantly different results.

	TO 1003			TO 1005			TO03 TO05	TO03 TO05
Parameter tested	**control**		**low Cu**	**control**		**low Cu**	**control**	**lowCu**
[Fe] (nmol)	1370.00		1370.00	1370.00		1370.00		
[Cu] (nmol)	10.20		0.20	14.32		6.08		
µ (dd-1)	1.52 ± 0.06	↓	**0.73 ± 0.10 *** **	1.82 ± 0.02	↓	**1.19 ± 0.03 *** **	↓	↓
µ (d-1)	1.05 ± 0.07	↓	**0.51 ± 0.10*** **	1.26 ± 0.02	↓	**0.82 ± 0.03*** **	↓	↓
µ (% µmax)	100.50 ± 4.21	↓	**47.86 ± 6.45 **** **	99.82 ± 1.19	↓	**65.46 ± 1.61 **** **		
cell diameter (µm)	5.22 ± 0.05	↓	**4.72 ± 0.04 **** **	5.42 ± 0.16	↓	**4.82 ± 0.23 **** **		
cell vol (fl)	74.68 ± 1.93	↓	**55.16 ± 1.43 **** **	83.69 ± 7.74	↓	**59.54 ± 8.78 **** **		.
cell surface area (µm^2)	85.73 ± 1.52	↓	**70.1 ± 1.23 ** **	92.34 ± 5.65	↓	**73.31 ± 7.13 ** **		
cell SA / V (µm^2 / fL)	1.15 ± 0.01	↑	**1.27 ± 0.01 ** **	1.11 ± 0.03	↑	**1.25 ± 0.06 ** **		
Chl a conc (pg/cell)	0.30 ± 0.01		0.34 ± 0.05	0.35 ± 0.05		0.23 ± 0.05 .		.
Chl a conc (fg/fl) cell vol	4.34 ± 0.11	↑	**7.40 ± 0.46 *** **	4.28 ± 0.80		3.79 ± 0.41		↑
Fv/Fm (A.U.)	0.60 ± 0.01^	↓	**0.29 ± 0.01 **** **	0.61 ± 0.01		0.58 ± 0.02 .	↓	↓
Sigma (Å / RCII)	584.40 ± 4.95^	↑	**764.01 ± 12.50 *** **	579.15 ± 3.58^		572.76 ± 24.94^		↑
PQ-Pool size (mol PQ / mol Qb)	4.34 ± 0.47^		5.98 ± 0.35 .	5.65 ± 0.18^		5.12 ± 0.19^		
sigma ' @ growth irradiance (Å / RCII)	583.09 ± 18.30	↑	**664.04 ± 10.95 ** **	585 ± 3.23^		575.61 ± 2.47^		↑
Fq'/Fv' @ growth irradiance (A.U.)	0.7 ± 0.04	↓	**0.58 ± 0.02 * **	0.69 ± 0.02^		0.66 ± 0.01^		
Fv'/Fm' @ growth irradiance (A.U.)	0.61 ± 0.01	↓	**0.29 ± 0.01 **** **	0.60 ± 0.01^		0.62 ± 0.00^		↓
Fq'/Fm' @ growth irradiance (A.U.)	0.43 ± 0.03	↓	**0.16 ± 0.01 *** **	0.41 ± 0.01^		0.41 ± 0.01^		↓
ETR @ growth irradiance (mol e-/RCII * s)	398.33 ± 31.51		373.65 ± 16.77	390.88 ± 7.34^		368.45 ± 5.97^		
NPQ (nsv) @ growth irradiance	0.63 ± 0.03	↑	**2.43 ± 0.15 **** **	0.66 ± 0.01^		0.59 ± 0.01^		↑
ETR - PE curve - alpha (mol e-/RCII)/(µmol quanta / m^2 * s)	3.49 ± 0.11	↑	**4.04 ± 0.11 * **	3.29 ± 0.01^		3.46 ± 0.03^		↑
ETR - PE curve - pmax pmax (mol e-/RCII * s)	493.72 ± 54.98		425.67 ± 23.75	502.11 ± 23.46^		431.17 ± 4.69^		
ETR - PE curve - ek (µmol quanta / m^2 * s)	140.79 ± 12.48	↓	**105.34 ± 5.07 * **	152.55 ± 7.65^		124.6 ± 0.031^		
Conversion factor (ETR / 14C uptake)	192.24 ± 22.23	↑	**406.85 ± 20.43 * **	117.55 ± 61.89^		111.99 ± 56.03^		↑
14C - PvsE - curve - α (g C / g Chla * h)/(µmol quanta / m^2 * s)	0.0151 ± 1.69E-03	↓	**5.66E-03 ± 1.75E-03 * **	1.41E-02 ± 3.32E-03		2.06E-02 ± 4.70E-03		↓
14C - PvsE - curve - eK (µmol quanta / m^2 * s)	251.97 ± 23.73	↓	**172.00 ± 2.51 ** **	249.05 ± 10.46		223.04 ± 20.76		↓
14C - PvsE - curve - Pmax (g C / g Chla * h)	3.89 ± 0.81	↓	**0.97 ± 0.29 ** **	3.46 ± 0.70		4.40 ± 0.54		↓
14C uptake @ 155 uEinstein (g C / g Chla * h)	2.09 ± 0.27	↓	**0.70 ± 0.21 * **	1.94 ± 0.44		2.71 ± 0.53		↓

	TO 1003			TO 1005			TO03 TO05	TO03 TO05
Parameter tested	**control**		**low Cu**	**control**		**low Cu**	**control**	**lowCu**
FeDFB uptake (zmol / µm^2 * h)	4.23 ± 1.62		1.03 ± 0.24	5.47 ± 2.83		2.01 ± 2.00 .		
Gross O2 Prod (mol O2 / mol Chla * h)	366.59 ± 28.16	↓	**101.02 ± 26.53*** **	362.04 ± 33.22		295.11 ± 58.21		.
Gross O2 Prod (µmol O2 / cell * h)	1.23E-07 ± 1.15E-08	↓	**3.60E-08 ± 4.27E-09****	1.39E-07 ± 1.04E-08	↓	**6.94E-08 ± 1.99E-09****		
Respiration (mol O2 / mol Chla * h)	0.07 ± 0.03		0.04 ± 0.01	0.05 ± 0.01		0.06 ± 0.00		.
Respiration (µmol O2 / cell * h)	1.16E-08 ± 2.32E-9		9.10E-09 ± 1.16E-9	1.79E-08 ± 3.79E-9		1.60E-08 ± 3.76E-9		
14C uptake @ 155 uE (mol C / mol Chla * h)	0.16 ± 0.03	↓	**0.05 ± 0.02***	0.15 ± 0.04		0.20 ± 0.04		
Protein content (pg/cell)	12.61 ± 1.47		15.44 ± 2.32	31.15 ± 2.18	↓	**15.36 ± 1.22**** **	↑	
AOX activity	48.84 ± 0.9		53.60 ± 7.05	60.56 ± 6.23		63.69 ± 7.12		

. *p*-value< 0.1

* *p*-value< 0.05

** *p*-value< 0.01

*** *p*-value< 0.001

**** *p*-value< 0.0001

A.6 Table of raw physiological data for all three biological replicates of each treatment (control and low Cu) and strain (CCMP 1003 and CCMP 1005)

Table A.3: Physiological raw data of all three biological replicates for both strains (CCMP 1003 and CCMP 1005) and treatments (control and lowCu)

Culture	TO1003 control			TO1003 lowCu			TO1005 control			TO1005 lowCu		
µ (dd-1)	1.43	1.48	1.65	0.59	0.92	0.67	1.85	1.77	1.83	1.19	1.14	1.24
µ (d-1)	0.99	1.03	1.14	0.41	0.64	0.47	1.28	1.23	1.27	0.82	0.79	0.86
% µ/µmax	94.26	97.64	108.24	38.89	60.37	44.32	101.41	97.50	100.56	65.34	62.74	68.30
cell size (µm)	5.13	5.27	5.27	4.64	4.76	4.77	5.30	5.74	5.21	4.59	4.59	5.28
cell vol (fl/cell)	70.83	76.73	76.48	52.29	56.53	56.66	77.92	99.01	74.15	50.79	50.72	77.10
cell SA (µm2)	82.68	87.25	87.25	67.64	71.18	71.48	88.25	103.51	85.28	66.19	66.19	87.58
Chla per cell (pg/ cell)	0.29	0.31	0.30	0.26	0.33	0.44	0.46	0.32	0.28	0.22	0.15	0.32
Chla per cell vol (fg/ fL)	4.52	4.35	4.14	6.49	7.92	7.80	5.85	3.27	3.71	4.28	2.97	4.12
FvFm	0.59	0.60		0.27	0.29	0.31	0.63	0.59	0.62	0.53	0.61	0.59
Sig	590.00	578.00		786.00	763.00	743.00		575.00	584.00	542.00	603.00	
PQ_Siz	4.90	3.80		6.70	5.50	5.80		5.90	5.40	4.90	5.30	
sig'	609.97	548.13	591.17	685.03	659.00	648.11		588.95	581.05	578.64	572.58	
F'q/F'v	0.71	0.64	0.77	0.61	0.59	0.55		0.67	0.71	0.67	0.65	
F'v/F'm	0.60	0.60	0.64	0.27	0.29	0.32		0.60	0.61	0.63	0.62	
F'q/F'm	0.43	0.38	0.49	0.16	0.17	0.17		0.40	0.43	0.43	0.41	
ETR @ growth irradiance	417.45	336.77	440.78	400.61	377.47	342.89		381.89	399.87	375.76	361.14	
NPQ(nsv)	0.66	0.66	0.57	2.70	2.46	2.16		0.67	0.65	0.58	0.61	
ETR alpha	3.47	3.31	3.70	4.25	3.91	3.96		3.31	3.28	3.51	3.42	
ETR pmax	542.03	384.02	555.13	456.14	442.02	378.88		473.39	530.84	436.92	425.44	
ETR ek	156.20	116.10	150.10	107.27	113.01	95.76		143.18	161.93	124.64	124.57	

Culture	TO1003 control			TO1003 lowCu			TO1005 control			TO1005 lowCu		
Conversion factor @ growth irradiance	155.98	188.12	232.64	1513.34	431.88	381.83		209.90	142.78	164.41	171.56	
14C per Chla alpha	0.02	0.01	0.01	0.00	0.01	0.01	0.01	0.01	0.02	0.02	0.02	0.03
14C per Chla ek	297.00	216.47	242.44	176.98	170.12	168.91	269.71	241.60	235.84	248.97	238.15	181.99
14C per Chla pmax	5.50	2.89	3.28	0.38	1.25	1.27	2.42	3.16	4.79	4.07	3.67	5.45
14C per Chla @ growth irradiance	2.64	1.78	1.85	0.27	0.90	0.92	1.25	1.79	2.76	2.25	2.10	3.77
FeDFB (zmol um 2 h)	3.00	2.20	7.40	1.40	0.60	1.10	6.87	0.01	9.52	4.01	0.01	
Gross Productivity (mol O2/ (mol Chla * h))	370.23	413.44	316.10	153.16	83.46	66.43	296.68	405.11	384.32	274.01	404.81	206.50
Gross Productivity / cell (mol O2 / cell * h)	0.00	0.00	0.00	0.00	0.00	0.00	0.00	0.00	0.00	0.00	0.00	0.00
Respiration (mol O2 / mol Chla * h)	22.40	34.84	45.92	34.79	18.53	21.04	25.73	42.29	82.41	63.88	57.45	64.01
Respiration (µmol O2 / cell * h)	0.00	0.00	0.00	0.00	0.00	0.00	0.00	0.00	0.00	0.00	0.00	0.00
14C (molC / mol Chla * h)	0.14	0.13	0.21	0.02	0.07	0.07	0.09	0.13	0.22	0.17	0.16	0.28
cellular protein (pg / cell)	11.71	15.48	10.64	15.97	11.18	19.17	28.97	33.33		16.58	14.14	
AOX activity (%)	47.05	49.74	49.73	53.14	41.62	66.04	57.93	72.43	51.33	50.77	75.35	64.94
Cell Density	1.65E+05	1.10E+05	3.12E+05	7.99E+04	1.11E+05	9.67E+04	1.37E+05	1.21E+05	9.95E+04	3.16E+05	2.95E+05	2.50E+05

A.7 Differential expression of all 48 predicted LHCs in *T. oceanica* (CCMP 1003 and CCMP 1005) across all four datasets

Table A.4: Expression of all 48 predicted LHC in TO03 and TO05 across all four datasets

Expression of all 48 predicted LHCs in *T. oceanica* (CCMP 1003 and CCMP 1005) across all four datasets

				differential expression[h]							
clade[a]	**gene name[b]**	**closest homolog in Tp[c]**	**expr[d]**	**TO03 I (original)[e]**	**sig[g]**	**TO03 II (+EST)[f]**	**sig[g]**	**TO05 I (original)[e]**	**sig[g]**	**TO05 II (+EST)[f]**	**sig[g]**
17531	THAOC_01290	**Tp17531**	y					-1.06		-1.05	
Lhcf - Group I	THAOC_02510	**TpLhcf**	y	-1.18		-1.20		-1.13		-1.17	
	THAOC_06305	**TpLhcf**	y	-4.2		**-10.34**	**y**	-1.21		-1.23	
	THAOC_17964	**TpLhcf**	y	1.19		1.06		-1.07		-1.10	
	THAOC_17964, contig_83951_1_204_+	**TpLhcf**	y							-1.07	
	THAOC_20854	**TpLhcf**	y	**-5.56**	**y**	**-5.56**	**y**	-1.28		-1.27	
	THAOC_20855	**TpLhcf**	y	-1.63		-1.63		-1.21		-1.20	
	THAOC_25270	**TpLhcf**	y	1.23		1.24		-1.13		-1.06	
	THAOC_25270, contig_119270_60_376_-	**TpLhcf**	y							-1.32	
	THAOC_25270, contig_123884_1_219_-	**TpLhcf**	y			-1.70					
	THAOC_25270, contig_70472_60_300_-	**TpLhcf**	y			1.52				-1.07	
	THAOC_25963	TpLhcf									
	THAOC_33280	TpLhcf									
	THAOC_36248	**TpLhcf**	y	-1.38		-1.31		-1.09		-1.12	
	THAOC_37647	**TpLhcf**	y.	**-2.04**	**y**						
	THAOC_08131	**TpLhcf8**	y					-1.32		-1.31	
	THAOC_08131, contig_91916_1_273_+	**TpLhcf8**	y							1.04	
	THAOC_32932	**TpLhcf8**	y	**-2.12**	**y**	**-2.16**	**y**	-1.15		-1.15	
	THAOC_01207	TpLhcf									
	THAOC_01208	**TpLhcf**	y	**-2.79**	**y**	**-2.81**	**y**	-1.13		-1.10	
	THAOC_16761	TpLhcf									
	THAOC_25269	TpLhcf									
	THAOC_25594	TpLhcf									
Lhcf - Group II	**THAOC_09684**	**TpLhcf11**	y	**4.83**	**y**	**3.89**	**y**	-1.23		-1.24	
Lhcf - Group III	**THAOC_05777**	**TpFCP10**	y	**2.40**	**y**	**2.32**	**y**	-1.16		-1.16	
	THAOC_18180	**TpFCP11**	y	2.02				1.09		-1.16	
	THAOC_06968	**TpFCP2**	y	**-2.52**	**y**	**-2.52**	**y**	-1.09		-1.10	
	THAOC_04469	**TpFCP4**	y	**2.06**	**y**	2.16		-1.26		-1.24	
	THAOC_16345	**TpFCP4**	y	**2.68**	**y**	**2.68**	**y**	-1.30		-1.29	
	THAOC_18994	TpFCP4									
	THAOC_08587	**TpFCP7**	y	**2.79**	**y**	2.90		**2.07**	**y**	2.00	
	THAOC_16412	**TpFCP9**	y	1.97		1.97		-1.09		-1.09	

clade[a]	gene name[b]	closest homolog in Tp[c]	expr[d]	differential expression[h)] TO03 I (original)[e]	sig[g]	TO03 II (+EST)[f]	sig[g]	TO05 I (original)[e]	sig[g]	TO05 II (+EST)[f]	sig[g]
Lhcr	THAOC_06811	TpLhcr									
	THAOC_35171	**TpLhcr1**	y	3.48		3.48		-1.39		-1.37	
	THAOC_35518	**TpLhcr10**	y	**-2.55**	**y**	**-2.56**	**y**	-1.04		1.03	
	THAOC_00550	**TpLhcr11**	y	2.75		**2.39**	**y**	-1.14		-1.19	
	THAOC_07034	**TpLhcr13**	y	1.66		1.63		-1.11		-1.12	
	THAOC_07036	**TpLhcr13**	y	**-6.57**	**y**	**-6.32**	**y**	-1.19		-1.12	
	THAOC_05708	**TpLhcr14**	y	-1.06		1.04		1.13		1.12	
	THAOC_34573	**TpLhcr2**	y	4.44		4.42		-1.32		-1.44	
	THAOC_16963	**TpLhcr3**	y	-1.56		-1.45		-1.13		-1.14	
	THAOC_05707	**TpLhcr4**	y	1.24		1.24		-1.21		-1.15	
Lhcx	**THAOC_09937**	**TpLhcx1**	y	**3.29**	**y**			-1.222			
	THAOC_12734	TpLhcx1									
	THAOC_32497	TpLhcx1									
	THAOC_31988	**TpLhcx1**	y			**3.29**	**y**			-1.22	
	THAOC_23429	TpLhcx4									
	THAOC_14109	TpLhcx5									
	THAOC_31495	TpLhcx6									
	THAOC_08095	**TpLhcx7**	y	1.14		**2.76**	**y**	-1.15		-1.13	
	THAOC_08095, contig_119183_41_788_+	**TpLhcx7**	y			-1.41					
Lhcz	THAOC_09862	TpLhcr5									
	THAOC_09825	TpLhcr8									
	THAOC_37813	**TpFCP5**	y					-1.46		-1.44	

[a]clades as per phylogenetic tree in Figure 4

[b]content in bold indicates significantly differentially expressed proteins in TO03, as defined in methods; blue, significantly down-regulated; red, significantly up-regulated

[c]bold names indicate proteins are found expressed in at least one dataset

[d]"y" indicates proteins are found expressed in at least one dataset

[e]original dataset, peptides from LC-MS/MS were mapped against database of predicted proteins of TO05 genome,

[f]EST dataset, peptides from LC-MS/MS were mapped against predicted proteins of combined database consisting of both TO05 genome and our own TO03 Transcriptome (assembled EST contigs)

[g]"y" indicates that the differential expression in the column left of it is significantly regulated as per methods

[h]differential expression given in fold-change, bold content indicates significantly regulated as per methods

Tp, *Thalassiosira pseudonana*; expr, expressed; sig, significant differential expression

A.8 Differential expression of all identified proteins involved in the photosynthetic ETC in *T. oceanica* (CCMP 1003 and CCMP 1005) across all four datasets

Table A.5: Differential expression of all identified proteins involved in photosynthetic ETC across all datasets

Part_of	gene name (NCBI)[a]	Protein Description[a]	differential expression TO03 I (original) [a,b]	differential expression TO05 I (original) [a,b]	where encoded	differential expression TO03 II (EST) [a,c]	differential expression TO05 II (EST) [c]
PS II	THAOC_34020	psb27-like, involved in Mn cluster formation	1.73	1	Nuc	1.73	1.05
	psbA	psbA, photosystem II protein D1	-1.92	-1.03	C	-1.63	1.07
	psbB	psbB, photosystem II CP47 reaction center protein	-1.61	-1.1	C	-1.65	-1.09
	psbC, THAOC_26185	**psbC, photosystem II CP43 reaction center protein**	**-2.1**	1.05	C		1.01
	psbD, THAOC_24371	**psbD, photosystem II D2 protein**	**-2.1**	-1.01	C	**-2.01**	
	psbE, THAOC_24363	**psbE, cytochrome b559 subunit alpha**	**-2.25**	-1.21	C	**-2.27**	-1.20
	psbH	psbH, photosystem II reaction center protein H		-1.49	C		-1.56
	THAOC_03193	psbO, Mn-stabilizing protein	-1.41		Nuc	-1.40	1.04
	THAOC_15373	psbP, oxygen-evolving enhancer protein 2 (OEE2)		-1.03	Nuc		1.04
	THAOC_08500	**psbQ, oxygen-evolving enhancer protein 3 (OEE3)**	**-2.96**		Nuc	-3.94	1.37
	THAOC_09685	psbU-like, small extrinsic protein	1.62	1.32	Nuc	1.63	1.32
	psbV, THAOC_30541	psbV, cytochrome c-550	1.07	1.18	C	1.03	1.18
	psbY	psbY, photosystem II protein Y		-1.11	C		-1.18
PET	petA	petA, cytochrome f	-1.63	-1.11	C	-1.65	
	petB, THAOC_26188	**petB, cytochrome b6**	**-2.33**		C	**-2.33**	-1.14
	THAOC_33417	petC, Fe-S subunit (Rieske protein)	-1.51		Nuc		-1.48
	petD, THAOC_24366	petD, cytochrome b6-f complex subunit 4		1.1	C		-1.15
	THAOC_29732	**petE, plastocyanin**	**-4.41**	1.31	Nuc	**-4.71**	1.52

Part_of	gene name (NCBI)[a]	Protein Description[a]	differential expression TO03 I (original) [a,b]	differential expression TO05 I (original) [a,b]	where encoded	differential expression TO03 II (EST) [a,c]	differential expression TO05 II (EST) [c]
PS I	psaA	psaA, photosystem I P700 chlorophyll a apoprotein A1	-1.21	1.14	C	-1.17	1.09
	psaB	psaB, photosystem I P700 chlorophyll a apoprotein A2	1.11	1.01	C	1.46	1.02
	psaC	psaC, photosystem I iron-sulfur center	-1.18	1.2	C	1.15	
	psaD, THAOC_24369	psaD, photosystem I reaction centre subunit II	1.2	1	C	1.20	-1.02
	psaF	psaF, photosystem I reaction centre subunit III	-1.2	1.04	C	-1.14	1.01
	THAOC_24361	psaL, photosystem I reaction centre subunit XI	-1.56	-1.02	C	-2.08	1.31
PET	**THAOC_25559**	**petF, ferredoxin**	**43.79**	-1.1	Nuc	**43.79**	-2.52
	THAOC_36724	**petH, FNR - ferredoxin--NADP+ reductase**	**2.47**		Nuc	**2.44**	-1.09
	THAOC_36724, contig_64183_1_637_+	**petH, FNR - ferredoxin--NADP+ reductase**				**5.50**	
	THAOC_06509	petH - FNR - ferredoxin--NADP+ reductase		-1.13	Nuc	-1.49	-1.17

[a] content in bold indicates significantly differentially expressed proteins in TO03, as defined in methods

[b] significant differential expression in original dataset as defined in methods, given in fold-change

[c] significant differential expression in EST dataset as defined in methods, given in fold-change

A.9 Overview of the number of identified proteins in the four different proteomic datasets

Table A.6 Overview of the number of identified proteins in the four different proteomic datasets.

	TO03 (original)[e]	TO03 (EST)[f]	TO03II (%)	TO05 (original)[e]	TO05 (EST)[f]	TO05II (%)	Diff TO03 (EST and original)	%	Diff TO05 (EST) and (original)	%
peptides identified by LC-MS/MS[a]	4,055	4,055		8,967	8,967					
proteins identified[b]	730	**844**	100%	1431	**1622**	100%	114	16%	191	13%
proteins mapped to TO05 genome[c]		**705**	84%		**1327**	82%				
proteins mapped to TO03 EST[d]		**139**	16%		**295**	18%				
proteins mapped to TO03 EST[d]		**139**	100%		**295**	100%				
TO03 ESTs mapped to TO05 chloroplast proteins		**2**	1%		**1**	0%				
TO03 ESTs mapped to TO05 nuclear proteins		**100**	72%		**207**	70%				
TO03 ESTs mapped to TO05 genome (excluding predicted proteins)		**28**	20%		**69**	23%				
TO03 ESTs NOT mapped to any published TO5 sequences		**9**	6%		**18**	6%				

[a]peptides of the initial LC-MS/Ms were used in searches against

[b]all proteins identified

[c]all proteins identified that map to the TO05 genome

[d]all proteins identified that map to the TO03 transcriptome

[e]original dataset in which peptides were mapped against database containing predicted proteins of TO05 genome

[f]second dataset in which peptides were mapped against a combined database of TO05 proteins and predicted proteins in TO03 transcriptome

Appendix B − Supplementary material for Chapter 4: Proteomic Analysis Revealed the Intricate Interaction Between the Carbon and Nitrogen Metabolisms in Copper-Limited *T. oceanica*

B.1 The Calvin-Benson-Bassham cycle - Differential expression of proteins involved in Calvin-Benson-Bassham cycle in *T. oceanica* CCMP 1003 (TO03) and 1005 (TO05) grown under Cu-limiting conditions

Table B.1 Differential expression and predicted cellular location of proteins involved in the Calvin-Benson-Bassham cycle in TO03 and TO05 cultured in low Cu conditions *vs.* control.

Calvin-Benson-Bassham Cycle			TO03[c]				TO05[c]			
			original		+EST		original		+EST	
Gene name[a]	Diatom homolog[b]	Name	sol	insol	sol	insol	sol	insol	sol	insol
cbbX, THAOC_24360	Tp24123, Pt 36139	cbbX, rubisco expression protein	**-2.25**		**-2.25**		-1.34	-1.03	-1.28	-1.08
rbcS		rbcS, ribulose-bisphosphate carboxylase small chain	1.12	1.23	1.14	1.2	-1.63	-1.49	-1.62	-1.44
rbcL		rbcL, ribulose-bisphosphate carboxylase large chain	1.03	1.33	1.01	1.39	-1.09	-1.34	-1.08	-1.38
THAOC_07617	Tp270304	PGK, phosphoglycerate kinase	1.54	-1.08			**2.98**	-1.71		
THAOC_07617 contig_117075_1_571_+					**6.85**				1.02	
THAOC_07617 contig_55250_138_1396_+					1.89	-1.16			1.17	1.05
THAOC_13085	Tp270231	GAPDH, glyceraldehyde 3-phosphate dehydrogenase	-1.29	**-4.16**	-1.43	**-4**	1.19	-1.11	1.17	-1.09

Calvin-Benson-Bassham Cycle			TO03[c]				TO03[c]			
			original		+EST		original		+EST	
Gene name[a]	Diatom homolog[b]	Name	sol	insol	sol	insol	sol	insol	sol	insol
THAOC_02438	Tp30380, Pt54738, Fc274452	TPI2, triose-phosphate isomerase	**3.3**		**3.13**		-1.06		-1.12	
THAOC_35826	Tp8590	TPI1, triose-phosphate isomerase	1.94		1.91		1		1	
THAOC_32006	Tp8590	TPI3, triose-phosphate isomerase	1.45		1.43		1.09		1.14	
THAOC_00388	Tp270396, PtBd825	FBA II, fructose-bisphosphate aldolase class-II	1.36				-1.23			
THAOC_12069	Tp21748, Pt22993	FBA II, fructose-bisphosphate aldolase class-II	**2**		1.99		1.15		1.2	
THAOC_02112	no Tp, Pt51289	FBA I, fructose-bisphosphate aldolase class-I	-1.73		-1.73		-1.18	1.08	-1.35	1.18
THAOC_31290		RPI, ribose-5-phosphate-isomerase	-1.12		-1.12		-1.09		-1.09	
THAOC_31290 contig_19155_129_974_+					**4.9**					
THAOC_09031		RPE, ribulose-5-phosphate epimerase	1.22		-1.19		-1.1		-1.1	

[a]Gene name as per Lommer et al., 2012; if identified based on EST data, the respective contig identifier is given as well

[b]using blastp, this is the closest diatom homolog

[c]average fold-change in Cu-limited compared to control cultures, bold indicates highly differentially expressed (> ± 2-fold, $p<0.05$), underlined indicates differential expression ratio of ±1.3- to 2-fold ($p<0.05$). original, original proteomics dataset in which peptides where mapped to the TO05 genome; +EST, second proteomics dataset in which peptides where mapped to both the TO05 genome and our EST library; sol, soluble protein fraction; insol, insoluble protein fraction

B.2 Putative triose-phosphate transporters and their differential expression in *T. oceanica* CCMP 1003 (TO03) and 1005 (TO05) grown under Cu-limiting conditions

Table B.2: Proteins with triose-phosphate transporter PFAM and their expression in TO03 and TO05 in response to Cu limitation *vs.* control

Putative triose-P-transporters			TO03[c]				TO05[c]			
			original		+EST		original		+EST	
Gene name[a]	Diatom homolog[b]	TargetP/ASAFind	sol	insol	sol	insol	sol	insol	sol	insol
Cytosol										
THAOC_31045	triose-phosphate transporter	_(3) / Not plastid						-1.08		-1.07
THAOC_33538	triose-phosphate transporter	_(2) / Not plastid								
Chloroplast										
THAOC_05244	triose-phosphate transporter	S(2) / Plastid				-1.82		-1.06		-1.06
THAOC_11183	triose-phosphate transporter	S(1) / Plastid								
Mitochondria										
THAOC_35890	triose-phosphate transporter	M(3) / Not plastid						1.36		1.36
Signal Sequence										
THAOC_04741	triose-phosphate transporter	S(5) / Not plastid		-1.31		-1.31		1.34		1.35
THAOC_13820	triose-phosphate transporter	S(3) / Not plastid								

[a]Gene name as per Lommer et al., 2012; if identified based on EST data, the respective contig identifier is given as well

[b]using blastp, this is the closest diatom homolog

[c]average fold-change in Cu-limited compared to control cultures, bold indicates highly differentially expressed (> ± 2-fold, $p<0.05$), underlined indicates differential expression ratio of ±1.3- to 2-fold ($p<0.05$). original, original proteomics dataset in which peptides where mapped to the TO05 genome; +EST, second proteomics dataset in which peptides where mapped to both the TO05 genome and our EST library; sol, soluble protein fraction; insol, insoluble protein fraction

B.3 Glycolysis - Differential expression of proteins involved in glycolysis in *T. oceanica* CCMP 1003 (TO03) and 1005 (TO05) grown under Cu-limiting conditions

Table B.3: Differential expression and predicted cellular location of proteins involved in glycolysis in TO03 and TO05 cultured in low Cu conditions *vs.* control

Glycolysis			TO03[c]				TO05[c]			
			original		+EST		original		+EST	
Gene name[a]	Diatom homolog[b]	Name	sol	insol	sol	insol	sol	insol	sol	insol
Cytosol										
THAOC_06412	Pt50444	PGM, phosphoglucomutase	-1.79		**-3.17**		-1.01	1.13	-1.01	1.13
THAOC_06412 contig_11427_139_3309_+					-1.71					
THAOC_25871	Tp38266, Pt23924	GPI, glucose-6-phosphate isomerase	-1.27		-1.26		1.45		1.34	
THAOC_16559	Tp22213	PFK, phosphofructokinase	-1.8		-1.75		-1.03		1.02	
THAOC_05494	Tp256250	F2BP, fructose-1-6-bisphosphatase	1.23		1.21		-1.18		-1.21	
THAOC_24977	Tp270288, Pt29014	FBA II, fructose-bisphosphate aldolase class-II	-1.18		-1.22		-1.32		-1.18	
THAOC_24978	Tp11761	FBA I, fructose-bisphosphate aldolase class-I	-1.6		-1.53		-1.06	**-2.37**	-1.09	-2.26
THAOC_24978 contig_128882_77_667_-					**-2.79**					
THAOC_21096	Tp30380, Pt54738	TPI2, triose-phosphate isomerase	-1.01		1.04		1.13		1.25	
THAOC_21095	Pt54738	TPI2, triose-phosphate isomerase	-1.25		-1.49		1.01		-1.07	
THAOC_34937	Tp40393	PK, pyruvate kinase	1.58		1.58		1.28	-1.61	1.25	-1.61

Glycolysis			TO03[c]				TO05[c]			
			original		+EST		original		+EST	
Gene name[a]	Diatom homolog[b]	Name	sol	insol	sol	insol	sol	insol	sol	insol
Chloroplast										
THAOC_12069	Tp21748, Pt22993	FBA II, Fructose-bisphosphate aldolase class-II	**2**		1.99		1.15		1.2	
THAOC_00388	Tp270396, PtBd825	FBA II, Fructose-bisphosphate aldolase class-II	1.36				-1.23			
THAOC_02112	no Tp, Pt51289	FBA I, Fructose-bisphosphate aldolase class-I	-1.73		-1.73		-1.18	1.08	-1.35	1.18
THAOC_02438	Tp30380, Pt54738, Fc274452	TPI2, triose-phosphate isomerase	**3.3**		**3.13**		-1.06		-1.12	
THAOC_35826	Tp8590	TPI1, triose-phosphate isomerase	1.94		1.91		1		1	
THAOC_32006	Tp8590	TPI3, triose-phosphate isomerase	1.45		1.43		1.09		1.14	
THAOC_13085	Tp270231	GAPD1, glyceraldehyde 3-phosphate dehydrogenase	-1.29	**-4.16**	-1.43	**-4**	1.19	-1.11	1.17	-1.09
THAOC_07617	Tp270304	PGK, phosphoglycerate kinase	1.54	-1.08			**2.98**	-1.71		
THAOC_07617 contig_117075_1_571_+					**6.85**				1.02	
THAOC_07617 contig_55250_138_1396_+					1.89	-1.16			1.17	1.05
THAOC_21902	Tp28350	PGAM2, phosphoglycerate mutase	**-2.25**		**-2.25**		-1.46		-1.19	
Mitochondria										
THAOC_33331	Tp28334	GAPDH, glyceraldehyde 3-phosphate dehydrogenase	**2**	-2.15	1.75		1.42	1.19	1.29	1.32
THAOC_33331 contig_105735_1_207_+					**3.79**				1.55	1.3
THAOC_33331 contig_105693_1_204_+									1.34	
THAOC_07275	Tp28241	GAPDH, glyceraldehyde 3-phosphate dehydrogenase	1.06		1.04		1.14	1.06	1.07	1.09
THAOC_08963	Tp27850	PGAM, phosphoglycerate mutase	-1.03		-1.06		1.12		1.06	
THAOC_34936	Tp40391	ENO, Enolase	1.44		1.54		1.2	1.04	1.26	1.04
THAOC_07097	Pt561725	PK, pyruvate kinase	-1.31		-1.31		-1.24	-1.34	-1.25	-1.34

Glycolysis			TO03[c]				TO05[c]			
			original		+EST		original		+EST	
Gene name[a]	Diatom homolog[b]	Name	sol	insol	sol	insol	sol	insol	sol	insol
THAOC_10009	Pt34120, Fc267632, Tp38807	EDA, 2-keto-3-deoxy phosphogluconate aldolase	1.06		1.06		1.26		1.26	1.32

[a]Gene name as per Lommer et al., 2012; if identified based on EST data, the respective contig identifier is given as well

[b]using blastp, this is the closest diatom homolog

[c]average fold-change in Cu-limited compared to control cultures, bold indicates highly differentially expressed (> ± 2-fold, $p<0.05$), underlined indicates differential expression ratio of ±1.3- to 2-fold ($p<0.05$). original, original proteomics dataset in which peptides where mapped to the TO05 genome; +EST, second proteomics dataset in which peptides where mapped to both the TO05 genome and our EST library; sol, soluble protein fraction; insol, insoluble protein fraction

B.4 Citrate Cycle (TCA) - Differential expression of proteins involved in glycolysis in *T. oceanica* CCMP 1003 (TO03) and 1005 (TO05) grown under Cu-limiting conditions

Table B.4: Differential expression and predicted cellular location of proteins involved in the tricarboxylic acid (TCA) / citrate cycle in TO03 and TO05 cultured in low Cu conditions *vs.* control. (for diagram, see Figure 4.4)

Citrate / TCA Cycle			TO03[c]				TO05[c]			
			original		+EST		original		+EST	
NCBI protein identifier[a]	Diatom homolog[b]	Name	sol	insol	sol	insol	sol	insol	sol	insol
Mitochondria										
THAOC_19912	Tp11411, Pt30145	CS, citrate synthase	1.06		-1.05		1.15		1.07	1.14
THAOC_20545	Tp268965	ACO, aconitase hydratase	**-4.73**		**-4.17**		1.26		1.3	
THAOC_37807	Tp21640, Pt14762, Fc168262	IDH, isocitrate/ isopropylmalate dehydrogenase	-1.64		-1.66		1.14		1.14	
THAOC_34595	Tp1456, Pt45017	IDH1, isocitrate dehydrogenase (monomeric)	**-3.02**		**-2.79**		1.41		1.45	
THAOC_34595 contig_117709_1_1294_+					**-5.5**		1.41		-1.23	
THAOC_28027	Tp269718, Pt29016	OGD1, 2-oxoglutarate dehydrogenase E1 component	1.08		1.08		1.2		1.03	
THAOC_28027 contig_117377_84_1088_-									1.34	
THAOC_13425	Fc226444	SUCLA, succinate CoA synthetase, beta chain	1.29		1.29		1.43		1.57	
THAOC_24310	Tp24123, Pt 36139	FH, fumarate hydratase, class II	-1.09		-1.09		-1.23		-1.18	
THAOC_03405	Tp20726, Pt51297	MDH1, malate dehydrogenase	1.6		1.54		1.15	1.05	1.15	1.05

[a]Gene name as per Lommer et al., 2012; if identified based on EST data, the respective contig identifier is given as well

[b]using blastp, this is the closest diatom homolog

[c]average fold-change in Cu-limited compared to control cultures, bold indicates highly differentially expressed (> ± 2-fold, $p<0.05$), underlined indicates differential expression ratio of ±1.3- to 2-fold ($p<0.05$). original, original proteomics dataset in which peptides where mapped to the TO05 genome; +EST, second proteomics dataset in which peptides where mapped to both the TO05 genome and our EST library; sol, soluble protein fraction; insol, insoluble protein fraction

B.5 Urea and nitrogen metabolism - Differential expression of proteins involved in urea and nitrogen metabolism in *T. oceanica* CCMP 1003 (TO03) and 1005 (TO05) grown under Cu-limiting conditions

Table B.5: Differential expression and predicted cellular location of proteins involved in nitrogen metabolism including the urea cycle in TO03 and TO05 cultured in low Cu conditions *vs.* control.

Nitrogen Metabolism			TO03[c]				TO05[c]			
			original		+EST		original		+EST	
Gene name[a]	Diatom homolog[b]	Name	sol	insol	sol	insol	sol	insol	sol	insol
Transporters										
THAOC_04919	Tp, Pt, Fc	NRT, nitrate/nitrite transporter		**11**		**11**				
THAOC_01055	Tp, Pt, Fc	NRT, nitrate/nitrite transporter						1.69		
THAOC_01056	Tp, Pt, Fc	NRT, nitrate/nitrite transporter						1.36		1.56
THAOC_31656	Tp24250, Pt20424, Fc214292	URT, Na/urea-polyamine transporter		**6.93**		**6.93**		1.66		1.32
THAOC_07247	Tp13996, Pt27877, Fc275907	AMT, ammonium transporter		-1.39		-1.39		-1.07		-1.11
THAOC_00240	Tp3393, Pt46427, Fc262069	NiRT, formate/nitrite transporter		-1.14		-1.14		1.29		1.14
Cytosol										
THAOC_34460	Tp25299, Pt54983, Fc206583	NR, nitrate reductase	1.49		1.45		-1.05	-1.32	-1.05	-1.32

Nitrogen Metabolism			TO03[c]				TO05[c]			
			original		+EST		original		+EST	
Gene name[a]	Diatom homolog[b]	Name	sol	insol	sol	insol	sol	insol	sol	insol
THAOC_37170	Tp42719, Pt, Fc207847	AsuS, argininosuccinate synthase	2.59		-1.28		1.39		1.37	
THAOC_12984	Tp29075, Pt34526, Fc262171	AsL, argininosuccinate lyase	-1.51		-1.51		1.08		1.12	
THAOC_04380	Tp260953, Pt260953, Fc187231	OCD, ornithine cyclodeaminase	1.24		1.24		1.04		1.22	
THAOC_22587	Tp34595, Pt25183, Fc190753	ATCase, aspartate carbamoyltransferase	-1.05		-1.05		1.2		1.2	
THAOC_06254	Tp38359, Pt13951, Fc192073	GDH, glutamate dehydrogenase, NADP dependent	2.09		2.77		1.38		1.5	
THAOC_06254 contig_96116_1_202_-					1.07				1.34	
Chloroplast										
THAOC_00016	Tp262125, Pt27757, Fc185143	NR, nitrite reductase	1.34		1.34		1.07		1.08	
THAOC_02363	Tp270365, Pt, Fc172194	Fe-NiR, nitrite/sulfite reductase ferredoxin-like half-domain	**2.27**		**2.32**		-1.13		-1.1	
THAOC_35252	Tp26941, Pt, Fc200565	NAD(P)H-NiR, nitrite reductase	-1.63		-1.65		1.06		1.07	
THAOC_31900	Tp26051, Pt51092, Fc228642	GSII, glutamine synthetase	1.71	1.76	1.59	1.81	1.27	1.46	1.28	1.5
THAOC_31900 contig_127491_284_455_+					**3.83**					

Nitrogen Metabolism			TO03[c]				TO05[c]			
			original		+EST		original		+EST	
Gene name[a]	Diatom homolog[b]	Name	sol	insol	sol	insol	sol	insol	sol	insol
THAOC_13288	Tp269900, Pt, Fc225787	GOGAT, glutamate synthase	1.55		1.57		1.05		1.1	
THAOC_16827	Tp31394, Pt22909, Fc273803	AAT, aspartate aminotransferase	**-2.33**		**-2.33**		1.04		1.03	
THAOC_32466	Tp270136, Pt50577, Fc277974	argD, n-acetylornithine aminotransferase	-3.01		-2.97		1.09		1.09	
Mitochondria										
THAOC_17688	Tp36208, Pt, Fc224733	GDCT, glycine decarboxylase t-protein	-1.23		-1.23					
THAOC_36273	Tp39799, Pt22187, Fc276117	GDCP, glycine decarboxylase p-protein	-1.86		-1.43		-1.17		-1.17	
THAOC_01996	Tp40323, Pt24195, Fc169332	unCPS (CPSase III), carbamoyl-phosphate synthase	-1.14		-1.11		-1.06		-1.05	
THAOC_05385	Tp997, Pt30514, Fc268473	OTC, ornithine carbamoyltransferase	1.67		1.67		-1.05		-1.05	
THAOC_06032	Tp270138, Pt22357, Fc277211	GSIII, glutamine synthetase	**-5.29**	-2.62	-7.01	-2.62	1.34	1.16	1.18	
THAOC_06032 contig_17263_419_2602_-									1.37	1.22
THAOC_15049	Tp31424, Pt23059, Fc170472	AAT, aspartate aminotransferase	**3.57**		**3.57**					

[a]Gene name as per Lommer et al., 2012; if identified based on EST data, the respective contig identifier is given as well
[b]using blastp, this is the closest diatom homolog

[c]average fold-change in Cu-limited compared to control cultures, bold indicates highly differentially expressed (> ± 2-fold, $p<0.05$), underlined indicates differential expression ratio of ±1.3- to 2-fold ($p<0.05$). original, original proteomics dataset in which peptides where mapped to the TO05 genome; +EST, second proteomics dataset in which peptides where mapped to both the TO05 genome and our EST library; sol, soluble protein fraction; insol, insoluble protein fraction

B.6 Glutathione metabolism - Differential expression of proteins involved in glutathione metabolism in *T. oceanica* CCMP 1003 (TO03) and 1005 (TO05) grown under Cu-limiting conditions

Table B.6: Differential expression and predicted cellular location of proteins involved in glutathione metabolism in TO03 and TO05 cultured in low Cu conditions *vs.* control.

Glutathione			TO03[c]				TO05[c]			
			original		+EST		original		+EST	
Gene name[a]	Diatom homolog[b]	Name	sol	insol	sol	insol	sol	insol	sol	insol
Cytosol										
THAOC_29696	Tp262753 , Pt47395 , Fc173923	APX, ascorbate peroxidase	-1.17		-1.17		-1.27		-1.31	
THAOC_37364	Tp38724 , Pt___ , Fc___, Ehux444342	APX, ascorbate peroxidase	1.42		1.37		1.11	1.75	1.08	1.75
THAOC_05931	Tp267987 , Pt___ , Fc172515	CYS2, cysteine synthase	-1.01		-1.01		1.1		1.06	
THAOC_05931, contig_111591_1_205_-									1.16	
THAOC_05931, contig_68507_1_219_+					-1.26				-1.02	
THAOC_23355	Tp13064 , Pt27240 , Fc291479	GCS, γ-glutamyl-cysteine synthase	4.53		4.53					
THAOC_09062	Tp___ , Pt__ , Fc___, (*Hydra*, polyp)	GST, glutathione-S-transferase	**7.28**		**12.4**					

Glutathione			TO03[c]				TO05[c]			
			original		+EST		original		+EST	
Gene name[a]	Diatom homolog[b]	Name	sol	insol	sol	insol	sol	insol	sol	insol
THAOC_24526	Tp269866 Pt37658 , Fc196320	GST, glutathione-S-transferase					**2.11**		**2.33**	0.03
THAOC_10112	Tp40669 , Pt49037 , Fc267154	NiSOD, nickel-dependent superoxide dismutase	1.04	1.38	1.15	1.38	1.08	1.25	1.15	1.24
THAOC_14269	Tp___ , Pt49037 , Fc267154	NiSOD, nickel-dependent superoxide dismutase	-2.68		-2.79		1.54	1.15	1.54	1.15
THAOC_05213	Tp41697 , Pt56471 , Fc231810	TXN, thioredoxin	2.62		**4.16**		1.33		1.35	
THAOC_06254	Tp38359, Pt13951, Fc192073	GDH, glutamate dehydrogenase, NADP dependent	2.09		2.77		1.38		1.5	
THAOC_06254, contig_96116_1_202_-					1.07				1.34	
Chloroplast										
THAOC_27524	Tp270338 , Pt_bd542 , Fc168185	CYS, cysteine synthase	**2.43**		**2.5**		1.38	-1.44	1.28	
THAOC_10442	Tp267987 , Pt__ , Fc172515	CYS2, cysteine synthase	1.51				-1.3		-1.32	
THAOC_10442, contig_37614_97_1300_+					1.61				1.6	
THAOC_19132	Tp23356 , Pt36641 , Fc229440	DHAR, dehydroascorbate reductase								
THAOC_13288	Tp269900 , Pt , Fc	GOGAT, glutamate synthase	1.55		1.57		1.05		1.1	
THAOC_07268	Tp26457 , Pt__ , Fc228584	GR, glutathione reductase	**2.47**		**2.4**		1.16		1.34	

Glutathione			TO03[c]				TO05[c]			
			original		+EST		original		+EST	
Gene name[a]	Diatom homolog[b]	Name	sol	insol	sol	insol	sol	insol	sol	insol
THAOC_07269	Tp11178 , Pt , Fc259160, Ehux58907	GRX, glutaredoxin	-1.3		-1.3		1.1		1.1	
THAOC_07269, contig_70896_7_411_-					-1.4				1.01	
THAOC_18234	Tp270300 , Pt9035 , Fc225878	GRX, glutaredoxin	-1.29		-1.4		1.01		-1.24	
THAOC_04546	Tp29212 , Pt25876 , Fc291481	GSS, glutathione synthetase	1.48		1.48		-1.18		-1.27	
THAOC_08875		GST, glutathione-S-transferase					1.29		1.29	
THAOC_02860	Tp32874 , Pt12583 , Fc 269011	MnSOD, Mn/Fe binding superoxide dismutase	1.77		1.77		1.07		1.27	
THAOC_31425	Tp270230 , Pt46280 , Fc221387	TXN, thioredoxin	1.47		1.47		1.54		1.64	
Mitochondria										
THAOC_02323	Tpbd718 , Pt38124 , Fc182589	GRX, glutaredoxin	1.01		1.01		1.05		-1.11	
THAOC_13865	Tp19991 , Pt , Fc235520	TXN, thioredoxin	1.79		1.77		1.27		1.26	

[a]Gene name as per Lommer et al., 2012; if identified based on EST data, the respective contig identifier is given as well
[b]using blastp, this is the closest diatom homolog
[c]average fold-change in Cu-limited compared to control cultures, bold indicates highly differentially expressed (> ± 2-fold, $p<0.05$), underlined indicates differential expression ratio of ±1.3- to 2-fold ($p<0.05$). original, original proteomics dataset in which peptides where mapped to the TO05 genome; +EST, second proteomics dataset in which peptides where mapped to both the TO05 genome and our EST library; sol, soluble protein fraction; insol, insoluble protein fraction

B.7 Malate Shunt - Differential expression of proteins involved in the putative malate shunt in *T. oceanica* CCMP 1003 (TO03) and 1005 (TO05) grown under Cu-limiting conditions

Table B.7: Differential expression and predicted cellular location of proteins involved in the putative malate shunt in TO03 and TO05 cultured in low Cu conditions *vs.* control.

Malate-Shunt			TO03[c]				TO05[c]			
			original		+EST		original		+EST	
Gene name[a]	Diatom homolog[b]	Name	sol	insol	sol	insol	sol	insol	sol	insol
Transporter										
THAOC_27515	Tp26366, Pt23908, Fc180618	malate-2-oxoglutarate antiporter						1.24		1.24
THAOC_25255	Tp16746, Pt__, Fc226900	malate-2-oxoglutarate antiporter						1.09		1.09
Mitochondria										
THAOC_03405	Tp20726, Pt51297	MDH1, malate dehydrogenase	1.6		1.54		1.15	1.05	1.15	1.05
THAOC_19570	no Tp homolog, Pt30519, Fc183259	PC(1), pyruvate carboxylase	-1.63		-1.63		-1.14		-1.1	
THAOC_15049	Tp31424, Pt23059, Fc170472	AAT, aspartate aminotransferase	**3.57**		**3.57**					
THAOC_37124, contig_65096_132_669_+	Tp34030, Pt56501, Fc277202	ME, malic enzyme						-1.15		
Chloroplast										
THAOC_30817	Tp25953, Fc291625	MDH2, malate dehydrogenase	**2.64**		**2.64**					
THAOC_31413	Tp269908, Pt49339, Fc186955	PC(2), pyruvate carboxylase	**2.64**		**2.7**		1.02		1.01	

Malate-Shunt			TO03[c]				TO05[c]			
			original		+EST		original		+EST	
Gene name[a]	Diatom homolog[b]	Name	sol	insol	sol	insol	sol	insol	sol	insol
THAOC_31413 contig_117322_1_422_-					2.43		1.02		1.01	
THAOC_16827	Tp31394, Pt22909, Fc273803	AAT, aspartate aminotransferase	**-2.33**		**-2.33**		1.04		1.03	

[a]Gene name as per Lommer et al., 2012; if identified based on EST data, the respective contig identifier is given as well
[b]using blastp, this is the closest diatom homolog
[c]average fold-change in Cu-limited compared to control cultures, bold indicates highly differentially expressed (> ± 2-fold, $p<0.05$), underlined indicates differential expression ratio of ±1.3- to 2-fold ($p<0.05$). original, original proteomics dataset in which peptides where mapped to the TO05 genome; +EST, second proteomics dataset in which peptides where mapped to both the TO05 genome and our EST library; sol, soluble protein fraction; insol, insoluble protein fraction

B.8 Pyruvate Hub - Differential expression of proteins involved in the pyruvate hub in *T. oceanica* CCMP 1003 (TO03) and 1005 (TO05) grown under Cu-limiting conditions

Table B.8: Differential expression and predicted cellular location of proteins involved in pyruvate metabolism in TO03 and TO05 cultured in low Cu conditions *vs.* control.

Pyruvate-HUB			TO03[c]				TO05[c]			
			original		+EST		original		+EST	
Gene name[a]	Diatom homolog[b]	Name	sol	insol	sol	insol	sol	insol	sol	insol
Chloroplast										
THAOC_31413	Tp269908, Pt49339, Fc186955	PC, pyruvate carboxylase	**2.64**		**2.7**		1.02		1.01	
THAOC_31413 contig_117322_1_422_-					2.43					
THAOC_30817	Tp25953, Fc291625	MDH, malate dehydrogenase	**2.64**		**2.64**					
THAOC_34740	Tp16169, Pt20360, Fc263399	PDH-E1, pyruvate dehydrogenase-E1 component	-1.12		-1.14		-1.06		-1.07	
THAOC_19934	Tp24399, Pt30113, Fc186500	DLDH, dihydrolipoamide dehydrogenase	-1.23		-1.4		-1.18	1.1	-1.08	1.56
Cytosol										
THAOC_34937	Tp 40393, Pt49098	PK, pyruvate kinase	1.58		1.58		1.28	-1.61	1.25	-1.61
THAOC_00276	Tp34543, Pt 51136, Fc259279	PEPC, phosphoenolpyruvate carboxylase	**-4.26**				1.04	-1.17		

Pyruvate-HUB			TO03[c]				TO05[c]			
			original		+EST		original		+EST	
Gene name[a]	Diatom homolog[b]	Name	sol	insol	sol	insol	sol	insol	sol	insol
THAOC_08200	Tp8778, Pt20183	PDH-E1, pyruvate dehydrogenase-E1 component	-1.29	1.48	-1.29	1.48	1.37	1.22	-1.07	1.21
THAOC_03499	Tp547, Pt, Fc166615	PDH-E2, pyruvatedehydrogenase E2 component (dihydrolipoamideacetyltransferase)	0.29		0.06		0.26	0.3	0.33	0.36
THAOC_33506	Tp3353, Pt50804, Fc274468	LDH, L-lactate dehydrogenase		-3.62		-3.62		1.06		1.03
THAOC_05626	Tp34187, PT22974, FC239808	ACAS, acetyl-CoA synthase	-1.3		-1.3		1.04	1.25	1.07	1.35
Mitochondria										
THAOC_07097	Tp31810, Pt56172	PK, pyruvate kinase	-1.31		-1.31		-1.24	-1.34	-1.25	-1.34
THAOC_33731	Tp268546, Pt27976, Fc241035	PEPC, phosphoenolpyruvate carboxylase	-1.13		-1.13		1.39		1.37	
THAOC_19570	Pt30519, Fc183259	PC, pyruvate carboxylase	-1.63		-1.63		-1.14		-1.1	
THAOC_03405	Tp20726, Pt51297	MDH, malate dehydrogenase	1.6		1.54		1.15	1.05	1.15	1.05
THAOC_30825	Tp36716, Pt26432, Fc271375	DLDH, dihydrolipoamide dehydrogenase	-1.4		-1.4		-1.2	1.27	-1.2	1.42

[a]Gene name as per Lommer et al., 2012; if identified based on EST data, the respective contig identifier is given as well

[b]using blastp, this is the closest diatom homolog

[c]average fold-change in Cu-limited compared to control cultures, bold indicates highly differentially expressed (> ± 2-fold, $p<0.05$), underlined indicates differential expression ratio of ±1.3- to 2-fold ($p<0.05$). original, original proteomics dataset in which peptides where mapped to the TO05 genome; +EST, second proteomics dataset in which peptides where mapped to both the TO05 genome and our EST library; sol, soluble protein fraction; insol, insoluble protein fraction

B.9 Respiration - Differential expression of proteins involved in respiration in *T. oceanica* CCMP 1003 (TO03) and 1005 (TO05) grown under Cu-limiting conditions

Table B.9: Differential expression and predicted cellular location of proteins involved in respiration in TO03 and TO05 cultured in low Cu conditions *vs.* control.

Respiration			TO03[c]				TO05[c]			
			original		+EST		original		+EST	
Gene name[a]	Diatom homolog[b]	Name	sol	insol	sol	insol	sol	insol	sol	insol
THAOC_05862		NAD(P)H dehydrogenase (ubiquinone), alpha/beta subcomplex I	1.91		1.91		1.21	1.42	1.47	1.48
THAOC_04072		ubiquinol-cytochrome *c* reductase subunit VII		-1.42		-1.34	0	1.24		1.27
THAOC_04852		cytochrome *c* oxidase subunit IV		1.52		1.52	0	**2.06**		**2.06**
THAOC_22544		cytochrome *c* oxidase subunit Vb	-2.21	2.59	-2.21	2.59	-1.19	**2.1**	-1.19	1.84
THAOC_12811		cytochrome *c* oxidase subunit VIb	-1.15	4.03	-1.15	4.03	-1.12		-1.12	

[a]Gene name as per Lommer et al., 2012; if identified based on EST data, the respective contig identifier is given as well

[b]using blastp, this is the closest diatom homolog

[c]average fold-change in Cu-limited compared to control cultures, bold indicates highly differentially expressed (> ± 2-fold, $p<0.05$), underlined indicates differential expression ratio of ±1.3- to 2-fold ($p<0.05$). original, original proteomics dataset in which peptides where mapped to the TO05 genome; +EST, second proteomics dataset in which peptides where mapped to both the TO05 genome and our EST library; sol, soluble protein fraction; insol, insoluble protein fraction

Appendix C − Supplementary material for Chapter 4: Comparative Proteomic Analysis of the Photosynthetic Apparatus of Copper and/or Iron Limited *T. oceanica*

C.1 Intraspecific differences in the effects of chronic metal limitation on physiology in two strains of the open ocean diatom *Thalassiosira oceanica*.

Table C.1 Intraspecific differences in the effects of chronic metal limitation on physiology in 2 strains of the open ocean diatom *Thalassiosira oceanica*. Arrows ("↓" and "↑") indicate a significantly lower or higher response in TO03 compared to TO05 (p<0.05). Note that only three parameters −absolute growth rate, F_v/F_m, and total cellular protein− are significantly different in the control, whereas responses differ greatly under the three metal limiting conditions. "·" indicates p<0.1

Treatment	**TO03 TO05** control	**TO03 TO05** lowCu	**TO03 TO05** lowFe	**TO03 TO05** lowFeCu
[Fe] (nmol)				
[Cu] (nmol)				
µ (dd-1)	↓	↓		
µ (d-1)	↓	↓		
µ (% µmax)			↑	.
cell diameter (µm)			↑	
Chl a conc (pg/cell)		.	↑	
Chl a conc (fg/fl) cell vol		↑	↑	
Fv/Fm (A.U.)	↓	↓		↓
Sigma (Å / RCII)		↑	↓	↑
PQ-Pool size (mol PQ / mol Qb)				
sigma ' @ growth irradiance (Å / RCII)		↑		↓
Fq'/Fv' @ growth irradiance (A.U.)				↑
Fv'/Fm' @ growth irradiance (A.U.)		↓		↓
Fq'/Fm' @ growth irradiance (A.U.)		↓		↓
ETR @ growth irradiance (mol e-/RCII * s)				
NPQ (nsv) @ growth irradiance		↑		↑
ETR - PE curve - alpha (mol e-/RCII)/(µmol quanta / m^2 * s)		↑		
ETR - PE curve - pmax pmax (mol e-/RCII * s)				
ETR - PE curve - ek (µmol quanta / m^2 * s)				.
Conversion factor (ETR / 14C uptake)		↑		
14C - PvsE - curve - α (g C / g Chla * h)/(µmol quanta / m^2 * s)		↓		
14C - PvsE - curve - eK (µmol quanta / m^2 * s)		↓	↓	.
14C - PvsE - curve - Pmax (g C / g Chla * h)		↓		
14C uptake @ 155 uEinstein (g C / g Chla * h)		↓		
Gross O2 Prod (mol O2 / mol Chla * h)		.		
Respiration (mol O2 / mol Chla * h)		.		
Respiration (µmol O2 / cell * h)			.	
AOX activity (%)				
protein concentration (pg/cell)	↓		↑	↑

C.2 Effect of all three low metal treatments (lowCu, lowFe, lowFeCu) on physiology in the open ocean diatom *Thalassiosira oceanica* (CCMP 1003, TO03).

Table C.2: Effect of all three low metal treatments (lowCu, lowFe, lowFeCu) on physiology in the open ocean diatom *Thalassiosira oceanica* (CCMP 1003, TO03). Arrows indicate if the response to low Cu statistically increases ↑ or decreases ↓ compared to the control. Shown are means with standard errors for parameters derived from three biological replicates (^ indicates measurements have only been done on two of the three biological triplicates, see raw data). Results in bold indicate statistically significant differences compared to the respective control treatment. Stars (., *, **, ***, ****) indicate the level of significance of a 2-way ANOVA with post-hoc interaction analysis (see methods for details).

	TO03			
Treatment	**control**	**low Cu**	**lowFe**	**low FeCu**
[Fe] (nmol)	1370.00	1370.00	12.5	12.5
[Cu] (nmol)	10.20	0.20	10.20	1.96
µ (dd-1)	1.52 ± 0.06 ↓	**0.73 ± 0.10 *** ↓**	**1.28 ±0.03* ↓**	**0.86 ±0.08**** ↓**
µ (d-1)	1.05 ± 0.07 ↓	**0.51 ± 0.10*** ↓**	**0.89 ±0.02* ↓**	**0.59 ±0.05**** ↓**
µ (% µmax)	100.50 ± 4.21 ↓	**47.86 ± 6.45 **** ↓**	**84.04 ±1.98* ↓**	**56.17 ±4.91**** ↓**
cell diameter (µm)	5.22 ± 0.05 ↓	**4.72 ± 0.04 **** **	5.36 ±0.02 ↓	**4.7 ±0.03** ↓**
Chl a conc (pg/cell)	0.30 ± 0.01	0.34 ± 0.05	0.37 ±0.01 ↓	**0.16 ±0.01** ↓**
Chl a conc (fg/fl) cell vol	4.34 ± 0.11 ↑	**7.40 ± 0.46 *** ↑**	4.61 ±0.04 ↓	**3.02 ±0.17* ↓**
Fv/Fm (A.U.)	0.60 ± 0.01^ ↓	**0.29 ± 0.01 **** ↓**	**0.35 ±0.03**** ↓**	**0.28 ±0.02**** ↓**
Sigma (Å / RCII)	584.40 ± 4.95^ ↑	**764.01 ± 12.50 *** ↑**	606 ±21.94 ↑	**796.67 ±28.04**** ↑**
PQ-Pool size (mol PQ / mol Qb)	4.34 ± 0.47^	5.98 ± 0.35 .	2.9 ±1.48	5.67 ±0.77
sigma ' @ growth irradiance (Å / RCII)	583.09 ± 18.30 ↑	**664.04 ± 10.95 ** ↑**		549.79 ±9.1
Fq'/Fv' @ growth irradiance (A.U.)	0.7 ± 0.04 ↓	**0.58 ± 0.02 * ↓**	↑	**0.81 ±0.01* ↑**
Fv'/Fm' @ growth irradiance (A.U.)	0.61 ± 0.01 ↓	**0.29 ± 0.01 **** ↓**	↓	**0.2 ±0.01**** ↓**
Fq'/Fm' @ growth irradiance (A.U.)	0.43 ± 0.03 ↓	**0.16 ± 0.01 *** ↓**	↓	**0.17 ±0.01**** ↓**
ETR @ growth irradiance (mol e-/RCII * s)	398.33 ± 31.51	373.65 ± 16.77		431.34 ±8.44

	TO03							
Treatment	**control**		**low Cu**		**lowFe**		**low FeCu**	
NPQ (nsv) @ growth irradiance	0.63 ± 0.03	↑	2.43 ± 0.15 ****			↑	**3.93 ±0.27****	
ETR - PE curve - alpha (mol e-/RCII)/(µmol quanta / m^2 * s)	3.49 ± 0.11	↑	**4.04 ± 0.11 ***				3.72 ±0.03.	
ETR - PE curve - pmax pmax (mol e-/RCII * s)	493.72 ± 54.98		425.67 ± 23.75				585.25 ±38.13.	
ETR - PE curve - ek (µmol quanta / m^2 * s)	140.79 ± 12.48	↓	**105.34 ± 5.07 ***				157.18 ±10.3	
Conversion factor (ETR / 14C uptake)	192.24 ± 22.23	↑	406.85 ± 20.43 *			↑	**378.09 ±32.2***	
14C - PvsE - curve - α (g C / g Chla * h)/(µmol quanta / m^2 * s)	0.0151 ± 1.69E-03	↓	**5.66E-03 ± 1.75E-03 ***		0.02 ±0		0.01 ±0.	
14C - PvsE - curve - eK (µmol quanta / m^2 * s)	251.97 ± 23.73	↓	**172.00 ± 2.51 ****	↓	**162.51 ±3.9*****	↓	**201.03 ±6.51***	
14C - PvsE - curve - Pmax (g C / g Chla * h)	3.89 ± 0.81	↓	**0.97 ± 0.29 ****		2.59 ±0.19	↓	**1.82 ±0.13****	
14C uptake @ 155 uEinstein (g C / g Chla * h)	2.09 ± 0.27	↓	**0.70 ± 0.21 ***		1.91 ±0.12	↓	**1.18 ±0.07***	
Gross O2 Prod (mol O2 / mol Chla * h)	366.59 ± 28.16	↓	**101.02 ± 26.53*****	↓	**210.53 ±36.49***	↓	**258.21 ±37.02****	
Respiration (mol O2 / mol Chla * h)	0.07 ± 0.03		0.04 ± 0.01		0.08 ±0.02	↓	**0.06 ±0.02***	
Respiration (µmol O2 / cell * h)	1.16E-08 ± 2.32E-9		9.10E-09 ± 1.16E-9		0 ±0.		0 ±0	
AOX activity	48.84 ± 0.9		53.60 ± 7.05		68.55 ±0.79		63.45 ±6.01	
protein concentration (pg/cell)	12.61 ± 1.47		15.44 ± 2.32	↑	**23.21 ±5.14***	↑	**31.46 ±1.57****	

. *p*-value< 0.1

* *p*-value< 0.5

** *p*-value< 0.01

*** *p*-value< 0.001

**** *p*-value< 0.0001

C.3 Effect of all three low metal treatments (lowCu, lowFe, lowFeCu) on physiology in the open ocean diatom *Thalassiosira oceanica* (CCMP 1005, TO05).

Table C.3: Effect of all three low metal treatments (lowCu, lowFe, lowFeCu) on physiology in the open ocean diatom *Thalassiosira oceanica*(CCMP 1005, TO05). Arrows indicate if the response to low Cu statistically increases ↑ or decreases ↓ compared to the control. Shown are means with standard errors for parameters derived from three biological replicates (^ indicates measurements have only been done on two of the three biological triplicates, see raw data). Results in bold indicate statistically significant differences compared to the respective control treatment. Stars (., *, **, ***, ****) indicate the level of significance of a 2-way ANOVA with post-hoc interaction analysis (see methods for details).

		TO05					
Treatment	**control**		**low Cu**		**lowFe**		**low FeCu**
[Fe] (nmol)	1370.00		1370.00	↓	12.5	↓	12.5
[Cu] (nmol)	14.32		6.08	↑	14.32	↑	6.08
µ (dd-1)	1.82 ± 0.02	↓	**1.19 ± 0.03 *** **	↓	**1.24 ±0.08****	↓	**0.77 ±0.08****
µ (d-1)	1.26 ± 0.02	↓	**0.82 ± 0.03*****	↓	**0.86 ±0.06****	↓	**0.54 ±0.05****
µ (% µmax)	99.82 ± 1.19	↓	**65.46 ± 1.61 ****	↓	**67.96 ±4.4*****	↓	**42.46 ±4.25****
cell diameter (µm)	5.42 ± 0.16	↓	**4.82 ± 0.23 ****	↓	**4.92 ±0.03***	↓	**4.56 ±0.03****
Chl a conc (pg/cell)	0.35 ± 0.05		0.23 ± 0.05 .	↓	**0.15 ±0****	↓	**0.15 ±0*****
Chl a conc (fg/fl) cell vol	4.28 ± 0.80		3.79 ± 0.41	↓	**2.32 ±0.02****	↓	**2.95 ±0.03***
Fv/Fm (A.U.)	0.61 ± 0.01		0.58 ± 0.02 .	↓	**0.5 ±0.05***	↓	**0.47 ±0.02****
Sigma (Å / RCII)	579.15 ± 3.58^		572.76 ± 24.94^	↑	**695 ±7.35****	↑	**706 ±10.6*****
PQ-Pool size (mol PQ / mol Qb)	5.65 ± 0.18^		5.12 ± 0.19^		4.25 ±1.18	↓	**2.9 ±0.17***
sigma ' @ growth irradiance (Å / RCII)	585 ± 3.23^		575.61 ± 2.47^	↑	**760.92 ±48.58*****	↑	**763.33 ±8.57******
Fq'/Fv' @ growth irradiance (A.U.)	0.69 ± 0.02^		0.66 ± 0.01^		0.56 ±0.06.	↓	**0.57 ±0.01***
Fv'/Fm' @ growth irradiance (A.U.)	0.60 ± 0.01^		0.62 ± 0.00^	↓	**0.47 ±0.05****	↓	**0.47 ±0.02****
Fq'/Fm' @ growth irradiance (A.U.)	0.41 ± 0.01^		0.41 ± 0.01^	↓	**0.27 ±0.06****	↓	**0.27 ±0.02****
ETR @ growth irradiance (mol e-/RCII * s)	390.88 ± 7.34^		368.45 ± 5.97^		409.66 ±16.65		416.48 ±6.32
NPQ (nsv) @ growth irradiance	0.66 ± 0.01^		0.59 ± 0.01^		1.15 ±0.22		1.15 ±0.1

	TO05			
Treatment	**control**	**low Cu**	**lowFe**	**low FeCu**
ETR - PE curve - alpha (mol e-/RCII)/(µmol quanta / m^2 * s)	3.29 ± 0.01^	3.46 ± 0.03^ ↑	**3.93 ±0.11**** ↑	**3.91 ±0.04*****
ETR - PE curve - pmax pmax (mol e-/RCII * s)	502.11 ± 23.46^	431.17 ± 4.69^	491.99 ±22.08	500.07 ±10.97
ETR - PE curve - ek (µmol quanta / m^2 * s)	152.55 ± 7.65^	124.6 ± 0.031^	125.15 ±2.14	127.76 ±1.93.
Conversion factor (ETR / 14C uptake)	117.55 ± 61.89^	111.99 ± 56.03^	132.5 ±66.25	238.43 ±9.45
14C - PvsE - curve - α (g C / g Chla * h)/(µmol quanta / m^2 * s)	1.41E-02 ± 3.32E-03	2.06E-02 ± 4.70E-03	0.02 ±0	0.01 ±0
14C - PvsE - curve - eK (µmol quanta / m^2 * s)	249.05 ± 10.46	223.04 ± 20.76	229 ±5.47 ↓	**162.82 ±4.52*****
14C - PvsE - curve - Pmax (g C / g Chla * h)	3.46 ± 0.70	4.40 ± 0.54	4 ±0.52	2.38 ±0.09
14C uptake @ 155 uEinstein (g C / g Chla * h)	1.94 ± 0.44	2.71 ± 0.53	2.35 ±0.27	1.76 ±0.09
Gross O2 Prod (mol O2 / mol Chla * h)	362.04 ± 33.22	295.11 ± 58.21	284.81 ±17.91	352.28 ±28.73
Respiration (mol O2 / mol Chla * h)	0.05 ± 0.01	0.06 ± 0.00	0.04 ±0.02	0.07 ±0.01
Respiration (µmol O2 / cell * h)	1.79E-08 ± 3.79E-9	1.60E-08 ± 3.76E-9	0 ±0	0 ±0.
AOX activity	60.56 ± 6.23	63.69 ± 7.12	59.2 ±6.25	81.43 ±20.89
protein concentration (pg/cell)	31.15 ± 2.18 ↓	**15.36 ± 1.22****** ↓	**7.97 ±1.43***** ↓	**7.38 ±0.77******

. *p*-value< 0.1

* *p*-value< 0.5

** *p*-value< 0.01

*** *p*-value< 0.001

**** *p*-value< 0.0001

C.4 All gene models of iron-responsive proteins and their expression across all three metal limitation treatments in two strains of *T. oceanica*.

Table C.4: All gene models of iron-responsive proteins and their expression across all three metal limitation treatments in two strains of *T. oceanica*.

		TO03 lowCu[a]		TO03 lowFe[a]		TO03 lowFeCu[a]		TO05 lowCu[a]		TO05 lowFe[a]		TO05 lowFeCu[a]	
Gene name	**Protein name**	sol	insol	sol	insol	sol	insol	sol	insol	sol	insol	sol	insol
ISIPS (iron starvation induced proteins)													
THAOC_21195	ISIP2												
THAOC_21560	ISIP2A												
THAOC_24851	ISIP2A												
THAOC_24852	ISIP2A												
THAOC_27288	ISIP1B												
THAOC_30995	ISIP1A	1.56		**2.57**	1.52	**9.41**	**16.19**	*1.51*	1.41	**7.14**	**34.12**	**6.64**	**9.04**
THAOC_32281	ISIP2B												
THAOC_34562	ISIP2A												
THAOC_34758, contig_117647_681_1617_-	ISIP3							*1.01*	*1.37*	***18.32***	***19.16***	***15.33***	*18.94*
THAOC_36410	ISIP2A								1		-1.37	-1.58	-1.15
ferredoxin													
THAOC_13269	fdx												
THAOC_20937	fdx												
THAOC_25559	petF	**43.79**		-1.46		**-11.02**		-1.48		*-5.31*		-1.21	-1.85
THAOC_27092	fdx												
THAOC_32402	fdx												

Gene name	Protein name	TO03 lowCu[a] sol	TO03 lowCu[a] insol	TO03 lowFe[a] sol	TO03 lowFe[a] insol	TO03 lowFeCu[a] sol	TO03 lowFeCu[a] insol	TO05 lowCu[a] sol	TO05 lowCu[a] insol	TO05 lowFe[a] sol	TO05 lowFe[a] insol	TO05 lowFeCu[a] sol	TO05 lowFeCu[a] insol
flavodoxin													
THAOC_05010	fld	**2.95**		**2.32**		**3.82**							
THAOC_09647	fld												
THAOC_16198	fld												
THAOC_16623	fld												
THAOC_19008	fldB, isoform B												
THAOC_31152	fldA, isoform A	1.44		**2.35**		**218.8**		1.4		**8.09**		**17.24**	**20.77**
FNR, ferredoxin-NADP+ reductase													
THAOC_06509	FNR	-1.46		-1.27		-1.05		-1.14	-1.14	1.27		1.34	1.35
THAOC_34226	FNR												
THAOC_34645	FNR												
THAOC_36724	FNR	**2.47**		**2.71**		**2.88**		-1.34		-1.32		-1.62	*-1.83*
THAOC_36724, contig_64183_1_637_+	FNR	***5.5***		***4.15***		***3.92***							

[a]expression of proteins given in fold-change as per original proteomic analysis (see methods for details); bold highlights significant changes in expression as defined in Methods (>± 2-fold, $p<0.05$); underlined highlights significant changes in expression (±1.3- to 2-fold, $p<0.05$), italic indicates that expression value is derived from EST proteomic analysis.

C.5 Expression of light-harvesting complex (LHC) proteins across all three metal limitation treatments in two strains of *T. oceanica*

Table C.5: Expression of light-harvesting complex (LHC) proteins across all three metal limitation treatments in two strains of *T. oceanica*

		TO03 lowCu[c]		TO03 lowFe[c]		TO03 lowFeCu[c]		TO05 lowCu[c]		TO05 lowFe[c]		TO05 lowFeCu[c]	
Gene name[a]	**closest homolog[b]**	sol	insol	sol	insol	sol	insol	sol	insol	sol	insol	sol	insol
Lhcf - Group I													
THAOC_01208	TpLhcf	**-2.79**	2.05	-3.49	1.07	1.55	1.22		-1.13		-1.36	-1.43	-1.39
THAOC_01927	TpLhcf		**-2.04**		**-2.04**		-1.61						
THAOC_02510	TpLhcf	-1.41	-1.18	-1.54	-1.06	1.23	*-1.37*	-1.19	-1.13	-1.17	-1.19	1.05	*-1.26*
THAOC_06305	TpLhcf	***-10.34***	1.04	**-8.21**	1.02	**-5.15**	**-2.07**	1.54	-1.21		-1.29	-1.24	*-1.24*
THAOC_08131	TpLhcf8								*-1.31*		-1.32	-1.13	1.08
THAOC_08131, contig_91916_1_273_+	TpLhcf8							*-1.14*	*-1.32*		*-1.46*		*-1.1*
THAOC_17964	TpLhcf		1.19		1.05		1.27		-1.07		-1.02	1.03	*1.05*
THAOC_17964, contig_83951_1_204_+	TpLhcf								*-1.07*		*-1.37*		*-1.49*
THAOC_20854	TpLhcf	**-5.56**	-1.49	**-5.1**	*-1.49*	**-2.79**	-1.47	1.32	-1.28	-1.58	1.21	*-1.96*	*1.27*
THAOC_20855	TpLhcf		-1.63		-1.66		**-3.9**		-1.21		-1.08	-1.25	-1.22
THAOC_25270	TpLhcf		1.23		1.31		1.74		-1.13		-1.16	-1.23	-1.2
THAOC_25270, contig_119270_60_376_-	TpLhcf								*-1.32*		*-1.2*		*-1.36*
THAOC_25270, contig_123884_1_219_-	TpLhcf		*-1.7*		***-2.23***		*-1.67*						
THAOC_25270, contig_70472_60_300_-	TpLhcf		*1.52*		*1.1*		*1.33*		*-1.07*		*-1.39*		*-1.36*
THAOC_32932	TpLhcf8	-5	**-2.12**	-3.59	**-2.05**	**-2.23**	-1.92		-1.15		-1.22	-1.23	-1.18
THAOC_36248	TpLhcf	1.45	-1.38	-1.01	-1.5	**3.55**	*1.15*		-1.09		1.19	1.32	1.35

Gene name[a]	closest homolog[b]	TO03 lowCu[c] sol	TO03 lowCu[c] insol	TO03 lowFe[c] sol	TO03 lowFe[c] insol	TO03 lowFeCu[c] sol	TO03 lowFeCu[c] insol	TO05 lowCu[c] sol	TO05 lowCu[c] insol	TO05 lowFe[c] sol	TO05 lowFe[c] insol	TO05 lowFeCu[c] sol	TO05 lowFeCu[c] insol
Lhcf - Group II													
THAOC_09684	TpLhcf11	-1.07	**4.83**	**9.06**	**3.7**	1.18	**2.52**	-1.05	-1.23	-1.64	-1.6	-1.62	-1.52
Lhcf - Group III													
THAOC_04469	TpFCP4	**-8.68**	**2.06**	-5.94	**2.09**	**-5.65**	1.24	1.53	-1.26	1.2	-1.64	-1.56	-1.73
THAOC_05777	TpFCP10	-1.04	**2.4**	**-2.24**	**2.28**	**-2.22**	-1.38	1.33	-1.16	-1.15	**-2.14**	-1.76	-1.67
THAOC_06968	TpFCP2	**-2.52**	1.4	-1.43	*1.7*	**-2.37**	1.06		-1.09		-1.36	-1.3	-1.11
THAOC_08587	TpFCP7	**-2.73**	**2.79**	-2.81	**2.54**	**-2.72**	1.83	**2.07**	-1.22		-1.34	-1.09	*-1.12*
THAOC_16345	TpFCP4		**2.68**		**2.17**		1.61		-1.3		-1.25	-1.13	-1.34
THAOC_16412	TpFCP9	-3.31	1.97		1.2	-3.79	-1.99	1.54	-1.09	-1.11	1.01	1.04	-1.16
THAOC_18180	TpFCP11		2.02				1.06	1.31	1.09		-1.7	-1.6	-1.33
THAOC_18994	TpFCP4									*1.93*	**2.48**	**2.58**	***2.87***
Lhcr													
THAOC_00550	TpLhcr11	-6.06	***2.39***	***-7.12***	***2.33***	**-6.64**	1.02	1.34	-1.14	-1.42	-1.26	-1.83	-1.49
THAOC_05707	TpLhcr4		1.24	**-9.33**	1.2	-2.8	-1.49	1.7	-1.21	1	-1.35	-1.51	-1.37
THAOC_05708	TpLhcr14		-1.06		-1.47		**-2.21**		1.13		-1.69	-1.98	-1.51
THAOC_07034	TpLhcr13		1.66		**2.08**		-1.26	1.83	-1.11	*1.38*	-1.2	-1.19	-1.26
THAOC_07036	TpLhcr13	**-6.57**	1.06	**-5.79**	*1.09*	**-7.66**	**-2.75**	1.24	-1.19		**-2.09**	**-2.18**	-1.76
THAOC_16963	TpLhcr3		-1.56		1.73		**-6.51**	-1.21	-1.13		-1.96	**-2.28**	**-2.23**
THAOC_34573	TpLhcr2		4.44		**3.06**		**3.12**	1.34	-1.32	-1.25	-1.6	-1.62	-1.72
THAOC_35171	TpLhcr1		3.48		1.52		1.18		-1.39		-1.42	-1.3	-1.26
THAOC_35518	TpLhcr10	**-2.55**	-1.26		*1.21*	**-4.93**	*-1.89*		-1.04	1.02	-1.64	-1.47	-1.86

Gene name[a]	closest homolog[b]	TO03 lowCu[c] sol	TO03 lowCu[c] insol	TO03 lowFe[c] sol	TO03 lowFe[c] insol	TO03 lowFeCu[c] sol	TO03 lowFeCu[c] insol	TO05 lowCu[c] sol	TO05 lowCu[c] insol	TO05 lowFe[c] sol	TO05 lowFe[c] insol	TO05 lowFeCu[c] sol	TO05 lowFeCu[c] insol
Lhcx													
THAOC_08095	TpLhcx7	1.26	***2.76***	-2.1	1.34	**-2.78**	-1.53		-1.15		-1.32	-1.25	-1.4
THAOC_08095, contig_119183_41_788_+	TpLhcx7	*-1.86*	*-1.41*	*-4.31*	*1.12*	***-3.01***	***-2.39***	*-1.16*	*-1.13*	*-1.24*	*-1.51*	*-1.53*	*-1.36*
THAOC_09937	TpLhcx1	**3.29**		**3.09**		**12.57**		-1.22		-2.25		-1.77	-1.24
THAOC_31988	TpLhcx1	***3.29***		***3.14***		***12.41***		*-1.22*				*-1.24*	
17531													
THAOC_01290	Tp17531								-1.06		-1.81	-1.87	-1.81
Lhcz													
THAOC_37813	TpFCP5								-1.46		-1.26	-1.27	-1.34

[a]grouped into different LHC clades as per phylogenetic analysis (Chapter 3)
[b]closest homolog as per phylogenetic analysis (Chapter 3)
[c]expression of proteins given in fold-change as per original proteomic analysis (see methods for details); bold highlights significant changes in expression as defined in Methods (>± 2-fold, $p<0.05$); underlined highlights significant changes in expression (±1.3- to 2-fold, $p<0.05$), italic indicates that expression value is derived from EST proteomic analysis. (2248)